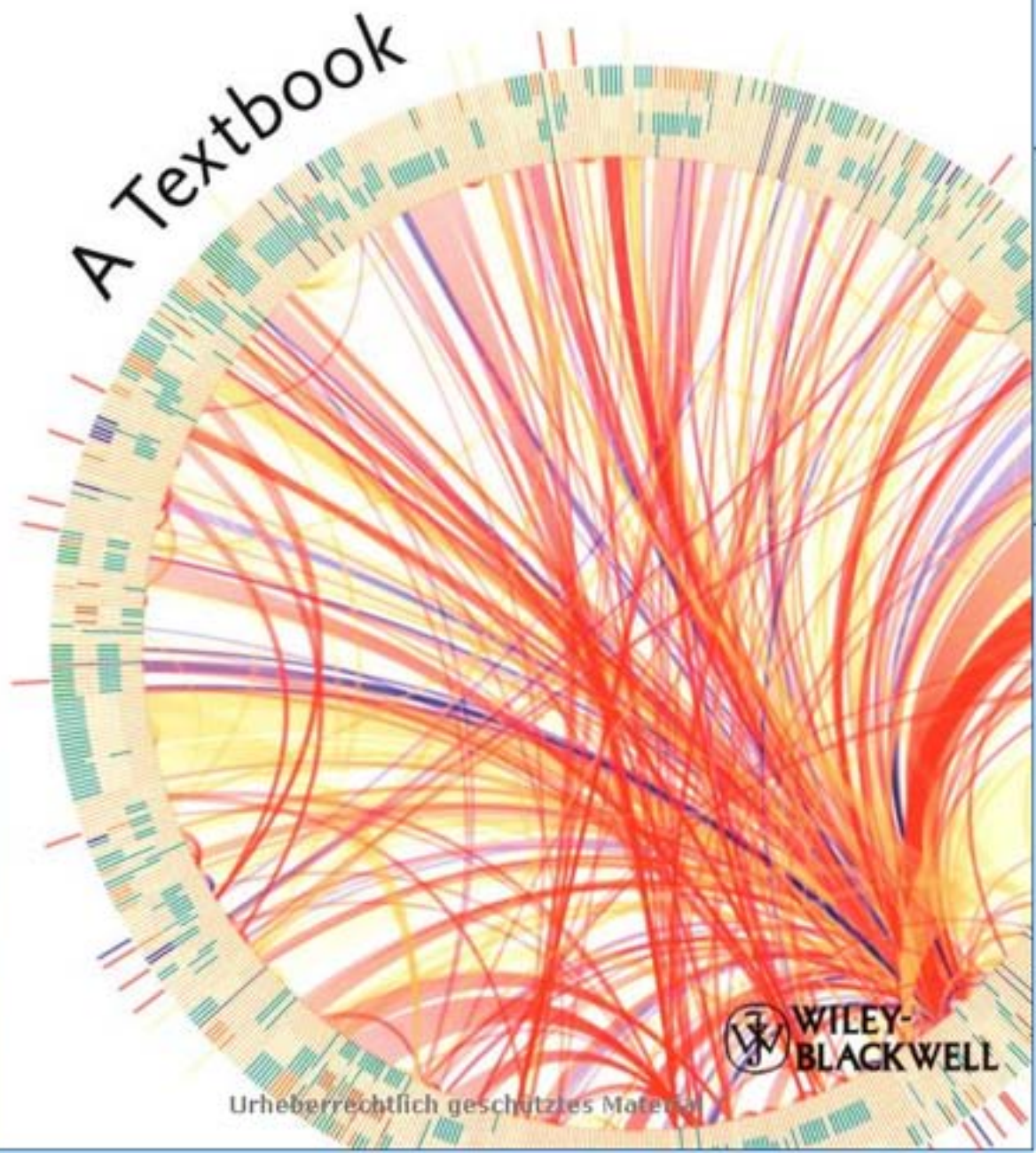# Systems Biology

Edda Klipp, Wolfram Liebermeister, Christoph Wierling,
Axel Kowald, Hans Lehrach, and Ralf Herwig

A Textbook

WILEY-
BLACKWELL

Edda Klipp, Wolfram Liebermeister,
Christoph Wierling, Axel Kowald,
Hans Lehrach, and Ralf Herwig
Systems Biology

Related Titles

Helms, V.

Principles of Computational Cell Biology

From Protein Complexes to Cellular Networks

2008
Softcover
ISBN: 978-3-527-31555-0

Baxevanis, A. D., Ouellette, B. F. F. (eds.)

Bioinformatics

A Practical Guide to the Analysis of Genes and Proteins

560 pages
2004
Hardcover
ISBN: 978-0-471-47878-2

Edda Klipp, Wolfram Liebermeister, Christoph Wierling,
Axel Kowald, Hans Lehrach, and Ralf Herwig

Systems Biology

A Textbook

The Authors

Prof. Edda Klipp
Humboldt-Universität Berlin
Institut für Biologie
Theoretische Biophysik
Invalidenstr. 42
10115 Berlin

Dr. Wolfram Liebermeister
Humboldt-Universität Berlin
Institut für Biologie
Theoretische Biophysik
Invalidenstr. 42
10115 Berlin

Dr. Christoph Wierling
MPI für Molekulare Genetik
Ihnestr. 73
14195 Berlin
Germany

Dr. Axel Kowald
Protagen AG
Otto-Hahn-Str. 15
44227 Dortmund

Prof. Hans Lehrach
MPI für Molekulare Genetik
Ihnestr. 73
14195 Berlin
Germany

Prof. Ralf Herwig
MPI für Molekulare Genetik
Ihnestr. 73
14195 Berlin
Germany

Cover
The cover pictures were provided with kind permission by Santiago Ortiz and Dr. Michael Erlowitz

Contents

Preface

Life is probably the most complex phenomenon in the universe. We see kids growing, people aging, plants blooming, and microbes degrading their remains. We use yeast for brewery and bakery, and doctors prescribe drugs to cure diseases. But can we understand how life works? Since the 19th century, the processes of life have no longer been explained by special "living forces," but by the laws of physics and chemistry. By studying the structure and physiology of living systems more and more in detail, researchers from different disciplines have revealed how the mystery of life arises from the structural and functional organization of cells and from the continuous refinement by mutation and selection.

In recent years, new imaging techniques have opened a completely new perception of the cellular microcosm. If we zoom into the cell, we can observe how structures are built, maintained, and reproduced while various sensing and regulation systems help the cell to respond appropriately to environmental changes. But along with all these fascinating observations, many open questions remain. Why do we age? How does a cell know when to divide? How can severe diseases such as cancer or genetic disorders be cured? How can we convince – i.e., manipulate – microbes to produce a desirable substance? How can the life sciences contribute to environmental safety and sustainable technologies?

This book provides you with a number of tools and approaches that can help you to think in more detail about such questions from a theoretical point of view. A key to tackle such questions is to combine biological experiments with computational modeling in an approach called systems biology: it is the combined study of biological systems through (i) investigating the components of cellular networks and their interactions, (ii) applying experimental high-throughput and whole-genome techniques, and (iii) integrating computational methods with experimental efforts.

The systemic approach in biology is not new, but it recently gained new thrust due to the emergence of powerful experimental and computational methods. It is based on the accumulation of an increasingly detailed biological knowledge, on the emergence of new experimental techniques in genomics and proteomics, on a tradition of mathematical modeling of biological processes, on the exponentially growing computer power (as prerequisite for databases and the calculation of large

systems), and on the Internet as the central medium for a quick and comprehensive exchange of information.

Systems Biology has influenced modern biology in two major ways: on the one hand, it offers computational tools for analyzing, integrating and interpreting biological data and hypotheses. On the other hand, it has induced the formulation of new theoretical concepts and the application of existing ones to new questions. Such concepts are, for example, the theory of dynamical systems, control theory, the analysis of molecular noise, robustness and fragility of dynamic systems, and statistical network analysis. As systems biology is still evolving as a scientific field, a central issue is the standardization of experiments, of data exchange, and of mathematical models.

In this book, we attempt to give a survey of this rapidly developing field. We will show you how to formulate your own model of biological processes, how to analyze such models, how to use data and other available information for making your model more precise – and how to interpret the results. This book is designed as an introductory course for students of biology, biophysics and bioinformatics, and for senior scientists approaching Systems Biology from a different discipline. Its nine chapters contain material for about 30 lectures and are organized as follows.

Chapter 1 – Introduction (E. Klipp, W. Liebermeister, A. Kowald, 1 lecture)

Introduction to the subject. Elementary concepts and definitions are presented. Read this if you want to start right from the beginning.

Chapter 2 – Modeling of Biochemical Systems (E. Klipp, C. Wierling, 4 lectures)

This chapter describes kinetic models for biochemical reaction networks, the most common computational technique in Systems Biology. It includes kinetic laws, stoichiometric analysis, elementary flux modes, and metabolic control analysis. Introduces tools and data formats necessary for modeling.

Chapter 3 – Specific Biochemical Systems (E. Klipp, C. Wierling, W. Liebermeister, 5 lectures)

Using specific examples from metabolism, signaling, and cell cycle, a number of popular modeling techniques are discussed. The aim of this chapter is to make the reader familiar with both modeling techniques and biological phenomena.

Chapter 4 – Model Fitting (W. Liebermeister, A. Kowald, 4 lectures)

Models in systems biology usually contain a large number of parameters. Assigning appropriate numerical values to these parameters is an important step in the creation of a quantitative model. This chapter shows how numerical values can be obtained from the literature or by fitting a model to experimental data. It also discusses how model structures can be simplified and how they can be chosen if several different models can potentially describe the experimental observations.

Chapter 5 – Analysis of High-Throughput Data (R. Herwig, 2 lectures)

Several techniques that have been developed in recent years produce large quantities of data (e.g., DNA and protein chips, yeast two-hybrid, mass spectrometry). But such large quantities often go together with a reduced quality of the individual measurement. This chapter describes techniques that can be used to handle this type of data appropriately.

Chapter 6 – Gene Expression Models (R. Herwig, W. Liebermeister, E. Klipp, 3 lectures)

Thousands of gene products are necessary to create a living cell, and the regulation of gene expression is a very complex and important task to keep a cell alive. This chapter discusses how the regulation of gene expression can be modeled, how different input signals can be integrated, and how the structure of gene networks can be inferred from experimental data.

Chapter 7 – Stochastic Systems and Variability (W. Liebermeister, 4 lectures)

Random fluctuations in transcription, translation and metabolic reactions make mathematics complicated, computation costly and interpretation of results not straight forward. But since experimentalists find intriguing examples for macroscopic consequences of random fluctuation at the molecular level, the incorporation of these effects into the simulations becomes more and more important. This chapter gives an overview where and how stochasticity enters cellular life.

Chapter 8 – Network Structures, Dynamics and Function (W. Liebermeister, 3 lectures)

Many complex systems in biology can be represented as networks (reaction networks, interaction networks, regulatory networks). Studying the structure, dynamics, and function of such networks helps to understand design principles of living cells. In this chapter, important network structures such as motifs and modules as well as the dynamics resulting from them are discussed.

Chapter 9 – Optimality and Evolution (W. Liebermeister, E. Klipp, 3 lectures)

Theoretical research suggests that constraints of the evolutionary process should have left their marks in the construction and regulation of genes and metabolic pathways. In some cases, the function of biological systems can be well understood by models based on an optimality hypothesis. This chapter discusses the merits and limitations of such optimality approaches.

Various aspects of systems biology – the biological systems themselves, types of mathematical models to describe them, and practical techniques – reappear in different contexts in various parts of the book. The following diagram, which shows the contents of the book sorted by a number of different aspects, may serve as an orientation.

Biological systems

Metabolism (3.1, 8.1, 9.1)
Transcription (6.1, 6.2, 8.2)
Genetic network (6.3, 6.4, 8.1, 8.2)
Signaling systems (3.2, 7.4, 8.2)
Cell cycle (3.3)
Development (3.4)
Apoptosis (3.5)

Perspectives on biological function

Qualitative behavior (2.3, 3.3)
Parameter sensitivity/robustness (7.3, 7.4)
Robustness against failure (7.4)
Modularity (8.3)
Optimality (9.1, 9.2)
Evolution (9.3)
Game-theoretical requirements (9.3)

Model types with different
levels of abstraction

Thermodynamic/many particles (7.1)
Kinetic models (2.1, 2.3)
Dynamical systems (2.3)
Optimization/control theory (2.3, 9.1, 9.2)

Mathematical frameworks to
describe cell states

Topological (8.1)
Structural stoichiometric (2.2)
Deterministic linear (15)
Deterministic kinetic (2.1, 2.3)
Spatial (3.4)
Discrete (6.3, 6.4)
Stochastic dynamics (7.1, 7.2, 14)
Uncertain parameters (7.3)

Modeling skills

Model building (2.1 – 2.4)
Model reduction and combination (4.3)
Data collection (4.1, 5.1)
Statistical data analysis (5.2)
Parameter estimation (4.2)
Model testing and selection (4.4)
Local sensitivity/control theory (2.3, 7.3)
Global sensitivity/uncertainty analysis (7.3)
Parameter optimization (9.1, 9.2)
Optimal control (9.2)

Practical issues in modeling

Data formats (2.4)
Data sources (2.4, 16)
Modeling software (2.4, 17)
Experimental techniques (11)
Statistical methods (4.2, 4.4, 13)

At the end of the regular course material, you will find a number of additional chapters that summarize important biological and mathematical methods. The first chapters deal with to cell biology (chapter 10, C. Wierling) and molecular biological methods (chapter 11, A. Kowald). For looking up mathematical and statistical definitions and methods, turn to chapters 12 and 13 (R. Herwig, A. Kowald). Chapters 14 and 15 (W. Liebermeister) concentrate on random processes and control theory. The final chapters provide an overview over useful databases (chapter 16, C. Wierling) as well as a huge list of available software tools including a short description of their purposes (chapter 17, A. Kowald).

Further material is available on an accompanying website

(www.wiley-vch.de/home/systemsbiology)

Beside additional and more specialized topics, the website also contains solutions to the exercises and problems presented in the book.

Part One
Introduction to Systems Biology

Part One
Introduction to Systems Biology

1
Introduction

1.1
Biology in Time and Space

Biological systems like organisms, cells, or biomolecules are highly organized in their structure and function. They have developed during evolution and can only be fully understood in this context. To study them and to apply mathematical, computational, or theoretical concepts, we have to be aware of the following circumstances.

The continuous reproduction of cell compounds necessary for living and the respective flow of information is captured by the central dogma of molecular biology, which can be summarized as follows: genes code for mRNA, mRNA serves as template for proteins, and proteins perform cellular work. Although information is stored in the genes in form of DNA sequence, it is made available only through the cellular machinery that can decode this sequence and can translate it into structure and function. In this book, this will be explained from various perspectives.

A description of biological entities and their properties encompasses different levels of organization and different time scales. We can study biological phenomena at the level of populations, individuals, tissues, organs, cells, and compartments down to molecules and atoms. Length scales range from the order of meter (e.g., the size of whale or human) to micrometer for many cell types, down to picometer for atom sizes. Time scales include millions of years for evolutionary processes, annual and daily cycles, seconds for many biochemical reactions, and femtoseconds for molecular vibrations. Figure 1.1 gives an overview about scales.

In a unified view of cellular networks, each action of a cell involves different levels of cellular organization, including genes, proteins, metabolism, or signaling pathways. Therefore, the current description of the individual networks must be integrated into a larger framework.

Many current approaches pay tribute to the fact that biological items are subject to evolution. The structure and organization of organisms and their cellular machinery has developed during evolution to fulfill major functions such as growth, proliferation, and survival under changing conditions. If parts of the organism or of the cell fail to perform their function, the individual might become unable to survive or replicate.

Size

		Time

Size scale (top to bottom):

- m — Human
- 10 cm — Mouse
- cm
- mm — D. melanogaster, C. elegans
- 100 µm — Body sizes
- 10 µm — Eukaryote, Cell sizes
- µm — Bacterium, Mitochondrion
- 100 nm — Wavelengths of visible light
- 10 nm — Ribosome, Membrane thickness
- nm — Small molecules, Hydrogen bond, Molecules
- 0.1 nm

Time scale (top to bottom):

- billion years — Life (Evolution)
- million years — Human
- year — E. coli genes (Cell regulation)
- day — Circadian oscillation
- hour — Glycolytic osc. (yeast), Cell cycle (E.coli), Gene expression
- min — Metabolism, signaling
- s — LacZ production (RNA)
- ms — Translation (AA), Transcription (nucleotide)
- µs — Protein–DNA binding (Molecules)
- ns
- fs — High-energy transition state

Figure 1.1 Length and time scales in biology. Data from the BioNumbers database http://bionumbers.hms.harvard.edu.

One consequence of evolution is the similarity of biological organisms from different species. This similarity allows for the use of model organisms and for the critical transfer of insights gained from one cell type to other cell types. Applications include, e.g., prediction of protein function from similarity, prediction of network properties from optimality principles, reconstruction of phylogenetic trees, or the identification of regulatory DNA sequences through cross-species comparisons. But the evolutionary process also leads to genetic variations within species. Therefore, personalized medicine and research is an important new challenge for biomedical research.

1.2
Models and Modeling

If we observe biological processes, we are confronted with various complex processes that cannot be explained from first principles and the outcome of which cannot reliably be foreseen from intuition. Even if general biochemical principles are well established (e.g., the central dogma of transcription and translation, the biochemistry of enzyme-catalyzed reactions), the biochemistry of individual molecules and systems is often unknown and can vary considerably between species. Experiments lead to biological hypotheses about individual processes, but it often remains unclear if these hypotheses can be combined into a larger coherent picture because it is often

difficult to foresee the global behavior of a complex system from knowledge of its parts. Mathematical modeling and computer simulations can help us understand the internal nature and dynamics of these processes and to arrive at predictions about their future development and the effect of interactions with the environment.

1.2.1
What is a Model?

The answer to this question will differ among communities of researchers. In a broad sense, a model is an abstract representation of objects or processes that explains features of these objects or processes (Figure 1.2). A biochemical reaction network can be represented by a graphical sketch showing dots for metabolites and arrows for reactions; the same network could also be described by a system of differential equations, which allows simulating and predicting the dynamic behavior of that network. If a model is used for simulations, it needs to be ensured that it faithfully predicts the system's behavior – at least those aspects that are supposed to be covered by the model. Systems biology models are often based on well-established physical laws that justify their general form, for instance, the thermodynamics of chemical reactions; besides this, a computational model needs to make specific statements about a system of interest – which are partially justified by experiments and biochemical knowledge, and partially by mere extrapolation from other systems. Such a model can summarize established knowledge about a system in a coherent mathematical formulation. In experimental biology, the term "model" is also used to denote a species that is especially suitable for experiments, for example, a genetically modified mouse may serve as a model for human genetic disorders.

1.2.2
Purpose and Adequateness of Models

Modeling is a subjective and selective procedure. A model represents only specific aspects of reality but, if done properly, this is sufficient since the intention of modeling is to answer particular questions. If the only aim is to predict system outputs from given input signals, a model should display the correct input–output relation, while its interior can be regarded as a black box. But if instead a detailed biological mechanism has to be elucidated, then the system's structure and the relations between its parts must be described realistically. Some models are meant to be generally applicable to many similar objects (e.g., Michaelis–Menten kinetics holds for many enzymes, the promoter–operator concept is applicable to many genes, and gene regulatory motifs are common), while others are specifically tailored to one particular object (e.g., the 3D structure of a protein, the sequence of a gene, or a model of deteriorating mitochondria during aging). The mathematical part can be kept as simple as possible to allow for easy implementation and comprehensible results. Or it can be modeled very realistically and be much more complicated. None of the characteristics mentioned above makes a model wrong or right, but they determine whether a model is appropriate to the problem to be solved. The phrase "essentially,

(a) Biological system

(b) Mental model

(c) Model scheme

X → Activation   Protein X

Y → Protein Y

(d) Process model

$$0 \rightarrow X \ : \quad a_1 = v_0 \ \text{(const.)}$$
$$X \rightarrow 0 \ : \quad a_2 = \kappa_x \cdot [X]$$
$$0 \rightarrow Y \ : \quad a_3 = f_y \cdot [X]$$
$$Y \rightarrow 0 \ : \quad a_4 = \kappa_y \cdot [Y]$$

(e) Dynamical model

$$\mathrm{d}x/\mathrm{d}t = v_0 - \kappa_x\, x$$
$$\mathrm{d}y/\mathrm{d}t = f_y\, x - \kappa_y\, y$$
$$x(0) = x_0$$
$$y(0) = y_0$$

(f) Quantitative results

Concentration / Time (axes); curves X and Y
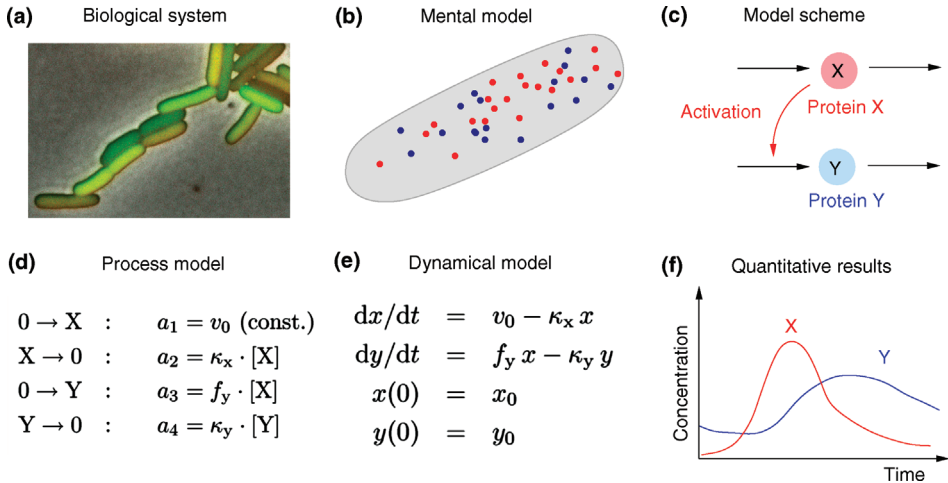
Figure 1.2 Typical abstraction steps in mathematical modeling. (a) *Escherichia coli* bacteria produce thousands of different proteins. If a specific protein type is fluorescently labeled, cells glow under the microscope according to the concentration of this enzyme (Courtesy of M. Elowitz). (b) In a simplified mental model, we assume that cells contain two enzymes of interest, X (red) and Y (blue) and that the molecules (dots) can freely diffuse within the cell. All other substances are disregarded for the sake of simplicity. (c) The interactions between the two protein types can be drawn in a wiring scheme: each protein can be produced or degraded (black arrows). In addition, we assume that proteins of type X can increase the production of protein Y. (d) All individual processes to be considered are listed together with their rates *a* (occurrence per time). The mathematical expressions for the rates are based on a simplified picture of the actual chemical processes. (e) The list of processes can be translated into different sorts of dynamic models; in this case, deterministic rate equations for the protein concentrations *x* and *y*. (f) By solving the model equations, predictions for the time-dependent concentrations can be obtained. If these predictions do not agree with experimental data, it indicates that the model is wrong or too much simplified. In both cases, it has to be refined.

all models are wrong, but some are useful" coined by the statistician George Box is indeed an appropriate guideline for model building.

1.2.3
Advantages of Computational Modeling

Models gain their reference to reality from comparison with experiments, and their benefits therefore depend on the quality of the experiments used. Nevertheless, modeling combined with experimentation has a lot of advantages compared to purely experimental studies:

- Modeling drives conceptual clarification. It requires verbal hypotheses to be made specific and conceptually rigorous.

- Modeling highlights gaps in knowledge or understanding. During the process of model formulation, unspecified components or interactions have to be determined.

- Modeling provides independence of the modeled object.

- Time and space may be stretched or compressed *ad libitum*.

- Solution algorithms and computer programs can be used independently of the concrete system.

- Modeling is cheap compared to experiments.

- Models exert by themselves no harm on animals or plants and help to reduce ethical problems in experiments. They do not pollute the environment.

- Modeling can assist experimentation. With an adequate model, one may test different scenarios that are not accessible by experiment. One may follow time courses of compounds that cannot be measured in an experiment. One may impose perturbations that are not feasible in the real system. One may cause precise perturbations without directly changing other system components, which is usually impossible in real systems. Model simulations can be repeated often and for many different conditions.

- Model results can often be presented in precise mathematical terms that allow for generalization. Graphical representation and visualization make it easier to understand the system.

- Finally, modeling allows for making well-founded and testable predictions.

The attempt to formulate current knowledge and open problems in mathematical terms often uncovers a lack of knowledge and requirements for clarification. Furthermore, computational models can be used to test whether proposed explanations of biological phenomena are feasible. Computational models serve as repositories of current knowledge, both established and hypothetical, about how systems might operate. At the same time, they provide researchers with quantitative descriptions of this knowledge and allow them to simulate the biological process, which serves as a rigorous consistency test.

1.3
Basic Notions for Computational Models

1.3.1
Model Scope

Systems biology models consist of mathematical elements that describe properties of a biological system, for instance, mathematical variables describing the concentrations of metabolites. As a model can only describe certain aspects of the system, all other properties of the system (e.g., concentrations of other substances or the environment of a cell) are neglected or simplified. It is important – and to some extent, an art – to construct models in such ways that the disregarded properties do not compromise the basic results of the model.

1.3.2
Model Statements

Besides the model elements, a model can contain various kinds of statements and equations describing facts about the model elements, most notably, their temporal behavior. In kinetic models, the basic modeling paradigm considered in this book, the dynamics is determined by a set of ordinary differential equations describing the substance balances. Statements in other model types may have the form of equality or inequality constraints (e.g., in flux balance analysis), maximality postulates, stochastic processes, or probabilistic statements about quantities that vary in time or between cells.

1.3.3
System State

In dynamical systems theory, a system is characterized by its *state*, a snapshot of the system at a given time. The state of the system is described by the set of variables that must be kept track of in a model: in deterministic models, it needs to contain enough information to predict the behavior of the system for all future times. Each modeling framework defines what is meant by the state of the system. In kinetic rate equation models, for example, the state is a list of substance concentrations. In the corresponding stochastic model, it is a probability distribution or a list of the current number of molecules of a species. In a Boolean model of gene regulation, the state is a string of bits indicating for each gene whether it is expressed ("1") or not expressed ("0"). Also the temporal behavior can be described in fundamentally different ways. In a *dynamical system*, the future states are determined by the current state, while in a *stochastic process*, the future states are not precisely predetermined. Instead, each possibly future history has a certain probability to occur.

1.3.4
Variables, Parameters, and Constants

The quantities in a model can be classified as variables, parameters, and constants. A *constant* is a quantity with a fixed value, such as the natural number e or Avogadro's number (number of molecules per mole). *Parameters* are quantities that have a given value, such as the K_m value of an enzyme in a reaction. This value depends on the method used and on the experimental conditions and may change. *Variables* are quantities with a changeable value for which the model establishes relations. A subset of variables, the *state variables*, describes the system behavior completely. They can assume independent values and each of them is necessary to define the system state. Their number is equivalent to the dimension of the system. For example, the diameter d and volume V of a sphere obey the relation $V = \pi d^3/6$, where π and 6 are constants, V and d are variables, but only one of them is a state variable since the relation between them uniquely determines the other one.

Whether a quantity is a variable or a parameter depends on the model. In reaction kinetics, the enzyme concentration appears as a parameter. However, the enzyme concentration itself may change due to gene expression or protein degradation and in an extended model, it may be described by a variable.

1.3.5
Model Behavior

Two fundamental factors that determine the behavior of a system are (i) influences from the environment (input) and (ii) processes within the system. The system structure, that is, the relation among variables, parameters, and constants, determines how endogenous and exogenous forces are processed. However, different system structures may still produce similar system behavior (output); therefore, measurements of the system output often do not suffice to choose between alternative models and to determine the system's internal organization.

1.3.6
Model Classification

For modeling, processes are classified with respect to a set of criteria.

- A structural or *qualitative* model (e.g., a network graph) specifies the interactions among model elements. A *quantitative* model assigns values to the elements and to their interactions, which may or may not change.
- In a *deterministic* model, the system evolution through all following states can be predicted from the knowledge of the current state. *Stochastic* descriptions give instead a probability distribution for the successive states.
- The nature of values that time, state, or space may assume distinguishes a *discrete* model (where values are taken from a discrete set) from a *continuous* model (where values belong to a continuum).
- *Reversible* processes can proceed in a forward and backward direction. Irreversibility means that only one direction is possible.
- *Periodicity* indicates that the system assumes a series of states in the time interval $\{t, t + \Delta t\}$ and again in the time interval $\{t + i\Delta t, t + (i + 1)\Delta t\}$ for $i = 1, 2, \ldots$.

1.3.7
Steady States

The concept of stationary states is important for the modeling of dynamical systems. *Stationary states* (other terms are *steady states* or *fixed points*) are determined by the fact that the values of all state variables remain constant in time. The asymptotic behavior of dynamic systems, that is, the behavior after a sufficiently long time, is often stationary. Other types of asymptotic behavior are oscillatory or chaotic regimes.

The consideration of steady states is actually an abstraction that is based on a separation of time scales. In nature, everything flows. Fast and slow processes – ranging from formation and breakage of chemical bonds within nanoseconds to growth of individuals within years – are coupled in the biological world. While fast processes often reach a quasi-steady state after a short transition period, the change of the value of slow variables is often negligible in the time window of consideration. Thus, each steady state can be regarded as a quasi-steady state of a system that is embedded in a larger nonstationary environment. Despite this idealization, the concept of stationary states is important in kinetic modeling because it points to typical behavioral modes of the system under study and it often simplifies the mathematical problems.

Other theoretical concepts in systems biology are only rough representations of their biological counterparts. For example, the representation of gene regulatory networks by Boolean networks, the description of complex enzyme kinetics by simple mass action laws, or the representation of multifarious reaction schemes by black boxes proved to be helpful simplification. Although being a simplification, these models elucidate possible network properties and help to check the reliability of basic assumptions and to discover possible design principles in nature. Simplified models can be used to test mathematically formulated hypothesis about system dynamics, and such models are easier to understand and to apply to different questions.

1.3.8
Model Assignment is not Unique

Biological phenomena can be described in mathematical terms. Models developed during the last decades range from the description of glycolytic oscillations with ordinary differential equations to population dynamics models with difference equations, stochastic equations for signaling pathways, and Boolean networks for gene expression. But it is important to realize that a certain process can be described in more than one way: a biological object can be investigated with different experimental methods and each biological process can be described with different (mathematical) models. Sometimes, a modeling framework represents a simplified limiting case (e.g., kinetic models as limiting case of stochastic models). On the other hand, the same mathematical formalism may be applied to various biological instances: statistical network analysis, for example, can be applied to cellular-transcription networks, the circuitry of nerve cells, or food webs.

The choice of a mathematical model or an algorithm to describe a biological object depends on the problem, the purpose, and the intention of the investigator. Modeling has to reflect essential properties of the system and different models may highlight different aspects of the same system. This ambiguity has the advantage that different ways of studying a problem also provide different insights into the system. However, the diversity of modeling approaches makes it still very difficult to merge established models (e.g., for individual metabolic pathways) into larger supermodels (e.g., models of complete cell metabolism).

1.4
Data Integration

Systems biology has evolved rapidly in the last years driven by the new high-throughput technologies. The most important impulse was given by the large sequencing projects such as the human genome project, which resulted in the full sequence of the human and other genomes [1, 2]. Proteomics technologies have been used to identify the translation status of complete cells (2D-gels, mass spectrometry) and to elucidate protein–protein interaction networks involving thousands of components [3]. However, to validate such diverse high-throughput data, one needs to correlate and integrate such information. Thus, an important part of systems biology is data integration.

On the lowest level of complexity, data integration implies common schemes for data storage, data representation, and data transfer. For particular experimental techniques, this has already been established, for example, in the field of transcriptomics with minimum information about a microarray experiment [4], in proteomics with proteomics experiment data repositories [5], and the Human Proteome Organization consortium [6]. On a more complex level, schemes have been defined for biological models and pathways such as Systems Biology Markup Language (SBML) [7] and CellML [8], which use an XML-like language style.

Data integration on the next level of complexity consists of data correlation. This is a growing research field as researchers combine information from multiple diverse data sets to learn about and explain natural processes [9, 10]. For example, methods have been developed to integrate the results of transcriptome or proteome experiments with genome sequence annotations. In the case of complex disease conditions, it is clear that only integrated approaches can link clinical, genetic, behavioral, and environmental data with diverse types of molecular phenotype information and identify correlative associations. Such correlations, if found, are the key to identifying biomarkers and processes that are either causative or indicative of the disease. Importantly, the identification of biomarkers (e.g., proteins, metabolites) associated with the disease will open up the possibility to generate and test hypotheses on the biological processes and genes involved in this condition. The evaluation of disease-relevant data is a multistep procedure involving a complex pipeline of analysis and data handling tools such as data normalization, quality control, multivariate statistics, correlation analysis, visualization techniques, and intelligent database systems [11]. Several pioneering approaches have indicated the power of integrating data sets from different levels: for example, the correlation of gene membership of expression clusters and promoter sequence motifs [12]; the combination of transcriptome and quantitative proteomics data in order to construct models of cellular pathways [10]; and the identification of novel metabolite-transcript correlations [13]. Finally, data can be used to build and refine dynamical models, which represent an even higher level of data integration.

1.5
Standards

As experimental techniques generate rapidly growing amounts of data and large models need to be developed and exchanged, standards for both experimental procedures and modeling are a central practical issue in systems biology. Information exchange necessitates a common language about biological aspects. One seminal example is the gene ontology which provides a controlled vocabulary that can be applied to all organisms, even as the knowledge about genes and proteins continues to accumulate. The SBML [7] has been established as exchange language for mathematical models of biochemical reaction networks. A series of "minimum-information-about" statements based on community agreement defines standards for certain types of experiments. *M*inimum *i*nformation *r*equested *i*n the *a*nnotation of biochemical *m*odels (MIRIAM) [14] describes standards for this specific type of systems biology models.

References

1 Lander, E.S. *et al.* (2001b) Initial sequencing and analysis of the human genome. *Nature*, **409**, 860–921.

2 Venter, J.C. *et al.* (2001a) The sequence of the human genome. *Science*, **291**, 1304–1351.

3 von Mering, C. *et al.* (2002) Comparative assessment of large-scale data sets of protein–protein interactions. *Nature*, **417**, 399–403.

4 Brazma, A. *et al.* (2001) Minimum information about a microarray experiment (MIAME)-toward standards for microarray data. *Nature Genetics*, **29**, 365–371.

5 Taylor, C.F. *et al.* (2003) A systematic approach to modeling, capturing, and disseminating proteomics experimental data. *Nature Biotechnology*, **21**, 247–254.

6 Hermjakob, H. *et al.* (2004) The HUPO PSI's molecular interaction format – a community standard for the representation of protein interaction data. *Nature Biotechnology*, **22**, 177–183.

7 Hucka, M. *et al.* (2003) The systems biology markup language (SBML): a medium for representation and exchange of biochemical network models. *Bioinformatics*, **19**, 524–531.

8 Lloyd, C.M. *et al.* (2004) CellML: its future present and past. *Progress in Biophysics and Molecular Biology*, **85**, 433–450.

9 Gitton, Y. *et al.* (2002) A gene expression map of human chromosome 21 orthologues in the mouse. *Nature*, **420**, 586–590.

10 Ideker, T. *et al.* (2001) Integrated genomic and proteomic analyses of a systematically perturbed metabolic network. *Science*, **292**, 929–934.

11 Kanehisa, M. and Bork, P. (2003) Bioinformatics in the post-sequence era. *Nature Genetics*, **33** (Suppl), 305–310.

12 Tavazoie, S. *et al.* (1999) Systematic determination of genetic network architecture. *Nature Genetics*, **22**, 281–285.

13 Urbanczyk-Wochniak, E. *et al.* (2003) Parallel analysis of transcript and metabolic profiles: a new approach in systems biology. *EMBO Reports*, **4**, 989–993.

14 Le Novere, N. *et al.* (2005) Minimum information requested in the annotation of biochemical models (MIRIAM). *Nature Biotechnology*, **23**, 1509–1515.

2
Modeling of Biochemical Systems

2.1
Kinetic Modeling of Enzymatic Reactions

Summary
The rate of an enzymatic reaction, i.e., the velocity by which the execution of the reaction changes the concentrations of its substrates, is determined by concentrations of its substrates, concentration of the catalyzing enzyme, concentrations of possible modifiers, and by certain parameters. We introduce different kinetic laws for reversible and irreversible reactions, for reactions with varying numbers of substrates, and for reactions that are subject to inhibition or activation. The derivations of the rate laws are shown and the resulting restrictions for their validity and applicability. Saturation and sigmoidal kinetics are explained. The connection to thermodynamics is shown.

Deterministic kinetic modeling of individual biochemical reactions has a long history. The Michaelis–Menten model for the rate of an irreversible one-substrate reaction is an integral part of biochemistry, and the K_m value is a major characteristic of the interaction between enzyme and substrate. Biochemical reactions are catalyzed by enzymes, i.e., specific proteins which often function in complex with cofactors. They have a catalytic center, are usually highly specific, and remain unchanged by the reaction. One enzyme molecule can catalyze thousands of reactions per second (this so-called turnover number ranges from $10^2\,s^{-1}$ to $10^7\,s^{-1}$). Enzyme catalysis leads to a rate acceleration of about 10^6- up to 10^{12}-fold compared to the noncatalyzed, spontaneous reaction.

In this chapter, we make you familiar with the basic concepts of the mass action rate law. We will show how you can derive and apply more advanced kinetic expressions. The effect of enzyme inhibitors and activators will be discussed. The thermodynamic foundations and constraints are introduced.

The basic quantities are the concentration S of a substance S, i.e., the number n of molecules (or, alternatively, moles) of this substance per volume V, and the rate v of a reaction, i.e., the change of concentration S per time t. This type of modeling is

macroscopic and phenomenological, compared to the microscopic approach, where single molecules and their interactions are considered. Chemical and biochemical kinetics rely on the assumption that the reaction rate v at a certain point in time and space can be expressed as a unique function of the concentrations of all substances at this point in time and space. Classical enzyme kinetics assumes for sake of simplicity a spatial homogeneity (the "well-stirred" test tube) and no direct dependency of the rate on time

$$v(t) = v(S(t)). \tag{2.1}$$

In more advanced modeling approaches, longing toward whole-cell modeling, spatial inhomogeneities are taken into account, paying tribute to the fact that many components are membrane-bound or that cellular structures hinder the free movement of molecules. But, in the most cases, one can assume that diffusion is rapid enough to allow for an even distribution of all substances in space.

2.1.1
The Law of Mass Action

Biochemical kinetics is based on the mass action law, introduced by Guldberg and Waage in the nineteenth century [1–3]. It states that the reaction rate is proportional to the probability of a collision of the reactants. This probability is in turn proportional to the concentration of reactants to the power of the molecularity, that is the number in which they enter the specific reaction. For a simple reaction such as

$$S_1 + S_2 \rightleftharpoons 2P, \tag{2.2}$$

the reaction rate reads

$$v = v_+ - v_- = k_+ S_1 \cdot S_2 - k_- P^2. \tag{2.3}$$

where v is the net rate; v_+ and v_- are the rates of the forward and backward reactions; and k_+ and k_- are the *kinetic* or *rate constants*, i.e., the respective proportionality factors.

The molecularity is 1 for S_1 and for S_2 and 2 for P, respectively. If we measure the concentration in mol l^{-1} (or M) and the time in seconds (s), then the rate has the unit M s^{-1}. Accordingly, the rate constants for bimolecular reactions have the unit M^{-1}s^{-1}. Rate constants of monomolecular reactions have the dimension s^{-1}. The general mass action rate law for a reaction transforming m_i substrates with concentrations S_i into m_j products with concentrations P_j reads

$$v = v_+ - v_- = k_+ \prod_{i=1}^{m_i} S_i^{n_i} - k_- \prod_{j=1}^{m_j} P_j^{n_j}, \tag{2.4}$$

where n_i and n_j denote the respective molecularities of S_i and P_j in this reaction.

The equilibrium constant K_{eq} (we will also use the simpler symbol q) characterizes the ratio of substrate and product concentrations in equilibrium (S_{eq} and P_{eq}), i.e., the state with equal forward and backward rate. The rate constants are related to K_{eq} in the

following way:

$$K_{eq} = \frac{k_+}{k_-} = \frac{\prod\limits_{j=1}^{m_j} P_{j,eq}^{n_j}}{\prod\limits_{i=1}^{m_i} S_{i,eq}^{n_i}} \tag{2.5}$$

The relation between the thermodynamic and the kinetic description of biochemical reactions will be outlined in Section 2.1.2.

The equilibrium constant for the reaction given in Eq. (2.2) is $K_{eq} = P_{eq}^2/(S_{1,eq} \cdot S_{2,eq})$. The dynamics of the concentrations away from equilibrium is described by the ODEs.

$$\frac{d}{dt} S_1 = \frac{d}{dt} S_2 = -v \quad \text{and} \quad \frac{d}{dt} P = 2v. \tag{2.6}$$

The time course of S_1, S_2, and P is obtained by integration of these ODEs (see Section 2.3).

Example 2.1

The kinetics of a simple decay like

$$S \to \tag{2.7}$$

is described by $v = kS$ and $dS/dt = -kS$. Integration of this ODE from time $t = 0$ with the initial concentration S_0 to an arbitrary time t with concentration $S(t)$, $\int_{S_0}^{S} dS/S = -\int_{t=0}^{t} k\, dt$, yields the temporal expression $S(t) = S_0 e^{-kt}$.

2.1.2
Reaction Kinetics and Thermodynamics

An important purpose of metabolism is to extract energy from nutrients, which is necessary for the synthesis of molecules, growth, and proliferation. We distinguish between energy-supplying reactions, energy-demanding reactions, and energetically neutral reactions. The principles of reversible thermodynamics and their application to chemical reactions allow understanding of energy circulation in the cell.

A biochemical process is characterized by the direction of the reaction, by whether it occurs spontaneously or not, and by the position of the equilibrium. The first law of thermodynamics, i.e., the law of energy conservation, tells us that the total energy of a closed system remains constant during any process. The second law of thermodynamics states that a process occurs spontaneous only if it increases the total entropy of the system. Unfortunately, entropy is usually not directly measurable. A more suitable measure is the Gibbs free energy G, which is the energy capable of carrying out work under isotherm–isobar conditions, i.e., at constant temperature and constant pressure. The change of the free energy is given as

$$\Delta G = \Delta H - T\Delta S, \tag{2.8}$$

where ΔH is the change in enthalpy, ΔS the change in entropy, and T the absolute temperature in Kelvin. ΔG is a measure for the driving force, the spontaneity of a chemical reaction. The reaction proceeds spontaneous under release of energy, if $\Delta G < 0$ (exergonic process). If $\Delta G > 0$, then the reaction is energetically not favorable and will not occur spontaneously (endergonic process). $\Delta G = 0$ means that the system has reached its equilibrium. Endergonic reactions may proceed if they obtain energy from a strictly exergonic reaction by energetic coupling. In tables, free energy is usually given for standard conditions ($\Delta G°$), i.e., for a concentration of the reaction partners of 1 M, a temperature of $T = 298$ K, and, for gaseous reactions, a pressure of $p = 98$, 1 kPa $= 1$ atm. The unit is kJ mol^{-1}. Free energy differences satisfy a set of relations as follows. The free energy difference for a reaction can be calculated from the balance of free energies of formation of its products and substrates:

$$\Delta G = \sum G_P - \sum G_S. \tag{2.9}$$

The enzyme cannot change the free energies of the substrates and products of a reaction, neither their difference, but it changes the way the reaction proceeds microscopically, the so-called reaction path, thereby lowering the activation energy for the reaction. The *Transition State Theory* explains this as follows. During the course of a reaction, the metabolites must pass one or more transition states of maximal free energy, in which bonds are solved or newly formed. The transition state is unstable; the respective molecule configuration is called an activated complex. It has a lifetime of around one molecule vibration, 10^{-14}–10^{-13} s, and it can hardly be experimentally verified. The difference $\Delta G^{\#}$ of free energy between the reactants and the activated complex determines the dynamics of a reaction: the higher this difference, the lower the probability that the molecules may pass this barrier and the lower the rate of the reaction. The value of $\Delta G^{\#}$ depends on the type of altered bonds, on steric, electronic, or hydrophobic demands, and on temperature.

Figure 2.1 presents a simplified view of the reaction course. The substrate and the product are situated in local minima of the free energy; the active complex is assigned to the local maximum. The free energy difference ΔG is proportional to the logarithm of the equilibrium constant K_{eq} of the respective reaction:

$$\Delta G = -RT \ln K_{eq}, \tag{2.10}$$

where R is the gas constant, 8.314 J mol^{-1} K^{-1}. The value of $\Delta G^{\#}$ corresponds to the kinetic constant k_+ of the forward reaction (Eqs. (2.3)–(2.5)) by $\Delta G^{\#} = -RT \ln k_+$, while $\Delta G^{\#} + \Delta G$ is related to the rate constant k_- of the backward reaction.

The interaction of the reactants with an enzyme may alter the reaction path and, thereby, lead to lower values of $\Delta G^{\#}$ as well as higher values of the kinetic constants. Furthermore, the free energy may assume more local minima and maxima along the path of reaction. They are related to unstable intermediary complexes. Values for the difference of free energy for some biologically important reactions are given in Table 2.1.
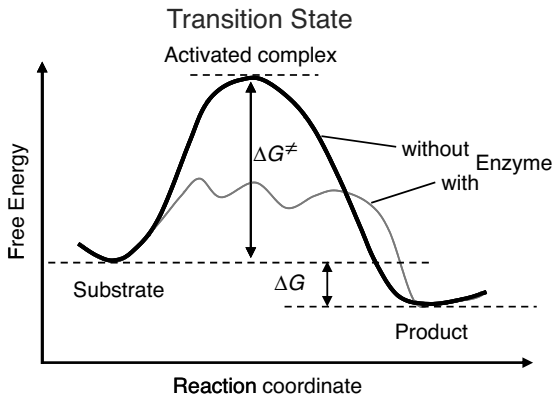
Figure 2.1 Change of free energy along the course of a reaction. The substrate and the product are situated in local minima of the free energy; the active complex is assigned to the local maximum. The enzyme may change the reaction path and thereby lower the barrier of free energy.

A biochemical reaction is reversible if it may proceed in both directions, leading to a positive or negative sign of the rate v. The actual direction depends on the current reactant concentrations. In theory, every reaction should be reversible. In practice, we can consider many reactions as irreversible since (i) reactants in cellular environment cannot assume any concentration, (ii) coupling of a chemical conversion to ATP consumption leads to a severe drop in free energy and therefore makes a reaction reversal energetically unfavorable, and (iii) for compound destruction, such as protein degradation, reversal by chance is extremely unlikely.

The detailed consideration of enzyme mechanisms by applying the mass action law for the single events has led to a number of standard kinetic descriptions, which will be explained in the following.

Table 2.1 Values of $\Delta G^{0'}$ and K_{eq} for some important reactions[a].

Reactions	$\Delta G^{0'}$ (kJ mol^{-1})
$2H_2 + O_2 \rightarrow 2H_2O$	-474
$2H_2O_2 \rightarrow 2H_2O + O_2$	-99
$PP_i + H_2O \rightarrow 2P_i$	-33.49
$ATP + H_2O \rightarrow ADP + P_i$	-30.56
Glucose-6-phosphate $+ H_2O \rightarrow$ Glucose $+ P_i$	-13.82
Glucose $+ P_i \rightarrow$ Glucose-6-phosphate $+ H_2O$	$+13.82$
Glucose-1-phosphate $\rightarrow$ Glucose-6-phosphate	-7.12
Glucose-6-phosphate $\rightarrow$ Fructose-6-phosphate	$+1.67$
Glucose $+ 6O_2 \rightarrow 6CO_2 + 6H_2O$	-2890

[a]*Source:* ZITAT: Lehninger, A.L. Biochemistry, 2nd edition, New York, Worth, 1975, p. 397.

2.1.3
Michaelis–Menten Kinetics

Brown [4] proposed an enzymatic mechanism for invertase, catalyzing the cleavage of saccharose to glucose and fructose. This mechanism holds in general for all one-substrate reactions without backward reaction and effectors, such as

$$\mathrm{E} + \mathrm{S} \underset{k_{-1}}{\overset{k_1}{\rightleftharpoons}} \mathrm{ES} \overset{k_2}{\longrightarrow} \mathrm{E} + \mathrm{P}. \tag{2.11}$$

It comprises a reversible formation of an enzyme–substrate complex ES from the free enzyme E and the substrate S and an irreversible release of the product P. The ODE system for the dynamics of this reaction reads

$$\frac{\mathrm{d}S}{\mathrm{d}t} = -k_1 E \cdot S + k_{-1} ES, \tag{2.12}$$

$$\frac{\mathrm{d}ES}{\mathrm{d}t} = k_1 E \cdot S - (k_{-1} + k_2) ES, \tag{2.13}$$

$$\frac{\mathrm{d}E}{\mathrm{d}t} = -k_1 E \cdot S + (k_{-1} + k_2) ES, \tag{2.14}$$

$$\frac{\mathrm{d}P}{\mathrm{d}t} = k_2 ES. \tag{2.15}$$

The reaction rate is equal to the negative decay rate of the substrate as well as to the rate of product formation:

$$v = -\frac{\mathrm{d}S}{\mathrm{d}t} = \frac{\mathrm{d}P}{\mathrm{d}t}. \tag{2.16}$$

This ODE system (Eqs. (2.12)–(2.16)) cannot be solved analytically. Different assumptions have been used to simplify this system in a satisfactory way. Michaelis and Menten [5] considered a *quasi-equilibrium* between the free enzyme and the enzyme–substrate complex, meaning that the reversible conversion of E and S to ES is much faster than the decomposition of ES into E and P, or in terms of the kinetic constants,

$$k_1, k_{-1} \gg k_2. \tag{2.17}$$

Briggs and Haldane [6] assumed that during the course of reaction a state is reached where the concentration of the ES complex remains constant, the so-called quasi-steady state. This assumption is justified only if the initial substrate concentration is much larger than the enzyme concentration, $S(t = 0) \gg E$, otherwise such a state will never be reached. In mathematical terms, we obtain

$$\frac{\mathrm{d}ES}{\mathrm{d}t} = 0. \tag{2.18}$$

In the following, we derive an expression for the reaction rate from the ODE system (2.12)–(2.15) and the quasi-steady-state assumption for ES. First, adding Eqs. (2.13) and (2.14) results in

$$\frac{dES}{dt} + \frac{dE}{dt} = 0 \quad \text{or} \quad E_{total} = E + ES = \text{constant}. \tag{2.19}$$

This expression shows that enzyme is neither produced nor consumed in this reaction; it may be free or part of the complex, but its total concentration remains constant. Introducing (2.19) into (2.13) under the steady-state assumption (2.18) yields

$$ES = \frac{k_1 E_{total} S}{k_1 S + k_{-1} + k_2} = \frac{E_{total} S}{S + (k_{-1} + k_2)/k_1}. \tag{2.20}$$

For the reaction rate, this gives

$$v = \frac{k_2 E_{total} S}{S + ((k_{-1} + k_2)/k_1)}. \tag{2.21}$$

In enzyme kinetics, it is convention to present Eq. (2.21) in a simpler form, which is important in theory and practice

$$v = \frac{V_{max} S}{S + K_m}. \tag{2.22}$$

Equation (2.22) is the expression for Michaelis–Menten kinetics. The parameters have the following meaning: the *maximal velocity*,

$$V_{max} = k_2 E_{total}, \tag{2.23}$$

is the maximal rate that can be attained, when the enzyme is completely saturated with substrate. The *Michaelis constant*,

$$K_m = \frac{k_{-1} + k_2}{k_1}, \tag{2.24}$$

is equal to the substrate concentration that yields the half-maximal reaction rate. For the quasi-equilibrium assumption (Eq. (2.17)), it holds that $K_m \cong k_{-1}/k_1$. The maximum velocity divided by the enzyme concentration (here $k_2 = v_{max}/E_{total}$) is often called the turnover number, k_{cat}. The meaning of the parameters is illustrated in the plot of rate versus substrate concentration (Figure 2.2).

2.1.3.1 How to Derive a Rate Equation

Below, we will present some enzyme kinetic standard examples to derive a rate equation. Individual mechanisms for your specific enzyme of interest may be more complicated or merely differ from these standards. Therefore, we summarize here the general way of deriving a rate equation.

1. Draw a wiring diagram of all steps to consider (e.g., Eq. (2.11)). It contains all substrates and products (S and P) and n free or bound enzyme species (E and ES).
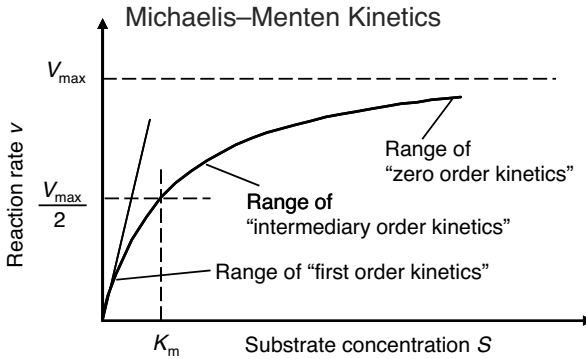
Figure 2.2 Dependence of reaction rate v on substrate concentration S in Michaelis–Menten kinetics. V_{max} denotes the maximal reaction rate that can be reached for large substrate concentration. K_m is the substrate concentration that leads to half-maximal reaction rate. For low substrate concentration, v increases almost linearly with S, while for high substrate concentrations v is almost independent of S.

2. The right sites of the ODEs for the concentrations changes sum up the rates of all steps leading to or away from a certain substance (e.g., Eqs. (2.12)–(2.15)). The rates follow mass action kinetics (Eq. (2.3)).
3. The sum of all enzyme-containing species is equal to the total enzyme concentration E_{total} (the right site of all differential equations for enzyme species sums up to zero). This constitutes one equation.
4. The assumption of quasi-steady state for $n - 1$ enzyme species (i.e., setting the right sites of the respective ODEs equal to zero) together with (3.) result in n algebraic equations for the concentrations of the n enzyme species.
5. The reaction rate is equal to the rate of product formation (e.g., Eq. (2.16)). Insert the respective concentrations of enzyme species resulting from (4.).

2.1.3.2 Parameter Estimation and Linearization of the Michaelis–Menten Equation

To assess the values of the parameters V_{max} and K_m for an isolated enzyme, one measures the initial rate for different initial concentrations of the substrate. Since the rate is a nonlinear function of the substrate concentration, one has to determine the parameters by nonlinear regression. Another way is to transform Eq. (2.22) to a linear relation between variables and then apply linear regression.

The advantage of the transformed equations is that one may read the parameter value more or less directly from the graph obtained by linear regression of the measurement data. In the plot by Lineweaver and Burk [7] (Table 2.2), the values for V_{max} and K_m can be obtained from the intersections of the graph with the ordinate and the abscissa, respectively. The Lineweaver–Burk plot is also helpful to easily discriminate different types of inhibition (see below). The drawback of the transformed equations is that they may be sensitive to errors for small or high substrate

Table 2.2 Different approaches for the linearization of Michaelis–Menten enzyme kinetics.

	Lineweaver–Burk	Eadie–Hofstee	Hanes–Woolf
Transformed equation	$\dfrac{1}{v} = \dfrac{K_m}{V_{max}}\dfrac{1}{S} + \dfrac{1}{V_{max}}$	$v = V_{max} - K_m\dfrac{v}{S}$	$\dfrac{S}{v} = \dfrac{S}{V_{max}} + \dfrac{K_m}{V_{max}}$
New variables	$\dfrac{1}{v}, \dfrac{1}{S}$	$v, \dfrac{v}{S}$	$\dfrac{S}{v}, S$
Graphical representation	Plot of $1/v$ vs $1/S$; Slope $= K_m/V_{max}$; intercepts $-1/K_m$ and $1/V_{max}$	Plot of v vs v/S; Slope $= -K_m$; V_{max}; V_{max}/K_m	Plot of S/v vs $1/S$; Slope $= 1/V_{max}$; K_m/V_{max}

concentrations or rates. Eadie and Hofstee [8] and Hanes and Woolf [9] have introduced other types of linearization to overcome this limitation.

2.1.3.3 The Michaelis–Menten Equation for Reversible Reactions

In practice, many reactions are reversible. The enzyme may catalyze the reaction in both directions. Consider the following mechanism:

$$E + S \underset{k_{-1}}{\overset{k_1}{\rightleftarrows}} ES \underset{k_{-2}}{\overset{k_2}{\rightleftarrows}} E + P \tag{2.25}$$

The product formation is given by

$$\frac{dP}{dt} = k_2 ES - k_{-2} E \cdot P = v. \tag{2.26}$$

The respective rate equation reads

$$
\begin{aligned}
v &= E_{\text{total}} \frac{Sq - P}{Sk_1/(k_{-1}k_{-2}) + 1/k_{-2} + k_2/(k_{-1}k_{-2}) + P/k_{-1}} \\
&= \frac{(V_{\text{max}}^{\text{for}}/K_{mS})S - (V_{\text{max}}^{\text{back}}/K_{mP})P}{1 + S/K_{mS} + P/K_{mP}}.
\end{aligned}
\tag{2.27}
$$

While the parameters $k_{\pm1}$ and $k_{\pm2}$ are the kinetic constants of the individual reaction steps, the phenomenological parameters $V_{\text{max}}^{\text{for}}$ and $V_{\text{max}}^{\text{back}}$ denote the maximal velocity in forward or backward direction, respectively, under zero product or substrate concentration, and the phenomenological parameters K_{mS} and K_{mP} denote the substrate or product concentration causing half maximal forward or backward rate. They are related in the following way [10]:

$$K_{\text{eq}} = \frac{V_{\text{max}}^{\text{for}} K_{mP}}{V_{\text{max}}^{\text{back}} K_{mS}}. \tag{2.28}$$

2.1.4
Regulation of Enzyme Activity by Effectors

Enzymes may immensely increase the rate of a reaction, but this is not their only function. Enzymes are involved in metabolic regulation in various ways. Their production and degradation is often adapted to the current requirements of the cell. Furthermore, they may be targets of effectors, both inhibitors and activators.

The effectors are small molecules, or proteins, or other compounds that influence the performance of the enzymatic reaction. The interaction of effector and enzyme changes the reaction rate. Such regulatory interactions that are crucial for the fine-tuning of metabolism will be considered here [11].

Basic types of inhibition are distinguished by the state, in which the enzyme may bind the effector (i.e., the free enzyme E, the enzyme–substrate complex ES, or both), and by the ability of different complexes to release the product. The general pattern of inhibition is schematically represented in Figure 2.3. The different types result, if some of the interactions may not occur.
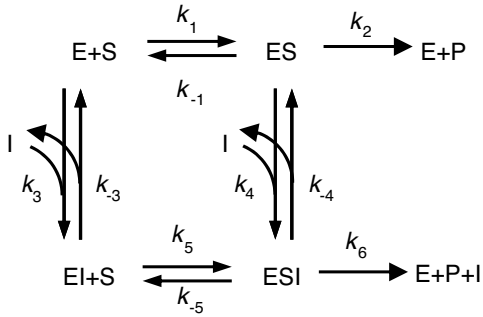
Figure 2.3 General scheme of inhibition in Michaelis–Menten kinetics. Reactions 1 and 2 belong to the standard scheme of Michaelis–Menten kinetics. Competitive inhibition is given, if in addition reaction 3 (and not reactions 4, 5, or 6) occurs. Uncompetitive inhibition involves reactions 1, 2, and 4, and noncompetitive inhibition comprises reactions 1, 2, 3, 4, and 5. Occurrence of reaction 6 indicates partial inhibition.

The rate equations are derived according to the following scheme:

1. Consider binding equilibriums between compounds and their complexes:

$$K_{\mathrm{m}} \cong \frac{k_{-1}}{k_1} = \frac{E \cdot S}{ES}, \ K_{\mathrm{I},3} = \frac{k_{-3}}{k_3} = \frac{E \cdot I}{EI}, \ K_{\mathrm{I},4} = \frac{k_{-4}}{k_4} = \frac{ES \cdot I}{ESI}, \ K_{\mathrm{I},5} = \frac{k_{-5}}{k_5} = \frac{EI \cdot S}{ESI}. \tag{2.29}$$

Note that, if all reactions may occur, the Wegscheider condition [12] holds in the form

$$\frac{k_1 k_4}{k_{-1} k_{-4}} = \frac{k_3 k_5}{k_{-3} k_{-5}}, \tag{2.30}$$

which means that the difference in the free energies between two compounds (e.g., E and ESI) is independent of the choice of the reaction path (here via ES or via EI).

2. Take into account the moiety conservation for the total enzyme (include only those complexes, which occur in the course of reaction):

$$E_{\mathrm{total}} = E + ES + EI + ESI. \tag{2.31}$$

3. The reaction rate is equal to the rate of product formation

$$v = \frac{\mathrm{d}P}{\mathrm{d}t} = k_2\, ES + k_6\, ESI. \tag{2.32}$$

Equations (2.29)–(2.31) constitute four independent equations for the four unknown concentrations of E, ES, EI, and ESI. Their solution can be inserted into Eq. (2.32). The effect of the inhibitor depends on the concentrations of substrate and inhibitor and on the relative affinities to the enzyme. Table 2.3 lists the different types of inhibition for irreversible and reversible Michaelis–Menten kinetics together with the respective rate equations.

Table 2.3 Types of inhibition for irreversible and reversible Michaelis–Menten kinetics[a].

Name	Implementation	Equation – irreversible case	Equation – reversible case	Characteristics
Competitive inhibition	I binds only to free E; P-release only from ES complex $k_{\pm4} = k_{\pm5} = k_6 = 0$	$v = \dfrac{V_{max} S}{K_m \cdot i_3 + S}$	$v = \dfrac{V^f_{max}(S/K_{mS}) - V^r_{max}(P/K_{mP})}{(S/K_{mS}) + (P/K_{mP}) + i_3}$	K_m changes, V_{max} remains same. S and I compete for the binding place; high S may out compete I.
Uncompetitive inhibition	I binds only to the ES complex; P-release only from ES complex $k_{\pm3} = k_{\pm5} = k_6 = 0$	$v = \dfrac{V_{max} S}{K_m + S \cdot i_4}$	$v = \dfrac{V^f_{max}(S/K_{mS}) - V^r_{max}(P/K_{mP})}{1 + ((S/K_{mS}) + (P/K_{mP})) i_4}$	K_m and V_{max} change, but their ratio remains same. S may not out compete I
Noncompetitive inhibition	I binds to E and ES; P-release only from ES $K_{I,3} = K_{I,4},\ k_6 = 0$	$v = \dfrac{V_{max} S}{(K_m + S) i_3}$	$v = \dfrac{V^f_{max}(S/K_{mS}) - V^r_{max}(P/K_{mP})}{(1 + (S/K_{mS}) + (P/K_{mP})) i_4}$	K_m remains, V_{max} changes. S may not out compete I
Mixed inhibition	I binds to E and ES; P-release only from ES $K_{I,3} \neq K_{I,4},\ k_6 = 0$	$v = \dfrac{V_{max} S}{K_m \cdot i_4 + S \cdot i_3}$		K_m and V_{max} change. $K_{I,3} > K_{I,4}$: competitive–noncompetitive inhibition $K_{I,3} < K_{I,4}$: noncompetitive–uncompetitive inhibition
Partial Inhibition	I may bind to E and ES; P-release from ES and ESI $K_{I,3} \neq K_{I,4},\ K_6 \neq 0$	$v = \dfrac{V_{max} S[1 + \{(k_6 I)/(k_2 K_{I,3})\}]}{K_m i_4 + S i_3}$		K_m and V_{max} change. if $k_6 > k_2$: activation instead of inhibition.

[a]These abbreviations are used: $K_{I,3} = \frac{k_{-3}}{k_3}$, $K_{I,4} = \frac{k_{-4}}{k_4}$, $i_3 = 1 + \frac{I}{K_{I,3}}$, $i_4 = 1 + \frac{I}{K_{I,4}}$.

In the case of *competitive* inhibition, the inhibitor competes with the substrate for the binding site (or inhibits substrate binding by binding elsewhere to the enzyme) without being transformed itself. An example for this type is the inhibition of succinate dehydrogenase by malonate. The enzyme converts succinate to fumarate forming a double bond. Malonate has two carboxyl groups, like the proper substrates, and may bind to the enzyme, but the formation of a double bond cannot take place. Since substrates and inhibitor compete for the binding sites, a high concentration of one of them may displace the other one. For very high substrate concentrations, the same maximal velocity as without inhibitor is reached, but the effective K_m value is increased.

In the case of *uncompetitive* inhibition, the inhibitor binds only to the ES complex. The reason may be that the substrate binding caused a conformational change, which opened a new binding site. Since S and I do not compete for binding sites, an increase in the concentration of S cannot displace the inhibitor. In the presence of inhibitor, the original maximal rate cannot be reached (lower V_{max}). For example, an inhibitor concentration of $I = K_{I,4}$ halves the K_m-value as well as V_{max}. Uncompetitive inhibition occurs rarely for one-substrate reactions, but more frequently in the case of two substrates. One example is inhibition of arylsulphatase by hydracine.

Noncompetitive inhibition is present, if substrate binding to the enzyme does not alter the binding of the inhibitor. There must be different binding sites for substrate and inhibitor. In the classical case, the inhibitor has the same affinity to the enzyme with or without bound substrate. If the affinity changes, this is called mixed inhibition. A standard example is inhibition of chymotrypsion by H^+-ions.

If the product may also be formed from the enzyme–substrate–inhibitor complex, the inhibition is only partial. For high rates of product release (high values of k_6), this can even result in an activating instead of an inhibiting effect.

The general types of inhibition, competitive, uncompetitive, and noncompetitive inhibition also apply for the reversible Michaelis–Menten mechanism. The respective rate equations are also listed in Table 2.3.

2.1.4.1 Substrate Inhibition

A common characteristic of enzymatic reaction is the increase of the reaction rate with increasing substrate concentration S up to the maximal velocity V_{max}. But in some cases, a decrease of the rate above a certain value of S is recorded. A possible reason is the binding of a further substrate molecule to the enzyme–substrate complex yielding the complex ESS that cannot form a product. This kind of inhibition is reversible if the second substrate can be released. The rate equation can be derived using the scheme of uncompetitive inhibition by replacing the inhibitor by another substrate. It reads

$$v = k_2 ES = \frac{V_{max} S}{K_m + S(1 + (S/K_I))}. \tag{2.33}$$

This expression has an optimum, i.e., a maximal value of v, at

$$S_{opt} = \sqrt{K_m K_I} \quad \text{with} \quad v_{opt} = \frac{V_{max}}{1 + 2\sqrt{K_m/K_I}}. \tag{2.34}$$
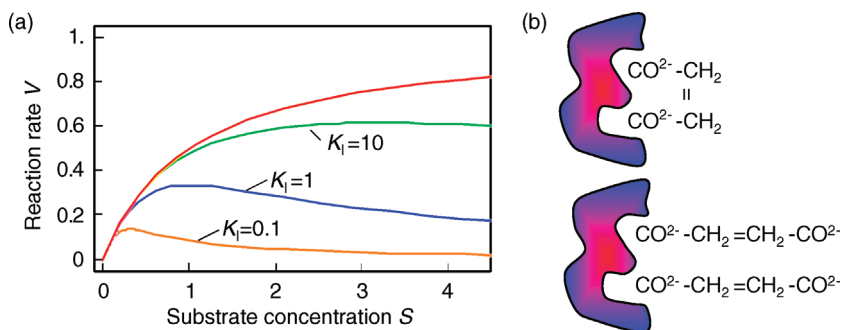
Figure 2.4 Plot of reaction rate v against substrate concentration S for an enzyme with substrate inhibition. The upper curve shows Michaelis–Menten kinetics without inhibition, the lower curves show kinetics for the indicated values of binding constant K_I. Parameter values: $V_{max} = 1$, $K_m = 1$. The left part visualizes a possible mechanism for substrate inhibition: The enzyme (gray item) has two binding pockets to bind different parts of a substrate molecule (upper scheme). In case of high substrate concentration, two different molecules may enter the binding pockets, thereby preventing the specific reaction (lower scheme).

The dependence of v on S is shown in Figure 2.4. A typical example for substrate inhibition is the binding of two succinate molecules to malonate dehydrogenase, which possesses two binding pockets for the carboxyl group. This is schematically represented in Figure 2.4.

2.1.4.2 Binding of Ligands to Proteins

Every molecule that binds to a protein is a ligand, irrespective of whether it is subject of a reaction or not. Below we consider binding to monomer and oligomer proteins. In oligomers, there may be interactions between the binding sites on the subunits.

Consider binding of one ligand (S) to a protein (E) with only one binding site:

$$E + S \rightleftharpoons ES \tag{2.35}$$
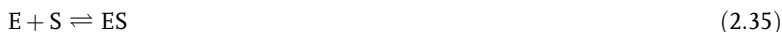
The binding constant K_B is given by

$$K_B = \left(\frac{ES}{E \cdot S} \right)_{eq}. \tag{2.36}$$

The reciprocal of K_B is the dissociation constant K_D. The fractional saturation Y of the protein is determined by the number of subunits that have bound ligands, divided by the total number of subunits. The fractional saturation for one subunit is

$$Y = \frac{ES}{E_{total}} = \frac{ES}{ES + E} = \frac{K_B \cdot S}{K_B \cdot S + 1}. \tag{2.37}$$

The plot of Y versus S at constant total enzyme concentration is a hyperbola, like the plot of v versus S in the Michaelis–Menten kinetics (Eq. (2.22)). At a process where the binding of S to E is the first step followed by product release and where the initial concentration of S is much higher than the initial concentration of E, the rate is proportional to the concentration of ES and it holds

$$\frac{v}{V_{\text{max}}} = \frac{ES}{E_{\text{total}}} = Y. \tag{2.38}$$

If the protein has several binding sites, then interactions may occur between these sites, i.e., the affinity to further ligands may change after binding of one or more ligands. This phenomenon is called *cooperativity*. Positive or negative cooperativity denote increase or decrease in the affinity of the protein to a further ligand, respectively. Homotropic or heterotropic cooperativity denotes that the binding to a certain ligand influences the affinity of the protein to a further ligand of the same or another type, respectively.

2.1.4.3 Positive Homotropic Cooperativity and the Hill Equation

Consider a dimeric protein with two identical binding sites. The binding to the first ligand facilitates the binding to the second ligand.

$$
\begin{aligned}
E_2 + S &\xrightarrow{\text{slow}} E_2 S \\
E_2 S + S &\xrightarrow{\text{fast}} E_2 S_2
\end{aligned}
\tag{2.39}
$$

where E is the monomer and E_2 is the dimer. The fractional saturation is given by

$$Y = \frac{E_2 S + 2 \cdot E_2 S_2}{2 \cdot E_{2,\text{total}}} = \frac{E_2 S + 2 \cdot E_2 S_2}{2 \cdot E_2 + 2 \cdot E_2 S + 2 \cdot E_2 S_2}. \tag{2.40}$$

If the affinity to the second ligand is strongly increase by binding to the first ligand, then $E_2 S$ will react with S as soon as it is formed and the concentration of $E_2 S$ can be neglected. In the case of complete *cooperativity*, i.e., every protein is either empty or fully bound, Eq. (2.39) reduces to

$$E_2 + 2S \rightarrow E_2 S_2 \tag{2.41}$$

The binding constant reads

$$K_B = \frac{E_2 S_2}{E_2 \cdot S^2}, \tag{2.42}$$

and the fractional saturation is

$$Y = \frac{2 \cdot E_2 S_2}{2 \cdot E_{2,\text{total}}} = \frac{E_2 S_2}{E_2 + E_2 S_2} = \frac{K_B \cdot S^2}{1 + K_B \cdot S^2}. \tag{2.43}$$

Generally, for a protein with n subunits, it holds:

$$v = V_{\text{max}} \cdot Y = \frac{V_{\text{max}} \cdot K_B \cdot S^n}{1 + K_B \cdot S^n}. \tag{2.44}$$

This is the general form of the *Hill equation*. To derive it, we assumed complete homotropic cooperativity. The plot of the fractional saturation Y versus substrate concentration S is a sigmoid curve with the inflection point at $1/K_B$. The quantity n (often "h" is used instead) is termed the *Hill coefficient*.

The derivation of this expression was based on experimental findings concerning the binding of oxygen to hemoglobin (Hb) [13, 14]. In 1904, Bohr *et al.* found that the

plot of the fractional saturation of Hb with oxygen against the oxygen partial pressure had a sigmoid shape. Hill (1913) explained this with interactions between the binding sites located at the Hb subunits [14]. At this time, it was already known that every subunit Hb binds one molecule of oxygen. Hill assumed complete cooperativity and predicted an experimental Hill coefficient of 2.8. Today it is known that Hb has four binding sites, but that the cooperativity is not complete. The sigmoid binding characteristic has the advantage that Hb binds strongly to oxygen in the lung with a high oxygen partial pressure while it can release O_2 easily in the body with low oxygen partial pressure.

2.1.4.4 The Monod–Wyman–Changeux Model for Sigmoid Kinetics

The Monod model [15] explains sigmoid enzyme kinetics by taking into account the interaction of subunits of an enzyme. We will show here the main characteristics and assumptions of this kinetics. The full derivation is given in the web material. It uses the following assumptions: (i) the enzyme consists of n identical subunits, (ii) each subunit can assume an active (R) or an inactive (T) conformation, (iii) all subunits change their conformations at the same time (concerted change), and (iv) the equilibrium between the R and the T conformation is given by an allosteric constant

$$L = \frac{T_0}{R_0}. \tag{2.45}$$

The binding constants for the active and inactive conformations are given by K_R and K_T, respectively. If substrate molecules can only bind to the active form, i.e., if $K_T = 0$, the rate can be expressed as

$$V = \frac{V_{max} K_R S}{(1 + K_R S)} \frac{1}{[1 + \{L/((1 + K_R S)^n)\}]}, \tag{2.46}$$

where the first factor $(V_{max} K_R S)/(1 + K_R S)$ corresponds to the Michaelis–Menten rate expression, while the second factor $[1 + (L/(1 + K_R S)^n)]^{-1}$ is a regulatory factor (Figure 2.5).

For $L = 0$, the plot v versus S is hyperbola as in Michaelis–Menten kinetics. For $L > 0$, we obtain a sigmoid curve shifted to the right. A typical value for the allosteric constant is $L \cong 10^4$.

Up to now we considered in the model of Monod, Wyman, and Changeux only homotropic and positive effects. But this model is also well suited to explain the dependence of the reaction rate on activators and inhibitors. Activators A bind only to the active conformation and inhibitors I bind only to the inactive conformation. This shifts the equilibrium to the respective conformation. Effectively, the binding to effectors changes L:

$$L' = L \frac{(1 + K_I I)^n}{(1 + K_A A)^n}, \tag{2.47}$$

where K_I and K_A denote binding constants. The interaction with effectors is a heterotropic effect. An activator weakens the sigmoidity, while an inhibitor strengthens it.
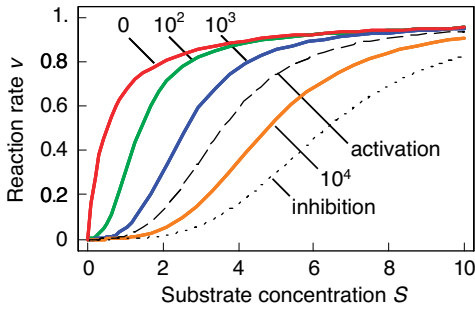
Figure 2.5 Model of Monod, Wyman, and Changeux: Dependence of the reaction rate on substrate concentration for different values of the allosteric constant L, according to equation. The binding constants for the active and inactive conformations are given by K_R and K_T, respectively. If substrate molecules can only bind to the active form, i.e., if $K_T = 0$, the rate can be expressed as

$$V = \frac{V_{max} K_R S}{(1 + K_R S)} \frac{1}{[1 + \{L/((1 + K_R S)^n)\}]}, \quad (2.46).$$

Parameters: $V_{max} = 1$, $n = 4$, $K_R = 2$, $K_T = 0$. The value of L is indicated at the curves. Obviously, increasing value of L causes stronger sigmoidity. The influence of activators or inhibitors (compare Eq. (2.47)) is illustrated with the dotted line for $K_I I = 2$ and with the dashed line for $K_A A = 2$ ($L = 10^4$ in both cases).

A typical example for an enzyme with sigmoid kinetics that can be described with the Monod model is the enzyme phosphofructokinase, which catalyzes the transformation of fructose-6-phosphate and ATP to fructose-1,6-bisphosphate. AMP, NH_4, and K^+ are activators, ATP is an inhibitor.

2.1.5
Generalized Mass Action Kinetics

Mass action kinetics (see Section 2.1.1) has experienced refinements in different ways. The fact that experimental results frequently do not show the linear dependence of rate on concentrations as assumed in mass action laws is acknowledged in power law kinetics used in the S-systems approach [16]. Here, the rate reads

$$\frac{v_j}{v_j^0} = k_j \prod_{i=1}^{n} \left(\frac{S_i}{S_i^0} \right)^{g_{j,i}}, \quad (2.48)$$

where the concentrations S_i and rates v_j are normalized to some standard value denoted by superscript 0, and $g_{i,j}$ is a real number instead of an integer as in Eq. (2.4). The normalization yields dimensionless quantities. The power law kinetics can be considered as a generalization of the mass action rate law. The exponent $g_{i,j}$ is equal to the concentration elasticities, i.e., the scaled derivatives of rates with respect to substrate concentrations (see Section 2.3, Eq. (2.107)). Substrates and effectors (their concentrations both denoted by S_i) enter expression (2.48) in the same formal way, but the respective exponents $g_{i,j}$ will be different. The exponents $g_{i,j}$ will be positive for substrates and activators, but should assume a negative value for inhibitors.

2.1.6
Approximate Kinetic Formats

In metabolic modeling studies, approximate kinetic formats are used (for a recent review, see [17]). They preassume that each reaction rate v_j is proportional to the enzyme concentration E_j. The rates, enzyme concentrations, and substrate concentrations are normalized with respect to a reference state, which is usually a steady state. This leads to the general expression

$$\frac{v_j}{v_j^0} = \frac{E_j}{E_j^0} \cdot f\left(\frac{S}{S^0}, \varepsilon_c^0\right), \tag{2.49}$$

where ε_c is the matrix of concentration elasticities as explained in Section 2.3. One example is the so-called lin-log kinetics

$$\frac{v}{v^0} = \frac{E}{E^0}\left(I + \varepsilon_c^0 \ln \frac{S}{S^0}\right), \tag{2.50}$$

where I is the $r \times r$ identity matrix. Another example is an approximation of the power-law kinetics

$$\ln \frac{v}{v^0} = \ln \frac{E}{E^0} + \varepsilon_c^0 \ln \frac{S}{S^0}. \tag{2.51}$$

Approximative kinetics simplify the determination of model parameters and, especially, of concentration elasticities, since Eq. (2.51) is a set of linear equations in the elasticity coefficients.

2.1.7
Convenience Kinetics

The convenience kinetics [18] has been introduced to ease parameter estimation and to have a kinetic mechanism, where all parameters are independent of each other and not related via the Haldane relation (Eq. (2.28)). It is a generalized form of Michaelis–Menten kinetics that covers all possible stoichiometries, and describes enzyme regulation by activators and inhibitors. For a reaction with stoichiometry

$$n_{-1}S_1 + n_{-2}S_2 + \cdots \leftrightarrow n_{+1}P_1 + n_{+2}P_2 + \cdots, \tag{2.52}$$
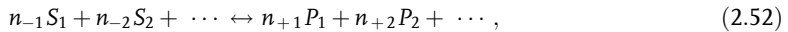
it reads

$$v = E_{\text{total}} \cdot f_{\text{reg}}$$
$$\cdot \frac{k_{\text{cat}}^{\text{for}} \prod_i (S_i/K_{\text{m},S_i})^{n_{-i}} - k_{\text{cat}}^{\text{back}} \prod_j (P_j/K_{\text{m},P_j})^{n_{+j}}}{\prod_i (1 + (S_i/K_{\text{m},S_i}) + \cdots + (S_i/K_{\text{m},S_i})^{n_{-i}}) + \prod_j (1 + (P_j/K_{\text{m},P_j}) + \cdots + (P_j/K_{\text{m},P_j})^{n_{+j}}) - 1}, \tag{2.53}$$

with enzyme concentration E_{total} and turnover rates $k_{\text{cat}}^{\text{for}}$ and $k_{\text{cat}}^{\text{back}}$. The regulatory prefactor f_{reg} is either 1 (in case of no regulation) or a product of terms $M/(K_A + M)$ or $1 + M/K_A$ for activators and $K_I/(K_I + M)$ for inhibitors. Activation constants K_A and

inhibition constants K_I are measured in concentration units. M is the concentration of the modifier.

In analogy to Michaelis–Menten kinetics, K_m values denote substrate concentrations, at which the reaction rate is half-maximal if the reaction products are absent; K_I and K_A values denote concentrations, at which the inhibitor or activator has its half-maximal effect. In this respect, many parameters in convenience kinetics are comparable to the kinetic constants measured in enzyme assays. This is important for parameter estimation (see Section 4.2).

To facilitate thermodynamic independence of the parameters, we introduce new system parameters that can be varied independently, without violating any thermodynamic constraints (see Section 2.1.1). For each reaction, we define the velocity constant $K_V = (k_{cat}^{for} \cdot k_{cat}^{back})^{1/2}$ (geometric mean of the turnover rates in both directions). Given the equilibrium and velocity constants, the turnover rates can be written as $k_{cat}^{for} = K_V(K_{eq})^{-1/2}$, $k_{cat}^{back} = K_V(K_{eq})^{1/2}$. The equilibrium constants K_{eq} can be expressed by independent parameters such as the Gibbs free energies of formation: for each substance i, we define the dimensionless energy constant $K_i^G = \exp(G_i(0)/(RT))$ with Boltzmann's gas constant $R = 8.314 \, J \, (mol^{-1} \, K^{-1})$ and absolute temperature T. The equilibrium constants then satisfy $\ln K_{eq} = -N^T \ln K^G$.

2.2
Structural Analysis of Biochemical Systems

Summary

We discuss basic structural and dynamic properties of biochemical reaction networks. We introduce a stoichiometric description of networks and learn how moieties and fluxes are balanced within networks.

The *basic elements* of a metabolic or regulatory network model are

1. the compounds with their concentrations or activities and
2. the reactions or transport processes changing the concentrations or activities of the compounds.

In biological environments, reactions are usually catalyzed by enzymes, and transport steps are carried out by transport proteins or pores, thus they can be assigned to identifiable biochemical compounds. In the following, we will mainly refer to metabolic networks. However, the analysis can also be applied to regulatory networks, if different activity states or complexes of regulatory molecules are considered as individual compounds that are converted into each other by modifying reactions.

2.2.1
System Equations

Stoichiometric coefficients denote the proportion of substrate and product molecules involved in a reaction. For example, for the reaction

$$S_1 + S_2 \rightleftharpoons 2P, \tag{2.54}$$

the stoichiometric coefficients of S_1, S_2, and P are -1, -1, and 2, respectively. The assignment of stoichiometric coefficients is not unique. We could also argue that for the production of one mole P, half a mole of each S_1 and S_2 have to be used and, therefore, choose $-1/2$, $-1/2$, and 1. Or, if we change the direction of the reaction, then we may choose 1, 1, and -2.

The change of concentrations in time can be described using ODEs. For the reaction depicted in Eq. (2.54) and the first choice of stoichiometric coefficients, we obtain

$$\frac{dS_1}{dt} = -v, \qquad \frac{dS_2}{dt} = -v, \quad \text{and} \quad \frac{dP}{dt} = 2v. \tag{2.55}$$

This means that the degradation of S_1 with rate v is accompanied by the degradation of S_2 with the same rate and by the production of P with the double rate.

For a metabolic network consisting of m substances and r reactions, the system dynamics is described by the *system equations* (or *balance equations*, since the balance of substrate production and degradation is considered) [19, 20]:

$$\frac{dS_i}{dt} = \sum_{j=1}^{r} n_{ij} v_j \quad \text{for} \quad i = 1, \ldots, m. \tag{2.56}$$

The quantities n_{ij} are the stoichiometric coefficients of the ith metabolite in the jth reaction. Here, we assume that the reactions are the only reason for concentration changes and that no mass flow occurs due to convection or to diffusion. The balance equations (2.56) can also be applied, if the system consists of several compartments. In this case, every compound in different compartments has to be considered as an individual compound and transport steps are formally considered as reactions transferring the compound belonging to one compartment into the same compound belonging to the other compartment. In case, volume differences must be considered (see Section 3.4).
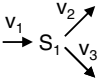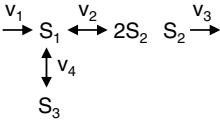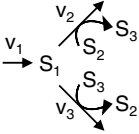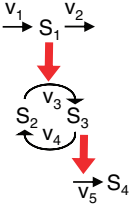
The stoichiometric coefficients n_{ij} assigned to the compounds S_i and the reactions v_j can be comprehended into the *stoichiometric matrix*

$$N = \{n_{ij}\} \quad \text{for} \quad i = 1, \ldots, m \quad \text{and} \quad j = 1, \ldots, r, \tag{2.57}$$

where each column belongs to a reaction and each row to a compound. Table 2.4 shows some examples for reaction networks and their respective stoichiometric matrices.

Note that all reactions may be reversible. In order to determine the signs is N, the direction of the arrows is artificially assigned as positive "from left to right" and "from top down." If the net flow of a reaction proceeds in the opposite direction as the arrow indicates, the value of rate v is negative.

Table 2.4 Different reaction networks and their stoichiometric matrices[a].

	Network	Stoichiometric matrix
N1	$S_1 + S_2 + S_3 \xleftrightarrow{v_1} S_4 + 2S_5$	$N = \begin{pmatrix} -1 \\ -1 \\ -1 \\ 1 \\ 2 \end{pmatrix}$
N2	$\xrightarrow{v_1} S_1 \xrightarrow{v_2} S_2 \xrightarrow{v_3} S_3 \xrightarrow{v_4} S_4 \xrightarrow{v_5}$	$N = \begin{pmatrix} 1 & -1 & 0 & 0 & 0 \\ 0 & 1 & -1 & 0 & 0 \\ 0 & 0 & 1 & -1 & 0 \\ 0 & 0 & 0 & 1 & -1 \end{pmatrix}$
N3		$N = (1 \quad -1 \quad -1)$
N4		$N = \begin{pmatrix} 1 & -1 & 0 & -1 \\ 0 & 2 & -1 & 0 \\ 0 & 0 & 0 & 1 \end{pmatrix}$
N5		$N = \begin{pmatrix} 1 & -1 & -1 \\ 0 & -1 & 1 \\ 0 & 1 & -1 \end{pmatrix}$
N6		$N = \begin{pmatrix} 1 & -1 & 0 & 0 & 0 \\ 0 & 0 & -1 & 1 & 0 \\ 0 & 0 & 1 & -1 & 0 \\ 0 & 0 & 0 & 0 & 1 \end{pmatrix}$

[a]Note that external metabolites are neither drawn in the network nor included in the stoichiometric matrix. Thin arrows denote reactions, bold arrows denote activation.

Altogether, the mathematical description of the metabolic system consists of a vector $S = (S_1, S_2, S_n)^T$ of concentrations values, a vector $v = (v_1, v_2,\ldots,v_r)^T$ of reaction rates, a parameter vector $p = (p_1, p_2, \ldots, p_m)^T$, and the stoichiometric matrix N. If the system is in steady state, we can also consider the vector $J = (J_1, J_2,\ldots,J_r)^T$ containing the steady-state fluxes. With these notions, the balance equation reads

$$\frac{dS}{dt} = Nv, \tag{2.58}$$

a compact form that is suited for various types of analysis.

2.2.2
Information Encoded in the Stoichiometric Matrix *N*

The stoichiometric matrix contains important information about the structure of the metabolic network. Using the stoichiometric matrix, we may calculate which combinations of individual fluxes are possible in steady state (i.e., calculate the admissible steady-state flux space). We may easily find out dead ends and unbranched reaction pathways. In addition, we may find out the conservation relations for the included reactants.

In steady state, it holds that

$$\frac{dS}{dt} = Nv = 0. \tag{2.59}$$

The right equality sign denotes a linear equation system for determination of the rates *v*. From linear algebra, it is known that this equation has nontrivial solutions only for Rank $N < r$. A kernel matrix *K* fulfilling

$$NK = 0 \tag{2.60}$$

shows the respective linear dependencies [21]. The choice of the kernel is not unique. It can be determined using the Gauss Algorithm (see mathematical textbooks). It contains as columns r–Rank *N* basis vectors. Every possible set *J* of steady-state fluxes can be expressed as linear combination of the columns k_i of *K*

$$J = \sum_{i=1}^{r-\text{Rank } N} \alpha_i \cdot k_i. \tag{2.61}$$

The coefficients must have units corresponding to the units of reaction rates (M s^{-1} or $\text{mol l}^{-1}\text{s}^{-1}$).

Example 2.2

For the network N2 in Table 2.4, we have $r = 5$ reactions and Rank $N = 4$. The kernel matrix contains just $1 = 5 - 4$ basis vectors, which are multiples of $k = (1 \quad 1 \quad 1 \quad 1 \quad 1)^\text{T}$. This means that in steady state, the flux through all reactions must be equal. Network N3 comprises $r = 3$ reactions and has Rank $N = 1$. Each representation of the kernel matrix contains $3 - 1 = 2$ basis vectors, e.g.,

$$K = (k_1 \quad k_2) \quad \text{with} \quad k_1 = \begin{pmatrix} 1 \\ -1 \\ 0 \end{pmatrix}, \quad k_2 = \begin{pmatrix} 1 \\ 0 \\ 1 \end{pmatrix}, \tag{2.62}$$

and for the steady-state flux holds

$$J = \alpha_1 \cdot k_1 + \alpha_2 \cdot k_2. \tag{2.63}$$

Network N6 can present a small signaling cascade. It has five reactions and Rank $N = 3$. The resulting two basis vectors of the kernel are linear combinations of

$$k_1 = (1 \quad 1 \quad 0 \quad 0 \quad 0)^T, \quad k_2 = (0 \quad 0 \quad 1 \quad 1 \quad 0)^T. \tag{2.64}$$

If we calculate the possible steady-state fluxes according to Eq. (2.63), we can easily see that in every steady state, it holds that production and degradation of S_1 are balanced ($J_1 = J_2$) and that the fluxes through the cycle are equal ($J_3 = J_4$). In addition, J_5 must be equal to zero, otherwise S_4 would accumulate. One could prevent the last effect by also including the degradation of S_4 into the network.

If the entries in a certain row are zero in all basis vectors, we have found an equilibrium reaction. In any steady state, the net rate of this reaction must be zero. For the reaction system N4 in Table 2.4, it holds that $r = 4$ and Rank $N = 3$. Its kernel consists of only one column $K = (1 \quad 1 \quad 1 \quad 0)^T$. Hence, $v_4 = \sum_{i=1}^{1} \alpha \cdot 0 = 0$. In any steady state, the rates of production and degradation of S_3 must equal.

If all basis vectors contain the same entries for a set of rows, this indicates an unbranched reaction path. In each steady state, the net rate of all respective reactions is equal.

Example 2.3

Consider the reaction scheme

$$(2.65)$$
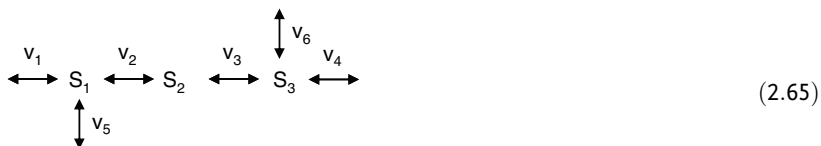
The system comprises $r = 6$ reactions. The stoichiometric matrix reads

$$N = \begin{pmatrix} 1 & -1 & 0 & 0 & -1 & 0 \\ 0 & 1 & -1 & 0 & 0 & 0 \\ 0 & 0 & 1 & -1 & 0 & 1 \end{pmatrix}$$

with Rank $N = 3$. Thus, the kernel matrix is spanned by three basis vectors, for example, $k_1 = (1 \quad 1 \quad 1 \quad 0 \quad 0 \quad -1)^T$, $k_2 = (1 \quad 0 \quad 0 \quad 0 \quad 1 \quad 0)^T$, and $k_3 = (-1 \quad -1 \quad -1 \quad -1 \quad 0 \quad 0)^T$. The entries for the second and third reactions are always equal, thus in any steady state, the fluxes through reactions 2 and 3 must be equal.

Up to now, we have not been concerned about (ir)reversibility of reactions in the network. If a certain reaction is considered irreversible, this has no consequences for the stoichiometric matrix N but rather for the kernel K. The set of vectors belonging to K is restricted by the condition that some values may not become negative (or positive – depending on the definition of flux direction).

2.2.3
Elementary Flux Modes and Extreme Pathways

The definition of the term "pathway" in a metabolic network is not straightforward. A descriptive definition of a pathway is a set of subsequent reactions that are linked by common metabolites. Typical examples include glycolysis or different amino acid synthesis pathways. More detailed inspection of metabolic maps like the *Boehringer Chart* [22] shows that metabolism is highly interconnected. Pathways that are known for a long time from biochemical experience are already hard to recognize, and it is even harder to find out new pathways, for example in metabolic maps that have been reconstructed from sequenced genomes of bacteria.

This problem has been elaborated in the concept of *elementary flux modes* [21, 23–27]. Here, the stoichiometry of a metabolic network is investigated to find out which direct routes are possible that lead from one external metabolite to another external metabolite. The approach takes into account that some reactions are reversible, while others are irreversible.

A *flux mode M* is set of flux vectors that represent such direct routes through the metabolic networks. In mathematical terms, it is defined as the set

$$M = \{v \in R^r | v = \lambda v^*, \lambda > 0\}, \tag{2.66}$$

where v^* is an r-dimensional vector (unequal to the null vector) fulfilling two conditions: (i) steady state, i.e., Eq. (2.59), and (ii) sign restriction, i.e., the flux directions in v^* fulfill the prescribed irreversibility relations.

A flux mode M comprising v is called reversible if the set M' comprising $-v$ is also a flux mode. A flux mode is an elementary flux mode if it uses a minimal set of reactions and cannot be further decomposed, i.e., the vector v cannot be represented as nonnegative linear combination of two vectors that fulfill conditions (i) and (ii) but contain more zero entries than v. An elementary flux mode is a minimal set of enzymes that could operate at steady state, with all the irreversible reactions used in the appropriate direction. The number of elementary flux modes is at least as high as the number of basis vectors of the null space.

Example 2.4

The systems (A) and (B) differ by the (ir)reversibility of reaction 2.
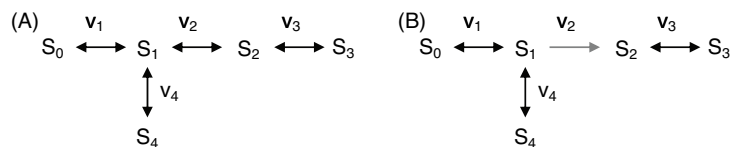
$$\tag{2.67}$$

The elementary flux modes connect the external metabolites S_0 and S_3, S_0 and S_4, or S_3 and S_4. The stoichiometric matrix and the flux modes read for case (A) and case (B)

$$N = \begin{pmatrix} 1 & -1 & 0 & -1 \\ 0 & 1 & -1 & 0 \end{pmatrix}, \quad v^A = \begin{pmatrix} 1 \\ 1 \\ 1 \\ 0 \end{pmatrix}, \begin{pmatrix} 1 \\ 0 \\ 0 \\ 1 \end{pmatrix}, \begin{pmatrix} 0 \\ -1 \\ -1 \\ 1 \end{pmatrix}, \begin{pmatrix} -1 \\ -1 \\ -1 \\ 0 \end{pmatrix}, \begin{pmatrix} -1 \\ 0 \\ 0 \\ -1 \end{pmatrix}, \begin{pmatrix} 0 \\ 1 \\ 1 \\ -1 \end{pmatrix},$$

$$\text{and } v^B = \begin{pmatrix} 1 \\ 1 \\ 1 \\ 0 \end{pmatrix}, \begin{pmatrix} 1 \\ 0 \\ 0 \\ 1 \end{pmatrix}, \begin{pmatrix} -1 \\ 0 \\ 0 \\ -1 \end{pmatrix}, \begin{pmatrix} 0 \\ 1 \\ 1 \\ -1 \end{pmatrix}.$$

$$(2.68)$$

The possible routes are illustrated in Figure 2.6.

Elementary Flux Modes
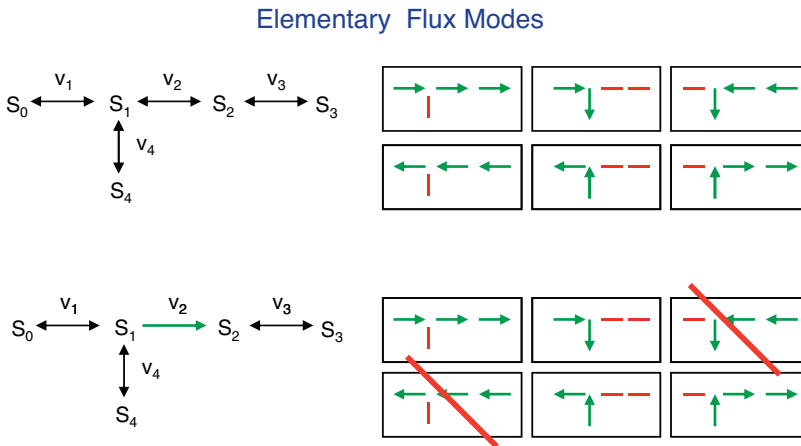
Figure 2.6 Schematic representation of elementary flux modes for the reaction network depicted in Eq. (2.67).

2.2.3.1 **Flux Cone**

The stoichiometric analysis of biochemical network analysis can be modified by considering only irreversible reactions (e.g., by splitting reversible reactions into two irreversible ones). Based on such a unidirectional representation, the basis vectors (Eq. (2.61)) form a convex cone in the flux space. This mapping relates stoichiometric analysis to the concepts of convex geometry as follows. The steady-state assumption requires that a flux vector is an element of the null space of the stoichiometry matrix N spanned by matrix K. A row of K can be interpreted as a hyperplane in flux space. The intersection of all these hyperplanes forms the null space. From thermodynamic

(a) (b) (c)
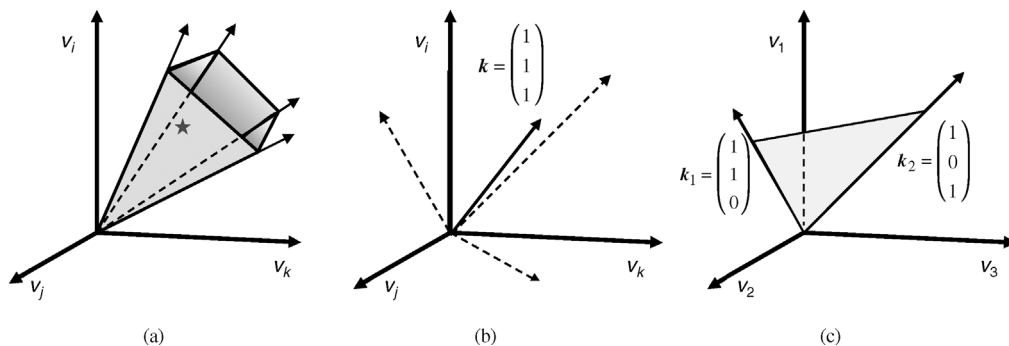
Figure 2.7 Flux cone: schematic representation of the subspace of feasible steady states within the space spanned by all positive-valued vectors for rates of irreversible reactions, v_i, $i = 1, \ldots, r$. Only three dimensions are shown. Feasible solutions are linear combinations of basis vectors of matrix K (see text). (a) Illustrative representation of the flux cone for a higher dimensional system (with r–Rank $(N) = 4$)). The basis vectors of K are rays starting at the origin. The line connecting the four rays indicates possible limits for real flux distributions set by constraints. The little star indicates one special feasible solution for the fluxes. (b) The flux cone for an unbranched reaction chain of arbitrary length, such as the network N2 in Table 2.4, is just a ray since K is represented by a single basis vector containing only 1s. (c) The flux cone for network N3 in Table 2.4 is the plane spanned by the basis vectors $k_1 = \begin{pmatrix} 1 & 1 & 0 \end{pmatrix}^T$, $k_2 = \begin{pmatrix} 1 & 0 & 1 \end{pmatrix}^T$.

considerations, some of the reactions can be assumed to proceed only in one direction so that the backward reaction can be neglected. Provided that all reactions are unidirectional or irreversible, the intersection of the null space with the semipositive orthant of the flux space forms a polyhedral cone, the flux cone. The intersection procedure results in a set of rays or edges starting at 0, which fully describe the cone. The edges are represented by vectors and any admissible steady state of the system is a positive combination of these vectors. An illustration is presented in Figure 2.7.

The set of elementary flux modes is uniquely defined. Pfeiffer *et al.* [23] developed a software ("Metatool") to calculate the elementary flux modes for metabolic networks. The concept of *extreme pathways* [28–30] is analogous to the concept of elementary flux modes, but here all reactions are constrained by flux directionality, while the concept of elementary flux modes allows for reversible reactions. To achieve this, reversible reactions are broken down into their forward and backward components. This way, the set of extreme pathways is a subset of the set of elementary flux modes and the extreme pathways are systemically independent.

Elementary flux modes and extreme pathways can be used to understand the range of metabolic pathways in a network, to test a set of enzymes for production of a desired product and detect nonredundant pathways, to reconstruct metabolism from annotated genome sequences and analyze the effect of enzyme deficiency, to reduce drug effects, and to identify drug targets. A specific application, the flux balance analysis, will be explained in Section 8.1.

2.2.4
Conservation Relations: Null Space of N^T

If a substance is neither added to nor removed from the reaction system (neither produced nor degraded), its total concentration remains constant. This also holds if the substance interacts with other compounds by forming complexes. We have seen already as an example the constancy of the total enzyme concentration (Eq. (2.19)) when deriving the Michaelis–Menten rate equation. This was based on the assumption that enzyme production and degradation takes place on a much faster timescale than the catalyzed reaction.

For the mathematical derivation of the conservation relations [21], we consider a matrix G fulfilling

$$GN = 0. \tag{2.69}$$

Due to Eq. (2.58), it follows

$$G\dot{S} = GNv = 0. \tag{2.70}$$

Integrating this equation leads directly to the conservation relations

$$GS = \text{constant}. \tag{2.71}$$

The number of independent rows of G is equal to n–Rank N, where n is the number of metabolites in the system. G^T is the kernel matrix of N^T, hence it has similar properties as K. Matrix G can also be found using the Gauss algorithm. It is not unique, but every linear combination of its rows is again a valid solution. There is a simplest representation $G = (\ G_0\quad I_{n-\text{Rank } N}\ )$. Finding this representation may be helpful for a simple statement of conservation relations, but this may necessitate renumbering and reordering of metabolite concentrations (see below).

Example 2.5

Consider a set of two reactions comprising a kinase and a phosphatase reaction

$$\begin{array}{c} \overset{v_1}{\curvearrowright} \\ \text{ATP}\quad\text{ADP} \\ \underset{v_2}{\curvearrowleft} \end{array} \tag{2.72}$$

The metabolite concentration vector reads $S = (\ ATP\quad ADP\ )^T$, the stoichiometric matrix is $N = \begin{pmatrix} -1 & 1 \\ 1 & -1 \end{pmatrix}$ yielding $G = (\ 1\quad 1\ )$. From the condition $GS = $ constant, it follows $ATP + ADP = $ constant. Thus, we have a conservation of adenine

nucleotides in this system. The actual values of $ATP + ADP$ must be determined from the initial conditions.

Example 2.6

For the following model of the upper part of glycolysis

$$
\begin{array}{l}
\text{Glucose} \xrightarrow{v_1} \text{Gluc-6P} \xleftrightarrow{v_2} \text{Fruc-6P} \xrightarrow{v_3} \text{Fruc-1,6P}_2 \\
(S_1) \quad\;\; \text{ATP ADP} \;\;(S_2) \qquad (S_3)\; \text{ATP ADP} \qquad (S_4) \\
\qquad\quad (S_5)\;\;(S_6) \qquad\qquad\qquad (S_5)\;\;(S_6)
\end{array}
\tag{2.73}
$$
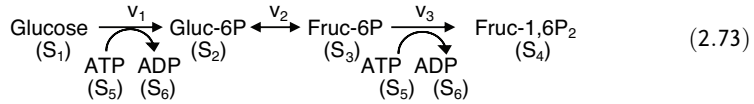
the stoichiometric matrix N (note the transpose!) and a possible representation of the conservation matrix G are given by

$$
N^{\mathrm{T}} = \begin{pmatrix} -1 & 1 & 0 & 0 & -1 & 1 \\ 0 & -1 & 1 & 0 & 0 & 0 \\ 0 & 0 & -1 & 1 & -1 & 1 \end{pmatrix} \text{ and } G = \begin{pmatrix} 2 & 1 & 1 & 0 & 0 & 1 \\ 0 & 0 & 0 & 0 & 1 & 1 \\ 1 & 1 & 1 & 1 & 0 & 0 \end{pmatrix} = \begin{pmatrix} g_1 \\ g_2 \\ g_3 \end{pmatrix}.
\tag{2.74}
$$

The interpretation of the second and third row is straightforward, showing the conservation of adenine nucleotides (g_2, $ADP + ATP =$ constant) and the conservation of sugars (g_3), respectively. The interpretation of the first row is less intuitive. If we construct the linear combination $g_4 = -g_1 + 3 \cdot g_2 + 2 \cdot g_3 = (0\;\;1\;\;1\;\;2\;\;3\;\;2)$, we find the conservation of phosphate groups.

Importantly, conservation relations can be used to simplify the system of differential equations $\dot{S} = Nv$ describing the dynamics of our reaction system. The idea is to eliminate linear dependent differential equations and to replace them by appropriate algebraic equations. Below the procedure is explained systematically [20].

First we have to rearrange the rows in the stoichiometric matrix N as well as in the concentration vector S such that a set of independent rows is on top and the dependent rows are at the bottom. Then the matrix N is split into the independent part N_R and the dependent part N' and a *link matrix* L is introduced in the following way:

$$
N = \begin{pmatrix} N_R \\ N' \end{pmatrix} = LN_R = \begin{pmatrix} I_{\text{Rank } N} \\ L' \end{pmatrix} N_R.
\tag{2.75}
$$

$I_{\text{Rank } N}$ is the identity matrix of size Rank N. The differential equation system may be rewritten accordingly

$$
\dot{S} = \begin{pmatrix} \dot{S}_{\text{indep}} \\ \dot{S}_{\text{dep}} \end{pmatrix} = \begin{pmatrix} I_{\text{Rank } N} \\ L' \end{pmatrix} N_R v,
\tag{2.76}
$$

and the dependent concentrations fulfil

$$\dot{S}_{\text{dep}} = L' \cdot \dot{S}_{\text{indep}}. \tag{2.77}$$

Integration leads to

$$S_{\text{dep}} = L' \cdot S_{\text{indep}} + \text{constant}. \tag{2.78}$$

This relation is fulfilled during the entire time course. Thus, we may replace the original system by a reduced differential equation system

$$\dot{S}_{\text{indep}} = N_R v, \tag{2.79}$$

supplemented with the set of algebraic equations (2.78).

Example 2.7

For the reaction system,

$$\tag{2.80}$$

the stoichiometric matrix, the reduced stoichiometric matrix, and the link matrix read

$$N = \begin{pmatrix} 1 & -1 & 0 & 0 \\ 0 & 1 & -1 & 0 \\ 0 & -1 & 0 & 1 \\ 0 & 1 & 0 & -1 \end{pmatrix}, \quad N_R = \begin{pmatrix} 1 & -1 & 0 & 0 \\ 0 & 1 & -1 & 0 \\ 0 & -1 & 0 & 1 \end{pmatrix},$$

$$L = \begin{pmatrix} 1 & 0 & 0 \\ 0 & 1 & 0 \\ 0 & 0 & 1 \\ 0 & 0 & -1 \end{pmatrix}, \quad L' = \begin{pmatrix} 0 & 0 & -1 \end{pmatrix}$$

The conservation relation $S_3 + S_4 = \text{constant}$ is expressed by $G = (0 \quad 0 \quad 1 \quad 1)$. The ODE system

$$\begin{aligned} \dot{S}_1 &= v_1 - v_2 \\ \dot{S}_2 &= v_2 - v_3 \\ \dot{S}_3 &= v_4 - v_2 \\ \dot{S}_4 &= v_2 - v_4 \end{aligned}$$

can be replaced by the differential-algebraic system

$$\dot{S}_1 = v_1 - v_2$$
$$\dot{S}_2 = v_2 - v_3$$
$$\dot{S}_3 = v_4 - v_2 \quad ,$$
$$S_3 + S_4 = \text{constant}$$

which has one differential equation less.

Eukaryotic cells contain a variety of organelles like nucleus, mitochondria, or vacuoles, which are separated by membranes. Reaction pathways may cross the compartment boundaries. If a substance S occurs in two different compartments, e.g., in the cytosol and in mitochondria, the respective concentrations can be assigned to two different variables, S^{C1} and S^{C2}. Formally, the transport across the membrane can be considered as a reaction with rate v. It is important to note that both compartments have different volumes V^{C1} and V^{C2}. Thus, transport of a certain amount of S with rate v from compartment $C1$ into the compartment $C2$ changes the concentrations differently:

$$V^{C1} \cdot \frac{\mathrm{d}}{\mathrm{d}t} S^{C1} = -v \quad \text{and} \quad V^{C2} \cdot \frac{\mathrm{d}}{\mathrm{d}t} S^{C2} = v, \tag{2.81}$$

where $V \cdot S$ denotes substance amount in moles. Compartmental models are discussed in more detail in Section 3.4.

2.3
Kinetic Models of Biochemical Systems

Summary

An important problem in the modeling of biological systems is to characterize the dependence of certain properties on time and space. One frequently applied strategy is the description of the change of state variables by differential equations. If only temporal changes are considered, ODEs are used. For changes in time and space, partial differential equations (PDEs) are appropriate. In this chapter, we will deal with the solution, analysis, a numerical integration of ODEs, and with basic concepts of dynamical systems theory as state space, trajectory, steady states, and stability.

2.3.1
Describing Dynamics with ODEs

The time behavior of biological systems in a deterministic approach can be described by a set of differential equations

$$\frac{\mathrm{d}x_i}{\mathrm{d}t} = \dot{x}_i = f_i(x_1, \ldots, x_n, p_1, \ldots, p_l, t) \quad i = 1, \ldots, n, \tag{2.82}$$

where x_i are the variables, e.g., concentrations, and p_j are the parameters, e.g., enzyme concentrations or kinetic constants, and t is the time. We will use the notions dx/dt and $\dot{x}$ interchangeably. In vector notation, Eq. (2.82) reads

$$\frac{d}{dt}\boldsymbol{x} = \dot{\boldsymbol{x}} = f(\boldsymbol{x}, \boldsymbol{p}, t), \tag{2.83}$$

with $\boldsymbol{x} = (x_1, \ldots, x_n)^T$, $\boldsymbol{f} = (f_1, \ldots, f_n)^T$, and $\boldsymbol{p} = (p_1, \ldots, p_l)^T$. For biochemical reaction systems, the functions f_i are frequently given by the contribution of producing and degrading reactions as described for the balance equations in Section 1.2.

2.3.1.1 Notations

ODEs depend on one variable (e.g., time t). Otherwise, they are called PDEs. PDEs are not considered here.

An implicit ODE

$$F(t, x, x', \ldots, x^{(n)}) = 0 \tag{2.84}$$

includes the variable t, the unknown function x, and its derivatives up to nth order. An explicit ODE of nth order has the form

$$x^{(n)} = f(t, x, x', \ldots, x^{(n-1)}). \tag{2.85}$$

The highest derivative (here n) determines the order of the ODE.

Studying the time behavior of our system, we may be interested in finding solutions of the ODE, i.e., finding an n times differentiable function x fulfilling Eq. (2.85). Such a solution may depend on parameters, so-called integration constants, and represents a set of curves. A solution of an ODE of nth order depending on n integration parameters is a *general* solution. Specifying the integration constants, for example, by specifying n initial conditions (for $n = 1$: $x(t = 0) = x^0$) leads to a special or *particular* solution.

We will not show here all possibilities of solving ODEs, instead we will focus on some cases relevant for the following chapters.

If the right-hand sides of the ODEs are not explicitly dependent on time t ($\dot{\boldsymbol{x}} = f(\boldsymbol{x}, \boldsymbol{p})$), the system is called autonomous. Otherwise it is nonautonomous. This case will not be considered here.

The system state is a snapshot of the system at a given time that contains enough information to predict the behavior of the system for all future times. The state of the system is described by the set of variables. The set of all possible states is the state space. The number n of independent variables is equal to the dimension of the state space. For $n = 2$, the two-dimensional state space can be called phase plane.

A particular solution of the ODE system $\dot{\boldsymbol{x}} = f(\boldsymbol{x}, \boldsymbol{p}, t)$, determined from the general solution by specifying parameter values $\boldsymbol{p}$ and initial conditions $\boldsymbol{x}(t_0) = \boldsymbol{x}^0$, describes a path through the state space and is called trajectory.

Stationary states or steady states are points $\bar{\boldsymbol{x}}$ in the phase plane, where the condition $\dot{\boldsymbol{x}} = 0 (\dot{x}_1 = 0, \ldots, \dot{x}_n = 0)$ is met. At steady state, the system of n differential equations is represented by a system of n algebraic equations for n variables.

The equation system $\dot{x} = 0$ can have multiple solutions referring to multiple steady states. The change of number or stability of steady states upon changes of parameter values p is called a bifurcation.

Linear systems of ODEs have linear functions of the variables as right-hand sides, such as

$$
\frac{dx_1}{dt} = a_{11}x_1 + a_{12}x_2 + z_1
$$
$$
\frac{dx_2}{dt} = a_{21}x_1 + a_{22}x_2 + z_2
$$
\qquad (2.86)

or in general $\dot{x} = Ax + z$. The matrix $A = \{a_{ik}\}$ is the system matrix containing the system coefficients $a_{ik} = a_{ik}(p)$ and the vector $z = (z_1, \ldots, Z_n)^T$ contains inhomogeneities. The linear system is *homogeneous* if $z = 0$ holds. Linear systems can be solved analytically. Although in real-world problems, the functions are usually nonlinear, linear systems are important as linear approximations in the investigation of steady states.

Example 2.8

The simple linear system

$$
\frac{dx_1}{dt} = a_{12}x_2, \qquad \frac{dx_2}{dt} = -x_1
$$
\qquad (2.87)

has the general solution

$$
x_1 = \frac{1}{2}e^{-i\sqrt{a_{12}}t}(1 + e^{2i\sqrt{a_{12}}t})C_1 - \frac{1}{2}ie^{-i\sqrt{a_{12}}t}(-1 + e^{2i\sqrt{a_{12}}t})\sqrt{a_{12}}C_2
$$

$$
x_2 = \frac{i}{2\sqrt{a_{12}}}e^{-i\sqrt{a_{12}}t}(1 + e^{2i\sqrt{a_{12}}t})C_1 + \frac{1}{2}e^{-i\sqrt{a_{12}}t}(1 + e^{2i\sqrt{a_{12}}t})C_2
$$

with the integration constants C_1 and C_2. Choosing $a_{12} = 1$ simplifies the system to $x_1 = C_1 \cos t + C_2 \sin t$ and $x_2 = C_2 \cos t - C_1 \sin t$. Specification of the initial conditions to $x_1(0) = 2$, $x_2(0) = 1$ gives the particular solution $x_1 = 2 \cos t + \sin t$ and $x_2 = \cos t - 2\sin t$. The solution can be presented in the phase plane or directly as functions of time (Figure 2.8).

2.3.1.2 Linearization of Autonomous Systems

In order to investigate the behavior of a system close to steady state, it may be useful to linearize it. Considering the deviation $\hat{x}(t)$ from steady state with $x(t) = \bar{x} + \hat{x}(t)$, it follows

$$
\dot{x} = f(\bar{x} + \hat{x}(t)) = \frac{d}{dt}(\bar{x} + \hat{x}(t)) = \frac{d}{dt}\hat{x}(t).
$$
\qquad (2.88)
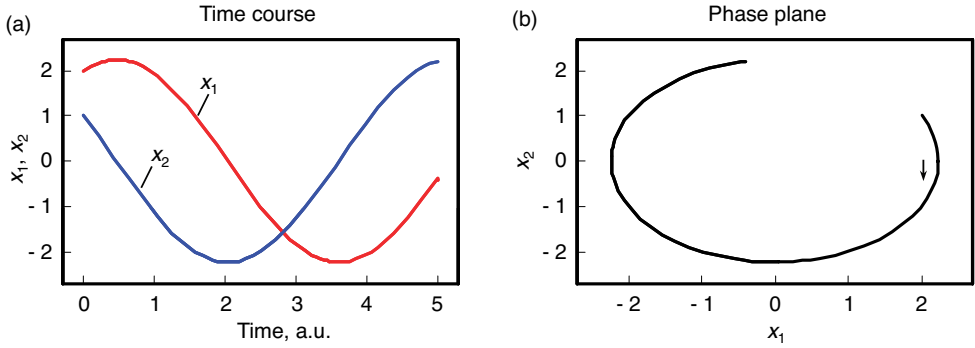
Figure 2.8 Phase plane and time course for the linear system of ODEs represented in Eq. (2.87). In time course panel: gray line $x_1(t)$, black line $x_2(t)$. Parameters: $a_{12} = 1$, $x_1(0) = 1$, $x_2(0) = 2$.

Taylor expansion of the temporal change of the deviation, $(d/dt)\hat{x}_i = f_i(\bar{x}_1 + \hat{x}_1, \ldots, \bar{x}_n + \hat{x}_n)$, gives

$$\frac{d}{dt}\hat{x}_i = f_i(\bar{x}_1, \ldots, \bar{x}_n) + \sum_{j=1}^{n} \frac{\partial f_i}{\partial x_j}\hat{x}_j + \frac{1}{2}\sum_{j=1}^{n}\sum_{k=1}^{n} \frac{\partial^2 f_i}{\partial x_j \partial x_k}\hat{x}_j\hat{x}_k + \cdots . \tag{2.89}$$

Since we consider steady state, it holds $f_i(\bar{x}_1, \ldots, \bar{x}_n) = 0$. Neglecting terms of higher order, we have

$$\frac{d}{dt}\hat{x}_i = \sum_{j=1}^{n} \frac{\partial f_i}{\partial x_j}\hat{x}_j = \sum_{j=1}^{n} a_{ij}\hat{x}_j. \tag{2.90}$$

The coefficients $a_{ij} = \partial f_i / \partial x_j$ are calculated at steady state and are constant. They form the so-called *Jacobian* matrix:

$$J = \{a_{ij}\} = \begin{pmatrix} \dfrac{\partial f_1}{\partial x_1} & \dfrac{\partial f_1}{\partial x_2} & \cdots & \dfrac{\partial f_1}{\partial x_n} \\ \dfrac{\partial f_2}{\partial x_1} & \dfrac{\partial f_2}{\partial x_2} & \cdots & \dfrac{\partial f_2}{\partial x_n} \\ \vdots & \vdots & \ddots & \vdots \\ \dfrac{\partial f_n}{\partial x_1} & \dfrac{\partial f_n}{\partial x_2} & \cdots & \dfrac{\partial f_n}{\partial x_n} \end{pmatrix}. \tag{2.91}$$

For linear systems, it holds $J = A$.

2.3.1.3 Solution of Linear ODE Systems

We are interested in two different types of problems: describing the temporal evolution of the system and finding its steady state. The problem of finding the steady state $\bar{x}$ of a linear ODE system, $\dot{x} = 0$, implies solution of $A\bar{x} + z = 0$. The problem can be solved by inversion of the system matrix A:

$$\bar{x} = -A^{-1}z. \tag{2.92}$$

The time course solution of homogeneous linear ODEs is described in the following. The systems can be solved with an exponential function as ansatz. In the simplest case $n = 1$, we have

$$\frac{dx_1}{dt} = a_{11} x_1. \tag{2.93}$$

Introducing the ansatz $x_1(t) = b_1 e^{\lambda t}$ with constant b_1 into Eq. (2.93) yields $b_1 \lambda e^{\lambda t} = a_{11} b_1 e^{\lambda t}$, which is true, if $\lambda = a_{11}$. This leads to the general solution $x_1(t) = b_1 e^{a_{11} t}$. To find a particular solution, we must specify the initial conditions $x_1(t = 0) = x_1^{(0)} = b_1 e^{a_{11} t}|_{t=0} = b_1$. Thus, the solution is

$$x_1(t) = x_1^{(0)} e^{a_{11} t}. \tag{2.94}$$

For a linear homogeneous system of n differential equations, $\dot{x} = Ax$, the approach is $x = b e^{\lambda t}$. This gives $\dot{x} = b \lambda e^{\lambda t} = Ab e^{\lambda t}$. The scalar factor $e^{\lambda t}$ can be cancelled out, leading to $b \lambda = Ab$ or the characteristic equation

$$(A - \lambda I_n) b = 0. \tag{2.95}$$

For homogeneous linear ODE systems, the *superposition principle* holds: if x_1 and x_2 are solutions of this ODE system, then also their linear combination is a solution. This leads to the general solution of the homogeneous linear ODE system:

$$x(t) = \sum_{i=1}^{n} c_i b^{(i)} e^{\lambda_i t}, \tag{2.96}$$

where $b^{(i)}$ is the eigenvectors of the system matrix A corresponding to the eigenvalues λ_i. A particular solution specifying the coefficients c_i can be found considering the initial conditions $x(t = 0) = x^{(0)} = \sum_{j=1}^{n} c_i b^{(i)}$. This constitutes an inhomogeneous linear equation system to be solved for c_i.

For the solution of inhomogeneous linear ODEs, the system $\dot{x} = Ax + z$ can be transformed into a homogeneous system by the coordination transformation $\hat{x} = x - \bar{x}$. Since $(d/dt)\bar{x} = A\bar{x} + z = 0$, it holds $(d/dt)\hat{x} = A\hat{x}$. Therefore, we can use the solution algorithm for homogeneous systems for the transformed system.

2.3.1.4 Stability of Steady States

If a system is at steady state, it should stay there – until an external perturbation occurs. Depending on the system behavior after perturbation, steady states are either

- *stable* – the system returns to this state
- *unstable* – the system leaves this state
- *metastable* – the system behavior is indifferent

A steady state is *asymptotically* stable, if it is stable and solutions based on nearby initial conditions tend to this state for $t \to \infty$. *Local* stability describes the behavior after small perturbations, *global* stability after any perturbation.

To investigate, whether a steady state $\bar{x}$ of the ODE system $\dot{x} = f(x)$ is asymptotically stable, we consider the linearized system $d\hat{x}/dt = A\hat{x}$ with $\hat{x}(t) = x(t) - \bar{x}$. The steady state $\bar{x}$ is asymptotically stable, if the Jacobian A has n eigenvalues with strictly

negative real parts each. The steady state is unstable, if at least one eigenvalue has a positive real part. This will now be explained in more detail for 1- and 2D systems.

We start with 1D systems, i.e., $n = 1$, and assume without loss of generality $\bar{x}_1 = 0$. The system $\dot{x}_1 = f_1(x_1)$ yields the linearized system $\dot{x}_1 = (\partial f_1 / \partial x_1)|_{\bar{x}_1} x_1 = a_{11} x_1$. The Jacobian matrix $A = \{a_{11}\}$ has only one eigenvalue $\lambda_1 = a_{11}$. The solution is $x_1(t) = x_1^{(0)} e^{\lambda_1 t}$. It is obvious that $e^{\lambda_1 t}$ increases for $\lambda_1 > 0$ and the system runs away from the steady state. For $\lambda_1 < 0$, the deviation from steady state decreases and $x_1(t) \to \bar{x}_1$ for $t \to \infty$. For $\lambda_1 = 0$, consideration of the linearized system allows no conclusion about stability of the original system because higher order terms in Eq. (2.89) play a role.

Consider the 2D case, $n = 2$. For the general (linear or nonlinear) system

$$\begin{aligned} \dot{x}_1 &= f_1(x_1, x_2) \\ \dot{x}_2 &= f_2(x_1, x_2) \end{aligned}, \tag{2.97}$$

we can compute the linearized system

$$\begin{aligned} \dot{x}_1 &= \frac{\partial f_1}{\partial x_1}\bigg|_{\bar{x}} x_1 + \frac{\partial f_1}{\partial x_2}\bigg|_{\bar{x}} x_2 \\ \dot{x}_2 &= \frac{\partial f_2}{\partial x_1}\bigg|_{\bar{x}} x_1 + \frac{\partial f_2}{\partial x_2}\bigg|_{\bar{x}} x_2 \end{aligned} \quad \text{or} \quad \dot{x} = \begin{pmatrix} \dfrac{\partial f_1}{\partial x_1}\bigg|_{\bar{x}} \dfrac{\partial f_1}{\partial x_2}\bigg|_{\bar{x}} \\ \dfrac{\partial f_2}{\partial x_1}\bigg|_{\bar{x}} \dfrac{\partial f_2}{\partial x_2}\bigg|_{\bar{x}} \end{pmatrix} x = \begin{pmatrix} a_{11} & a_{12} \\ a_{21} & a_{22} \end{pmatrix} x = Ax. \tag{2.98}$$

To find the eigenvalues of A, we have to solve the characteristic polynomial

$$\lambda^2 - \underbrace{(a_{11} + a_{22})}_{\text{Tr } A} \lambda + \underbrace{a_{11} a_{22} - a_{12} a_{21}}_{\text{Det } A} = 0, \tag{2.99}$$

with Tr A the trace and Det A the determinant of A, and get

$$\lambda_{1/2} = \frac{\text{Tr } A}{2} \pm \sqrt{\frac{(\text{Tr } A)^2}{4} - \text{Det } A}. \tag{2.100}$$

The eigenvalues are either real for $(\text{Tr } A)^2 / 4 - \text{Det } A \geq 0$ or complex (otherwise). For complex eigenvalues, the solution contains oscillatory parts.

For stability, it is necessary that Tr $A < 0$ and Det $A \geq 0$. Depending on the sign of the eigenvalues, steady states of a 2D system may have the following characteristics:

1. $\lambda_1 < 0$, $\lambda_2 < 0$, both real: stable node
2. $\lambda_1 > 0$, $\lambda_2 > 0$, both real: unstable node
3. $\lambda_1 > 0$, $\lambda_2 < 0$, both real: saddle point, unstable
4. $Re(\lambda_1) < 0$, $Re(\lambda_2) < 0$, both complex with negative real parts: stable focus
5. $Re(\lambda_1) > 0$, $Re(\lambda_2) > 0$, both complex with positive real parts: unstable focus
6. $Re(\lambda_1) = Re(\lambda_2) = 0$, both complex with zero real parts: center, unstable.
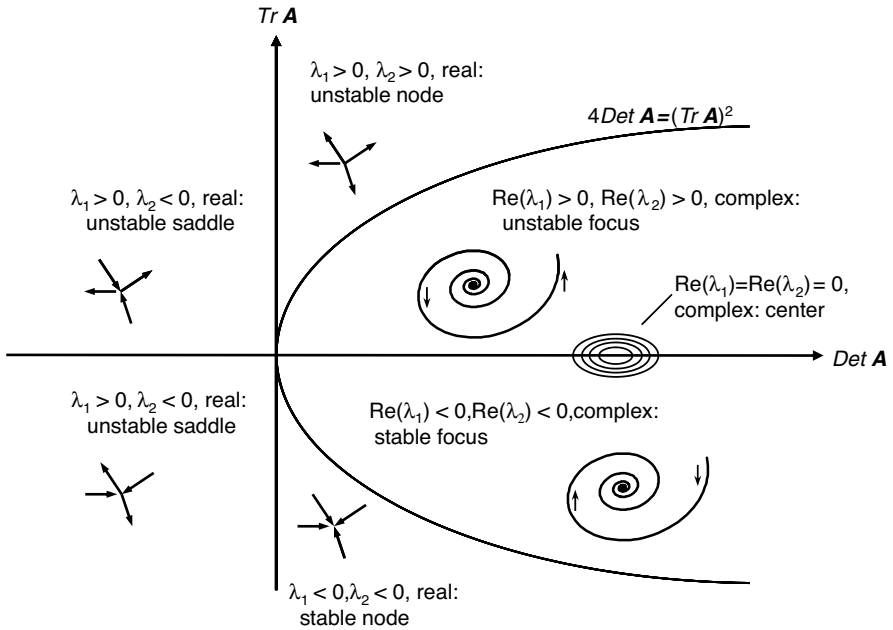
Figure 2.9 Stability of steady states in two-dimensional systems: the character of steady-state solutions is represented depending on the value of the determinant (*x*-axis) and the trace (*y*-axis) of the Jacobian matrix. Phase plane behavior of trajectories in the different cases is schematically represented.

Graphical representation of stability depending on trace and determinant is given in Figure 2.9.

Up to now, we considered only the linearized system. For the stability of the original system, the following holds. If the steady state of the linearized system is asymptotically stable, then the steady state of the complete system is also asymptotically stable. If the steady state of the linearized system is a saddle point, an unstable node or an unstable focus, then the steady state of the complete system is also unstable. This means that statements about the stability remain true, but the character of the steady state is not necessarily kept. For the center, no statement on the stability of the complete system is possible.

Routh–Hurwitz Theorem [31]   For systems with $n > 2$ differential equations, we obtain the characteristic polynomial

$$c_n\lambda^n + c_{n-1}\lambda^{n-1} + \cdots + c_1\lambda + c_0 = 0. \tag{2.101}$$

This is a polynomial of degree n, which frequently cannot be solved analytically (at least for $n > 4$). We can use the Hurwitz criterion to test whether the real parts of all eigenvalues are negative. We have to form the Hurwitz matrix H, containing the coefficients of the characteristic polynomial:

$$H = \begin{pmatrix} c_{n-1} & c_{n-3} & c_{n-5} & \ldots & 0 \\ c_n & c_{n-2} & c_{n-4} & \ldots & 0 \\ 0 & c_{n-1} & c_{n-3} & \ldots & 0 \\ 0 & c_n & c_{n-2} & \ldots & 0 \\ \vdots & \vdots & \vdots & \ddots & \vdots \\ 0 & 0 & 0 & \ldots & c_0 \end{pmatrix} = \{h_{ik}\} \text{ with } h_{ik} = \begin{cases} c_{n+i-2k}, & \text{if } 0 \le 2k-i \le n \\ 0, \text{else} \end{cases}.$$

$$(2.102)$$

It has been shown that all solutions of the characteristic polynomial have negative real parts, if all coefficients c_i of the polynomial as well as all principal leading minors of H have positive values.

2.3.1.5 Global Stability of Steady States

A state is globally stable, if the trajectories for all initial conditions approach it for $t \to \infty$. The stability of a steady state of an ODE system can be tested with a method proposed by Lyapunov:

Shift the steady state into the point of origin by coordination transformation $\hat{x} = x - \bar{x}$.

Find a function $V_L(x_1, \ldots, x_n)$, called Lyapunov function, with the following properties:

(1) $V_L(x_1, \ldots, x_n)$ has continuous derivatives with respect to all variables x_i.
(2) $V_L(x_1, \ldots, x_n)$ satisfies $V_L(x_1, \ldots, x_n) = 0$ for $x_i = 0$ and is positive definite elsewhere, i.e., $V_L(x_1, \ldots, x_n) > 0$ for $x_i \neq 0$.
(3) The time derivative of $V_L(x(t))$ is given by

$$\frac{dV_L}{dt} = \sum_{i=1}^{n} \frac{\partial V_L}{\partial x_i} \frac{dx_i}{dt} = \sum_{i=1}^{n} \frac{\partial V_L}{\partial x_i} f_i(x_1, \ldots, x_n). \quad (2.103)$$

A steady state $\bar{x} = 0$ is stable, if the time derivative of $V_L(x(t))$ in a certain region around this state has no positive values. The steady state is asymptotically stable, if the time derivative of $V_L(x(t))$ in this region is negative definite, i.e., $dV_L/dt = 0$ for $x_i = 0$ and $dV_L/dt < 0$ for $x_i \neq 0$.

Example 2.9

The system $\dot{x}_1 = -x_1$, $\dot{x}_2 = -x_2$ has the solution $x_1(t) = x_1^{(0)} e^{-t}$, $x_2(t) = x_2^{(0)} e^{-t}$ and the state $x_1 = x_2 = 0$ is asymptotically stable.

The global stability can also be shown using the positive definite function $V_L = x_1^2 + x_2^2$ as Lyapunov function. It holds $dV_L/dt = (\partial V_L/\partial x_1)\dot{x}_1 + (\partial V_L/\partial x_2)\dot{x}_2 = 2x_1(-x_1) + 2x_2(-x_2)$, which is negative definite.

2.3.1.6 Limit Cycles

Oscillatory behavior is a typical phenomenon in biology. The cause of the oscillation may be different either imposed by external influences or encoded by internal
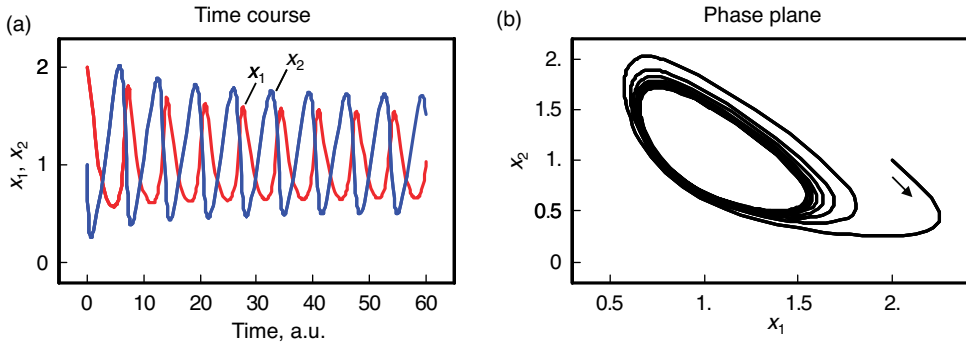
Figure 2.10 Solution of the Equation system in Example 2.10 represented as time course (left panel) and in phase plane (right panel). Initial conditions $x_1(0) = 2$, $x_2(0) = 1$.

structures and parameters. Internally caused stable oscillations can be found if we have a limit cycle in the phase space.

A *limit cycle* is an isolated closed trajectory. All trajectories in its vicinity are periodic solutions winding toward (stable limit cycle) or away from (unstable) the limit cycle for $t \to \infty$.

Example 2.10

The nonlinear system $\dot{x}_1 = x_1^2 x_2 - x_1$, $\dot{x}_2 = p - x_1^2 x_2$ has a steady state at $\bar{x}_1 = p$, $\bar{x}_2 = 1/p$. If we choose, e.g., $p = 0.98$, this steady state is unstable since Tr $\mathbf{A} = 1 - p^2 > 0$ (Figure 2.10).

For 2D systems, there are two criteria to check whether a limit cycle exists. Consider the system of differential equations

$$\begin{aligned} \dot{x}_1 &= f_1(x_1, x_2) \\ \dot{x}_2 &= f_2(x_1, x_2) \end{aligned}. \tag{2.104}$$

The *negative criterion of Bendixson* states: if the expression Tr $\mathbf{A} = \partial f_1/\partial x_1 + \partial f_2/\partial x_2$ does not change its sign in a certain region of the phase plane, then there is no closed trajectory in this area. Hence, a necessary condition for the existence of a limit cycle is the change of the sign of Tr $\mathbf{A}$.

Example 2.11

Example 2.10 holds Tr $\mathbf{A} = (2x_1 x_2 - 1) + (-x_1^2)$. Therefore, Tr $\mathbf{A} = 0$ is fulfilled at $x_2 = (x_1^2 + 1)/(2x_1)$ and Tr $\mathbf{A}$ may assume positive or negative values for varying x_1, x_2, and the necessary condition for the existence of a limit cycle is met.

The criterion of Poincaré–Bendixson states: if a trajectory in the 2D phase plane remains within a finite region without approaching a singular point (a steady state), then this trajectory is either a limit cycle or it approaches a limit cycle. This criterion provides a sufficient condition for the existence of a limit cycle. Nevertheless, the limit cycle trajectory can be computed analytically only in very rare cases.

2.3.2
Metabolic Control Analysis

Metabolic control analysis (MCA) is a powerful quantitative and qualitative framework for studying the relationship between steady-state properties of a network of biochemical reaction and the properties of the individual reactions. It investigates the sensitivity of steady-state properties of the network to small parameter changes. MCA is a useful tool for theoretical and experimental analysis of control and regulation in cellular systems.

MCA was independently founded by two different groups in the 1970s [32, 33] and was further developed by many different groups upon the application to different metabolic systems. A milestone in its formalization was provided by Reder [20]. Originally intended for metabolic networks, MCA has nowadays found applications also for signaling pathways, gene expression models, and hierarchical networks [34–38].

Metabolic networks are very complex systems that are highly regulated and exhibit a lot of interactions such as feedback inhibition or common substrates such as ATP for different reactions. Many mechanisms and regulatory properties of isolated enzymatic reactions are known. The development of MCA was motivated by a series of questions like the following: Can one predict properties or behavior of metabolic networks from the knowledge about their parts, the isolated reactions? Which individual steps control a flux or a steady-state concentration? Is there a rate-limiting step? Which effectors or modifications have the most prominent effect on the reaction rate? In biotechnological production processes, it is of interest which enzyme(s) should be activated in order to increase the rate of synthesis of a desired metabolite. There are also related problems in health care. Concerning metabolic disorders involving overproduction of a metabolite, which reactions should be modified in order to down-regulate this metabolite while perturbing the rest of the metabolism as weakly as possible?

In metabolic networks, the steady-state variables, i.e., the fluxes and the metabolite concentrations, depend on the value of parameters such as enzyme concentrations, kinetic constants (like Michaelis constants and maximal activities), and other model-specific parameters. The relations between steady-state variables and kinetic parameters are usually nonlinear. Up to now, there is no general theory that predicts the effect of large parameter changes in a network. The approach presented here is, basically, restricted to small parameter changes. Mathematically, the system is linearized at steady state, which yields exact results, if the parameter changes are infinitesimally small.

In this section, we will first define a set of mathematical expressions that are useful to quantify control in biochemical reaction networks. Later we will show the relations between these functions and their application for prediction of reaction network behavior.

2.3.2.1 The Coefficients of Control Analysis

Biochemical reaction systems are networks of metabolites connected by chemical reactions. Their behavior is determined by the properties of their components – the individual reactions and their kinetics – as well as by the network structure – the involvement of compounds in different reaction or in brief: the stoichiometry. Hence, the effect of a perturbation exerted on a reaction in this network will depend on both – the local properties of this reaction and the embedding of this reaction in the global network.

Let $y(x)$ denotes a quantity that depends on another quantity x. The effect of the change Δx on y is expressed in terms of sensitivity coefficients:

$$c_x^y = \left(\frac{x}{y} \frac{\Delta y}{\Delta x} \right)_{\Delta x \to 0}. \tag{2.105}$$

In practical applications, Δx might be, e.g., identified with 1% change of x and Δy with the percentage change of y. The factor x/y is a normalization factor that makes the coefficient independent of units and of the magnitude of x and y. In the limiting case $\Delta x \to 0$, the coefficient defined in Eq. (2.105) can be written as

$$c_x^y = \frac{x}{y} \frac{\partial y}{\partial x} = \frac{\partial \ln y}{\partial \ln x}. \tag{2.106}$$

Both right-hand expressions are mathematically equivalent.

Two distinct types of coefficients, local and global coefficients, reflect the relations among local and global effects of changes. *Elasticity coefficients* are local coefficients pertaining to individual reactions. They can be calculated in any given state. *Control coefficients* and *response coefficients* are global quantities. They refer to a given steady state of the entire system. After a perturbation of x, the relaxation of y to new steady state is considered.

The general form of the coefficients in control analysis as defined in Eq. (2.106) contains the normalization x/y. The normalization has the advantage that we get rid of units and can compare, e.g., fluxes belonging to different branches of a network. The drawback of the normalization is that x/y is not defined as soon as $y = 0$, which may happen for certain parameter combinations. In those cases, it is favorable to work with nonnormalized coefficients. Throughout this chapter, we will consider usually normalized quantities. If we use nonnormalized coefficients, they are flagged as $\tilde{c}$. In general, the use of one or the other type of coefficient is also a matter of personal choice of the modeler.

Changes reflected by the different coefficients are illustrated in Figure 2.11.

2.3.2.2 The Elasticity Coefficients

An elasticity coefficient quantifies the sensitivity of a reaction rate to the change of a concentration or a parameter while all other arguments of the kinetic law are kept
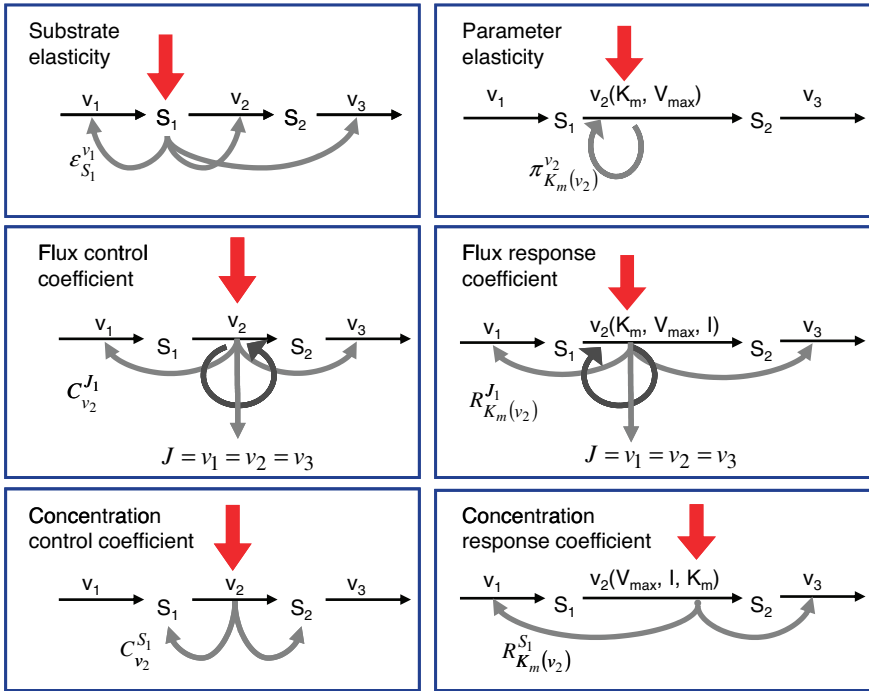
Figure 2.11 Schematic representation of perturbation and effects quantified by different coefficients of metabolic control analysis.

fixed. It measures the direct effect on the reaction velocity, while the rest of the network is not taken into consideration. The sensitivity of the rate v_k of a reaction to the change of the concentration S_i of a metabolite is calculated by the ε-*elasticity*:

$$\varepsilon_i^k = \frac{S_i}{v_k}\frac{\partial v_k}{\partial S_i}. \tag{2.107}$$

The π-*elasticity* is defined with respect to parameters p_m such as kinetic constants, concentrations of enzymes, or concentrations of external metabolites as follows:

$$\pi_m^k = \frac{p_m}{v_k}\frac{\partial v_k}{\partial p_m}. \tag{2.108}$$

Example 2.12

In Michaelis–Menten kinetics, the rate v of a reaction depends on the substrate concentration S in the form $v = V_{max}S/(K_m + S)$ (Eq. (2.22)). The sensitivity is given by the elasticity $\varepsilon_S^v = \partial \ln v / \partial \ln S$. Since the Michaelis–Menten equation defines a mathematical dependency of v on S, it is easy to calculate that

$$\varepsilon_S^v = \frac{S}{v}\frac{\partial}{\partial S}\left(\frac{V_{max}S}{K_m + S}\right) = \frac{S}{v}\frac{V_{max}(K_m + S) - V_{max}S}{(K_m + S)^2} = \frac{S}{K_m + S}. \qquad (2.109)$$

The normalized ε-elasticity in the case of mass action kinetics can be calculated similarly and is always 1. Whenever the rate does not depend directly on a concentration (e.g., for a metabolite of a reaction system that is not involved in the considered reaction), the elasticity is zero.

Example 2.13

Typical values of elasticity coefficients will be explained for an isolated reaction transforming substrate S into product P. The reaction is catalyzed by enzyme E with the inhibitor I, and the activator A as depicted below

$$
\begin{array}{c}
\text{E} \\
\downarrow \\
\text{S} \xrightarrow[\;\;\;\text{T}\;\;\uparrow\;]{} \text{P} \\
\quad\;\; \text{I} \quad \text{A}
\end{array}
\qquad (2.110)
$$
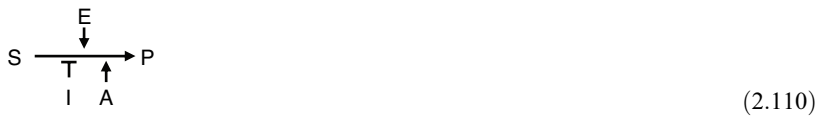
Usually, the elasticity coefficients for metabolite concentrations are in the following range:

$$\varepsilon_S^v = \frac{S}{v}\frac{\partial v}{\partial S} > 0 \quad \text{and} \quad \varepsilon_P^v = \frac{P}{v}\frac{\partial v}{\partial P} \leq 0. \qquad (2.111)$$

In most cases, the rate increases with the concentration of the substrate (compare, e.g., Eq. (2.109)) and decreases with the concentration of the product. An exception from $\varepsilon_S^v > 0$ occurs in the case of substrate inhibition (Eq. (2.33)), where the elasticity will become negative for $S > S_{opt}$. The relation $\varepsilon_P^v = 0$ holds, if the reaction is irreversible or if the product concentration is kept zero by external mechanisms. The elasticity coefficients with respect to effectors I or A should obey

$$\varepsilon_A^v = \frac{A}{v}\frac{\partial v}{\partial A} > 0 \quad \text{and} \quad \varepsilon_I^v = \frac{I}{v}\frac{\partial v}{\partial I} < 0, \qquad (2.112)$$

since this is essentially what the notions activator and inhibitor mean.

For the most kinetic laws, the reaction rate v is proportional to the enzyme concentration E. For example, E is a multiplicative factor in the mass action rate law as well as in the maximal rate of the Michaelis–Menten rate law. Therefore, it holds that

$$\varepsilon_E^v = \frac{\partial \ln v}{\partial \ln E} = 1. \qquad (2.113)$$

More complicated interactions between enzymes and substrates such as metabolic channeling (direct transfer of the metabolite from one enzyme to the next without release to the medium) may lead to exceptions from this rule.

2.3.2.3 Control Coefficients

When defining control coefficients, we refer to a stable steady state of the metabolic system characterized by steady-state concentrations $\mathbf{S}^{\text{st}} = \mathbf{S}^{\text{st}}(\mathbf{p})$ and steady-state fluxes $\mathbf{J} = \mathbf{v}(\mathbf{S}^{\text{st}}(\mathbf{p}), \mathbf{p})$. Any sufficiently small perturbation of an individual reaction rate, $v_k \to v_k + \Delta v_k$, by a parameter change $p_k \to p_k + \Delta p_k$ drives the system to a new steady state in close proximity with $\mathbf{J} \to \mathbf{J} + \Delta \mathbf{J}$ and $\mathbf{S}^{\text{st}} \to \mathbf{S}^{\text{st}} + \Delta \mathbf{S}$. A measure for the change of fluxes and concentrations are the control coefficients.

The *flux control coefficient* for the control of rate v_k over flux J_j is defined as

$$C_k^j = \frac{v_k}{J_j} \frac{\partial J_j / \partial p_k}{\partial v_k / \partial p_k}. \tag{2.114}$$

The control coefficients quantify the control that a certain reaction v_k exerts on the steady-state flux J_j. It should be noted that the rate change, Δv_k, is caused by the change of a parameter p_k that has a direct effect solely on v_k. Thus, it holds

$$\frac{\partial v_k}{\partial p_k} \neq 0 \quad \text{and} \quad \frac{\partial v_l}{\partial p_k} = 0 \quad (l \neq k). \tag{2.115}$$

Such a parameter might be the enzyme concentration, a kinetic constant, or the concentration of a specific inhibitor or effector.

In a more compact form the flux control coefficients read

$$C_k^j = \frac{v_k}{J_j} \frac{\partial J_j}{\partial v_k}. \tag{2.116}$$

Equivalently, the *concentration control coefficient* of concentrations S_i^{st} with respect to v_k reads

$$C_k^i = \frac{v_k}{S_i^{\text{st}}} \frac{\partial S_i^{\text{st}}}{\partial v_k}. \tag{2.117}$$

2.3.2.4 Response Coefficients

The steady state is determined by the values of the parameters. A third type of coefficients expresses the direct dependence of steady-state variables on parameters. The response coefficients are defined as

$$R_m^j = \frac{p_m}{J_j} \frac{\partial J_j}{\partial p_m} \quad \text{and} \quad R_m^i = \frac{p_m}{S_i^{\text{st}}} \frac{\partial S_i^{\text{st}}}{\partial p_m}, \tag{2.118}$$

where the first coefficient expresses the response of the flux to a parameter perturbation, while the latter describes the response of a steady-state concentration.

2.3.2.5 Matrix Representation of the Coefficients

Control, response, and elasticity coefficients are defined with respect to all rates, steady-state concentrations, fluxes, or parameters in the metabolic system and in the respective model. They can be arranged in matrices:

$$\mathbf{C}^J = \{C_k^j\}, \ \mathbf{C}^S = \{C_k^i\}, \ \mathbf{R}^J = \{R_m^j\}, \ \mathbf{R}^S = \{R_m^i\}, \ \boldsymbol{\varepsilon} = \{\varepsilon_i^k\}, \ \boldsymbol{\pi} = \{\pi_m^k\}. \tag{2.119}$$

Matrix representation can also be chosen for all types of nonnormalized coefficients. The arrangement in matrices allows us to apply matrix algebra in control analysis. In particular, the matrices of normalized control coefficients can be calculated from the matrices of nonnormalized control coefficient as follows:

$$\begin{aligned}
\boldsymbol{C}^J &= (\mathrm{dg}\boldsymbol{J})^{-1} \cdot \tilde{\boldsymbol{C}}^J \cdot \mathrm{dg}\boldsymbol{J} & \boldsymbol{C}^S &= (\mathrm{dg}\boldsymbol{S}^{\mathrm{st}})^{-1} \cdot \tilde{\boldsymbol{C}}^J \cdot \mathrm{dg}\boldsymbol{J} \\
\boldsymbol{R}^J &= (\mathrm{dg}\boldsymbol{J})^{-1} \cdot \tilde{\boldsymbol{R}}^J \cdot \mathrm{dg}\boldsymbol{p} & \boldsymbol{R}^S &= (\mathrm{dg}\boldsymbol{S}^{\mathrm{st}})^{-1} \cdot \tilde{\boldsymbol{R}}^S \cdot \mathrm{dg}\boldsymbol{p} \cdot \\
\boldsymbol{\varepsilon} &= (\mathrm{dg}\boldsymbol{v})^{-1} \cdot \tilde{\boldsymbol{\varepsilon}} \cdot \mathrm{dg}\boldsymbol{S}^{\mathrm{st}} & \boldsymbol{\pi} &= (\mathrm{dg}\boldsymbol{v})^{-1} \cdot \tilde{\boldsymbol{\pi}} \cdot \mathrm{dg}\boldsymbol{p}
\end{aligned} \tag{2.120}$$

The symbol "dg" stands for the diagonal matrix, e.g., for a system with three reaction holds

$$\mathrm{dg}\boldsymbol{J} = \begin{pmatrix} J_1 & 0 & 0 \\ 0 & J_2 & 0 \\ 0 & 0 & J_3 \end{pmatrix}.$$

2.3.2.6 The Theorems of Metabolic Control Theory

Let us assume that we are interested in calculating the control coefficients for a system under investigation. Usually, the steady-state fluxes or concentrations cannot be expressed explicitly as function of the reaction rates. Therefore, flux and concentration control coefficients cannot simply be determined by taking the respective derivatives, as we did for the elasticity coefficients in Example 2.12.

Fortunately, the work with control coefficients is eased by of a set of theorems. The first type of theorems, the *summation theorems*, makes a statement about the total control over a flux or a steady-state concentration. The second type of theorems, the *connectivity theorems*, relates the control coefficients to the elasticity coefficients. Both types of theorems together with network information encoded in the stoichiometric matrix contain enough information to calculate all control coefficients.

Here, we will first introduce the theorems. Then, we will present a hypothetical perturbation experiment (as introduced by Kacser and Burns) to illustrate the summation theorem. Finally, the theorems will be derived mathematically.

2.3.2.7 The Summation Theorems

The summation theorems make a statement about the total control over a certain steady-state flux or concentration. The flux control coefficients and concentration control coefficients fulfill, respectively,

$$\sum_{k=1}^{r} C_{v_k}^{J_j} = 1 \quad \text{and} \quad \sum_{k=1}^{r} C_{v_k}^{S_i} = 0, \tag{2.121}$$

for any flux J_j and any steady-state concentration S_i^{st}. The quantity r is the number of reactions. The flux control coefficients of a metabolic network for one steady-state flux sum up to one. This means that all enzymatic reactions can share the control over this flux. The control coefficients of a metabolic network for one steady-state concentration are balanced. This means again that the enzymatic reactions can share the control over this concentration, but some of them exert a negative control while

others exert a positive control. Both relations can also be expressed in matrix formulation. We get

$$C^J \cdot \boldsymbol{1} = \boldsymbol{1} \quad \text{and} \quad C^S \cdot \boldsymbol{1} = \boldsymbol{0}. \tag{2.122}$$

The symbols $\boldsymbol{1}$ and $\boldsymbol{0}$ denote column vectors with r rows containing as entries only ones or zeros, respectively. The summation theorems for the nonnormalized control coefficients read

$$\tilde{C}^J \cdot \boldsymbol{K} = \boldsymbol{K} \quad \text{and} \quad \tilde{C}^S \cdot \boldsymbol{K} = \boldsymbol{0}, \tag{2.123}$$

where $\boldsymbol{K}$ is the matrix satisfying $\boldsymbol{N} \cdot \boldsymbol{K} = \boldsymbol{0}$ (see Section 2.2). A more intuitive derivation of the summation theorems is given in the following example according to Kacser and Burns [33].

Example 2.14

The summation theorem for flux control coefficients can be derived using a thought experiment.

Consider the following unbranched pathway with fixed concentrations of the external metabolites, S_0 and S_3:

$$S_0 \overset{v_1}{\leftrightarrow} S_1 \overset{v_2}{\leftrightarrow} S_2 \overset{v_3}{\leftrightarrow} S_3 \tag{2.124}$$

What happens to steady-state fluxes and metabolite concentrations, if we perform an experimental manipulation of all three reactions leading to the same fractional change α of all three rates?

$$\frac{\delta v_1}{v_1} = \frac{\delta v_2}{v_2} = \frac{\delta v_3}{v_3} = \alpha. \tag{2.125}$$

The flux must increase to the same extent, $\delta J/J = \alpha$, but, since rates of producing and degrading reactions increase to the same amount, the concentrations of the metabolites remain constant $\delta S_1/S_1 = \delta S_2/S_2 = 0$.

The combined effect of all changes in local rates on the system variables S_1^{st}, S_2^{st}, and J can be written as the sum of all individual effects caused by the local rate changes. For the flux holds

$$\frac{\delta J}{J} = C_1^J \frac{\delta v_1}{v_1} + C_2^J \frac{\delta v_2}{v_2} + C_3^J \frac{\delta v_3}{v_3}. \tag{2.126}$$

It follows

$$\alpha = \alpha(C_1^J + C_2^J + C_3^J) \quad \text{or} \quad 1 = C_1^J + C_2^J + C_3^J. \tag{2.127}$$

This is just a special case of Eq. (2.121). In the same way, for the change of concentration S_1^{st}, we obtain

$$\frac{\delta S_1^{st}}{S_1^{st}} = C_1^{S_1} \frac{\delta v_1}{v_1} + C_2^{S_1} \frac{\delta v_2}{v_2} + C_3^{S_1} \frac{\delta v_3}{v_3}. \tag{2.128}$$

Finally, we get

$$0 = C_1^{S_1} + C_2^{S_1} + C_3^{S_1} \quad \text{as well as} \quad 0 = C_1^{S_2} + C_2^{S_2} + C_3^{S_2}. \tag{2.129}$$

Although shown here only for a special case, these properties hold in general for systems without conservation relations. The general derivation is given in Section 2.3.2.9.

2.3.2.8 The Connectivity Theorems

Flux control coefficients and elasticity coefficients are related by the expression

$$\sum_{k=1}^{r} C_{v_k}^{J_j} \varepsilon_{S_i}^{v_k} = 0. \tag{2.130}$$

Note that the sum runs over all rates v_k for any flux J_j. Considering the concentration S_i of a specific metabolite and a certain flux J_j, each term contains the elasticity $\varepsilon_{S_i}^{v_k}$ describing the direct influence of a change of S_i on the rates v_k and the control coefficient expressing the control of v_k over J_j.

The connectivity theorem between concentration control coefficients and elasticity coefficients reads

$$\sum_{k=1}^{r} C_{v_k}^{S_h} \varepsilon_{S_i}^{v_k} = -\delta_{hi}. \tag{2.131}$$

Again, the sum runs over all rates v_k, while S_h and S_i are the concentrations of two fixed metabolites. The symbol $\delta_{hi} = \begin{cases} 0, & \text{if} \quad h \neq i \\ 1, & \text{if} \quad h = i \end{cases}$ is the so-called Kronecker symbol.

In matrix formulation, the connectivity theorems read

$$C^J \cdot \boldsymbol{\varepsilon} = \boldsymbol{0} \quad \text{and} \quad C^S \cdot \boldsymbol{\varepsilon} = -I, \tag{2.132}$$

where I denotes the identity matrix of size $n \times n$. For nonnormalized coefficients, it holds

$$\tilde{C}^J \cdot \tilde{\boldsymbol{\varepsilon}} \cdot L = 0 \quad \text{and} \quad \tilde{C}^S \cdot \tilde{\boldsymbol{\varepsilon}} \cdot L = -L, \tag{2.133}$$

where L is the link matrix that expresses the relation between independent and dependent rows in the stoichiometric matrix (Eq. (2.75)) A comprehensive representation of both summation and connectivity theorems for nonnormalized coefficients is given by the following equation:

$$\begin{pmatrix} \tilde{C}^J \\ \tilde{C}^S \end{pmatrix} \cdot \begin{pmatrix} K & \tilde{\boldsymbol{\varepsilon}} L \end{pmatrix} = \begin{pmatrix} K & 0 \\ 0 & -L \end{pmatrix}. \tag{2.134}$$

The summation and connectivity theorem together with the structural information of the stoichiometric matrix are sufficient to calculate the control coefficients

for a metabolic network. This shall be illustrated for a small network in the next example.

Example 2.15

To calculate the control coefficients, we study the following reaction system:

$$P_0 \overset{v_1}{\leftrightarrow} S \overset{v_2}{\leftrightarrow} P_2 \qquad (2.135)$$

The flux control coefficients obey the theorems

$$C_1^J + C_2^J = 1 \quad \text{and} \quad C_1^J \varepsilon_S^1 + C_2^J \varepsilon_S^2 = 0, \qquad (2.136)$$

which can be solved for the control coefficients to yield

$$C_1^J = \frac{\varepsilon_S^2}{\varepsilon_S^2 - \varepsilon_S^1} \quad \text{and} \quad C_2^J = \frac{-\varepsilon_S^1}{\varepsilon_S^2 - \varepsilon_S^1}. \qquad (2.137)$$

Since usually $\varepsilon_S^1 < 0$ and $\varepsilon_S^2 > 0$ (see Example 2.13), both control coefficients assume positive values $C_1^J > 0$ and $C_2^J > 0$. This means that both reactions exert a positive control over the steady-state flux, and acceleration of any of them leads to increase of J, which is in accordance with common intuition.

The concentration control coefficients fulfil

$$C_1^S + C_2^S = 0 \quad \text{and} \quad C_1^S \varepsilon_S^1 + C_2^S \varepsilon_S^2 = -1, \qquad (2.138)$$

which yields

$$C_1^S = \frac{1}{\varepsilon_S^2 - \varepsilon_S^1} \quad \text{and} \quad C_2^S = \frac{-1}{\varepsilon_S^2 - \varepsilon_S^1}. \qquad (2.139)$$

With $\varepsilon_S^1 < 0$ and $\varepsilon_S^2 > 0$, we get $C_1^S > 0$ and $C_2^S < 0$, i.e., increase of the first reaction causes a raise in the steady-state concentration of S while acceleration of the second reaction leads to the opposite effect.

2.3.2.9 Derivation of Matrix Expressions for Control Coefficients

After having introduced the theorems of MCA, we will derive expressions for the control coefficients in matrix form. These expressions are suited for calculating the coefficients even for large-scale models. We start from the steady-state condition

$$N v(S^{\text{st}}(p), p) = 0. \qquad (2.140)$$

Implicit differentiation with respect to the parameter vector p yields

$$N \frac{\partial v}{\partial S} \frac{\partial S^{\text{st}}}{\partial p} + N \frac{\partial v}{\partial p} = 0. \qquad (2.141)$$

Since we have chosen reaction-specific parameters for perturbation, the matrix of nonnormalized parameter elasticities contains nonzero entries in the main diagonal and zeros elsewhere (compare Eq. (2.115)).

$$\frac{\partial \boldsymbol{v}}{\partial \boldsymbol{p}} = \begin{pmatrix} \dfrac{\partial v_1}{\partial p_1} & 0 & & 0 \\ 0 & \dfrac{\partial v_2}{\partial p_2} & & 0 \\ & & \cdots & \\ 0 & 0 & & \dfrac{\partial v_r}{\partial p_r} \end{pmatrix}. \tag{2.142}$$

Therefore, this matrix is regular and has an inverse. Furthermore, we consider the Jacobian matrix

$$\boldsymbol{M} = \boldsymbol{N} \frac{\partial \boldsymbol{v}}{\partial \boldsymbol{S}} = \boldsymbol{N} \tilde{\boldsymbol{\varepsilon}}. \tag{2.143}$$

The Jacobian $\boldsymbol{M}$ is a regular matrix if the system is asymptotically stable and contains no conservation relations. The case with conservation relations is considered below. Here, we may premultiply Eq. (2.141) by the inverse of $\boldsymbol{M}$ and rearrange to get

$$\frac{\partial \boldsymbol{S}^{\text{st}}}{\partial \boldsymbol{p}} = -\left(\boldsymbol{N}\frac{\partial \boldsymbol{v}}{\partial \boldsymbol{S}}\right)^{-1} \boldsymbol{N}\frac{\partial \boldsymbol{v}}{\partial \boldsymbol{p}} = -\boldsymbol{M}^{-1}\boldsymbol{N}\frac{\partial \boldsymbol{v}}{\partial \boldsymbol{p}} \equiv \tilde{\boldsymbol{R}}^S. \tag{2.144}$$

As indicated, $\partial \boldsymbol{S}^{\text{st}}/\partial \boldsymbol{p}$ is the matrix of nonnormalized response coefficients for concentrations. Postmultiplication by the inverse of the nonnormalized parameter elasticity matrix gives

$$\frac{\partial \boldsymbol{S}^{\text{st}}}{\partial \boldsymbol{p}} \left(\frac{\partial \boldsymbol{v}}{\partial \boldsymbol{p}}\right)^{-1} = -\left(\boldsymbol{N}\frac{\partial \boldsymbol{v}}{\partial \boldsymbol{S}}\right)^{-1} \boldsymbol{N} = \tilde{\boldsymbol{C}}^S. \tag{2.145}$$

This is the matrix of nonnormalized concentration control coefficients. The right (middle) site contains no parameters. This means, that the control coefficients do not depend on the particular choice of parameters to exert the perturbation as long as Eq. (2.115) is fulfilled. The control coefficients are only dependent on the structure of the network represented by the stoichiometric matrix $\boldsymbol{N}$, and on the kinetics of the individual reactions, represented by the nonnormalized elasticity matrix $\tilde{\boldsymbol{\varepsilon}} = \partial \boldsymbol{v}/\partial \boldsymbol{S}$.

The implicit differentiation of

$$\boldsymbol{J} = \boldsymbol{v}(\boldsymbol{S}^{\text{st}}(\boldsymbol{p}), \boldsymbol{p}), \tag{2.146}$$

with respect to the parameter vector $\boldsymbol{p}$ leads to

$$\frac{\partial \boldsymbol{J}}{\partial \boldsymbol{p}} = \frac{\partial \boldsymbol{v}}{\partial \boldsymbol{p}} + \frac{\partial \boldsymbol{v}}{\partial \boldsymbol{S}}\frac{\partial \boldsymbol{S}^{\text{st}}}{\partial \boldsymbol{p}} = \left(\boldsymbol{I} - \frac{\partial \boldsymbol{v}}{\partial \boldsymbol{S}}\left(\boldsymbol{N}\frac{\partial \boldsymbol{v}}{\partial \boldsymbol{S}}\right)^{-1}\boldsymbol{N}\right)\frac{\partial \boldsymbol{v}}{\partial \boldsymbol{p}} \equiv \tilde{\boldsymbol{R}}^J. \tag{2.147}$$

This yields, after some rearrangement, an expression for the nonnormalized flux control coefficients:

$$\frac{\partial \boldsymbol{J}}{\partial \boldsymbol{p}}\left(\frac{\partial \boldsymbol{v}}{\partial \boldsymbol{p}}\right)^{-1} = \boldsymbol{I} - \frac{\partial \boldsymbol{v}}{\partial \boldsymbol{S}}\left(\boldsymbol{N}\frac{\partial \boldsymbol{v}}{\partial \boldsymbol{S}}\right)^{-1}\boldsymbol{N} = \tilde{\boldsymbol{C}}^J. \tag{2.148}$$

The normalized control coefficients are (by use of Eq. (2.120))

$$C^J = I - (\mathrm{dg}J)^{-1} \left(\frac{\partial v}{\partial S} \left(N \frac{\partial v}{\partial S} \right)^{-1} N \right) (\mathrm{dg}J) \quad \text{and}$$

$$C^S = -(\mathrm{dg}S^{\,\mathrm{st}})^{-1} \left(\left(N \frac{\partial v}{\partial S} \right)^{-1} N \right) (\mathrm{dg}J). \tag{2.149}$$

These equations can easily be implemented for numerical calculation of control coefficients or used for analytical computation. They are also suited for derivation of the theorems of MCA. The summation theorems for the control coefficients follow from Eq. (2.149) by postmultiplication with the vector $\mathbf{1}$ (the row vector containing only 1s), and consideration of the relations $(\mathrm{dg}J) \cdot \mathbf{1} = J$ and $NJ = 0$. The connectivity theorems result from postmultiplication of Eq. (2.149) with the elasticity matrix $\boldsymbol{\varepsilon} = (\mathrm{dg}J)^{-1} \cdot (\partial v / \partial S) \cdot \mathrm{dg}S^{\mathrm{st}}$, and using that multiplication of a matrix with its inverse yields the identity matrix I of respective type.

If the reaction system involves conservation relations, we eliminate dependent variables as explained in Section 1.2.4. In this case, the nonnormalized coefficients read

$$\tilde{C}^J = I - \frac{\partial v}{\partial S} L \left(N_R \frac{\partial v}{\partial S} \right)^{-1} N_R \quad \text{and} \quad \tilde{C}^{\,\mathrm{S}} = -L \left(N_R \frac{\partial v}{\partial S} \right)^{-1} N_R \tag{2.150}$$

and the normalized control coefficients are obtained by applying Eq. (2.120).

An example for calculation of flux control coefficients can be found in the web material.

To investigate the implications of control distribution, we will now analyze the control pattern in an unbranched pathway:

$$S_0 \xrightarrow{v_1} S_1 \xrightarrow{v_2} S_2 \cdots S_{r-1} \overset{v_r}{\leftrightarrow} S_r \tag{2.151}$$

with linear kinetics $v_i = k_i S_{i-1} - k_{-i} S_i$, the equilibrium constants $q_i = k_i / k_{-i}$ and fixed concentrations of the external metabolites, S_0 and S_r. In this case, one can calculate an analytical expression for the steady-state flux,

$$J = \frac{S_0 \prod\limits_{j=1}^{r} q_j - S_r}{\sum\limits_{l=1}^{r} \frac{1}{k_l} \prod\limits_{m=l}^{r} q_m} \tag{2.152}$$

as well as an analytical expression for the flux control coefficients

$$C_i^J = \left(\frac{1}{k_i} \prod_{j=i}^{r} q_j \right) \cdot \left(\sum_{l=1}^{r} \frac{1}{k_l} \prod_{m=l}^{r} q_m \right)^{-1}. \tag{2.153}$$

Let us consider two very general cases. First assume that all reactions have the same individual kinetics, $k_i = k_+$, $k_{-i} = k_-$ for $i = 1, \ldots, r$ and that the equilibrium constants, which are also equal, satisfy $q = k_+ / k_- > 1$. In this case, the ratio of two subsequent flux control coefficients is

$$\frac{C_i^J}{C_{i+1}^J} = \frac{k_{i+1}}{k_i} q_i = q > 1. \tag{2.154}$$

Hence, the control coefficients of the preceding reactions are larger than the control coefficients of the succeeding reactions and flux control coefficients are higher in the beginning of a chain than in the end. This is in agreement with the frequent observation that flux control is strongest in the upper part of an unbranched reaction pathway.

Now assume that the individual rate constants might be different, but that all equilibrium constants are equal to one, $q_i = 1$ for $i = 1, \ldots, r$. This implies $k_i = k_{-i}$. Equation (2.153) simplifies to

$$C_i^J = \frac{1}{k_i} \cdot \left(\sum_{l=1}^{r} \frac{1}{k_l} \right)^{-1}. \tag{2.155}$$

Consider now the relaxation time $\tau_i = 1/(k_i + k_{-i})$ (see Section 4.3) as a measure for the rate of an enzyme. The flux control coefficient reads

$$C_i^J = \frac{\tau_i}{\tau_1 + \tau_2 + \cdots + \tau_r}. \tag{2.156}$$

This expression helps to elucidate two aspects of metabolic control. First, all enzymes participate in the control since all enzymes have a positive relaxation time. There is no enzyme that has all control, i.e., determines the flux through the pathway alone. Second, slow enzymes with a higher relaxation time exert in general more control than fast enzymes with a short relaxation time.

The predictive power of flux control coefficients for directed changes of flux is illustrated in the following example.

Example 2.16

Assume that we can manipulate the pathway shown in Figure 2.12 by changing the enzyme concentration in a predefined way. We would like to explore the effect of the perturbation of the individual enzymes. For a linear pathway (see Eqs. (2.151)–(2.153)) consisting of four consecutive reactions, we calculate the flux control coefficients. For $i = 1, \ldots, 4$, it shall hold that (i) all enzyme concentrations $E_i = 1$, (ii) the rate constants be $k_i = 2$, $k_{-i} = 1$, and (iii) the concentrations of the external reactants be $S_0 = S_4 = 1$. The resulting flux is $J = 1$ and the flux control coefficients are $\mathbf{C}^J = (\,0.533 \quad 0.267 \quad 0.133 \quad 0.067\,)^{\mathsf{T}}$ according to Eq. (2.149).

If we now perturb slightly the first enzyme, lets say perform a percentage change of its concentration, i.e., $E_1 \rightarrow E_1 + 1\%$, then Eq. (2.105) implies that the flux increases as $J \rightarrow J + C_1^J \cdot 1\%$. In fact, the flux in the new steady state is $J^{E_1 \rightarrow 1.01 \cdot E_1} = 1.00531$. Increasing E_2, E_3, or E_4 by 1% leads to flux values of 1.00265, 1.00132, and 1.00066, respectively. A strong perturbation would not yield similar effects. This is illustrated in Figure 2.12.
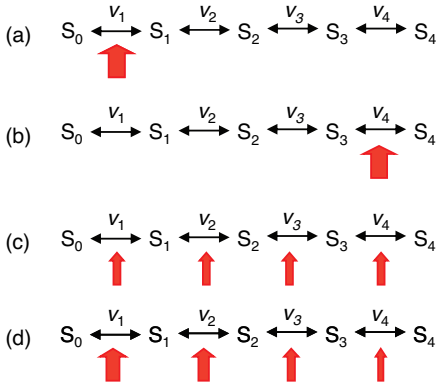
Figure 2.12 Effect of enzyme concentration change on steady-state flux and on flux control coefficients in an unbranched pathway consisting of four reactions. In the reference state, all enzymes have the concentration 1 (in arbitrary units), the control distribution is the same as in case (c), and the steady-state flux is $J = 1$. (a) Change of $E_1 \rightarrow 5E_1$ while keeping the other enzyme concentrations constant results in a remarkable drop of control of the first enzyme. The resulting flux is $J^{E_1 \rightarrow 5 \cdot E_1} = 1.7741$. (b) The change $E_4 \rightarrow 5E_4$ corresponds to $J^{E_4 \rightarrow 5 \cdot E_4} = 1.0563$. There is only slight change of control distribution. (c) Equal enzyme concentrations with $E_i \rightarrow 2E_i, i = 1, \ldots, 4$ results in $J^{E_i \rightarrow 2 \cdot E_i} = 2$. (d) Optimal distribution of enzyme concentration $E_1 = 3.124$, $E_2 = 2.209$, $E_3 = 1.562$, $E_4 = 1.105$ resulting in the maximal steady-state flux $J^{max} = 2.2871$.
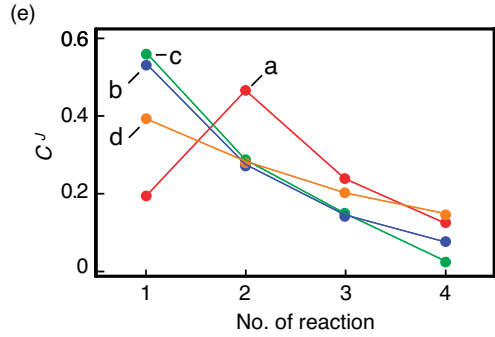
2.4
Tools and Data Formats for Modeling

Summary

This section gives an overview about different simulation techniques and introduces tools, resources, and standard formats used in systems biology. Modeling and simulation functionalities of the tools are presented and common data formats used by these tools and in general in systems biology are introduced. Furthermore, model databases and databases of cellular and biochemical reaction networks are discussed.

The development of models of biological and in particular cellular systems starts by the collection of the model components and its interactions. Usually, in the first step, one formulates the biochemical reaction equations that define the topological structure of the reaction network and the reaction stoichiometries. For this purpose, it is often also useful to draw a diagram that illustrates the network structure either of the whole model or of a particular part. Once the reaction network and its stoichiometry are defined, a more detailed mathematical model can be constructed. For this purpose, often systems of ODEs are applied. Usually, this requires very detailed

information about the kinetics of the individual reactions or appropriate assumptions have to be made.

In this section, databases are presented that provide information on the network structure of cellular processes such as metabolic pathways and signal transduction pathways. Moreover, data formats used for the structural, mathematical, and graphical description of biochemical reaction networks are introduced. We will start this section with an overview of simulation techniques and of software tools that support the user by the development of models.

2.4.1
Simulation Techniques

In systems biology, different simulation techniques are used such as systems of ODEs, stochastic methods, Petri nets, π-calculus, PDEs, cellular automata (CA) methods, agent-based systems, and hybrid approaches. The use of ODEs in biological modeling is widespread and by far the most common simulation approach in computational systems biology [39, 40]. The description of a biological model by a system of ODEs has already been discussed in the earlier sections. Some ODEs are simple enough to be solved analytically and have an exact solution. More complex ODE systems, as they are occurring in most systems biology simulations, must be solved numerically by appropriate algorithms. A first method for the numerical solution of ODEs was derived by Newton and Gauss. Methods that provide more improved computational accuracy are, for instance, Runge–Kutta algorithms and implicit methods that can also handle so-called stiff differential equations. Simulation tools for systems biology have to cope with systems of multiple reactants and multiple reactions. For the numerical integration of such complex ODE systems, they usually make use of more advanced programs such as LSODA [41, 42], CVODE [43], or LIMEX [44]. In the following, Petri nets and CA are described in more detail.

2.4.1.1 Petri Nets
An alternative to ODEs for the simulation of time-dependent processes are Petri nets. A Petri net is a graphical and mathematical modeling tool for discrete and parallel systems. The mathematical concept was developed in the early 1960s by Carl Adam Petri. The basic elements of a Petri net are places, transitions and arcs that connect places and transitions. When represented graphically, places are shown as circles and transitions as rectangles. Places represent objects (e.g., molecules, cars, and machine parts) and transitions describe if and how individual objects are inter-converted. Places can contain zero or more tokens, indicating the number of objects that currently exist. If a transition can take place (can fire) or not depends on the places that are connected to the transition by incoming arcs, to contain enough tokens. If this condition is fulfilled, the transition fires and changes the state of the system by removing tokens from the input places and adding tokens to the output places. The number of tokens that are removed and added depends on the weights of the arcs.

Petri nets are not only an optically pleasing representation of a system but can also be described mathematically in terms of integer arithmetic. For simple types of Petri nets, certain properties can thus be calculated analytically, but often the net has to be run to study the long-term system properties. Over the years many, extensions to the basic Petri net model have been developed for the different simulation purposes [45].

1. Hybrid Petri nets that add the possibility to have places that contain a continuous token number instead of discrete values.
2. Timed Petri nets extend transitions to allow for a specific time delay between the moment when a transition is enabled and the actual firing.
3. Stochastic Petri nets that go one step further and allow a random time delay drawn from a probability distribution.
4. Hierarchical Petri nets, in which modularity is introduced by representing whole nets as a single place or transition of a larger net.
5. Colored Petri nets that introduce different types (colors) or tokens and more complicated firing rules for transitions.

With these extensions, Petri nets are powerful enough to be used for models in systems biology. Biochemical pathways can be modeled with places representing metabolites, transitions representing reactions and stoichiometric coefficients are encoded as different weights of input and output arcs. Consequently, Petri nets have been used to model metabolic networks [46, 47] and signal transduction pathways [48]. Many free and commercial tools are available to explore the behavior of Petri nets. The *Petri Nets World* webpage (http://www.informatik. uni-hamburg.de/TGI/PetriNets/) is an excellent starting point for this purpose.

2.4.1.2 Cellular Automata
Cellular Automata (CA) are tools for the simulation of temporal or spatiotemporal processes using discrete time and/or spatial steps (see Section 3.4.1.3). A cellular automaton consists of a regular grid or lattice of nearly identical components, called cells, where each cell has a certain state of a finite number of states. The states of the cells evolve synchronously in discrete time steps according to a set of rules. Each particular state of cell is determined by the previous states of its neighbors. CA were invented in the late 1940s by von Neumann and Ulam. A well-known CA simulation is Conway's Game of Life [49].

2.4.2
Simulation Tools

In the following, three different simulation tools are presented that essentially make use of ODE systems for simulation, and come along with further functionalities important for modeling, such as graphical visualization of the reaction network, advanced analysis techniques, and interfaces to external model and pathway databases. Further modeling and simulation tools are presented in Chapter 17. Modeling

and simulations tools have also been reviewed by Alves *et al.* [50], Klipp *et al.* [51], Materi and Wishart [52], and Wierling *et al.* [53].

Modeling systems have to accomplish several requirements. They must have a well-defined internal structure for the representation of model components and reactions, and optionally functionalities for the storage of a model in a well-defined structure, standardized format, or database. Further desired aspects are a user-friendly interface for model development, a graphical representation of reaction networks, a detailed description of the mathematical model, integrated simulation engines, e.g., for deterministic or stochastic simulation, along with graphical representations of those simulation results, and functionalities for model analysis and model refinement. This is a very broad spectrum of functionalities. Existing tools cover different aspects of these functionalities. In the following, systems biology tools will be introduced that already accomplish several of the desired aspects. CellDesigner is one of those widely used in the systems biology community [51]. It has a user-friendly process diagram editor, uses the Systems Biology Markup Language (SBML; see Section 2.4.3.1) for model representation and exchange, and provides fundamental simulation and modeling functions. Another program with similar functionalities is COPASI. COPASI has an interface for the model definition and representation and provides several methods for simulation, model analysis, and refinement such as parameter scanning, MCA, optimization, or parameter estimation. Similarly, also PyBioS has rich functionalities for model design, simulation, and analysis. In contrast to the stand-alone programs CellDesigner and Copasi, PyBioS is a web application. A particular feature of PyBioS is its interfaces to pathway databases, like Reactome or KEGG, which can directly be used for model generation.

2.4.2.1 CellDesigner

CellDesigner provides an advanced graphical model representation along with an easy to use user-interface and an integrated simulation engine [54]. The current version of CellDesigner is 4.0.1. The process diagram editor of CellDesigner supports a rich set of graphical elements for the description of biochemical and gene-regulatory networks. Networks can be constructed from compartments, species, and reactions. CellDesigner comes with a large number of predefined shapes that can be used for different types of molecules, such as proteins, receptors, ion channels, small metabolites, etc. It is also possible to modify the symbols to indicate phosphor-ylations or other modifications. The program also provides several icons for special reaction types like catalysis, transport, inhibition, and activation. For version 4.0, it is announced that the graphical elements are compliant with the Systems Biology Graphical Notation (SBGN; see Section 2.4.3.3).

Reading and writing of the models is SBML-based (see Section 2.4.3.1 for more details on SBML) and the models written by CellDesigner pass the online validation at http://sbml.org/tools/htdocs/sbmltools.php and thus are conform with the SBML standard. A nice feature in this respect is the ability to display the SBML model structure as a tree (Figure 2.13, left side). A click on a species or reaction in this tree highlights the corresponding elements in the graphics canvas and in the matching tab on the right side showing further details. This tab is also the place where initial
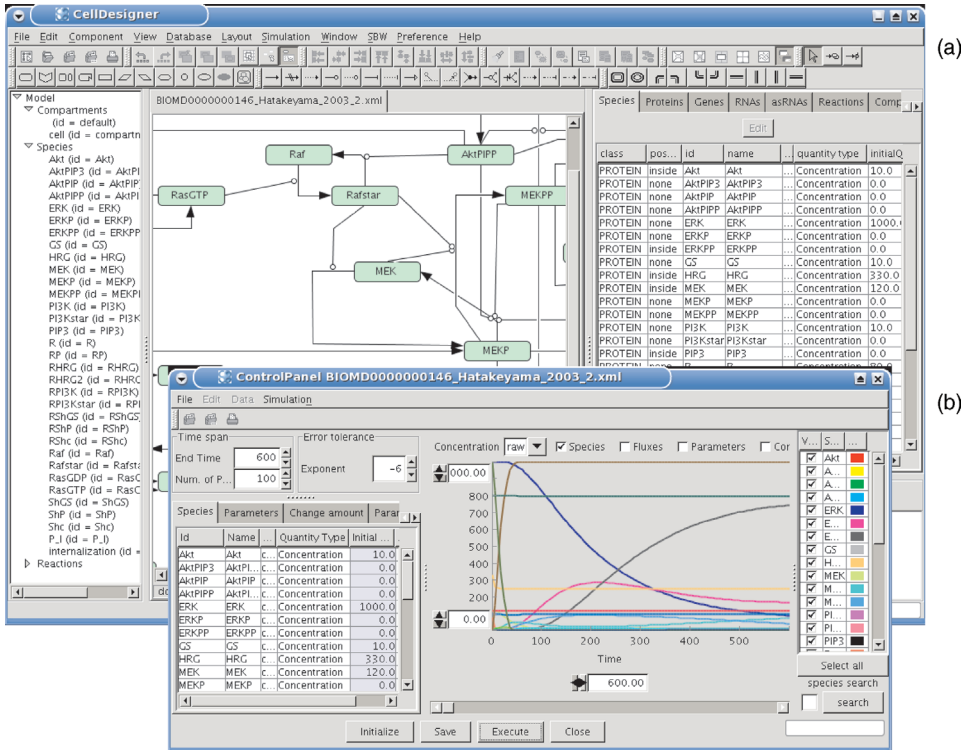
Figure 2.13 CellDesigner's process diagram editor (a) supports a rich set of graphical elements for different cellular species and reaction types. Simulations can be performed in CellDesigner using its integrated simulation engine (b).

concentrations and reaction details are entered. CellDesigner allows entering arbitrary kinetic equations, but has unfortunately no list of standard kinetics (mass action or Michaelis–Menten) that could be applied. For each reaction, the rate law has to be typed in by hand. A connection to the Systems Biology Workbench (SBW, see Section 17.4) is realized via the SBW menu and provides an interface to communicate with other SBW-compliant programs. For a further introduction to CellDesigner, a tutorial can be obtained at its website (http://www.celldesigner.org/). A movie introducing the usage of CellDesigner is availabe from the website of this book.

2.4.2.2 COPASI

Another platform-independent and user-friendly biochemical simulator that offers several unique features is COPASI [55]. COPASI is the successor to Gepasi [56, 57]. Its current version is 4.4 (http://www.copasi.org/). COPASI does not have such a rich visualization of the reaction network as CellDesigner, but it provides advanced functionalities for model simulation and analysis. In contrast to many other tools, it can switch between stochastic and deterministic simulation methods and supports hybrid deterministic-stochastic methods.
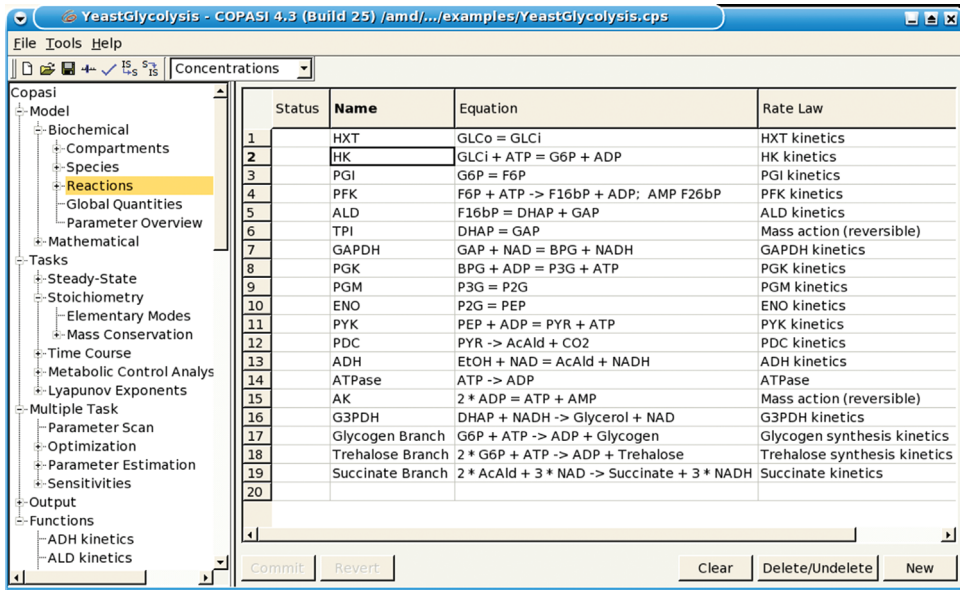
Figure 2.14 The different functionalities of COPASI are arranged in a hierarchical menu at left-hand side of its user interface. Details about the individual methods are listed in the right panel.

The user interface has a hierarchical menu (Figure 2.14, left side) that provides access to all the different functionalities of the tool. The biochemical model can be browsed according to its compartments, metabolites, and reactions including detailed list of the initial concentrations and kinetic parameters of the model. COPASI has a comprehensive set of standard methodologies for model analysis. It comprises the computation of steady states and their stability, supports the analysis of the stoichiometric network, e.g., the computation of elementary modes [25], supports MCA, and has methods for the optimization and parameter estimation. For compatibility with other tools, COPASI also supports the import and export of SBML-based models. For the definition of the kinetics, COPASI provides a copious set of predefined kinetic laws to choose from. A movie that is introducing the usage of COPASI is available from the website of this book.

2.4.2.3 PyBioS

Similarly as CellDesigner and Copasi, also PyBioS is designed for applications in systems biology and supports modeling and simulation [53]. PyBioS is a web-based environment (http://pybios.molgen.mpg.de/) that provides a framework for the conduction of kinetic models of various sizes and levels of granularity. The tool is a modeling platform for editing and analyzing biochemical models in order to predict the time-dependent behavior of the models. The platform has interfaces to external pathway databases (e.g., Reactome and KEGG) that can directly be used during model development for the definition of the structure of the reaction system. Figure 2.15
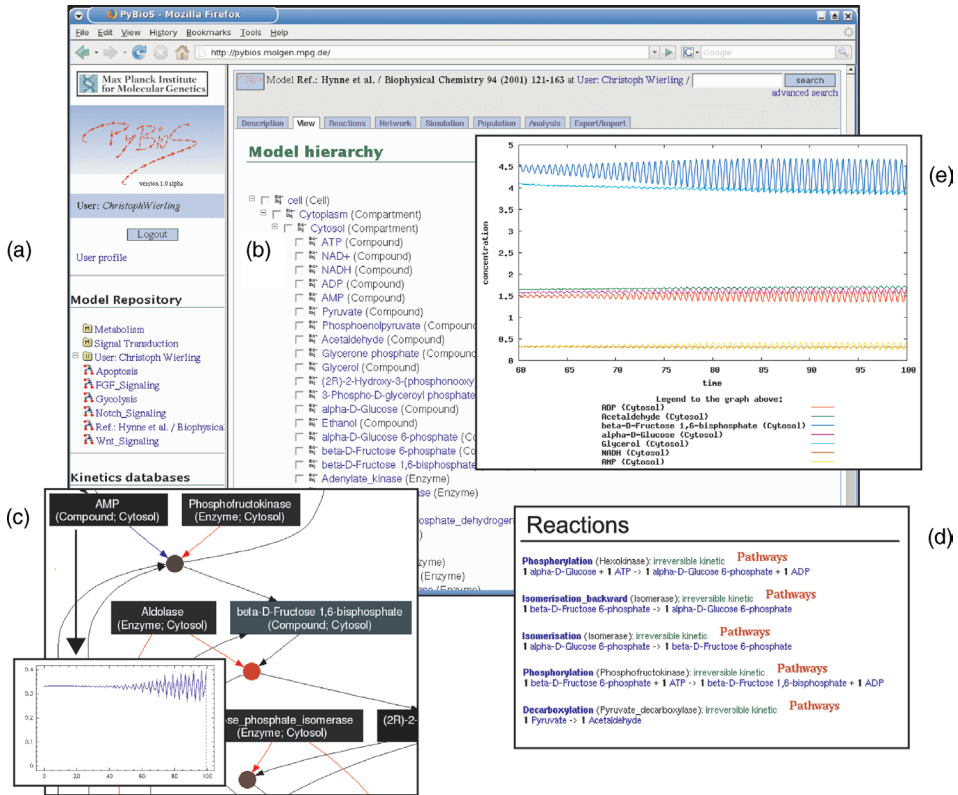
Figure 2.15 The PyBioS simulation environment. A particular model can be selected from the model repository (a) and its hierarchical model structure can be inspected via the View-tab at the top of the browser-window (b). A graphical representation of the model is provided by an automatically generated network diagram (accessible via the Network-tab), for example (c) shows the forward and reverse reaction of the isomerization of glucose-phosphate to fructose-phosphate of a glycolysis model. The Reactions-tab offers an overview of all reactions of the model (d). Simulations can be performed via the Simulation-tab (e). A simulation is based on an automatically generated mathematical model derived from the corresponding object-oriented model that comprises the network of all reactions and their respective kinetics.

shows screenshots of the PyBioS modeling and simulation environment. PyBioS defines a set of object classes (e.g., cell, compartment, compound, protein, complex, gene) for the definition of hierarchical models. Models are stored in a model repository. Support for the export and import of SBML-based models makes the platform compatible with other systems biology tools. Besides time course simulation, PyBioS also provides analysis methods, e.g., for the identification of steady states and their stability or for sensitivity analysis, such as the analysis of the steady-state behavior versus a varying parameter value or the computation of metabolic control coefficients. The reaction network of a model or individual parts of it can be visualized by network diagrams of the model components and their reactions that are

connected via edges. Time course results of simulation experiments can be plotted into the network graphs and used for the interpretation of the model behavior.

2.4.3
Data Formats

The documentation and exchange of models need to be done in a defined way. In the easiest way – as usually found in publications – the biochemical reactions and the mathematical equations that are describing the model can be listed, using common formalism for the representation of biochemical and mathematical equations. These conventions provide a good standard for the documentation and exchange in publications. However, these formats are suitable for humans but not for the direct processing by a computer. This gave rise to the development of standards for the description of models. During the last years, the eXtensible Markup Language (XML, http://www.w3.org/XML) has been proved to be a flexible tool for the definition of standard formats. In the following text, a brief introduction to XML as well as a description of SBML, a standard for model description that is based on XML, is given. Moreover, BioPAX, a standard for the description cellular reaction systems, and SBGN, a standard for the graphical representation of reaction networks, will be described.

2.4.3.1 Systems Biology Markup Language

The Systems Biology Markup Language (SBML, http://www.sbml.org) is a free and open format for the representation of models common to research in many areas of computational biology, including cell signaling pathways, metabolic pathways, gene regulation, and others [58]. It is already supported by many software tools [59]. In January 2009, the SBML homepage listed more than 110 software systems supporting SBML. Currently, there are two SBML specifications denoted Level 1 and Level 2. Level 2 is the most recent specification and therefore it is described in the following text.

SBML is defined as an XML compliant format. XML documents are written as plain text and have a very clear and simple syntax that can easily be read by both humans and computer programs; however, it is generally intended to be written and read by computers, not humans. In XML, information is associated with tags indicating the type or formatting of the information. Tags are used to delimit and denote parts of the document or to add further information to the document structure. Using miscellaneous start tags (e.g., `<tag>`) and end tags (e.g., `</tag>`), information can be structured as text blocks in a hierarchical manner.

Example 2.17

The following example of the phosphorylation reaction of aspartate catalyzed by the aspartate kinase illustrates the general structure of an SBML file.

$$\text{Aspartate} + \text{ATP} \xrightarrow{\text{Aspartate kinase}} \text{Aspartyl phosphate} + \text{ADP}$$
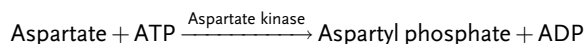
```
(1) <?xml version="1.0" encoding="UTF-8"?>
(2)  <sbml level="2" version="1" xmlns="http://www.
sbml.org/sbml/level2">
(3)  <model id="AK_reaction">
(4)   <listOfUnitDefinitions>
(5)    <unitDefinition id="mmol">
(6)     <listOfUnits>
(7)      <unit kind="mole" scale="-3" />
(8)     </listOfUnits>
(9)    </unitDefinition>
(10)    <unitDefinition id="mmol_per_litre_per_sec">
(11)     <listOfUnits>
(12)      <unit kind="mole" scale="-3" />
(13)      <unit kind="litre" exponent="-1" />
(14)      <unit kind="second" exponent="-1" />
(15)     </listOfUnits>
(16)    </unitDefinition>
(17)   </listOfUnitDefinitions>
(18)   <listOfCompartments>
(19)     <compartment id="cell" name="Cell" size="1"
units="volume" />
(20)   </listOfCompartments>
(21)   <listOfSpecies>
(22)     <species id="asp" name="Aspartate"
compartment="cell" initialConcentration="2"
substanceUnits="mmol" />
(23)     <species id="aspp" name="Aspartyl phosphate"
compartment="cell" initialConcentration="0"
substanceUnits="mmol" />
(24)    <species id="atp" name="ATP" compartment="cell"
initialConcentration="0" substanceUnits="mmol" />
(25)    <species id="adp" name="ADP" compartment="cell"
initialConcentration="0" substanceUnits="mmol" />
(26)   </listOfSpecies>
(27)   <listOfReactions>
(28)    <reaction id="AK" reversible="false">
(29)     <listOfReactants>
(30)      <speciesReference species="asp"
stoichiometry="1" />
(31)      <speciesReference species="atp"
stoichiometry="1" />
(32)     </listOfReactants>
(33)     <listOfProducts>
(34)      <speciesReference species="aspp"
stoichiometry="1" />
```

```
(35)      <speciesReference species="adp" stoichiometry=
"1" />
(36)      </listOfProducts>
(37)      <kineticLaw>
(38)       <math xmlns="http://www.w3.org/1998/Math/
MathML">
(39)       <apply>
(40)        <times />
(41)         <ci> k </ci>
(42)         <ci> asp </ci>
(43)         <ci> atp </ci>
(44)         <ci> cell </ci> <ci> cell </ci>
(45)        </apply>
(46)       </math>
(47)       <listOfParameters>
(48)       <parameter id="k" value="2.25" units="per_mM_
and_min" />
(49)       </listOfParameters>
(50)      </kineticLaw>
(51)    </reaction>
(52)   </listOfReactions>
(53)  </model>
(54) </sbml>
```

Line 1 in the above example defines the document as a XML document. The SBML model is coded in lines 2–54. It is structured into several lists that define different properties of the model. Most important lists that are usually used are the definition of units (lines 4–17), of compartments (lines 18–20), of species (lines 21–26), and finally of the reactions themselves (lines 27–52). Most entries in SBML have one required attribute, id, to give the instance a unique identifier by which other parts of the SBML model definition can refer to it. Some base units, like gram, meter, liter, mole, second, etc., are already predefined in SBML. More complex units derived from the base units are defined in the list of units. For instance, mM/s that is equal to $\text{mmol} \cdot l^{-1} \sec^{-1}$ can be defined as shown in lines 10–16 and used by its id in the subsequent definition of parameters and initial concentrations. Compartments are used in SBML as a construct for the grouping of model species. They are defined in the list of compartments (lines 18–20) and can be used not only for the definition of cellular compartments but also for grouping in general. Each compartment can have a name attribute and defines a compartment size. Model species are defined in the list of species. Each species has a recommended id attribute that can be used to refer it and can define its name and initial value with its respective unit. Species identifiers are used in the list of reactions (lines 27–52) for the definition of the individual biochemical reactions. Reversibility of a reaction is indicated by an attribute of the reaction tag

(lines 28). Reactants and products of a specific reaction along with their respective stoichiometry are specified in separate lists (lines 29–36).

The kinetic law of an individual reaction (lines 37–50) is specified in MathML for SBML Level 2. MathML is an XML-based markup language especially created for the representation of complicated mathematical expressions. In the above example, the rate law reads $k \cdot [asp] \cdot [atp] \cdot cell^2$, where k is a kinetic parameter [asp] and [atp] are the concentrations of aspartate and ATP, respectively, and cell is the volume of the cell. The consideration of the cell volume is needed, since rate laws in SBML are expressed in terms of amount of substance abundance per time instead of the traditional expression in terms of amount of substance concentration per time. The formulation of the rate law in the traditional way embodies the tacit assumption that the participating reaction species are located in the same, constant volume. This is done because attempting to describe reactions between species located in different compartments that differ in volume by the expression in terms of concentration per time quickly leads to difficulties.

2.4.3.2 BioPAX

Another standard format that is used in systems biology and designed for handling information on pathways and topologies of biochemical reaction networks is BioPAX (http://www.biopax.org). While SBML is tuned toward the simulation of models of molecular pathways, BioPAX is a more general and expressive format for the description of biological reaction systems even it is lacking definitions for the representation of dynamic data such as kinetic laws and parameters. BioPAX is defined by the BioPAX working group (http://www.biopax.org/). The BioPax Ontology defines a large set of classes for the description of pathways, interactions, and biological entities as well as their relations. Reaction networks described by BioPAX can be represented by the use XML. Many systems biology tools and databases make use of BioPAX for the exchange of data.

2.4.3.3 Systems Biology Graphical Notation

Graphical representations of reaction networks prove as very helpful tools for the work in systems biology. The graphical representation of a reaction system is not only helpful during the design of a new model and as a representation of the model topology, it is also helpful for the analysis and interpretation for instance of simulation results. Traditionally, diagrams of interacting enzymes and compounds have been written in an informal manner of simple unconstrained shapes and arrows. Several diagrammatic notations have been proposed for the graphical representation (e.g., [60–64]). As a consequence of the different proposals, the Systems Biology Graphical Notation (SBGN) has been set up recently. It provides a common graphical notation for the representation of biochemical and cellular reaction networks. SBGN defines a comprehensive set of symbols, with precise semantics, together with detailed syntactic rules defining their usage. Furthermore, SBGN defines how such graphical information is represented in a machine-readable form to ensure its proper storage, exchange, and reproduction of the graphical representation.

SBGN defines three different diagram types: (i) State Transition diagrams that are depicting all molecular interactions taking place, (ii) Activity Flow diagrams that are representing only the flux of information going from one entity to another, and (iii) Entity Relationship diagrams that are representing the relationships between different molecular species. In a State Transition diagram, each node represents a given state of a species, and therefore a given species may appear multiple times. State Transition diagrams are suitable for following the temporal process of interactions. A drawback of State Transition diagrams, however, is that the representation of each individual state of a species results quickly in very large diagram and due to this, it becomes difficult to understand what interactions actually exist for the species in question. In such a case, an Entity Relation diagram is more suitable. In an Entity Relation diagram, a biological entity appears only once.

SBGN defines several kinds of symbols, whereas two types of symbols are distinguished: nodes and arcs. There are different kinds of nodes defined. Reacting state or entity nodes represent, e.g., macromolecules, such as protein, RNA, DNA, polysaccharide, or simple chemicals, such as a radical, an ion, or a small molecule. Container nodes are defined for the representation of a complex, compartment, or module. Different transition nodes are defined for the representation of transitions like biochemical reactions, associations, like protein-complex formation, or dissociations, like the dissociation of a protein complex. The influence of a node onto another is visualized by different types of arcs representing, e.g., consumption, production, modulation, stimulation, catalysis, inhibition, or trigger effect. Not all node and arc symbols are defined for each of the three diagram types. A detailed description of the different nodes, arcs, and the syntax of their usage by the different diagram types is given in the specification of SBGN (see http://sbgn.org/).

Examples of a State Transition and an Entity Relationship diagram is given in Figure 2.16.

2.4.3.4 Standards for Systems Biology

With the increasing amount of data in modern biology the requirement of standards used for data integration became more and more important. For example, in the course of a microarray experiment, a lot of different information accumulates, as information about the samples, the type of microarray that is used, the experimental procedure including the hybridization experiment, the data normalization, and the expression data itself. It turns out that an important part of systems biology is data integration. This requires a conceptual design and the development of common standards.

The development of a standard involves four steps: an informal design of a conceptual model, a formalization, the development of a data exchange format, and the implementation of supporting tools [65]. For micorarray experiments, a conceptual model about the minimum information that is required for the description of such an experiment is specified by MIAME (Minimum Information About a Microarray Experiment [65]). Similar specifications have also been done for, e.g., proteomics data with MIAPE (Minimum Information About a Proteomics Experiment [66]), or systems biology models with MIRIAM (Minimum information
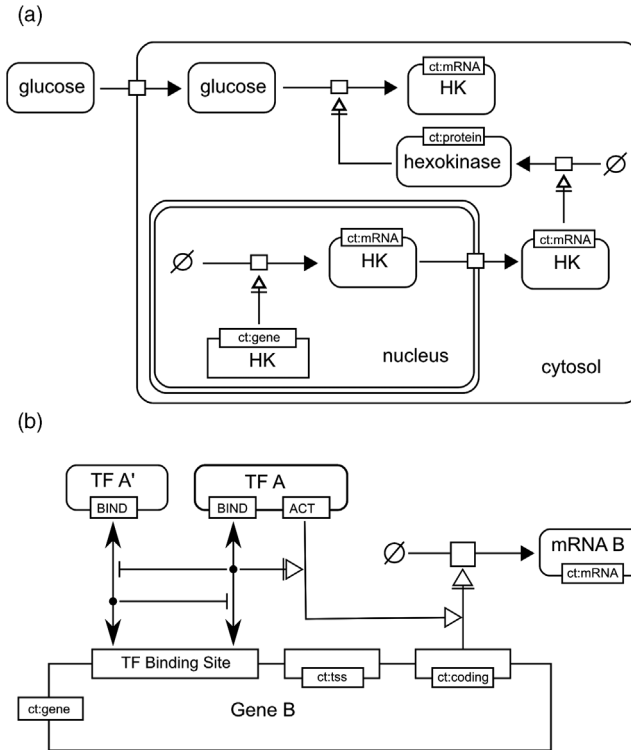
Figure 2.16 Systems Biology Graphical Notation (SBGN). (a) State transition diagram. (b) Entity relation diagram describing gene regulation and transcription of a gene. The two transcription factors TF A and TF A′ compete for the same transcription factor-binding site. If one of the transcription factors is bound, the binding site is blocked for the other one, but only TF A can activate the transcription of the gene. The abbreviation "ct" indicates conceptual types of the respective entity.

requested in the annotation of biochemical models). MIRIAM specifies a set of rules for curating quantitative models of biological systems that define procedures for encoding and annotating models represented in machine-readable form [67].

2.4.4
Data Resources

The development of models of biological systems requires diverse kind of data. This is, for instance, information about the different model components (e.g., metabolites, proteins, and genes) and their different functions and interactions. Such information can be extracted from literature or dedicated data resources, like pathway databases. Two pathway databases that are well known are KEGG und Reactome. Both are described below in more detail. Another important data for modeling are information about reaction kinetics. Database dealing with such data are described in

more detail in Sections 2.4.4.2 and 3.1. Further information about databases providing primary data is given in Chapter 16.

2.4.4.1 Pathway Databases

Kyoto Enzyclopedia of Genes and Genomes   Kyoto Enzyclopedia of Genes and Genomes (KEGG; http://www.genome.ad.jp/kegg/) is a reference knowledge base offering information about genes and proteins, biochemical compounds and reactions, and pathways. The data is organized in three parts: the gene universe (consisting of the GENES, SSDB, and KO database), the chemical universe (with the COMPOUND, GLYCAN, REACTION, and ENZYME databases which are merged as LIGAND database), and the protein network consisting of the PATHWAY database [68]. Besides this, the KEGG database is hierarchically classified into categories and subcategories at four levels. The five topmost categories are metabolism, genetic information processing, environmental information processing, cellular processes, and human diseases. Subcategories of metabolism are, e.g., carbohydrate, energy, lipid, nucleotide, or amino acid metabolism. These are subdivided into the different pathways, like glycolysis, citrate cycle, purine metabolism, etc. Finally, the fourth level corresponds to the KO (KEGG Orthology) entries. A KO entry (internally identified by a K number, e.g., K00001 for the alcohol dehydrogenase) corresponds to a group of orthologous genes that have identical functions.

The gene universe offers information about genes and proteins generated by genome sequencing projects. Information about individual genes is stored in the GENES database, which is semiautomatically generated from the submissions to GenBank, the NCBI RefSeq database, the EMBL database, and other publicly available organism-specific databases. K numbers are further assigned to entries of the GENES database. The SSDB database contains information about amino acid sequence similarities between protein-coding genes computationally generated from the GENES database. This is carried out for many complete genomes and results in a huge graph depicting protein similarities with clusters of orthologous and paralogous genes.

The chemical universe offers information about chemical compounds and reactions relevant to cellular processes. It includes more than 11,000 compounds (internally represented by C numbers, e.g., C00001 denotes water), a separate database for carbohydrates (nearly 11,000 entries; represented by a number preceded by G, e.g., G10481 for cellulose), more than 6000 reactions (with R numbers, e.g., R00275 for the reaction of the superoxide radical into hydrogen peroxide), and more than 4000 enzymes (denoted by EC numbers as well as K numbers for orthologous entries). All these data are merged as LIGAND database [69]. Thus, the chemical universe offers comprehensive information about metabolites with their respective chemical structures and biochemical reactions.

KEGG's protein network provides information about protein interactions comprising pathways and protein complexes. The 235 KEGG reference pathway diagrams (maps), offered on the website, give clear overviews of important pathways. Organism-specific pathway maps are automatically generated by coloring of organism-specific genes in the reference pathways.

The KEGG database can be queried via the web interface, e.g., for genes, proteins, compounds, etc. Access to the data via FTP (http://www.genome.ad.jp/anonftp) as well as access to it via a SOAP server (http://www.genome.ad.jp/kegg/soap) is possible for academic users, too.

Reactome   Reactome (formerly known as Genome Knowledgebase [70–72]) is an open, online database of fundamental human biological processes. The Reactome project is managed as a collaboration of the Cold Spring Harbor Laboratory, the European Bioinformatics Institute (EBI), and the Gene Ontology Consortium. The database is divided into several modules of fundamental biological processes that are thought to operate in humans. Each module of the database has one or more primary authors and is further peer reviewed by experts of the specific field. Each module can also be referenced by its revision date and thus can be cited like a publication.

On one hand, the Reactome database is intended to offer valuable information for the wet-lab scientist, who wants to know, e.g., more about a specific gene product she or he is unfamiliar with. On the other hand, the Reactome database can be used by the computational biologist to draw conclusions from large data sets like expression data gained by cDNA chip experiments.

Another tool offered by Reactome is the "Pathfinder." This utility enables the user to find the shortest path between two physical entities, e.g., the shortest path between the metabolites D-fructose and pyruvate, or the steps from the primary mRNA to its processed form. The computed path can be shown graphically. The pathfinder offers also the possibility to exclude specific entities, like the metabolites ATP or NADH that show high connectivity and thus their input might lead to a path that is not the one intended to be found.

Data from Reactome can be exported in various formats upon which are SBML and BioPAX.

2.4.4.2   Databases of Kinetic Data

High-throughput projects, such as the international genome sequencing efforts, accumulate large amounts of data at an amazing rate. These data are essential for the reconstruction of phylogenetic trees and gene-finding projects. However, for kinetic modeling, which is at the heart of systems biology, kinetic data of proteins and enzymes are needed. Unfortunately, this type of data is notoriously difficult and time-consuming to obtain since proteins often need individually tuned purification and reaction conditions. Furthermore, the results of such studies are published in a large variety of journals from different fields. In this situation, the databases BRENDA and SABIO-RK aim to be comprehensive resources of kinetic data. They are discussed in more detail in Section 4.1.1.

2.4.4.3   Model Databases

A lot of different mathematical models of biological systems have already been developed in the past and are described in the literature. However, these models are usually not available in a computer-amenable format. During the last years, big efforts have been done on the gathering and implementation of existing models in

databases. Two well-known databases on this are BioModels and JWS, which are described in more detail in the following.

BioModels The BioModels.net project (http://biomodels.net) is an international effort to (i) define agreed-upon standards for model curation, (ii) define agreed-upon vocabularies for annotating models with connections to biological data resources, and (iii) provide a free, centralized, publicly accessible database of annotated, computational models in SBML, and other structured formats. The ninth release of the databases has 192 models, of which 150 are in the curated and 42 are in the noncurated branch. Models can be browsed in the web interface, online simulations can be performed via the external simulation engine of JWS online (see below), or they can be exported in several prominent file formats (e.g., SBML, CellML, BioPAX) for external usage by other programs.

JWS Another model repository that is providing kinetic models of biochemical systems is JWS online [73]. As of February 2008, this model repository provides 84 models (http://jjj.biochem.sun.ac.za). Models in JWS online can be interactively run and interrogated over the internet.

Exercises and Problems

1. A canonical view of the upper part of glycolysis starts with glucose and comprises the following reactions (in brackets: possible abbreviations): The enzyme hexokinase (HK, E_1) phosphorylates glucose (Gluc, S_1) to glucose-6-phosphate (G6P, S_2) under consumption of ATP (S_5) and production of ADP (S_6). The enzyme phosphoglucoisomerase (PGI, E_2) converts glucose-6-phosphate to fructose-6-phosphate (F6P, S_3). The enzyme phosphofructokinase (PFK, E_3) phosphorylates F6P a second time to yield fructose-1,6-bisphosphate (F1,6,BP, S_4). The enzyme fructosebisphosphatase catalyzes the reverse reaction (E_4).

   (a) Sketch the reaction network and formulate a set of differential equations (without specifying the kinetics of the individual reactions).
   (b) Formulate the stoichiometric matrix N. What is the rank of N?
   (c) Calculate steady-state fluxes (matrix K) and conservation relations (matrix G).
   (d) Compare your results with Example 2.6.

2. (a) Write down the sets of differential equations for the networks N1–N6 given in Table 2.4 without specifying their kinetics.
   (b) Determine the rank of the stoichiometric matrices, independent steady-state fluxes, and conservation relations.
   Do all systems have a (nontrivial) steady state?

3. Inspect networks N3 and N4 in Table 2.4. Can you find elementary flux modes? Use an available tool (e.g., Metatool) to check out.

4. Assign the following kinetics to network N3 in Table 2.4: $\nu_1 = k_1$, $\nu_2 = (V_{max2} \cdot S_1)/(K_{m2} + S_1)$, $\nu_3 = (V_{max3} \cdot S_1)/(K_{m3} + S_1)$ with $k_1 = 10$, $V_{max2} = 3$, $K_{m2} = 0.2$, V_{max2} 5, and $K_{m2} = 0.4$. Compute the steady-state concentration of S_1 and calculate the flux control coefficients.

5. For the reaction system $A \xrightarrow{\nu_1} B$, $B \xrightarrow{\nu_2} C$, $C \xrightarrow{\nu_3} A$ with $\nu_1 = k_1 \cdot A$, $\nu_2 = k_2 \cdot B$, $\nu_3 = k_3 \cdot C$, and $k_1 = 2$, $k_2 = 2$, $k_3 = 1$, write down the set of systems equations.

   (a) Compute the Jacobian **J**!
   (b) Determine the eigenvalues and eigenvectors of the Jacobian **J**!
   (c) What is the general solution of the ODE system?
   (d) Compute the solution with the initial condition $A(0) = 1$, $B(0) = 1$, $C(0) = 0$!

6. The Jacobian $\mathbf{A}_a$ of the following ODE system depends on the parameter a:

$$\frac{d}{dt} \begin{pmatrix} x \\ y \end{pmatrix} = \begin{pmatrix} 0 & -1 \\ 10 + a & a \end{pmatrix} \begin{pmatrix} x \\ y \end{pmatrix}$$

   (a) To every specific choice of parameter a belongs a point $(\mathrm{Tr}\,\mathbf{A}_a, \mathrm{Det}\,\mathbf{A}_a)$ in the plane spaned by trace and determinate of $\mathbf{A}_a$. Draw the curve $(\mathrm{Tr}\,\mathbf{A}_a, \mathrm{Det}\,\mathbf{A}_a)$ in this space for a as a changing parameter.
   (b) For which values of a is $(x,y) = (0,0)$ a saddle point, node or focus?

7. What is the use of standards important for the development of new systems biology tools?

References

1 Guldberg, C.M. and Waage, P. (1879) Über die chemische Affinität. *Journal fur Praktische Chemie*, **19**, 69.

2 Guldberg, C.M. and Waage, P. (1867) *Études sur les affinités chimiques*, Christiana.

3 Waage, P. and Guldberg, C.M. (1864) *Studies concerning affinity*, Forhandlinger: Videnskabs-Selskabet, Christiana, pp 35.

4 Brown, A.J. (1902) Enzyme action. *Journal of the Chemical Society*, **81**, 373–386.

5 Michaelis, L. and Menten, M.L. (1913) Kinetik der invertinwirkung. *Biochemistry Zeitung*, **49**, 333–369.

6 Briggs, G.E. and Haldane, J.B.S. (1925) A note on the kinetics of enzyme action. *The Biochemical Journal*, **19**, 338–339.

7 Lineweaver, H. and Burk, D. (1934) The determination of enzyme dissocation

constants. *Journal of the American Chemical Society*, **56**, 658–660.

8 Eadie, G.S. (1942) The inhibition of cholinesterase by physostigmine and prostigmine. *The Journal of Biological Chemistry*, **146**, 85–93.

9 Hanes, C.S. (1932) Studies on plant amylases. I. The effect of starch concentratio upon the velocity of hydrolysis by the amylase of germinated barley. *The Biochemical Journal*, **26**, 1406–1421.

10 Haldane, J.B.S. (1930) *Enzymes*, Longmans, Green and Co., London.

11 Schellenberger, A. (1989) *Enzymkatalyse*, Fischer Verlag, Jena.

12 Wegscheider, R. (1902) Über simultane Gleichgewichte und die Beziehungen

zwischen Thermodynamik und Reaktionskinetik homogener Systeme. *Zeitschrift für Physikalische Chemie*, **39**, 257–303.

13 Hill, A.V. (1910) The possible effects of the aggregation of the molecules of hemoglobin on its dissociation curves. *The Journal of Physiology*, **40**, iv–vii.

14 Hill, A.V. (1913) The combinations of hemoglobin with oxygen and with carbon monoxide. *The Biochemical Journal*, **7**, 471–480.

15 Monod, J. *et al.* (1965) On the nature of allosteric transitions: A plausible model. *Journal of Molecular Biology*, **12**, 88–118.

16 Savageau, M. (1985) Mathematics of organizationally complex systems. *Biomed Biochim Acta*, **44**, 839–884.

17 Heijnen, J.J. (2005) Approximative kinetic formats used in metabolic network modelling. *Biotechnology and Bioengineering*, **91**, 534–545.

18 Liebermeister, W. and Klipp, E. (2006) Bringing metabolic networks to life: convenience rate law and thermodynamic constraints. *Theoretical Biology and Medical Modelling*, **3**, 42.

19 Glansdorff, P. and Prigogine, I. (1971) *Thermodynamic Theory of Structure, Stability and Fluctuations*, Wiley-Interscience, London.

20 Reder, C. (1988) Metabolic control theory: a structural approach. *Journal of Theoretical Biology*, **135**, 175–201.

21 Heinrich, R. and Schuster, S. (1996) *The Regulation of Cellular Systems*, Chapman & Hall, New York.

22 Michal, G. (1999) *Biochemical Pathways*, Spektrum Akademischer, Heidelberg.

23 Pfeiffer, T. *et al.* (1999) METATOOL: for studying metabolic networks. *Bioinformatics (Oxford, England)*, **15**, 251–257.

24 Schilling, C.H. *et al.* (1999) Metabolic pathway analysis: basic concepts and scientific applications in the post-genomic era. *Biotechnology Progress*, **15**, 296–303.

25 Schuster, S. *et al.* (1999) Detection of elementary flux modes in biochemical networks: a promising tool for pathway analysis and metabolic engineering. *Trends in Biotechnology*, **17**, 53–60.

26 Schuster, S. *et al.* (2000) A general definition of metabolic pathways useful for systematic organization and analysis of complex metabolic networks. *Nature Biotechnology*, **18**, 326–332.

27 Schuster, S. *et al.* (2002) Reaction routes in biochemical reaction systems: algebraic properties, validated calculation procedure and example from nucleotide metabolism. *Journal of Mathematical Biology*, **45**, 153–181.

28 Schilling, C.H. and Palsson, B.O. (2000) Assessment of the metabolic capabilities of *Haemophilus influenzae* Rd through a genome-scale pathway analysis. *Journal of Theoretical Biology*, **203**, 249–283.

29 Schilling, C.H. *et al.* (2000) Theory for the systemic definition of metabolic pathways and their use in interpreting metabolic function from a pathway-oriented perspective. *Journal of Theoretical Biology*, **203**, 229–248.

30 Wiback, S.J. and Palsson, B.O. (2002) Extreme pathway analysis of human red blood cell metabolism. *Biophysical Journal*, **83**, 808–818.

31 Bronstein, I.N. and Semendjajew, K.A. (1987) Taschenbuch der Mathematik, 23rd edition, Nauka, Moscow.

32 Heinrich, R. and Rapoport, T.A. (1974) A linear steady-state treatment of enzymatic chains. General properties, control and effector strength. *European Journal of Biochemistry*, **42**, 89–95.

33 Kacser, H. and Burns, J.A. (1973) The control of flux. *Symposia of the Society for Experimental Biology*, **27**, 65–104.

34 Bruggeman, F.J. *et al.* (2002) Modular response analysis of cellular regulatory networks. *Journal of Theoretical Biology*, **218**, 507–520.

35 Hofmeyr J.H. and Westerhoff, H.V. (2001) Building the cellular puzzle: control in multi-level reaction networks. *Journal of Theoretical Biology*, **208**, 261–285.

36 Kholodenko, B.N. *et al.* (2000) Diffusion control of protein phosphorylation in

signal transduction pathways. *The Biochemical Journal*, **350** (Pt 3), 901–907.

37 Liebermeister, W. *et al.* (2004) A theory of optimal differential gene expression. *Bio Systems*, **76**, 261–278.

38 Westerhoff, H.V. *et al.* (2002) ECA: control in ecosystems. *Molecular Biology Reports*, **29**, 113–117.

39 de Jong, H. (2002) Modeling and simulation of genetic regulatory systems: a literature review. *Journal of Computational Biology: A Journal of Computational Molecular Cell Biology*, **9**, 67–103.

40 Kitano, H. (2002) Computational systems biology. *Nature*, **420**, 206–210.

41 Hindmarsh, A.C. (1983) ODEPACK, A systematized collection of ODE solvers, in *Scientific Computing* (eds R.S. Stepleman *et al.*) North-Holland, Amsterdam, pp. 55–64.

42 Petzold, L. (1983) Automatic selection of methods for solving stiff and nonstiff systems of ordinary differential equations. *SIAM Journal on Scientific and Statistical Computing*, **4**, 136–148.

43 Cohen, S.D. and Hindmarsh, A.C. (1996) CVODE, a stiff/nonstiff ODE solver in C. *Computers in Physics*, **10**, 138–143.

44 Deuflhard, P. and Nowak, U. (1987) Extrapolation integrators for quasilinear implicit ODEs, in *Large Scale Scientific Computing* (eds P. Deuflhard and B. Engquist) Birkkäuser, Basel, pp. 37–50.

45 Bernardinello, L. and de Cindio, F. (1992) *A Survey of Basic Net Models and Modular Net Classes*, Springer, Berlin.

46 Küffner, R. *et al.* (2000) Pathway analysis in metabolic databases via differential metabolic display (DMD). *Bioinformatics*, **16**, 825–836.

47 Reddy, V.N. *et al.* (1996) Qualitative analysis of biochemical reaction systems. *Computers in Biology and Medicine*, **26**, 9–24.

48 Matsuno, H. *et al.* (2003) Biopathways representation and simulation on hybrid functional Petri net. *In Silico Biology*, **3**, 389–404.

49 Gardner, M. (1970) Mathematical games. *Scientific American*, **223**, 120–123.

50 Alves, R. *et al.* (2006) Tools for kinetic modeling of biochemical networks. *Nature Biotechnology*, **24**, 667–672.

51 Klipp, E. *et al.* (2007b) Systems biology standards – the community speaks. *Nature Biotechnology*, **25**, 390–391.

52 Materi, W. and Wishart, D.S. (2007) Computational systems biology in drug discovery and development: methods and applications. *Drug Discovery Today*, **12**, 295–303.

53 Wierling, C. *et al.* (2007) Resources, standards and tools for systems biology. *Briefings in Functional Genomics and Proteomics*, **6**, 240–251.

54 Funahashi, A. *et al.* (2003) CellDesigner: a process diagram editor for gene-regulatory and biochemical networks. *Biosilico*, **1**, 159–162.

55 Hoops, S. *et al.* (2006) COPASI – a COmplex PAthway SImulator. *Bioinformatics*, **22**, 3067–3074.

56 Mendes, P. (1993) GEPASI: a software package for modelling the dynamics steady states and control of biochemical and other systems. *Computer Applications in the Biosciences*, **9**, 563–571.

57 Mendes, P. (1997) Biochemistry by numbers: simulation of biochemical pathways with Gepasi 3. *Trends in Biochemical Sciences*, **22**, 361–363.

58 Hucka, M. *et al.* (2003) The systems biology markup language (SBML): a medium for representation and exchange of biochemical network models. *Bioinformatics*, **19**, 524–531.

59 Hucka, M. *et al.* (2004) Evolving a lingua franca and associated software infrastructure for computational systems biology: the Systems Biology Markup Language (SBML) project. *Systematic Biology (Stevenage)*, **1**, 41–53.

60 Kitano, H. (2003) A graphical notation for biochemical networks. *BIOSILICO*, **1**, 169–176.

61 Kitano, H. *et al.* (2005) Using process diagrams for the graphical representation of biological networks. *Nature Biotechnology*, **23**, 961–966.

62 Kohn, K.W. (1999) Molecular interaction map of the mammalian cell cycle control and DNA repair systems. *Molecular Biology of the Cell*, **10**, 2703–2734.

63 Moodie, S.L. *et al.* (2006) A graphical notation to describe the logical interactions of biological pathways. *Journal of Integrative Bioinformatics*, **3**, 36.

64 Pirson, I. *et al.* (2000) The visual display of regulatory information and networks. *Trends in Cell Biology*, **10**, 404–408.

65 Brazma, A. *et al.* (2001) Minimum information about a microarray experiment (MIAME)-toward standards for microarray data. *Nature Genetics*, **29**, 365–371.

66 Taylor, C.F. *et al.* (2007) The minimum information about a proteomics experiment (MIAPE). *Nature Biotechnology*, **25**, 887–893.

67 Le Novere, N. *et al.* (2005) Minimum information requested in the annotation of biochemical models (MIRIAM). *Nature Biotechnology*, **23**, 1509–1515.

68 Kanehisa, M. *et al.* (2004) The KEGG resource for deciphering the genome. *Nucleic Acids Research*, **32**, D277–D280.

69 Goto, S. *et al.* (2002) LIGAND: database of chemical compounds and reactions in biological pathways. *Nucleic Acids Research*, **30**, 402–404.

70 Joshi-Tope, G. *et al.* (2003) The genome knowledgebase: a resource for biologists and bioinformaticists. *Cold Spring Harbor Symposia on Quantitative Biology*, **68**, 237–243.

71 Joshi-Tope, G. *et al.* (2005) Reactome: a knowledgebase of biological pathways. *Nucleic Acids Research*, **33**, D428–D432.

72 Vastrik, I. *et al.* (2007) Reactome: a knowledge base of biologic pathways and processes. *Genome Biology*, **8**, R39.

73 Olivier, B.G. and Snoep, J.L. (2004) Web-based kinetic modelling using JWS Online. *Bioinformatics*, **20**, 2143–2144.

3
Specific Biochemical Systems

Systems biology aims to understand structure, function, regulation, or development of biological systems by combining experimental and computational approaches. It is important to understand that different parts of cellular organization are studied and understood in different ways and to different extent. This is related to diverse experimental techniques that can be used to measure the abundance of metabolites, proteins, mRNA, or other types of compounds. For example, enzyme kinetic measurements are performed for more than a century, while mRNA measurements (e.g., as microarray data) or protein measurements (e.g., as mass spectrometry analysis) have been developed more recently. Not all data can be provided with the same accuracy and reproducibility. These and other complications in studying life caused a nonuniform progress in modeling different parts of cellular life. Moreover, the diversity of scientific questions and the availability of computational tools to tackle them led to the development of very different types of models for different biological processes. In this chapter, we will introduce a number of classical and more recent areas of systems biological research. In the following, we discuss modeling of metabolic systems, signaling pathways, cell cycle regulation, and development and differentiation, primarily with ODE systems, as well as spatial modeling of biochemical systems. In the web-material, we introduce approaches to synthetic biology, population dynamics, aging, and pharmacokinetics.

3.1
Metabolic Systems

Summary

Living cells require energy and material for building membranes, storing molecules, turnover of enzymes, replication and repair of DNA, movement, and many other processes. Through metabolism, cells acquire energy and use it to build new cells. Metabolism is the means by which cells survive and reproduce. Metabolism is the general term for two kinds of reactions: (1) catabolic reactions (breakdown of complex compounds to get energy and building blocks) and (2) anabolic reactions

(construction of complex compounds used in cellular functioning). Metabolism is a highly organized process. It involves hundreds or thousands of reactions that are catalyzed by enzymes.

Metabolic networks consist of reactions transforming molecules of one type into molecules of another type. In modeling terms, the concentrations of the molecules and their rates of change are of special interest. In Chapter 2, we explained how to study such networks on three levels of abstraction:

1. Enzyme kinetics investigates the dynamic properties of the individual reactions in isolation.
2. The network character of metabolism is studied with stoichiometric analysis considering the balance of compound production and degradation.
3. Metabolic control analysis quantifies the effect of perturbations in the network employing the dynamics of individual concentration changes and their integration in the network.

Here, we will illustrate the theoretical concepts by applying them to a number of examples. We will specifically discuss cellular energy metabolism focusing on glycolysis and the threonine pathway as an example of amino acid synthesis. You may find the complete models and many other models also in modeling databases such as JWS online [1].

3.1.1
Basic Elements of Metabolic Modeling

Metabolic networks are defined by the enzymes converting substrates into products in a reversible or irreversible manner. Without enzymes, those reactions are essentially impossible or too slow. But networks are also characterized by the metabolites that are converted by the various enzymes. Biochemical studies have revealed a number of important catabolic pathways and pathways of the energy metabolism such as glycolysis, the pentose-phosphate pathway, the tricarboxylic acid (TCA) cycle, and oxidative phosphorylation. Among the known anabolic pathways are gluconeogenesis, amino acid synthesis pathways, and synthesis of fatty acids and nucleic acids. Databases such as the Kyoto Encyclopedia of Genes and Genomes Pathway (KEGG, http://http://www.genome.jp/kegg/pathway.html) provide a comprehensive overview of pathways in various organisms.

Here, we will focus on pathway characteristics, which are essential for modeling. Figure 3.1 provides a summary of the first steps to build a model. First, we can sketch the metabolites and the converting reactions in a cartoon to get an overview and an intuitive understanding. Based on that cartoon and on further information, we must set the limits of our model. That means, we must consider what kind of question we want to answer with our model, what information in terms of qualitative and quantitative data is available, and how we can make the model as simple as possible but as comprehensive as necessary. Then, for every compound, which is part of the system, we formulate the balance equations (see also Section 2.2) summing up all reaction that produce the compound (with a positive

(a) Basic Elements of Metabolic Networks
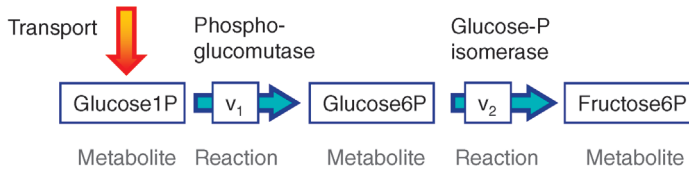
(b) Design of Structured Dynamic Models

1. Setting system limits

2. Balancing

$$\frac{d}{dt}G6P = v_1 - v_2$$

3. Assignment of Kinetics

$$v_1 = \frac{V_{\text{max},1} \cdot G1P}{K_{\text{m},1} + G1P} \qquad v_2 = \frac{V_{\text{max},2} \cdot G6P}{K_{\text{m},2} + G6P}$$
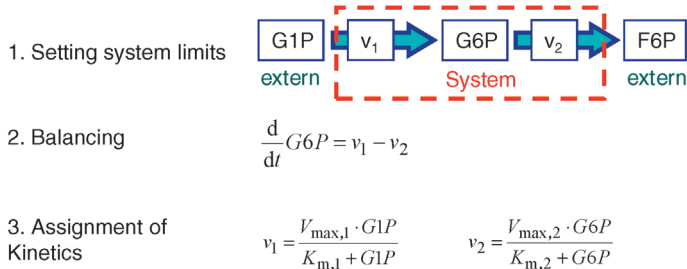
Figure 3.1 Designing metabolic models. (a) Basic elements of metabolic networks and (b) basic steps for designing structured dynamic models (see the text for further explanation).

sign) and all reaction that degrade the compound (with a negative sign). At this stage, the model is suited for a network analysis such as stoichiometric analysis (Section 2.2) or, with some additional information, flux balance analysis (Section 9.1). In order to study the dynamics of the system, we must add kinetic descriptions to the individual reactions. Keep in mind that the reaction kinetics may depend on

- the concentrations of substrates and products (here G1P and G6P),
- specific parameters such as K_{m}-values,
- the amount and activity of the catalyzing enzyme (here hidden in the V_{max} values, see Section 2.1), and
- the activity of modifiers, which are not shown in the example in Figure 3.1.

In the following, we will discuss in more detail models for three pathways: the upper glycolysis, the full glycolysis, and the threonine synthesis.

3.1.2
Toy Model of Upper Glycolysis

A first model of the upper part of glycolysis is depicted in Figure 3.2. It comprises six reactions and six metabolites. Note that we neglect the formation of phosphate P_i here. The ODE system reads
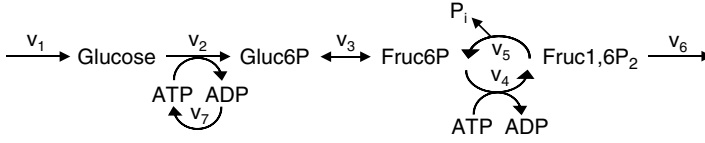
Figure 3.2 Toy model of the upper glycolysis. The model involves the reactions glucose uptake (v_1), the phosphorylation of glucose under conversion of ATP to ADP by the enzyme hexokinase (v_2), intramolecular rearrangments by the enzyme phosphoglucoisomerase (v_3), a second phosphorylation (and ATP/ADP conversion) by phosphofructokinase (v_4), dephosphorylation without involvement of ATP/ADP by fructose-bisphosphatase (v_5), and splitting of the hexose (6-C-sugar) into two trioses (3-C-sugars) by aldolase (v_6). Abbreviations: Gluc-6P – glucose-6-phosphate, Fruc-6P – fructose-6-phosphate, Fruc-1,6P$_2$ – fructose-1,6-bisphosphate.

$$\frac{\mathrm{d}}{\mathrm{d}t} Glucose = v_1 - v_2$$

$$\frac{\mathrm{d}}{\mathrm{d}t} Gluc6P = v_2 - v_3$$

$$\frac{\mathrm{d}}{\mathrm{d}t} Fruc6P = v_3 - v_4 + v_5 \tag{3.1}$$

$$\frac{\mathrm{d}}{\mathrm{d}t} Fruc1,6P_2 = v_4 - v_5 - v_6$$

$$\frac{\mathrm{d}}{\mathrm{d}t} ATP = -\frac{\mathrm{d}}{\mathrm{d}t} ADP = -v_2 - v_4 + v_7.$$

With mass action kinetics, the rate equations read $v_1 = \text{const.} = k_1$, $v_2 = k_2 \cdot Glucose \cdot ATP$, $v_3 = k_3 \cdot Gluc6P - k_{-3} \cdot Fruc6P$, $v_4 = k_4 \cdot Fruc6P \cdot ATP$, $v_5 = k_5 \cdot Fruc1,6P_2$, $v_6 = k_6 \cdot Fruc1,6P_2$, and $v_7 = k_7 \cdot ADP$. Given the values of the parameters k_i, $i = 1,\ldots,7$ and the initial concentrations, one may simulate the time behavior of the network as depicted in Figure 3.3.

We see that starting with zero concentrations of all hexoses (here glucose, fructose, and their phosphorylated versions), they accumulate until production and degradation are balanced. Finally, they approach a steady state. ATP rises and then decreases in the same way as ADP decreases and rises, while their sum remains constant. This is due to the conservation of adenine nucleotides, which could be revealed by stoichiometric analysis (Section 2.2).

For this upper glycolysis model, the concentration vector is $S = (Glucose, Gluc6P, Fruc6P, Fruc1,6P_2, ATP, ADP)^{\mathrm{T}}$, the vector of reaction rates is $\mathbf{v} = (v_1, v_2, \ldots, v_7)^{\mathrm{T}}$, and the stoichiometric matrix reads

$$N = \begin{pmatrix} 1 & -1 & 0 & 0 & 0 & 0 & 0 \\ 0 & 1 & -1 & 0 & 0 & 0 & 0 \\ 0 & 0 & 1 & -1 & 1 & 0 & 0 \\ 0 & 0 & 0 & 1 & -1 & -1 & 0 \\ 0 & -1 & 0 & -1 & 0 & 0 & 1 \\ 0 & 1 & 0 & 1 & 0 & 0 & -1 \end{pmatrix}. \tag{3.2}$$

It comprises $r = 7$ reactions and has Rank $N = 5$. Thus, the kernel matrix (see Section 2.2.2) has two linear independent columns. A possible representation is
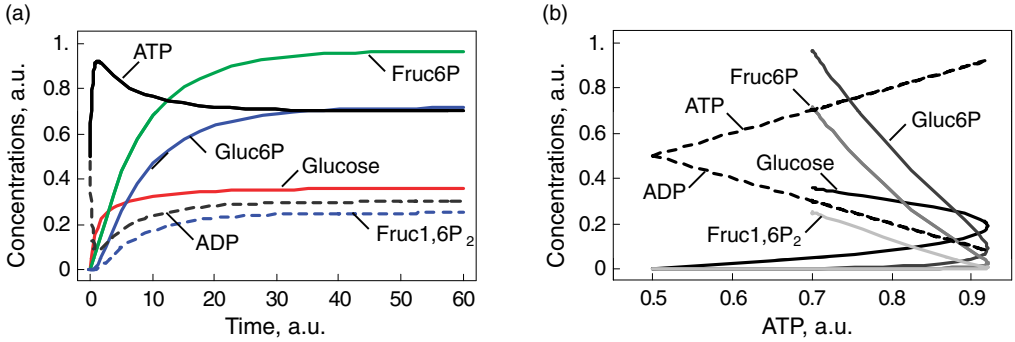
Figure 3.3 Dynamic behavior of the upper glycolysis model (Figure 3.2 and Eq. (3.1)). Initial conditions at $t = 0$: $Glucose(0) = Gluc\text{-}6P(0) = Fruc\text{-}6P(0) = Fruc\text{-}1,6P_2(0) = 0$ and $ATP(0) = ADP(0) = 0.5$ (arbitrary units). Parameters: $k_1 = 0.25, k_2 = 1, k_3 = 1, k_{-3} = 1, k_4 = 1, k_5 = 1, k_6 = 1,$ and $k_7 = 2.5$. The steady-state concentrations are $Glucose^{st} = 0.357, Gluc\text{-}6P^{st} = 0.714, Fruc\text{-}6P^{st} =$ $0.964, Fruc\text{-}1,6P_2^{st} = 0.2,$ and $ATP^{st} = 0.7,$ and $ADP^{st} = 0.25$. The steady-state fluxes are $J_1 = J_2 = J_3 = J_5 = J_6 = 0.25, J_4 = 0.5,$ and $J_7 = 0.75$. (a) Time-course plots (concentration versus time), (b) phase-plane plot (concentrations versus concentration of ATP with varying time); all curves start at $ATP = 0.5$ for $t = 0$.

$$K = (\ k_1 \quad k_2\ ) \quad \text{with} \quad \begin{aligned} k_1 &= (\ 0 \quad 0 \quad 0 \quad 1 \quad 1 \quad 0 \quad 1\ )^T, \\ k_2 &= (\ 1 \quad 1 \quad 1 \quad -1 \quad -2 \quad 1 \quad 0\ )^T. \end{aligned} \tag{3.3}$$

Figure 3.4 shows the flux and concentration control coefficients (see Section 2.3.2) for the model of upper glycolysis in gray scale (see scaling bar). Reaction v_1 has a
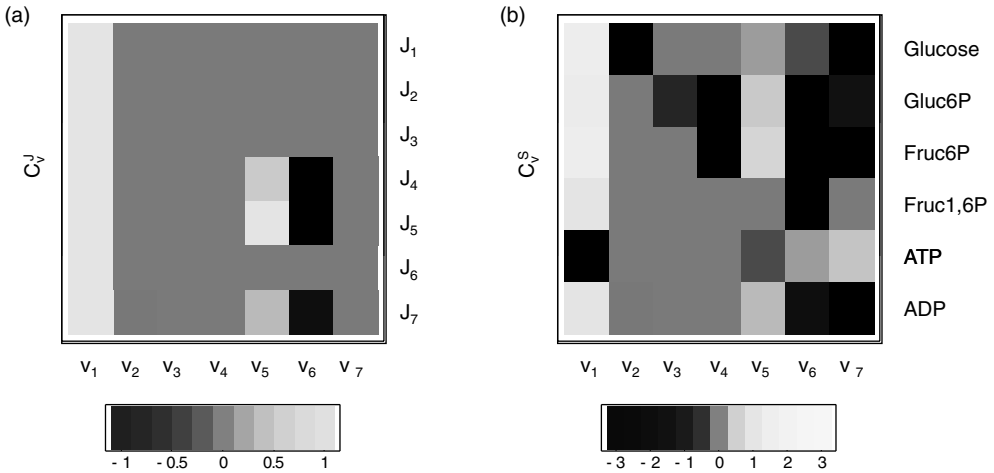
Figure 3.4 Flux and concentration control coefficients for the glycolysis model in Figure 3.2 with the parameters given in the legend of Figure 3.3. Values of the coefficients are indicated in gray-scale: gray means zero control, white or light gray indicates positive control, dark gray or black negative control, respectively.
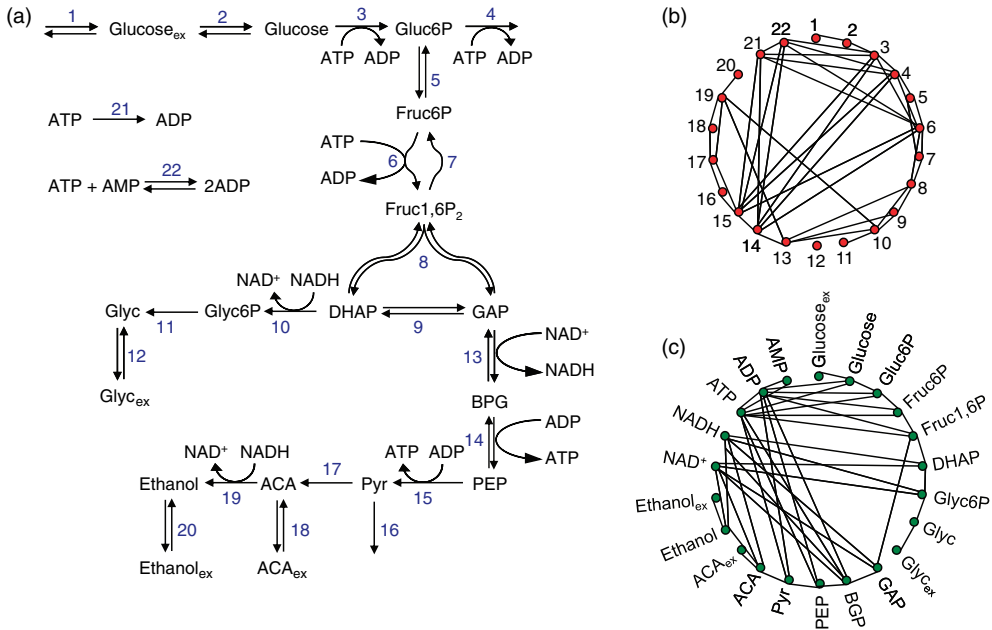
Figure 3.5 Full glycolysis models. (a) Main reactions and metabolites, (b) network of reactions connected by common metabolites, (c) network of metabolites connected by common reactions.

flux control of 1 over all steady-state fluxes, reactions v_2, v_3, v_4, and v_7 have no control over fluxes; they are dominated by v_1. Reactions v_5 and v_6 have positive or negative control over J_4, J_5, and J_7, respectively, since they control the turnover of fructose phosphates.

The concentration control shows a more interesting pattern. As a rule of thumb, it holds that producing reactions have a positive control and degrading reactions have a negative control, such as v_1 and v_2 for glucose. But also distant reactions can exert concentration control, such as v_4 to v_6 over Gluc6P.

More comprehensive models of glycolysis can be used to study details of the dynamics, such as the occurrence of oscillations or the effect of perturbations. Examples are the models of Hynne and colleagues [2] or the Reuss group [3, 4]. An overview of the most important reactions in glycolysis is given in Figure 3.5.

3.1.3
Threonine Synthesis Pathway Model

Threonine is an amino acid, which is essential for birds and mammals. The synthesis pathway from aspartate involves five steps (Figure 3.6). It is known for a long time and has attracted some interest with respect to its economic industrial production for a variety of uses. The kinetics of all the five enzymes from *Escherichia coli* have been
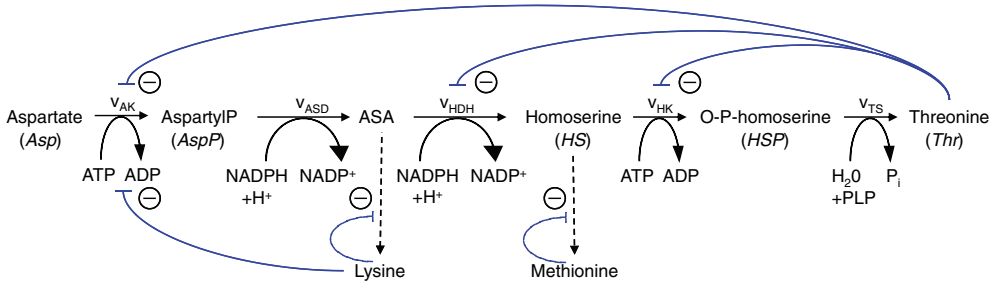
Figure 3.6 Model of the threonine pathway. Aspartate is converted into threonine in five steps. Threonine exerts negative feedback on its producing reactions. The pathway consumes ATP and NADPH.

studied extensively; the complete genome sequence of this organism is now known and there is an extensive range of genetic tools available. The intensive study and the availability of kinetic information make it a good example for metabolic modeling of the pathway.

The reaction system can be described with the following set of differential equations:

$$\frac{\mathrm{d}}{\mathrm{d}t} Asp = -v_{\mathrm{AKI}} - v_{\mathrm{AKIII}}$$

$$\frac{\mathrm{d}}{\mathrm{d}t} AspP = v_{\mathrm{AKI}} + v_{\mathrm{AKIII}} - v_{\mathrm{ASD}}$$

$$\frac{\mathrm{d}}{\mathrm{d}t} ASA = v_{\mathrm{ASD}} - v_{\mathrm{HDH}}$$

$$\frac{\mathrm{d}}{\mathrm{d}t} HS = v_{\mathrm{HDH}} - v_{\mathrm{HK}}$$

$$\frac{\mathrm{d}}{\mathrm{d}t} HSP = v_{\mathrm{HK}} - v_{\mathrm{TS}}$$

$$\frac{\mathrm{d}}{\mathrm{d}t} Thr = v_{\mathrm{TS}},$$

(3.4)

with

$$v_{\mathrm{AKI}} = \frac{V_{\mathrm{AKI}} \cdot \left(Asp \cdot ATP - \frac{AspP \cdot ADP}{K_{\mathrm{eq,AK}}} \right)}{\left(K_{\mathrm{Asp,AKI}} \cdot \frac{1 + \left(\frac{Thr}{K_{\mathrm{iThr,AKI}}} \right)^{h_1}}{1 + \left(\frac{Thr}{\alpha_{\mathrm{AKI}} \cdot K_{\mathrm{iThr,AKI}}} \right)^{h_1}} + AspP \cdot \frac{K_{\mathrm{Asp,AKI}}}{K_{\mathrm{AspP,AKI}}} + Asp \right) \cdot \left(K_{\mathrm{ATP,AKI}} \cdot \left(1 + \frac{ADP}{K_{\mathrm{ADP,AKI}}} \right) + ATP \right)}$$

$K_{\mathrm{eq,AK}} = 6.4 \times 10^{-4}$, $K_{\mathrm{Asp,AKI}} = 0.97 \pm 0.48$ mM, $K_{\mathrm{ATP,AKI}} = 0.98 \pm 0.5$ mM, $K_{\mathrm{AspP,AKI}} = 0.017 \pm 0.004$ mM, $K_{\mathrm{ADP,AKI}} = 0.25$ mM, $K_{\mathrm{iThr,AKI}} = 0.167 \pm 0.003$ mM, $h_1 = 4.09 \pm 0.26$,

$\alpha_{\text{AKI}} = 2.47 \pm 0.17,$

$$v_{\text{AKIII}} = \frac{V_{\text{AKIII}} \cdot \left(Asp \cdot ATP - \frac{AspP \cdot ADP}{K_{\text{eq, AK}}} \right)}{\left(1 + \left(\frac{Lys}{K_{\text{iLys}}} \right)^{h_{\text{Lys}}} \right) \left(K_{\text{Asp, AKIII}} \left(1 + \frac{AspP}{K_{\text{AspP, AKIII}}} \right) + Asp \right) \cdot \left(K_{\text{ATP, AKIII}} \left(1 + \frac{ADP}{K_{\text{ADP, AKIII}}} \right) + ATP \right)}$$

$K_{\text{eq,AK}} = 6.4 \times 10^{-4}, \quad K_{\text{Asp,AK III}} = 0.32 \pm 0.08 \text{ mM}, \quad K_{\text{ATP,AK III}} = 0.22 \pm 0.02 \text{ mM}$
$K_{\text{AspP,AK III}} = 0.017 \pm 0.004 \text{ mM}, \quad K_{\text{ADP,AKIII}} = 0.25 \text{ mM}, \quad K_{\text{iLys}} = 0.391 \pm 0.08 \text{ mM},$
$h_{\text{Lys}} = 2.8 \pm 1.4,$

$$v_{\text{ASD}} = \frac{V_{\text{ASD}} \cdot \left(AspP \cdot NADPH - \frac{ASA \cdot NADP^+ \cdot P_i}{K_{\text{eq, ASD}}} \right)}{\left(K_{\text{AspP, ASD}} \left(1 + \frac{ASA}{K_{\text{ASA, ASD}}} \right) \cdot \left(1 + \frac{P_i}{K_{P_i}} \right) + AspP \right) \cdot \left(K_{\text{NAPDH}} \left(1 + \frac{NADP^+}{K_{\text{NADP}^+}} \right) + NADPH \right)}$$

$K_{\text{eq,ASD}} = 2.84 \times 10^5, \quad K_{\text{AspP,ASD}} = 0.022 \pm 0.001 \text{ mM}, \quad K_{\text{NADPH,ASD}} = 0.029 \pm 0.002$
$\text{mM}, \quad K_{\text{ASA,ASD}} = 0.11 \pm 0.008 \text{ mM}, \quad K_{\text{NADP}^+,\text{ASD}} = 0.144 \pm 0.02 \text{ mM}, \quad K_{P_i} = 10.2 \pm$
$1.4 \text{ mM},$

$$v_{\text{HDH}} = \frac{V_{\text{HDH}} \cdot \left(ASA \cdot NADPH - \frac{HS \cdot NADP^+}{K_{\text{eq,HDH}}} \right)}{\left(\frac{1 + \left(\frac{Thr}{K_{\text{iThr,2}}} \right)^{h_2}}{1 + \left(\frac{Thr}{\alpha_2 \cdot K_{\text{iThr,2}}} \right)^{h_2}} \right) \left(K_{\text{ASA,HDH}} \left(1 + \frac{HS}{K_{\text{HS, HDH}}} \right) + ASA \right) \cdot \left(K_{\text{NADPH,HDH}} \left(1 + \frac{NADP^+}{K_{\text{NADP}^+,\text{AKIII}}} \right) + NADPH \right)}$$

$K_{\text{eq,HDH}} = 1 \times 10^{11} \text{ M}^{-1}, \quad K_{\text{ASA,HDH}} = 0.24 \pm 0.03 \text{ mM}, \quad K_{\text{NADPH,HDH}} = 0.037 \pm$
$0.006 \text{ mM}, \quad K_{\text{hs,HDH}} = 3.39 \pm 0.33 \text{ mM}, \quad K_{\text{NADP}^+,\text{HDH}} = 0.067 \pm 0.006 \text{ mM}, \quad K_{\text{iThr,2}} = 0.097$
$\text{mM}, \quad h_2 = 1.41, \quad \alpha_2 = 3.93,$

$$v_{\text{HK}} = \frac{V_{\text{HK}} \cdot hs \cdot ATP}{\left(K_{\text{HS, HK}} \left(1 + \frac{ATP}{K_{\text{iATP, HK}}} \right) \cdot \left(1 + \frac{Thr}{K_{\text{iThr, HK}}} \right) + hs \right) \cdot \left(K_{\text{ATP, HK}} \left(1 + \frac{hs}{K_{\text{iHS, HK}}} \right) + ATP \right) \cdot \left(1 + \frac{Lys}{K_{\text{iLys, HK}}} \right)}$$

$K_{\text{HS,HK}} = 0.11 \text{ mM}, \quad K_{\text{ATP,HK}} = 0.072 \text{ mM}, \quad K_{\text{iThr,HK}} = 1.09 \text{ mM}, \quad K_{\text{iLys,HK}} = 9.45 \text{ mM},$
$K_{\text{iHS,HK}} = 4.7 \text{ mM}, \quad K_{\text{iATP,HK}} = 4.35 \text{ mM}$

$$v_{\text{TS}} = \frac{V_{\text{TS}} \cdot HSP}{K_{\text{HSP,TS}} + HSP}$$
$$K_{\text{HSP,TS}} = 0.31 \pm 0.03 \text{ mM}.$$

This system has no nontrivial steady state, i.e., no steady state with nonzero flux, since aspartate is always degraded, while threonine is only produced. The same imbalance holds for the couples ATP/ADP and $NADPH + H^+/NADP^+$. The dynamics is shown in Figure 3.7.

Threonine exerts feedback inhibition on the pathway producing it. This is illustrated in Figure 3.8. The higher the threonine concentration, the lower the
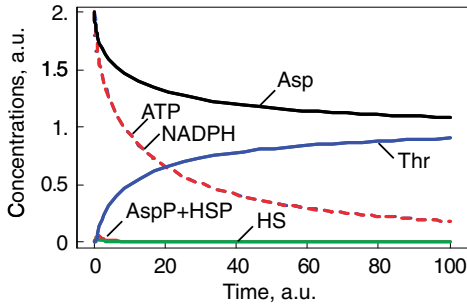
Figure 3.7 Dynamics of the threonine pathway model (Figure 3.6, Eq. (3.4)). The parameters are given in the text.
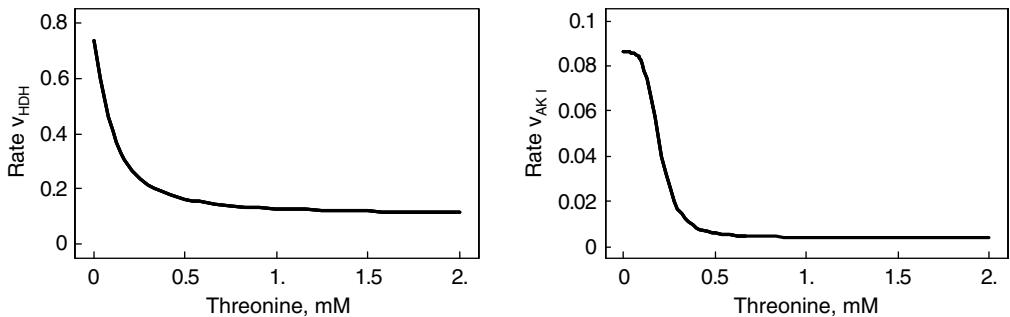
Figure 3.8 Effect of feedback inhibition in the model depicted in Figure 3.6.

rates of inhibited reactions. The effect is that production of threonine is down-regulated as long as its level is sufficient, thereby saving aspartate and energy.

3.2
Signaling Pathways

Summary

This section introduces the structure of different cellular signaling pathways and their typical constituents such as receptors, G proteins, MAP kinase cascades, or phosphorelay systems. Different modeling approaches and various specific models are discussed. We analyze how the structure of pathways encoded in respective model assumptions determines the steady states and dynamic properties of signaling pathways. To describe the dynamic properties of signaling pathways, quantitative measures are used to assess the amplitude and duration of a signal or the crosstalk between distinct signaling pathways.

3.2.1
Introduction

Upon intercellular communication or cellular stress response, the cell senses extracellular signals. They are transformed into intracellular signals and sequences of reactions. Different external changes or events may stimulate signaling. Typical stimuli are hormones, pheromones, heat, cold, light, osmotic pressure, appearance, or concentration change of substances like glucose or K^+, Ca^+, or cAMP.

On a molecular level, signaling involves the same type of processes as metabolism: production or degradation of substances, molecular modifications (mainly phosphorylation, but also methylation, acetylation), and activation or inhibition of reactions. From a modeling point of view, there are some important differences between signaling and metabolism. First, signaling pathways serve for information processing and transfer of information, while metabolism provides mainly mass transfer. Second, the metabolic network is determined by the present set of enzymes catalyzing the reactions. Signaling pathways involve compounds of different types; they may form highly organized complexes and may assemble dynamically upon occurrence of the signal. Third, the quantity of converted material is high in metabolism (amounts are usually given in concentrations on the order of μM or mM) compared to the number of molecules involved in signaling processes (typical abundance of proteins in signal cascades is on the order of $10–10^4$ molecules per cell). Finally, different amounts of components have an effect on the concentration ratio of catalysts and substrates. In metabolism, this ratio is usually low, i.e., the enzyme concentration is much lower than the substrate concentration, which gives rise to the quasi-steady state assumption used in Michaelis–Menten kinetics (Section 2.1). In signaling processes, amounts of catalysts and their substrates are frequently in the same order of magnitude.

Modeling of the dynamic behavior of signaling pathways is often not straightforward. Knowledge about components of the pathway and their interactions is still limited and incomplete. The interpretation of experimental data is context- and knowledge-dependent. Furthermore, the effect of a signal often changes the state of the whole cell, and this implies difficulties for determination of system limits. But in many cases, we may apply the same tools as introduced in Chapter 2.

3.2.2
Function and Structure of Intra- and Intercellular Communication

Cells have a broad spectrum of molecular "facilities" to receive and process signals; not all of them can be considered here. A typical sequence of events in signaling pathways is shown in Figure 3.9 and proceeds as follows.

The "signal" (a substance acting as ligand or a physical stimulus) approaches the cell surface and is bound or sensed by a transmembrane receptor. The receptor changes its state from susceptible to active and stimulates an internal signaling cascade. This cascade frequently includes a series of changes of protein phosphorylation states. Activated proteins may cross the nuclear membrane and, eventually, transcription factors are activated or deactivated. Such a transcription factor

Signaling Paradigm
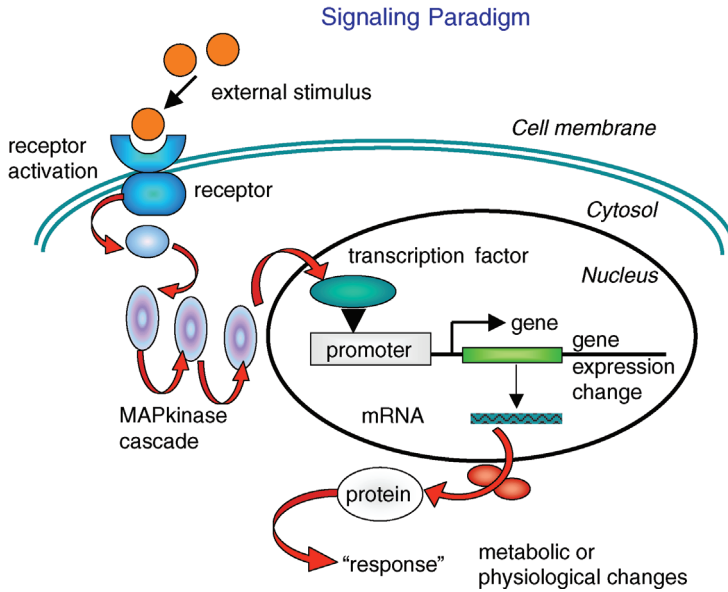
Figure 3.9 Visualization of the signaling paradigm (for description see the text). The receptor is stimulated by a ligand or another kind of signal, and it changes its own state from susceptible to active. The active receptor initiates the internal signaling cascade including a series of protein phosphorylation state changes. Subsequently, transcription factors are activated or deactivated. The transcription factors regulate the transcription rate of a set of genes. The absolute amount or the relative changes in protein concentrations alter the state of the cell and trigger the actual response to the signal.

changes its binding properties to regulatory regions on the DNA upstream of a set of genes; the transcription rate of these genes is altered (typically increased). Either newly produced proteins or the changes in protein concentration cause the actual response of the cell to the signal. In addition to this downstream program, signaling pathways are regulated by a number of control mechanisms including feedback and feed-forward activation or inhibition. Fast tracks of signal transduction work without changes in gene expression by changing binding properties or activity pattern of proteins (e.g., binding of Ste5 to $G\beta\gamma$ or regulation of Fps1 by Hog1P$_2$).

This is the typical picture; however, many pathways may work in completely different manner. As example, an overview on signaling pathways that are stimulated in yeast stress response is given in Figure 3.10.

3.2.3
Receptor–Ligand Interactions

Many receptors are transmembrane proteins; they receive the signal and transmit it. Upon signal sensing, they change their conformation. In the active form, they are able to initiate a downstream process within the cell (Figure 3.11).

Signaling Pathways in Baker's Yeast
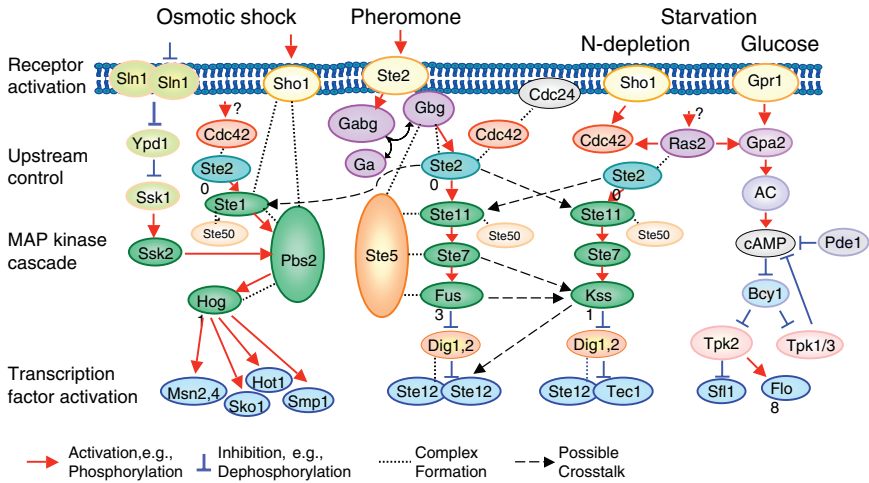
Figure 3.10 Overview on signaling pathways in yeast: HOG pathway activated by osmotic shock, pheromone pathway activated by a pheromone from cells of opposite mating type, and pseudohyphal growth pathway stimulated by starvation conditions. In each case, the signal interacts with the receptor. The receptor activates a cascade of intracellular processes including complex formations, phosphorylations, and transport steps. A MAP kinase cascade is a particular part of many signaling pathways; their components are indicated by bold border. Eventually, transcription factors are activated that regulate the expression of a set of genes. Beside the indicated connections, further interactions of components are possible. For example, crosstalk may occur, that is the activation of the downstream part of one pathway by a component of another pathway. This is supported by the frequent incidence of some proteins like Ste11 in the scheme.

The simplest concept of the interaction between receptor R and ligand L is reversible binding to form the active complex LR:
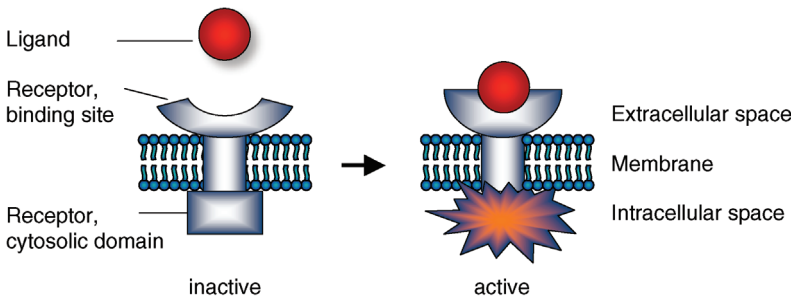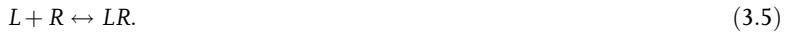
$$L + R \leftrightarrow LR. \tag{3.5}$$

Figure 3.11 Schematic representation of receptor activation.

The dissociation constant is calculated as

$$K_D = \frac{L \cdot R}{LR}. \tag{3.6}$$

Typical values for K_D are 10^{-12}–10^{-6} M.

Cells have the ability to regulate the number and the activity of specific receptors, for example, in order to weaken the signal transmission during long-term stimulation. Balancing production and degradation regulates the number of receptors. Phosphorylation of serine/threonine or tyrosine residues of the cytosolic domain by protein kinases mainly regulates the activity. Hence, a more realistic scenario for ligand–receptor interaction is depicted in Figure 3.12(a).

For a more detailed model, we assume that the receptor is present in an inactive state R_i or in a susceptible state R_s. The susceptible form can interact with the ligand to form the active state R_a. The inactive or the susceptible forms are produced from precursors (v_{pi}, v_{ps}); all three forms may be degraded (v_{di}, v_{ds}, v_{da}). The rates of production and degradation processes as well as the equilibria between different states might be influenced by the cell's state, for example, by the cell-cycle stage. In general, the dynamics of this scenario can be described by the following set of differential equations:

$$\frac{d}{dt} R_i = v_{pi} - v_{di} - v_{is} + v_{si} + v_{ai}$$

$$\frac{d}{dt} R_s = v_{ps} - v_{ds} + v_{is} - v_{si} - v_{sa} + v_{as} \tag{3.7}$$

$$\frac{d}{dt} R_a = -v_{da} + v_{sa} - v_{as} - v_{ai}.$$
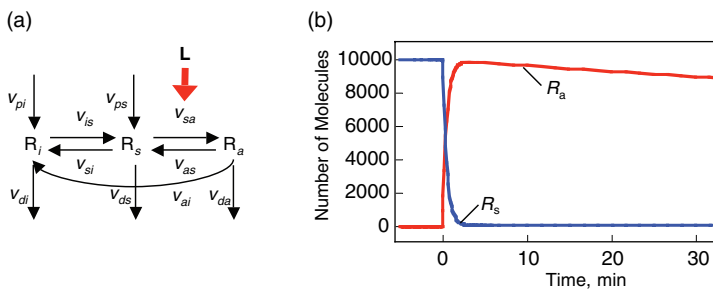
Figure 3.12 Receptor activation by ligand. (a) Schematic representation: L – ligand, R_i – inactive receptor, R_s – susceptible receptor, R_a – active receptor. v_{p*} – production steps, v_{d*} – degradation steps, other steps – transition between inactive, susceptible, and active state of receptor. (b) Time course of active (red line) and susceptible (blue line) receptor after stimulation with 1 µM α-factor at $t = 0$. The total number of receptors is 10,000. The concentration of the active receptor increases immediately and then declines slowly while the susceptible receptor is effectively reduced to zero.

For the production terms, we may either assume constant values or (as mentioned above) rates that depend on the current cell state. The degradation terms might be assumed to be linearly dependent on the concentration of their substrates ($v_{d*} = k_{d*} \cdot R_*$). This may also be a first guess for the state changes of the receptor (e.g., $v_{is} = k_{is} \cdot R_i$). The receptor activation is dependent on the ligand concentration (or any other value related to the signal). A linear approximation of the respective rate is $v_{sa} = k_{sa} \cdot R_s \cdot L$. If the receptor is a dimer or oligomer, it might be sensible to include this information into the rate expression for receptor activation as $v_{sa} = k_{sa} \cdot R_s \cdot K_B^n \cdot L^n / (1 + K_B^n \cdot L^n)$, where K_B denotes the binding constant to the monomer and n the Hill coefficient (Section 2.1, Eq. (2.44)).

Example 3.1

An experimentally confirmed example for the activation of receptor and G protein of the pheromone pathway has been presented by Yi and colleagues [5] for the binding of the pheromone α-factor to the receptor Ste2 in yeast. Concerning the receptor activation dynamics, they report a susceptible and an active form of the receptor, but no inactive form ($R_i = 0$, $v_{*i} = v_{i*} = 0$). The remaining rates are determined as follows:

$$v_{ps} = k_{ps}$$
$$v_{ds} = k_{ds} \cdot R_s$$
$$v_{da} = k_{da} \cdot R_a \qquad\qquad (3.8)$$
$$v_{sa} = k_{sa} \cdot R_s \cdot L$$
$$v_{as} = k_{as} \cdot R_a,$$

with the following values for the rate constants: $k_{ps} = 4$ molecules per cell per second, $k_{ds} = 4 \times 10^{-4}\,\mathrm{s}^{-1}$, $k_{da} = 4 \times 10^{-3}\,\mathrm{s}^{-1}$, $k_{sa} = 2 \times 10^6\,\mathrm{M}^{-1}\,\mathrm{s}^{-1}$, and $k_{as} = 1 \times 10^{-2}\,\mathrm{s}^{-1}$. The time course of receptor activation is depicted in Figure 3.12.

3.2.4
Structural Components of Signaling Pathways

Signaling pathways may constitute highly complex networks, but it has been discovered that they are frequently composed of typical building blocks. These components include Ras proteins, G protein cycles, phosphorelay systems, and MAP kinase cascades. In this section, we will discuss their general composition and function as well as modeling approaches.

3.2.4.1 G proteins

G proteins are essential parts of many signaling pathways. The reason for their name is that they bind the guanine nucleotides GDP and GTP. They are heterotrimers, i.e., they consist of three different subunits. Note the difference to small G proteins

consisting of one monomer, which are discussed below. G proteins are associated to cell surface receptors with a heptahelical transmembrane structure, the G protein-coupled receptors (GPCR). Signal transduction cascades involving (i) such a trans-membrane surface receptor, (ii) an associated G protein, and (iii) an intracellular effector that produces a second messenger play an important role in cellular communication and are well-studied [6, 7]. In humans, GPCR mediate responses to light, flavors, odors, numerous hormones, neurotransmitters, and other signals [8–10]. In unicellular eukaryotes, receptors of this type mediate signals that affect such basic processes as cell division, cell–cell fusion (mating), morphogenesis, and chemotaxis [8, 11–13].

The cycle of G protein activation and inactivation is shown in Figure 3.13. When GDP is bound, the G protein α subunit (Gα) is associated with the G protein βγ heterodimer (Gβγ) and is inactive. Ligand binding to a receptor promotes guanine nucleotide exchange; Gα releases GDP, binds GTP, and dissociates from Gβγ. The dissociated subunits Gα or Gβγ, or both, are then free to activate target proteins (downstream effectors), which initiates signaling. When GTP is hydrolyzed, the subunits are able to reassociate. Gβγ antagonizes receptor action by inhibiting guanine nucleotide exchange. Regulator of G protein signaling (RGS) proteins bind to Gα, stimulate GTP hydrolysis, and thereby reverse G protein activation. This general scheme also holds for the regulation of small monomeric Ras-like GTPases, such as Rho. In this case, the receptor, Gβγ, and RGS are replaced by GEF and GAP (see below).
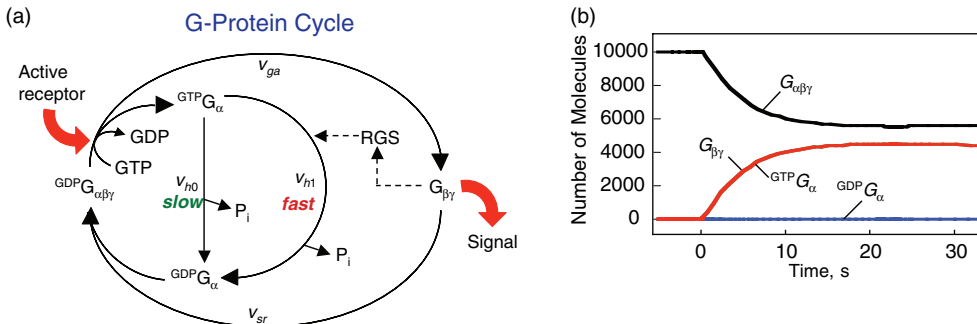
Figure 3.13 Activation cycle of G protein. (a) Without activation, the heterotrimeric G protein is bound to GPD. Upon activation by the activated receptor, an exchange of GDP with GTP occurs and the G protein is divided into GTP-bound Gα and the heterodimer Gβγ. Gα-bound GTP is hydrolyzed, either slowly in reaction v_{h0} or fast in reaction v_{h1} supported by the RGS protein. GDP-bound Gα can reassociate with Gβγ (reaction v_{sr}). (b) Time course of G protein activation. The total number of molecules is 10,000. The concentration of GDP-bound Gα is low for the whole period due to fast complex formation with the heterodimer Gβγ.

Direct targets include different types of effectors, such as adenylyl cyclase, phospholipase C, exchange factors for small GTPases, some calcium and potassium channels, plasma membrane Na^+/H^+ exchangers, and certain protein kinases [6, 14–16]. Typically, these effectors produce second messengers or other biochemical changes that lead to stimulation of a protein kinase or a protein kinase cascade (or, as mentioned, are themselves a protein kinase). Signaling persists until GTP is hydrolyzed to GDP and the $G\alpha$ and $G\beta\gamma$ subunits reassociate, completing the cycle of activation. The strength of the G protein–initiated signal depends on (i) the rate of nucleotide exchange, (ii) the rate of spontaneous GTP hydrolysis, (iii) the rate of RGS-supported GTP hydrolysis, and (iv) the rate of subunit reassociation. RGS proteins act as GTPase-activating proteins (GAPs) for a variety of different $G\alpha$ classes. Thereby, they shorten the lifetime of the activated state of a G protein, and contribute to signal cessation. Furthermore, they may contain additional modular domains with signaling functions and contribute to diversity and complexity of the cellular signaling networks [17–20].

Example 3.2

The model of the heterotrimeric G protein cycle of the yeast pheromone pathway was already mentioned in Example 3.1 and it is linked to the receptor activation model via the concentration of the active receptor. The G protein cycle model comprises two ODEs and two algebraic equations for the mass conservation of the subunits $G\alpha$ and $G\beta\gamma$:

$$\frac{d}{dt} G_{\alpha\beta\gamma} = -v_{ga} + v_{sr}$$
$$\frac{d}{dt} G_{\alpha}GTP = v_{ga} - v_{h0} - v_{h1} \tag{3.9}$$
$$G_{total\alpha} = G_{\alpha\beta\gamma} + G_{\alpha}GTP + G_{\alpha}GDP$$
$$G_{total\beta\gamma} = G_{\alpha\beta\gamma} + G_{\beta\gamma}.$$

The rate equations for the G protein activation, v_{ga}, the hydrolysis of $G_{\alpha}GTP$, v_{h0} and v_{h1}, and the subunit reassociation, v_{sr}, follow simple mass action kinetics:

$$v_{ga} = k_{ga} \cdot R_a \cdot G_{\alpha\beta\gamma}$$
$$v_{hi} = k_{hi} \cdot G_{\alpha}GTP, \quad i = 0, 1 \tag{3.10}$$
$$v_{sr} = k_{sr} \cdot G_{\beta\gamma} \cdot G_{\alpha}GDP.$$

The parameters are $k_{ga} = 1 \times 10^{-5}$ (molecule per cell)$^{-1}$s^{-1}, $k_{h0} = 0.004$ s^{-1}, $k_{h1} = 0.11$ s^{-1}, and $k_{sr} = 1$(molecule per cell)$^{-1}$s^{-1}. Note that in the original work, two different yeast strains have been considered. For the strains with a constantly active RGS (*SST2$^+$*) or with a deletion of RGS (*sst2Δ*), the rate constants k_{h1} and k_{h0} have been set to zero, respectively. The time courses are shown in Figure 3.13.

(a) Ras-Protein
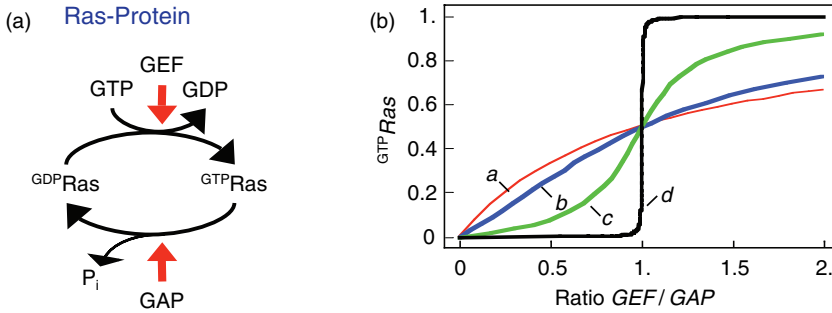
Figure 3.14 The Ras activation cycle. (a) Wiring diagram: GEF supports the transition form GDP-bound to GTP-bound states to activate Ras, while GAP induces hydrolysis of the bound GTP resulting in Ras deactivation. (b) Steady states of active Ras depending on the concentration ratio of its activator GEF and the inhibitor GAP. We compare the behavior for a model with mass action kinetics (curve a) with the behavior obtained with Michaelis–Menten kinetics for decreasing values of the K_m-value (curves b–d). The smaller the K_m-value, the more sigmoidal the response curve, leading to an almost steplike shape in the case of very low K_m-values. Parameters: $Ras_{total} = RasGTP + RasGDP = 1$, $k_1 = k_2 = 1$ (all curves), (b) $K_{m1} = K_{m2} = 1$, (c) $K_{m1} = K_{m2} = 0.1$, (d) $K_{m1} = K_{m2} = 0.001$.

3.2.4.2 Small G proteins

Small G proteins are monomeric G proteins with molecular weight of 20–40 kDa. Like heterotrimeric G proteins, their activity depends on the binding of GTP. More than a hundred small G proteins have been identified. They belong to five families: Ras, Rho, Rab, Ran, and Arf. They regulate a wide variety of cell functions as biological timers that initiate and terminate specific cell functions and determine the periods of time [21].

Ras proteins cycle between active and inactive states (Figure 3.14). The transition from GDP-bound to GTP-bound states is catalyzed by a guanine nucleotide exchange factor (GEF), which induces exchange between the bound GDP and the cellular GTP. The reverse process is facilitated by a GAP, which induces hydrolysis of the bound GTP. Its dynamics can be described with the following equation with appropriate choice of the rates v_{GEF} and v_{GAP}:

$$\frac{d}{dt} RasGTP = -\frac{d}{dt} RasGDP = v_{GEF} - v_{GAP}$$

$$v_{GEF} = \frac{k_1 \cdot GEF \cdot RasGDP}{(K_{m1} + RasGDP)} \quad \text{and} \quad v_{GAP} = \frac{k_2 \cdot GAP \cdot RasGTP}{(K_{m2} + RasGTP)}. \tag{3.11}$$

Figure 3.14 illustrates the wiring of a Ras protein and the dependence of its activity on the concentration ratio of the activating GEF and the deactivating GAP.

Mutations of the *Ras* protooncogenes (H-*Ras*, N-*Ras*, K-*Ras*) are found in many human tumors. Most of these mutations result in the abolishment of normal GTPase activity of *Ras*. The Ras mutants can still bind to GAP, but cannot catalyze GTP hydrolysis. Therefore, they stay active for a long time.

3.2.4.3 **Phosphorelay Systems**

Most phosphorylation events in signaling pathways take place under repeated consumption of ATP. Phosphorelay (also called phosphotransfer) systems employ another mechanism: after an initial phosphorylation using ATP (or another phosphate donor), the phosphate group is transferred directly from one protein to the next without further consumption of ATP (or external donation of phosphate). Examples are the bacterial phosphoenolpyruvate:carbohydrate phosphotransferase [22–25], the two-component system of *E. coli* (see also Section 6.4 on robustness) or the Sln1 pathway involved in osmoresponse of yeast [26].

Figure 3.15 shows a scheme of a phosphorelay system from the high osmolarity glycerol (HOG) signaling pathway in yeast as well as a schematic representation of a phosphorelay system.

The phosphorelay system in the yeast HOG pathway is organized as follows [27]. It involves the transmembrane protein Sln1, which is present as a dimer. Under normal conditions, the pathway is active, since Sln1 continuously autophosphorylates at a histidine residue, Sln1H-P, under consumption of ATP. Subsequently, this phosphate group is transferred to an aspartate residue of Sln1 (resulting in Sln1A-P), then to a histidine residue of Ypd1, and finally to an aspartate residue of Ssk1. Ssk1 is continuously dephosphorylated by a phosphatase. Without stress, the proteins are mainly present in their phosphorylated form. The pathway is blocked by an increase in the external osmolarity and a concomitant loss of turgor pressure in the cell. The phosphorylation of Sln1 stops, the pathway runs out of transferable phosphate groups, and the concentration of unphosphorylated Ssk1 rises. This is the signal for the next part of the pathway. The temporal behavior of a generalized
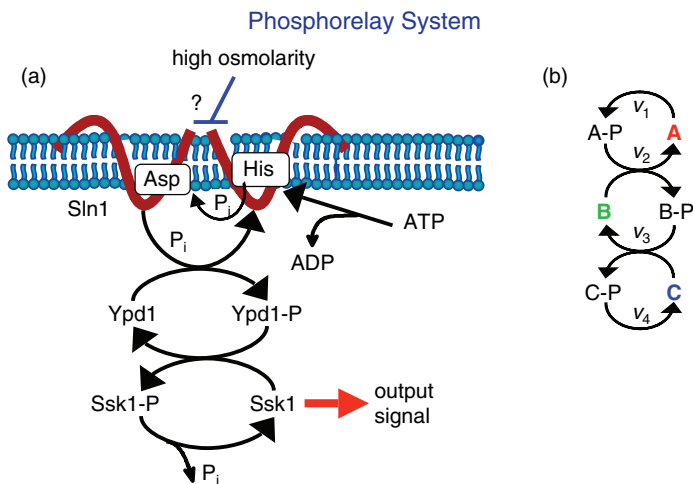
Figure 3.15 Schematic representation of a phosphorelay system. (a) Phosphorelay system belonging to the Sln1-branch of the HOG pathway in yeast. (b) General scheme of phosphorylation and dephosphorylation in a phosphorelay.

phosphorelay system (Figure 3.15) can be described with the following set of ODEs:

$$\frac{d}{dt}A = -k_1 \cdot A + k_2 \cdot AP \cdot B$$

$$\frac{d}{dt}B = -k_2 \cdot AP \cdot B + k_3 \cdot BP \cdot C \qquad (3.12)$$

$$\frac{d}{dt}C = -k_3 \cdot BP \cdot C + k_4 \cdot CP.$$

For the ODE system in Eq. (3.12), the following conservation relations hold:

$$A_{total} = A + AP$$

$$B_{total} = B + BP \qquad (3.13)$$

$$C_{total} = C + CP.$$

The existence of conservation relations is in agreement with the assumption that production and degradation of the proteins occurs on a larger time scale than the phosphorylation events.

The temporal behavior of a phosphorelay system upon external stimulation (here, setting the value of k_1 transiently to zero) is shown in Figure 3.16. Before the stimulus, the concentrations of A, B, and C assume low, but nonzero, levels due to continuous flow of phosphate groups through the network. During stimulation, they increase one after the other up to a maximal level that is determined by the total concentration of each protein. After removal of stimulus, all three concentrations return quickly to their initial values.

Figure 3.16(b) illustrates how the sensitivity of the phosphorelay system depends on the value of the terminal dephosphorylation of CP. For a low value of the rate constant k_4, e.g., $k_4 < 0.001$, the concentration C is low (almost) independent of the value of k_1, while for high k_4, e.g., $k_4 > 10$, the concentration C is (almost always) maximal. Changing of k_1 leads to a change of C-levels only in the range $0.001 < k_4 < 10$.
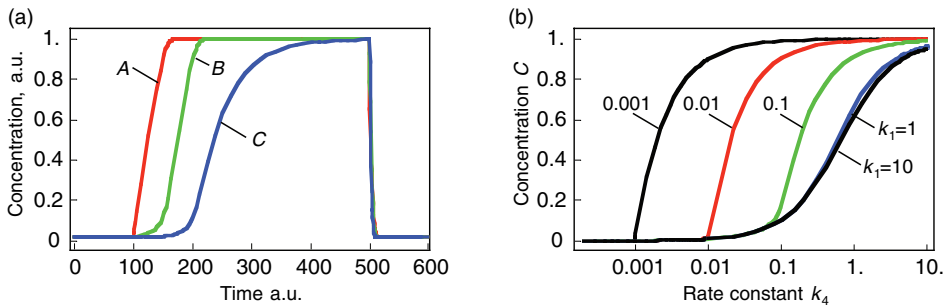
Figure 3.16 Dynamics of the phosphorelay system. (a) Time courses after stimulation from time 100 to time 500 (a.u.) by decreasing k_1 to zero. (b) Dependence of steady-state level of the phosphorelay output, C, on the cascade activation strength, k_1, and the terminal dephosphorylation, k_4. Parameter values: $k_1 = k_2 = k_3 = 1$, $k_4 = 0.02$, $A_{total} = B_{total} = C_{total} = 1$.

This system is an example for a case where we can draw preliminary conclusions about feasible parameter values just from the network structure and the task of the module. Another example for a phosphorelay system is discussed in Section 7.4.

3.2.4.4 MAP Kinase Cascades

Mitogen-activated protein kinases (MAPKs) are a family of serine/threonine kinases that transduce biochemical signals from the cell membrane to the nucleus in response to a wide range of stimuli. Independent or coupled kinase cascades participate in many different intracellular signaling pathways that control a spectrum of cellular processes, including cell growth, differentiation, transformation, and apoptosis. MAPK cascades are widely involved in eukaryotic signal transduction, and MAP kinase pathways are conserved from yeast to mammals.

A general scheme of a MAPK cascade is depicted in Figure 3.17. This pathway consists of several levels (usually three to four), where the activated kinase at each level phosphorylates the kinase at the next level down the cascade. The MAP kinase (MAPK) is at the terminal level of the cascade. It is activated by the MAPK kinase (MAPKK) by phosphorylation of two sites, conserved threonine and tyrosine residues. The MAPKK is itself phosphorylated at serine and threonine residues by the MAPKK kinase
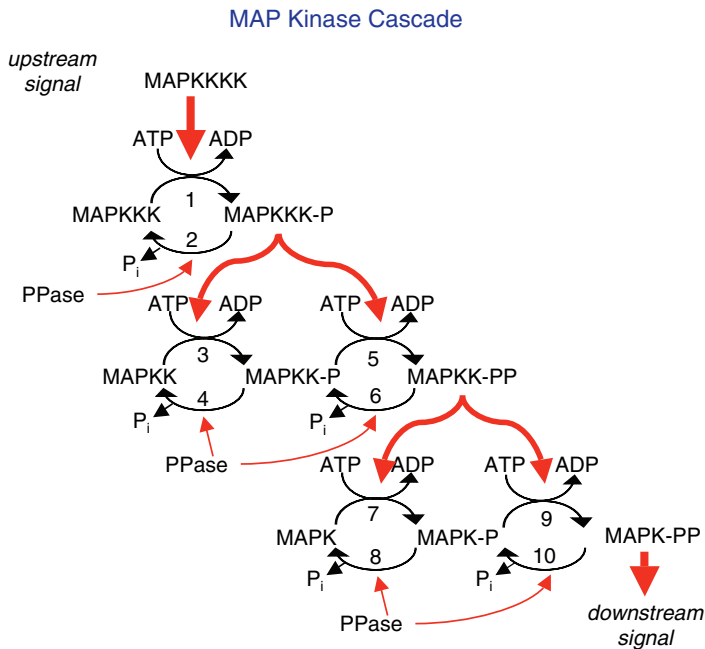
Figure 3.17 Schematic representation of the MAP kinase cascade. An upstream signal (often by a further kinase called MAP kinase kinase kinase kinase) causes phosphorylation of the MAPKKK. The phosphorylated MAPKKK in turn phosphorylates the protein at the next level. Dephosphorylation is assumed to occur continuously by phosphatases or autodephosphorylation.

Table 3.1 Names of the components of MAP kinase pathways in
different organisms and different pathways.

Organism	Budding yeast		Xensopus oocytes	Human, cell cycle regulation		
	HOG pathway	**Pheromone pathway**			**p38 pathway**	**JNK pathway**
MAPKKK	Ssk2/Ssk22	Ste11	Mos	Rafs (c-, A- and B-),	Tak1	MEKKs
MAPKK	Pbs2	Ste7	MEK1	MEK1/2	MKK3/6	MKK4/7
MAPK	Hog1	Fus3	p42 MAPK	ERK1/2	p38	JNK1/2

(MAPKKK). Several mechanisms are known to activate MAPKKKs by phosphorylation of a tyrosine residue. In some cases, the upstream kinase may be considered as a MAPKKK kinase (MAPKKKK). Dephosphorylation of either residue is thought to inactivate the kinases, and mutants lacking either residue are almost inactive. At each cascade level, protein phosphatases can inactivate the kinase, although it is in some cases a matter of debate whether this dephosphorylation is performed by an independent protein or by the kinase itself as autodephosphorylation. Also ubiquitin-dependent degradation of phosphorylated proteins has been reported.

Although they are highly conserved throughout different species, elements of the MAPK cascade got different names in various studied systems. Some examples are listed in. Table 3.1 (see also [28]).

In the following, we will present typical modeling approaches for MAPK cascades and then discuss their functional properties. Their dynamics may be represented by the following ODE system:

$$\frac{\mathrm{d}}{\mathrm{d}t} MAPKKK = -v_1 + v_2$$

$$\frac{\mathrm{d}}{\mathrm{d}t} MAPKKK\text{-}P = v_1 - v_2 \tag{3.14}$$

$$\frac{\mathrm{d}}{\mathrm{d}t} MAPKK = -v_3 + v_4$$

$$\frac{\mathrm{d}}{\mathrm{d}t} MAPKK\text{-}P = v_3 - v_4 - v_5 + v_6 \tag{3.15}$$

$$\frac{\mathrm{d}}{\mathrm{d}t} MAPKK\text{-}P_2 = v_5 - v_6.$$

$$\frac{\mathrm{d}}{\mathrm{d}t} MAPK = -v_7 + v_8$$

$$\frac{\mathrm{d}}{\mathrm{d}t} MAPK\text{-}P = v_7 - v_8 - v_9 + v_{10} \tag{3.16}$$

$$\frac{\mathrm{d}}{\mathrm{d}t} MAPK\text{-}P_2 = v_9 - v_{10}.$$

The variables in the ODE system fulfill a set of moiety conservation relations, irrespective of the concrete choice of expression for the rates $v_1, \ldots, v_{10}$. It holds,

$$MAPKKK_{\text{total}} = MAPKKK + MAPKKK\text{-}P$$
$$MAPKK_{\text{total}} = MAPKK + MAPKK\text{-}P + MAPKK\text{-}P_2 \tag{3.17}$$
$$MAPK_{\text{total}} = MAPK + MAPK\text{-}P + MAPK\text{-}P_2.$$

The conservation relations reflect the fact that we do not consider production or degradation of the involved proteins in this model. This is justified by the supposition that protein production and degradation take place on a different time scale than signal transduction.

The choice of the expressions for the rates is a matter of elaborateness of experimental knowledge and of modeling taste. We will discuss here different possibilities. First, assuming only mass action results in linear and bilinear expression such as

$$v_1 = k_{\text{kinase}} \cdot MAPKKK \cdot MAPKKKK$$
$$v_2 = k_{\text{phosphatase}} \cdot MAPKKK\text{-}P. \tag{3.18}$$

The kinetic constants k_{kinase} and $k_{\text{phosphatase}}$ are first- and second-order rate constants, respectively. In these expressions, the concentrations of the donor and acceptor of the transferred phosphate group, ATP and ADP, are assumed to be constant and included in the rate constants. Considering ATP and ADP explicitly results in

$$v_1 = k_{\text{kinase}^*} \cdot MAPKKK \cdot MAPKKKK \cdot ATP$$
$$v_2 = k_{\text{phosphatase}} \cdot MAPKKK\text{-}P. \tag{3.19}$$

In this case, we have to care about the ATP–ADP balance and add three more differential equations

$$\frac{\mathrm{d}}{\mathrm{d}t} ATP = -\frac{\mathrm{d}}{\mathrm{d}t} ADP = -\sum_{i \text{ odd}} v_i$$
$$\frac{\mathrm{d}}{\mathrm{d}t} P_i = \sum_{i \text{ even}} v_i. \tag{3.20}$$

Here we find two more conservation relations, the conservation of adenine nucleotides, $ATP + ADP = \text{const.}$ and the conservation of phosphate groups

$$MAPKKK\text{-}P + MAPKK\text{-}P + 2 \cdot MAPKK\text{-}P_2 + MAPK\text{-}P$$
$$+ 2 \cdot MAPK\text{-}P_2 + 3 \cdot ATP + 2 \cdot ADP + P = \text{const.} \tag{3.21}$$

Second, one may assume that the kinases catalyzing the phosphorylation of the next kinase behave like saturable enzymes (e.g., [29]) and, therefore, consider Michaelis–Menten kinetics for the individual steps (e.g., [30]). Taking again the first and second reaction as examples for kinase and phosphatase steps, we get

$$v_1 = k_1 \cdot MAPKKKK \frac{MAPKKK}{K_{\text{m1}} + MAPKKK}$$
$$v_2 = \frac{V_{\text{max2}} \cdot MAPKKK\text{-}P}{K_{\text{m2}} + MAPKKK\text{-}P}, \tag{3.22}$$
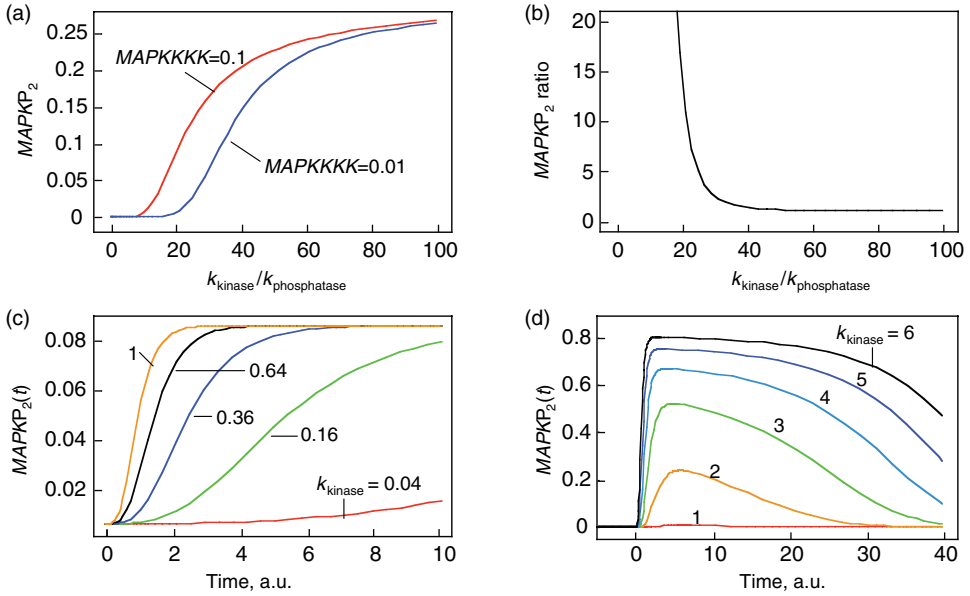
Figure 3.18 Parameter dependence of MAPK cascade performance. Steady-state simulations for changing values of rate constants for kinases, k_{kinase}, and phosphatases, $k_{phosphatase}$ are shown (in arbitrary units). (a) Absolute values of the output signal MAPK-PP depending on the input signal (high $MAPKKKK = 0.1$, or low $MAPKKKK = 0.01$) for varying ratio of $k_{kinase}/k_{phosphatase}$. (b) Ratio of the output signal for high versus low input signal ($MAPKKKK = 0.1$ or $MAPKKKK = 0.01$) for varying ratio of $k_{kinase}/k_{phosphatase}$. (c) Time course of MAPK activation for different values of k_{kinase} and a ratio $k_{kinase}/k_{phosphatase} = 20$. (d) Time course of MAPK activation for different values of k_{kinase} and fixed $k_{phosphatase} = 1$.

where k_1 is a first-order rate constant, K_{m1} and K_{m2} are Michaelis constants, and V_{max2} denotes a maximal enzyme rate. Reported values for Michaelis constants are 15 nM [30], 46 and 159 nM [31], and 300 nM [29]. For maximal rates, values of about $0.75 \, nM \cdot s^{-1}$ [30] are used in models.

The performance of MAPK cascades, i.e., their ability to amplify the signal, to enhance the concentration of the double phophorylated MAPK notably, and the speed of activation, depends crucially on the kinetic constants of the kinases, k_{kinase}, and phosphatases, $k_{phosphatase}$ (Eq. (3.19)), and, moreover, on their ratio (see Figure 3.18). If the ratio $k_{kinase}/k_{phosphatase}$ is low (phosphatases stronger than kinases), then the amplification is high, but at very low absolute concentrations of phosphorylated MAPK. High values of $k_{kinase}/k_{phosphatase}$ ensure high absolute concentrations of MAPK-P_2, but with negligible amplification. High values of both k_{kinase} and $k_{phosphatase}$ ensure fast activation of downstream targets.

Frequently, the proteins of MAPK cascades interact with scaffold proteins. Binding to scaffold proteins can bring the kinases together in the correct spatial order or can reduce their diffusion through the cytosol or provide an anchor to the plasma

membrane. This way, they contribute to the regulation of the efficiency, specificity, and localization of the signaling pathway.

3.2.4.5 Jak/Stat Pathways

Jak–Stat pathways play an important role in regulating immune responses and cellular homeostasis in human health and disease [32, 33]. They are activated by cytokines, a large family of extracellular ligands. The whole family of structurally and functionally conserved receptors comprises four Jaks and seven Stats. As is the case for many types of receptor families, downstream signaling entails tyrosine phosphorylation. Stat stands for "signal transducer and activator of transcription," because these proteins function both as signal transducer and transcription activator. They are inactive as monomers. Activation involves phosphorylation and dimerization.

A mathematical model of the Jak–Stat pathway presented by Swamaye and colleagues (2003) presupposes the binding of the ligand (here the hormone Epo) to the receptor (EpoR) that results in phosphorylation of Jak2 and of the cytoplasmatic domain of EpoR. The model involves the recruitment of monomeric Stat5 ($x_1 = Stat5$) to phosphorylated and thereby activated receptor, $EpoR_A$. Upon receptor recruitment, monomeric Stat5 is tyrosine phosphorylated ($x_2 = Stat5\text{-}P$). It dimerizes in a second step to yield x_3, and migrates in the third step to the nucleus (x_4), where it binds to the promoter of target genes. After it has fulfilled its task, it is dephosphorylated and exported to the cytoplasm (fourth step). Using simple mass action kinetics for the four steps indicated in Figure 3.19, the respective ODE system reads

$$\frac{dx_1(t)}{dt} = -k_1 \cdot x_1(t) \cdot EpoR_A + 2 \cdot k_4 \cdot x_3(t-\tau)$$

$$\frac{dx_2(t)}{dt} = -k_2 \cdot x_2^2(t) + k_1 \cdot x_1(t) \cdot EpoR_A$$

$$\frac{dx_3(t)}{dt} = -k_3 \cdot x_3(t) + \frac{1}{2}k_2 \cdot x_2^2(t)$$

$$\frac{dx_4(t)}{dt} = -k_4 \cdot x_3(t-\tau) + k_3 \cdot x_3(t).$$

(3.23)

The parameter τ represents the delay time that Stat5 molecules have to reside in the nucleus. This model has been used to show that recycling of Stat5 molecules is an important event in the activation cycle and necessary to explain experimental data.

In the web material, we present a model of the human Erbk signaling network consisting of a receptor and several signaling pathways including a MAPK pathway, which shows interesting feedback and crosstalk phenomena.

3.2.5
Signaling – Dynamic and Regulatory Features

Signaling pathways can exhibit interesting dynamic and regulatory features. Representative pathway structures that form the basis for characteristic dynamic behaviors

Jak-Stat Pathway
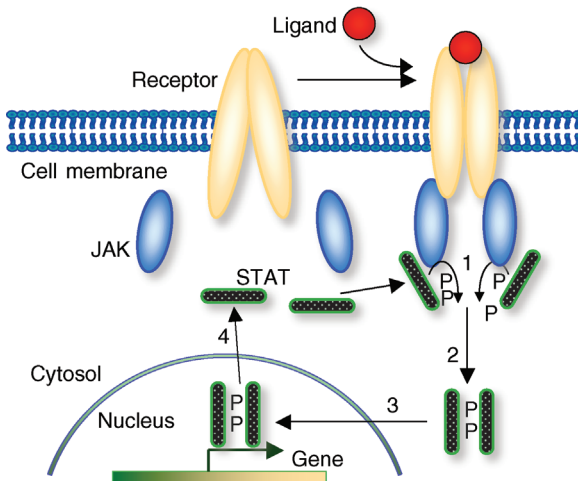
Figure 3.19 The Jak–Stat signaling pathway. Upon binding ligand, receptor-associated Jaks become activated and mediate phosphorylation of specific receptor tyrosine residues. This leads to the recruitment of specific Stats, which are then also tyrosine-phosphorylated. Activated Stats are released from the receptor, dimerize, translocate to the nucleus, and bind to enhancers.

(so-called dynamic motifs) are discussed in detail in Section 8.2. Among the various regulatory features of signaling pathways, negative feedback has attracted outstanding interest. It also plays an important role in metabolic pathways, for example, in amino acid synthesis pathways, where a negative feedback signal from the amino acid at the end to the precursors at the beginning of the pathway prevents an overproduction of this amino acid. The implementation of feedback and the respective dynamic behavior show a wide variation. Feedback can bring about limit cycle type oscillations, for instance, in cell cycle models [34]. In signaling pathways, negative feedback may cause an adjustment of the response or damped oscillations.

3.2.5.1 Quantitative Measures for Properties of Signaling Pathways

The dynamic behavior of signaling pathways can be quantitatively characterized by a number of measures [35]. Let $P_i(t)$ be the time-dependent concentration of the kinase i (or another interesting compound). The signaling time τ_i describes the average time to activate the kinase i. The signal duration ϑ_i gives the average time during which the kinase i remains activated. The signal amplitude S_i is a measure for the average concentration of activated kinase i. The following definitions have been introduced. The quantity

$$I_i = \int_0^\infty P_i(t)\,\mathrm{d}t \tag{3.24}$$

measures the total of active kinase i generated during the signaling period, i.e., the integrated response of X_i (the area covered by a plot $P_i(t)$ versus time). Further measures are

$$T_i = \int_0^\infty t \cdot P_i(t) \mathrm{d}t \quad \text{and} \quad Q_j = \int_0^\infty t^2 \cdot P_i(t) \mathrm{d}t. \qquad (3.25)$$

The signaling time can now be defined as

$$\tau_i = \frac{T_i}{I_i}, \qquad (3.26)$$

i.e., as the average of time, analogous to a center of time, or to the mean value of a statistical distribution. The signal duration

$$\vartheta_i = \sqrt{Q_j/I_i - \tau_i^2} \qquad (3.27)$$

gives a measure of how the signaling response extends around the mean time (compatible to standard deviation). The signal amplitude is defined as

$$A_i = \frac{I_i}{2\vartheta_i}. \qquad (3.28)$$

In a geometric representation, this is the height of a rectangle whose length is $2\vartheta_i$ and whose area equals the area under the curve $P_i(t)$. Note that this measure might be different from the maximal value $P_i^{\max}$ that $P_i(t)$ assumes during the time course.

Figure 3.20 shows a signaling pathway with successive activation of compounds and the respective time courses. The characteristic quantities are given in Table 3.2 and for $P_1(t)$ shown in the figure.
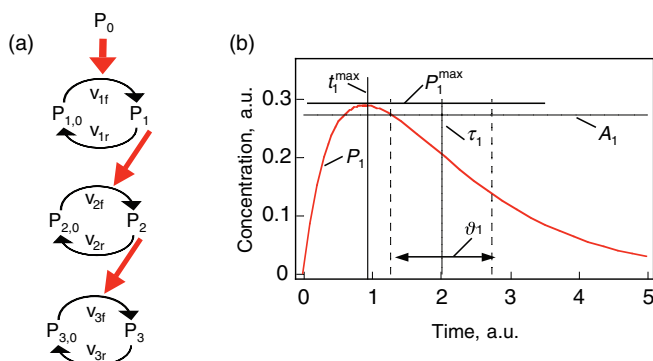
Figure 3.20 Characteristic measures for dynamic variables. (a) Wiring of an example signaling cascade with $v_{if} = k_{if} \cdot P_{i-1}(t) \cdot (1 - P_i(t))$, $v_{ir} = k_{ir} \cdot P_i(t)$, $k_{if} = k_{ir} = 1$, $\mathrm{d}P_0(t)/\mathrm{d}t = -P_0(t)$, $P_0(0) = 1$, $P_i(0) = 0$ for $i = 1, \ldots, 3$. (b) Time courses of X_i. The horizontal lines indicate the concentration measures for X_1, i.e., the calculated signal amplitude A_1 and $P_1^{\max}$, and vertical lines indicate time measures for P_1, i.e., the time $t_1^{\max}$ of $P_1^{\max}$, the characteristic time τ_1, and the dotted vertical lines cover the signaling time ϑ_1.

Table 3.2 Dynamic characteristics of the signaling cascade shown in Figure 3.15.

Compound	Integral, I_i	Maximum, X_i^{max}	Time (X_i^{max}), t_i^{max}	Characteristic time, τ_i	Signal duration, ϑ_i	Signal amplitude, A_i
X_1	0.797	0.288	0.904	2.008	1.458	0.273
X_2	0.695	0.180	1.871	3.015	1.811	0.192
X_3	0.629	0.133	2.855	4.020	2.109	0.149

3.2.5.2 Crosstalk in Signaling Pathways

Signal transmission in cellular context is often not as precise as in electric circuits in the sense that an activated protein has a high specificity for just one target. Instead, there might be crosstalk, i.e., proteins of one signaling pathway interact with proteins assigned to another pathway. Strictly speaking, the assignment of proteins to one pathway is often arbitrary and may result, for example, from the history of their function discovery. Frequently, protein interactions form a network with various binding, activation, and inhibition events, such as illustrated in Figure 3.10.

In order to introduce quantitative measures for crosstalk, let us consider the simplified scheme in Figure 3.21: external signal α binds to receptor R_A, which activates target T_A via a series of interactions. In the same way, external signal β binds to receptor R_B, which activates target T_B. In addition, there are processes that mediate an effect of receptor R_B on target T_A.

Let us concentrate on pathway A and define all measures from its perspective. Signaling from α via R_A to T_A shall be called intrinsic, while signals from β to T_A are extrinsic. Further, in order to quantify crosstalk, we need a quantitative measure for the effect of an external stimulus on the target. We have different choices: if we are interested in the level of activation, such a measure might be the integral over the time course of T_A (Eq. (3.24)), its maximal value, or its amplitude (Eq. (3.28)). If we are interested in the response timing, we can consider the time of the maximal value or the characteristic time (for an overview on measures, see Table 3.2). Whatever measure we chose, it shall be denoted by X in the following.
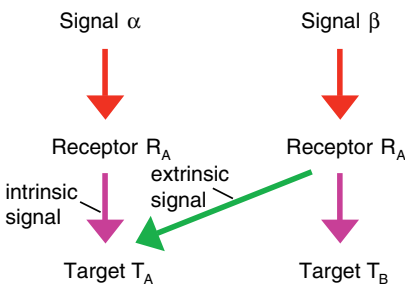
Figure 3.21 Crosstalk of signaling pathways.

Table 3.3 Effect of crosstalk on signaling.

	$S_e > 1$	$S_e < 1$
$S_i > 1$	Mutual signal inhibition	Dominance of intrinsic signal
$S_i < 1$	Dominance of extrinsic signal	Mutual signal amplification

The crosstalk measure C is the activation of pathway A by the extrinsic stimulus β relative to the intrinsic stimulus α

$$C = \frac{X_{\text{extrinsic}}}{X_{\text{intrinsic}}} = \frac{X_{T_A}(\beta)}{X_{T_A}(\alpha)}. \tag{3.29}$$

The fidelity F [36] is defined as output due to the intrinsic signal divided by the output in response to the extrinsic signal and reads in our notation:

$$F = \frac{X_{T_A}(\alpha)/X_{R_A}(\alpha)}{X_{T_A}(\alpha)/X_{R_B}(\beta)}. \tag{3.30}$$

In addition, the intrinsic sensitivity S_i expresses how an extrinsic signal modifies the intrinsic signal when acting in parallel, while the extrinsic sensitivity S_e quantifies the effect of the intrinsic signal on the extrinsic signal [37]:

$$S_i(A) = \frac{X_{T_A}(\alpha)}{X_{T_A}(\alpha, \beta)} \quad \text{and} \quad S_e(A) = \frac{X_{T_A}(\beta)}{X_{T_A}(\alpha, \beta)}. \tag{3.31}$$

Table 3.3 shows how different specificity values can be interpreted.

Example 3.3

Consider the coupling of a faster and a slower signaling pathway as depicted in Figure 3.21, described with rate equations used in Figure 3.22 with the exception $v_{3Af} = k_{3Af} \cdot (P_{2A}(t) + P_{2B}(t)) \cdot (1 - P_{3A}(t))$. Let A be the slower pathway (all $k_{iAf} = k_{iAr} = 1$) and B the faster pathway (all $k_{iBf} = k_{iBr} = 10$). The pathways are activated by setting either $P_{0A}(0)$ or $P_{0B}(0)$ or both from zero to one, respectively. The time courses show that crosstalk from pathway B to pathway A affects the pathway output $P_{3A}(t)$. Concomitant activation of A by α and B by β leads to faster activation of $P_{3A}(t)$ than α alone. Activation by β alone leads to drastically reduced $P_{3A}(t)$. Table 3.4. reports the quantitative crosstalk measures. We note mutual signal amplification in terms of integrated response (I_{3A}) and maximal response ($\text{Max}(P_{3A})$), but dominance of the intrinsic signal on the level of signal timing (here $t_{P_{3A}}^{\max}$).
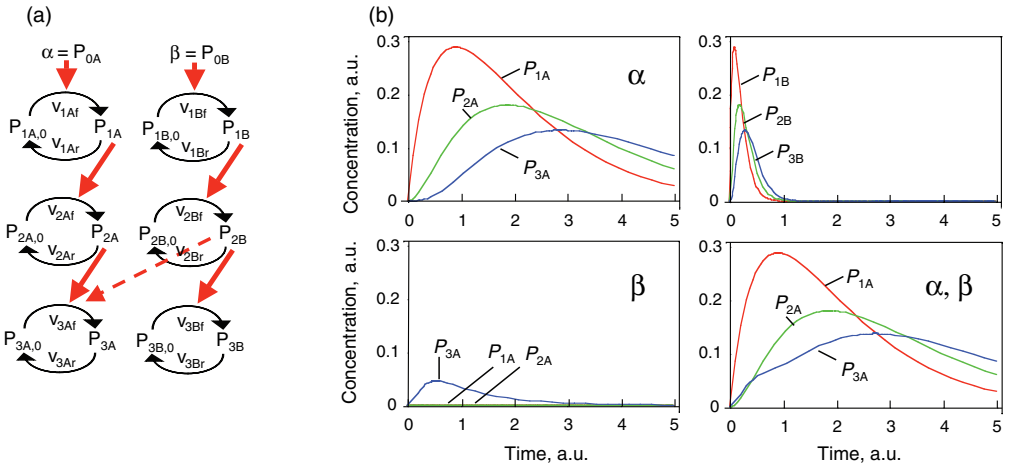
Figure 3.22 Crosstalk of MAP kinase pathways. (a) Pathway A leads to activation of P_{3A} upon stimulation by α, pathway B transmits signal from β to P_{3B}. Crosstalk occurs through signaling from P_{2B}. (b) Dynamics of pathways A and B upon stimulation by α, β, or both (as indicated).

3.3
The Cell Cycle

Summary

The cell cycle is a fundamental cellular process that dominates many aspects of cellular biochemistry. In this section, different phases of the mitotic cell cycle are introduced. The regulatory mechanisms that control the periodic process are discussed and mathematical models of different complexity that describe the oscillatory process are introduced.

Growth and reproduction are major characteristics of life. Crucial for these is the cell division by which one cell divides into two and all parts of the mother cell are distributed to the daughter cells. This also requires that the genome has to be

Table 3.4 Crosstalk measures for the pathway in Example 3.3.

	X_A (α)	X_A (β)	X_A (α, β)	$S_i(A) = \frac{X_A(\alpha)}{X_A(\alpha,\beta)}$	$S_e(A) = \frac{X_A(\beta)}{X_A(\alpha,\beta)}$	$C = \frac{X_A(\beta)}{X_A(\alpha)}$
$I_3 = \int_0^\infty P_{3A}(t)\,\mathrm{d}t$	0.628748	0.067494	0.688995	0.912557	0.09796	0.107347
$t_{P_{3A}}^{max}$	2.85456	0.538455	2.73227	1.04476	0.197072	0.18863
$\mathrm{Max}(P_{3A})$	0.132878	0.0459428	0.136802	0.971314	0.335833	0.345752

duplicated in advance, which is performed by the DNA polymerase, an enzyme that utilizes desoxynucleotide triphosphates (dNTPs) for the synthesis of two identical DNA double strands from one parent double strand. In this case, each single strand acts as template for one of the new double strands. Several types of DNA polymerases have been found in prokaryotic and eukaryotic cells, but all of them synthesize DNA only in $5' \to 3'$ direction. In addition to DNA polymerase, several further proteins are involved in DNA replication: proteins responsible for the unwinding and opening of the mother strand (template double strand), proteins that bind the opened single stranded DNA and prevent it from rewinding during synthesis, an enzyme called primase that is responsible for the synthesis of short RNA primers that are required by the DNA polymerase for the initialization of DNA polymerization, and a DNA ligase responsible for linkage of DNA fragments that are synthesized discontinuously on one of the two template strands because of the limitation to $5' \to 3'$ synthesis. Like the DNA, also other cellular organelles have to be doubled, such as the centrosome involved in the organization of the mitotic spindle.

The cell cycle is divided into two major phases: the interphase and the M phase (Figure 3.23). The interphase is often a relatively long period between two subsequent cell divisions. Cell division itself takes place during M phase and consists of two steps: first, the nuclear division in which the duplicated genome is separated into two parts, and second, the cytoplasmatic division or cytokinesis, where the cell divides into two cells. The latter not only distributes the two separated genomes between each of the newly developing cells, but also divides up cytoplasmatic organelles and substances between them. Finally, the centrosome is replicated and divided between both cells as well.

DNA replication takes place during interphase in the so-called S phase (S = synthesis) of the cell cycle (Figure 3.23). This phase is usually preceded by a gap phase, G_1, and followed by another gap phase, G_2. From G_1 phase, cells can also leave the cell cycle and enter a rest phase, G_0. The interphase normally represents 90% of the cell cycle. During interphase, the chromosomes are dispersed as chromatin in the nucleus. Cell division occurs during M phase, which follows the G_2 phase, and consists of mitosis and cytokinesis. Mitosis is divided into different stages. During the first stage – the prophase – chromosomes condense into their compact form and the two centrosomes of a cell begin recruiting microtubles for the formation of the mitotic spindle. In later stages of mitosis, this spindle is used for the equal segregation of the chromatides of each chromosome to opposite cellular poles. During the following prometaphase, the nuclear envelope dissolves and the micro-tubles of the mitotic spindle attach to protein structures, called kinetochores, at the centromeres of each chromosome. In the following metaphase, all chromosomes line up in the middle of the spindle and form the metaphase plate. Now, during anaphase, the proteins holding together both sister chromatids are degraded and each chromatid of a chromosome segregate into opposite directions. Finally, during telophase, new nuclear envelopes are recreated around the separated genetic materials and form two new nuclei. The chromosomes unfold again into chromatin. The mitotic reaction is often followed by a cytokinesis where the cellular
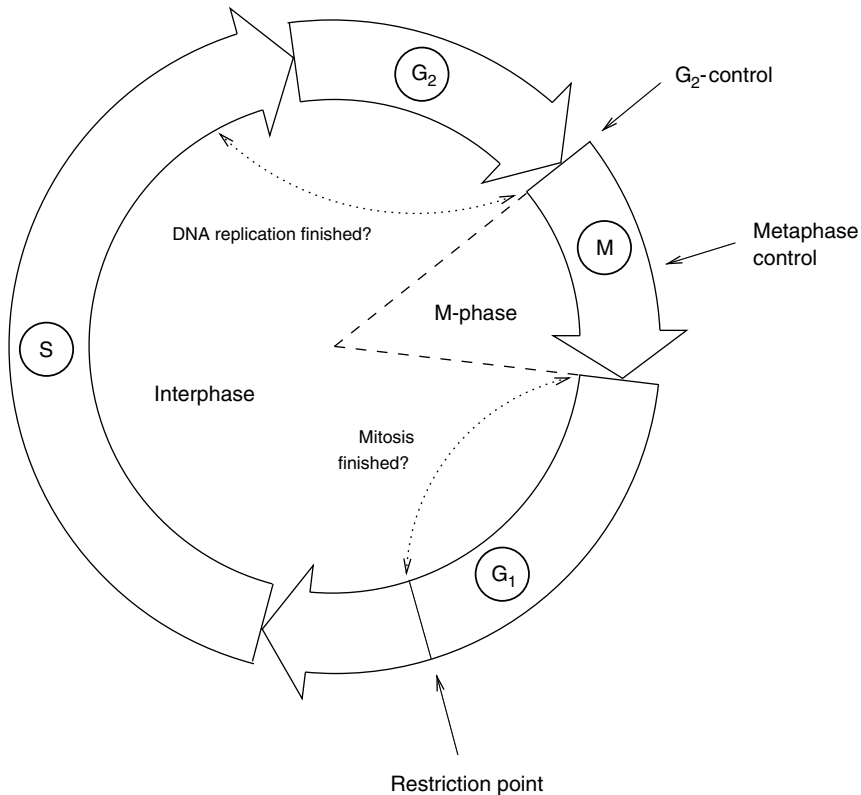
Figure 3.23 The cell cycle is divided into the interphase, which is the period between two subsequent cell divisions, and the M phase, during which one cell separates into two. Major control points of the cell cycle are indicated by arrows. More details are given in the text.

membrane pinches off between the two newly separated nuclei and two new cells are formed.

The cell cycle is strictly controlled by specific proteins. When a certain checkpoint, the restriction point, in the G_1 phase is passed, this leads to a series of specific steps that end up in cell division. At this point, the cell checks whether it has achieved a sufficient size and the external conditions are suitable for reproduction. The control system ensures that a new phase of the cycle is only entered if the preceding phase has been finished successfully. For instance, to enter a new M phase, it has to be assured that DNA replication during S phase has correctly been brought to an end. Similarly, entering in S phase requires a preceding mitosis.

Passage through the eukaryotic cell cycle is strictly regulated by the periodic synthesis and destruction of cyclins that bind and activate cyclin-dependent kinases (CDKs). The term "kinase" expresses that their function is phosphorylation of

proteins with controlling functions. A contrary function is carried out by a "phosphatase." Its function is to dephosphorylate a previously phosphorylated protein and by this toggle its activity. Cyclin-dependent kinase inhibitors (CKI) also play important roles in cell cycle control by coordinating internal and external signals and impeding proliferation at several key checkpoints.

The general scheme of the cell cycle is conserved from yeast to mammals. The levels of cyclins rise and fall during the stages of the cell cycle. The levels of CDKs appear to remain constant during cell cycle, but the individual molecules are either unbound or bound to cyclins. In budding yeast, one CDK (Cdc28) and nine different cyclins (Cln1–Cln3, Clb1–Clb6) that seem to be at least partially redundant are found. In contrast, mammals employ a variety of different cyclins and CDKs. Cyclins include a G1 cyclin (cyclin D), S phase cyclins (A and E), and mitotic cyclins (A and B). Mammals have nine different CDKs (referred to as CDK1-9) that are important in different phases of the cell cycle. The anaphase-promoting complex (APC) triggers the events leading to destruction of the cohesions, thus allowing the sister chromatids to separate and degrades the mitotic cyclins.

3.3.1
Steps in the Cycle

Let us take a course through the mammalian cell cycle starting in G1 phase. As the level of G_1 cyclins rises, they bind to their CDKs and signal the cell to prepare the chromosomes for replication. When the level of S phase promoting factor (SPF) rises, which includes cyclin A bound to CDK2, it enters the nucleus and prepares the cell to duplicate its DNA (and its centrosomes). As DNA replication continues, cyclin E is destroyed, and the level of mitotic cyclins begins to increase (in G_2). The M phase-promoting factor (the complex of mitotic cyclins with the M-phase CDK) initiates (i) assembly of the mitotic spindle, (ii) breakdown of the nuclear envelope, and (iii) condensation of the chromosomes. These events take the cell to metaphase of mitosis. At this point, the M phase-promoting factor activates the APC, which allows the sister chromatids at the metaphase plate to separate and move to the poles (anaphase), thereby completing mitosis. APC destroys the mitotic cyclins by coupling them to ubiquitin, which targets them for destruction by proteasomes. APC turns on the synthesis of G_1 cyclin for the next turn of the cycle and it degrades geminin, a protein that has kept the freshly synthesized DNA in S phase from being re-replicated before mitosis.

A number of checkpoints ensure that all processes connected with cell cycle progression, DNA doubling and separation, and cell division occur correctly. At these checkpoints, the cell cycle can be aborted or arrested. They involve checks on completion of S phase, on DNA damage, and on failure of spindle behavior. If the damage is irreparable, apoptosis is triggered. An important checkpoint in G_1 has been identified in both yeast and mammalian cells. Referred to as "Start" in yeast and as "restriction point" in mammalian cells, this is the point at which the cell becomes committed to DNA replication and completing a cell cycle [38–41]. All the checkpoints require the services of complexes of proteins. Mutations in the genes encoding

some of these proteins have been associated with cancer. These genes are regarded as oncogenes. Failures in checkpoints permit the cell to continue dividing despite damage to its integrity. Understanding how the proteins interact to regulate the cell cycle has become increasingly important to researchers and clinicians when it was discovered that many of the genes that encode cell cycle regulatory activities are targets for alterations that underlie the development of cancer. Several therapeutic agents, such as DNA-damaging drugs, microtubule inhibitors, antimetabolites, and topoisomerase inhibitors, take advantage of this disruption in normal cell cycle regulation to target checkpoint controls and ultimately induce growth arrest or apoptosis of neoplastic cells.

For the presentation of modeling approaches, we will focus on the yeast cell cycle since intensive experimental and computational studies have been carried out using different types of yeast as model organisms. Mathematical models of the cell cycle can be used to tackle, for example, the following relevant problems:

- The cell seems to monitor the volume ratio of nucleus and cytoplasm and to trigger cell division at a characteristic ratio. During oogenesis, this ratio is abnormally small (the cells accumulate maternal cytoplasm), while after fertilization cells divide without cell growth. How is the dependence on the ratio regulated?

- Cancer cells have a failure in cell cycle regulation. Which proteins or protein complexes are essential for checkpoint examination?

- What causes the oscillatory behavior of the compounds involved in the cell cycle?

3.3.2
Minimal Cascade Model of a Mitotic Oscillator

One of the first genes to be identified as being an important regulator of the cell cycle in yeast was *cdc2/cdc28* [42], where *cdc2* refers to fission yeast and *cdc28* to budding yeast. Activation of the *cdc2/cdc28* kinase requires association with a regulatory subunit referred to as a cyclin.

A minimal model for the mitotic oscillator involving a cyclin and the Cdc2 kinase has been presented by Goldbeter [43]. It covers the cascade of posttranslational modifications that modulate the activity of Cdc2 kinase during cell cycle. In the first cycle of the bicyclic cascade model, the cyclin promotes the activation of the Cdc2 kinase by reversible dephosphorylation, and in the second cycle, the Cdc2 kinase activates a cyclin protease by reversible phosphorylation. The model was used to test the hypothesis that cell cycle oscillations may arise from a negative feedback loop, i.e., the cyclin activates the Cdc2 kinase, while the Cdc2 kinase triggers the degradation of the cyclin.

The minimal cascade model is represented in Figure 3.24. It involves only two main actors, cyclin and CDK. Cyclin is synthesized at constant rate, v_i, and triggers the transformation of inactive (M+) into active (M) Cdc2 kinase by enhancing the rate of a phosphatase, v_1. A kinase with rate v_2 reverts this modification. In the lower cycle, the Cdc2 kinase phosphorylates a protease (v_3) shifting it from the inactive (X+) to the active (X) form. The activation of the cyclin protease is reverted by a

(a)

(b)

(c)

(d)
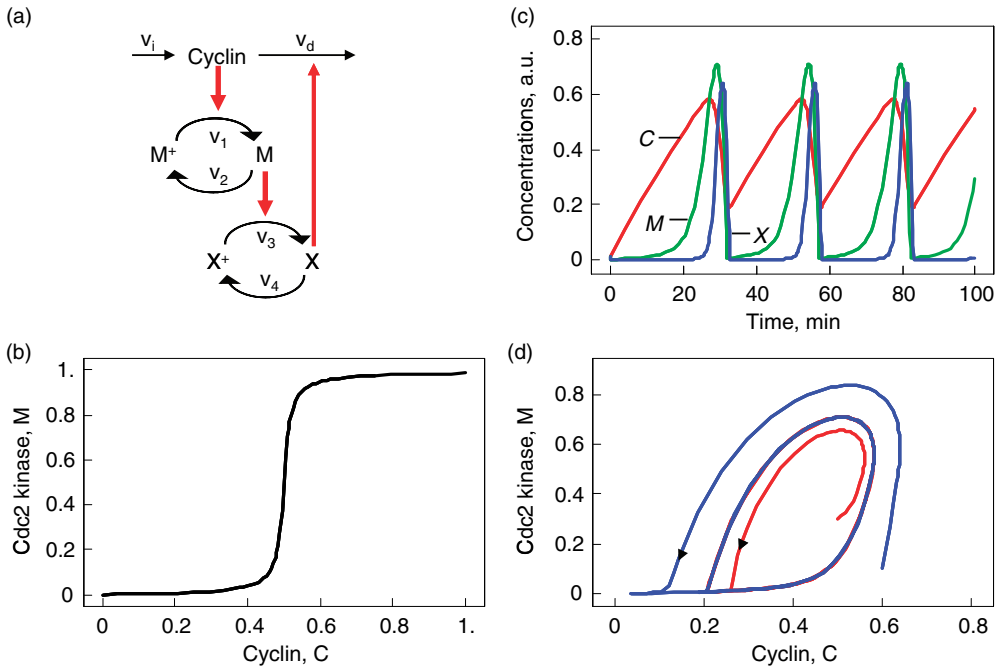
Figure 3.24 Goldbeter's minimal model of the mitotic oscillator. (a) Illustration of the model comprising cyclin production and degradation, phosphorylation and dephosphorylation of Cdc2 kinase, and phosphorylation and dephosphorylation of the cyclin protease (see text). (b) Threshold-type dependence of the fractional concentration of active Cdc2 kinase on the cyclin concentration. (c) Time courses of cyclin (C), active Cdc2 kinase (M), and active cyclin protease (X) exhibiting oscillations according to Equation system in Eq. (3.1). (d) Limit cycle behavior, represented for the variables C and M. Parameter values: $K_{mi} = 0.05$ ($i = 1, \ldots, 4$), $K_{mc} = 0.5$, $k_d = 0.01$, $v_i = 0.025$, $v_d = 0.25$, $V_{m1} = 3$, $V_{m2} = 1.5$, $V_{m3} = 1$, $V_{m4} = 0.5$. Initial conditions in (b) are $C(0) = M(0) = X(0) = 0.01$, and in (c) are $X(0) = 0.01$. Units: μM and min^{-1}.

further phosphatase with rate v_4. The dynamics is governed by the following ODE system:

$$\frac{dC}{dt} = v_i - v_d \frac{X \cdot C}{K_{md} + C} - k_d C$$

$$\frac{dM}{dt} = \frac{V_{m1} \cdot (1-M)}{K_{m1} + (1-M)} - \frac{V_{m2} \cdot M}{K_{m2} + M} \tag{3.32}$$

$$\frac{dX}{dt} = \frac{V_{m3} \cdot (1-X)}{K_{m3} + (1-X)} - \frac{V_{m4} \cdot X}{K_{m4} + X},$$

where C denotes the cyclin concentration; M and X represent the fractional concentrations of active Cdc2 kinase and active cyclin protease, while $(1 - M)$ and $(1 - X)$ are the fractions of inactive kinase and phosphatase, respectively. K_m values are Michaelis constants. $V_{m1} = V_1 C/(K_{mc} + C)$ and $V_{m3} = V_3 \cdot M$ are effective maximal

rates. Note that the differential equations for the changes of *M* and *X* are modeled with the so-called Goldbeter–Koshland switch.

This model involves only Michaelis–Menten type kinetics, but no form of positive cooperativity. It can be used to test whether oscillations can arise solely as a result of the negative feedback provided by the Cdc2-induced cyclin degradation and of the threshold and time delay involved in the cascade. The time delay is implemented by considering posttranslational modifications (phosphorylation/ dephosphorylation cycles v_1/v_2 and v_3/v_4). For certain parameters, they lead to a threshold in the dependence of steady-state values for *M* on *C* and for *X* on *M* (Figure 3.24(b)). Provided that this threshold exists, the evolution of the bicyclic cascade proceeds in a periodic manner (Figure 3.24(c)). Starting from low initial cyclin concentration, this value accumulates at constant rate, while *M* and *X* stay low. As soon as *C* crosses the activation threshold, *M* rises. If *M* crosses the threshold, *X* starts to increase sharply. X in turn accelerates cyclin degradation and consequently, *C*, *M*, and *X* drop rapidly. The resulting oscillations are of the limit cycle type. The respective limit cycle is shown in phase plane representation in Figure 3.24(d).

3.3.3
Models of Budding Yeast Cell Cycle

Tyson, Novak, and colleagues have developed a series of models describing the cell cycle of budding yeast in very detail [45–48]. These comprehensive models employ a set of assumptions that are summarized in the following.

The cell cycle is an alternating sequence of the transition from G_1 phase to S/M phase, called "Start" (in mammalian cells, it is called "restriction point"), and the transition from S/M to G_1, called "Finish." An overview is given in Figure 3.25.

The CDK (Cdc28) forms complexes with the cyclins Cln1 to Cln3 and Clb1 to Clb6, and these complexes control the major cell cycle events in budding yeast cells. The complexes Cln1-2/Cdc28 control budding, the complex Cln3/Cdc28 governs the executing of the checkpoint "Start," Clb5-6/Cdc28 ensures timely DNA replication, Clb3-4/Cdc28 assists DNA replication and spindle formation, and Clb1-2/Cdc28 is necessary for completion of mitosis.

The cyclin–CDK complexes are in turn regulated by synthesis and degradation of cyclins and by the Clb-dependent kinase inhibitor (CKI) Sic1. The expression of the gene for Cln2 is controlled by the transcription factor SBF, the expression of the gene for Clb5 by the transcription factor MBF. Both the transcription factors are regulated by CDKs. All cyclins are degraded by proteasomes following ubiquitination. APC is one of the complexes triggering ubiquitination of cyclins.

For the implementation of these processes in a mathematical model, the following points are important. Activation of cyclins and CDKs occurs in principle by the negative feedback loop presented in Goldbeter's minimal model (see Figure 3.24). Furthermore, the cells exhibit exponential growth. For the dynamics of the cell, mass *M* holds $dM/dt = \mu M$. At the instance of cell division, *M* is replaced by *M*/2. In some
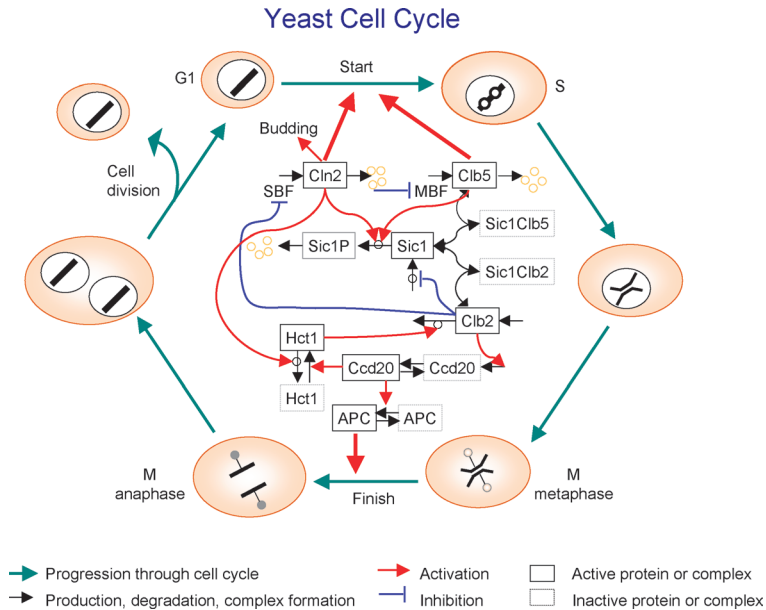
Yeast Cell Cycle

Figure 3.25 Schematic representation of the yeast cell cycle (inspired by Fall *et al.* [44]). The outer ring represents the cellular events. Beginning with cell division, it follows the G1 phase. The cells possess a single set of chromosomes (shown as one black line). At "Start," the cell goes into the S phase and replicates the DNA (two black lines). The sister chromatids are initially kept together by proteins. During M phase, they are aligned, attached to the spindle body, and segregated to different parts of the cell. The cycle closes with formation of two new daughter cells. The inner part represents main molecular events driving the cell cycle comprising (1) protein production and degradation, (2) phosphorylation and dephosphorylation, and (3) complex formation and disintegration. For the sake of clarity, CDK Cdc28 is not shown. The "Start" is initiated by activation of CDK by cyclins Cln2 and Clb5. The CDK activity is responsible for progression through S and M phase. At Finish, the proteolytic activity coordinated by APC destroys the cyclins and renders thereby the CDK inactive.

cases, uneven division is considered. Cell growth implies adaptation of the negative feedback model to growing cells.

The transitions "Start" and "Finish" characterize the wild-type cell cycle. At "Start," the transcription factor SBF is turned on and the levels of the cyclins Cln2 and Clb5 increase. They form complexes with Cdc28. The boost in Cln2/Cdc28 has three main consequences: it initiates bud formation, it phosphorylates the CKI Sic1 promoting its disappearance, and it inactivates Hct1, which in conjunction with APC was responsible for Clb2 degradation in G1 phase. Hence, DNA synthesis takes place and the bud emerges. Subsequently, the level of Clb2 increases and the spindle starts to form. Clb2/Cdc28 inactivates SBF and Cln2 decreases. Inactivation of MBF causes Clb5 to decrease. Clb2/Cdc28 induces progression through mitosis. Cdc20 and Hct1, which target proteins to APC for ubiquitination, regulate the metaphase–anaphase transition. Cdc20 has several tasks in the anaphase. Furthermore, it activates Hct,
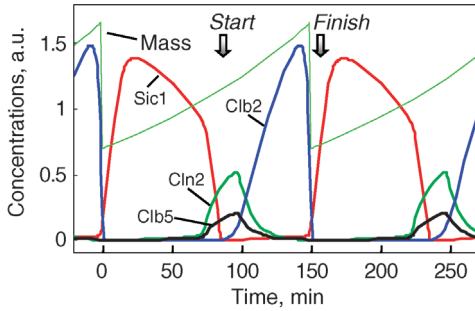
Figure 3.26 Temporal behavior of some key players during two successive rounds of yeast cell cycle. The dotted line indicates the cell mass that halves after every cell division. The levels of Cln2, $Clb2_{total}$, $Clb5_{total}$, and $Sic1_{total}$ are simulated according to the model presented by Chen *et al.* [47].

promoting degradation of Clb2, and it activates the transcription factor of Sic1. Thus, at "Finish," Clb2 is destroyed and Sic1 reappears.

The dynamics of some key players in cell cycle according to the model given in Chen *et al.* [47] is shown in Figure 3.26 for two successive cycles. At "Start," Cln2 and Clb5 levels rise and Sic1 is degraded, while at "Finish," Clb2 vanishes and Sic1 is newly produced.

3.3.4
Modeling Nucleo/Cytoplasmatic Compartmentalization

Compartmentalization is a major characteristic of eukaryotic cells. The partitioning of a cell by membranes results in a separation of functional units and in the formation of reaction spaces that might differ significantly in their molecular composition. This is due to a restricted permeability of the membranes and the controlled shuttling of molecules (e.g., mRNAs, proteins, protein-complexes) between compartments, e.g., between the cytosol and the nucleus. This compartmentalization has also regulatory aspects, e.g., for the cell cycle.

Barberis *et al.* [49] have set up a model of G_1/S transition of the budding yeast cell cycle that takes into account compartmentalization. The structure of the model is displayed in Figure 3.27. The model is composed of two compartments – the cytoplasm and the nucleus. The partitioning allows us to consider differences in the concentrations of same molecule species that are in different compartments. All proteins of the model have synthesis and degradation reactions. Protein synthesis takes place in the cytoplasm. Since the expression of the cyclins Cln1,2 and Clb5,6 is regulated by transcription factors of the mode (SBF, MBF), they are explicitly modeled by transcription events taking place in the nucleus, a transfer of the respective mRNAs into the cytoplasm, and their subsequent translation. Cln3 is the most upstream cyclin in the yeast cell cycle progression. In growing cells, the Cln3 protein enters the nucleus and forms a binary complex with Cdk1 (Cdk1–Cln3). Active nuclear Cdk1–Cln3 activates the transcription factors SBF and MBF. This
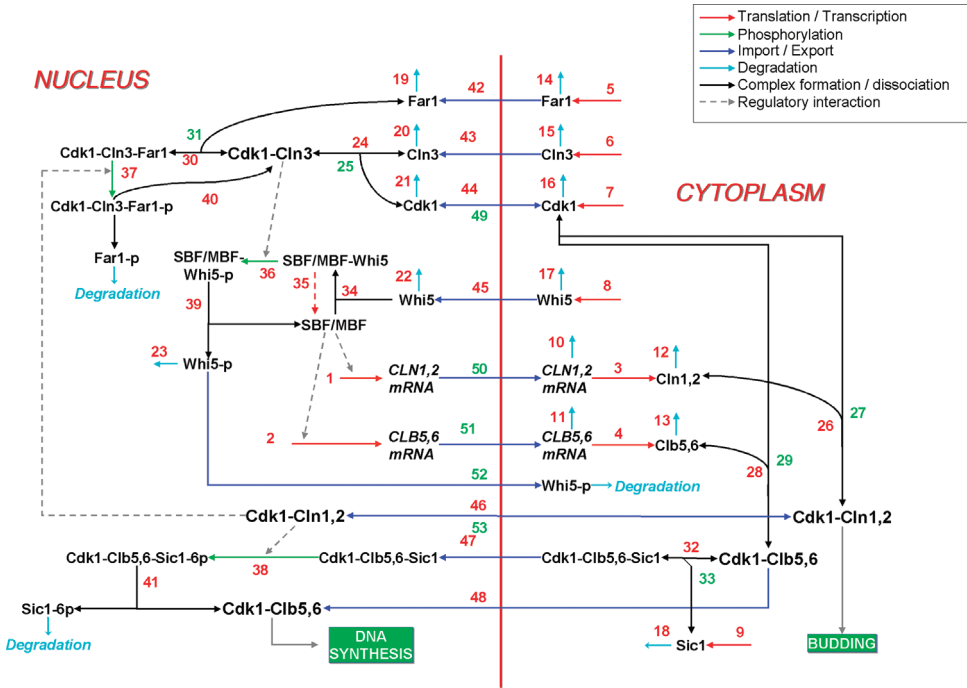
Figure 3.27 Processes regulating the G_1/S transition in budding yeast (this figure was kindly provided by M. Barberis [49]).

happens indirectly by Cdk1–Cln3 mediated phosphorylation of Whi5 and its subsequent dissociation from SBF and MBF. The activation of SBF and MBF commits a cell to DNA replication and budding. This happens due to SBF-mediated transcription of Cln1,2. Similarly, the transcription factor MBF activates Clb5,6 transcription. This activation cascade is modulated by the Cdk inhibitor protein Far1. Far1 is largely enriched in newborn cells and forms a ternary complex with Cdk1–Cln3. Given the presence of a substantial amount of Far1 in the cell, Far1 traps Cdk1–Cln3 in the inactive form. Growth-dependent accumulation of Cln3 allows it to overcome the threshold that is set by Far1. Furthermore, in the presence of Cdk1–Cln1,2, Far1 can be phosphorylated and hence primed for degradation. The degradation of Far1 yields in a substantial amount of active Cdk1–Cln3.

The newly expressed proteins Cln1 and Cln2 form a cytoplasmatic complex with Cdk1 that promotes the biochemical reactions relevant for budding. Moreover, Clb5 and Clb6 bind to Cdk1 and migrate into the nucleus where the Cdk1–Clb5,6 complex initiates DNA replication. Like Far1 is an inhibitor of Cdk1–Cln3 activity, Sic1 is an inhibitor of Cdk1–Clb5,6 activity. But in the same way as Far1 can be targeted for degradation by phosphorylation, also Sic1 can be phosphorylated by Cdk1–Cln1,2 and subsequently degraded.

The model defines two thresholds that subsequently have being overcome during the upstream events of "Start": (i) Cln3–Cdk1 has a threshold that is set by Far1 and
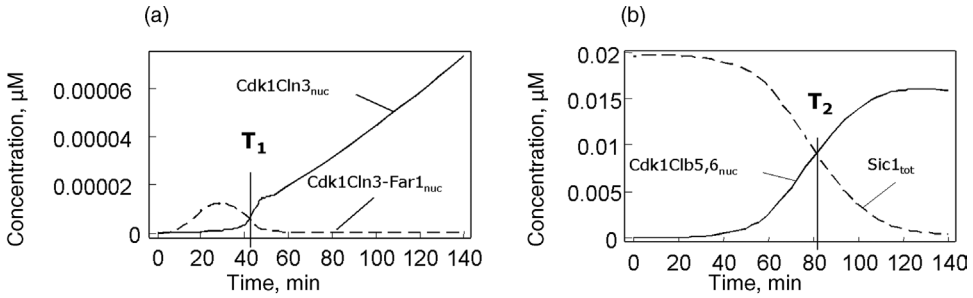
Figure 3.28 Simulation results of the G_1/S transition model. (a) Nuclear Cdk1-Cln3-Far1 complex reaches its maximal concentration after 30 min and becomes degraded upon overcoming Cln3/Far1 threshold (T_1). (b) The half-maximal concentration of nuclear Cdk1-Clb5,6 is reached at around 80 min, thereby setting the Clb5,6/Sic1 threshold (T_2) (this figure was kindly provided by Barberis [49]).

(ii) Cdk1–Clb5,6 has a threshold that is set by Sic1. The simulation results depicted in Figure 3.28 show these thresholds.

Compartmentalization as described by this model addresses the following regulatory issues:

1. Gene expression involves the migration of the mRNA from the nucleus to the cytosol, where proteins are synthesized.
2. Both import and export of proteins to or from the nucleus can be regulated independently.
3. Controlled partitioning affects binding equilibria by altering the actual concentration of a given protein available for binding to a given interactor within a subcellular compartment.

3.4
Spatial Models

Summary

Cells and organisms show complex spatial structures, which are vital for the processes of life. Biochemical reaction–diffusion systems can establish, maintain, and adapt spatial structures in a self-organized and robust manner. The body plan of animals, for instance, is shaped during embryonic development by spatial-temporal profiles of morphogen levels. Dynamic instabilities in such systems can give rise to spontaneous pattern formation. The spatiotemporal dynamics of substance concentrations can be modeled in different mathematical frameworks, including compartment models, reaction–diffusion equations, and stochastic simulations.

Cells, tissues, and organisms show complex spatial structures, and many biological processes involve spatiotemporal dynamics. Prominent examples are calcium waves within cells, neural activity in the brain, patterning during embryonic development, or the invasion of tissues by cancer cells. Such spatiotemporal processes can be modeled in different mathematical frameworks, including compartment and reaction–diffusion models [50]. Spatial simulation can increase the numerical cost quite drastically, but characteristic dynamic behavior like waves or pattern formation can already be studied in relatively simple models with one or two substances.

Spatial structures are vital for many processes in living cells. Organelles can contain different compositions of enzymes and provide suitable environments for different biochemical processes (e.g., presence of hydrolases and low pH in lysosomes); membranes allow to establish gradients of concentrations or chemical potential, e.g., proton gradients that provide an energy storage in bacteria and mitochondria. The localization of molecules also plays a role in signaling: in the Jak–Stat pathway, for instance, active Stat proteins accumulate in the nucleus to induce transcriptional changes. Besides the compartments, there is also structure on the microscopic scale: scaffold proteins can hold together protein complexes. By localizing several functions in close vicinity, they create a "critical mass" of enzymatic activity. In channeling, for instance, intermediates are directly passed from enzyme to enzyme, which increases the efficiency of enzymes.

3.4.1
Types of Spatial Models

How can spatial substance distributions be described in models? If molecules move freely and independently and if diffusion is much faster than chemical reactions, inhomogeneities will rapidly disappear, and substances may be described by their concentrations averaged over the cell. On the other hand, if molecules are not distributed homogeneously, e.g., because membranes slow down the diffusion of molecules, then spatial location and structure need to be modeled.

3.4.1.1   Compartment Models and Partial Differential Equations

One possibility is to describe substances by their concentrations in different compartments, e.g., organelles in the cell. Compartments are also used in pharmacokinetics, to model the distribution and degradation of substances in different organs [51, 52]. Compartment models are based on the assumption of fast diffusion within each compartment; if biological compartments resemble each other (e.g., the mitochondria in a cell) and rapid mixing between them would not make a difference, they can be treated as a single, effective compartment.

If diffusion is slow within compartments, it will not wear away the spatial inhomogeneities in substance concentrations: on the contrary, coupling between diffusion and chemical reactions may generate dynamic patterns (e.g., waves) out of homogeneous substance distributions. The dynamics of such patterns can be described by *reaction–diffusion systems*, which describe substance concentrations in continuous space and time. The partial differential equations can be solved

numerically by splitting the space in question into *finite elements*, small volume elements which formally resemble compartments, but are chosen according to numerical requirements.

3.4.1.2 Stochastic Models

Partial differential equation models assume that concentrations are smooth functions in space – which only holds on a spatial scale much larger than the average distance between molecules. If a substance is present in small amounts, the behavior of individual molecules – thermal movement and chemical reactions – can be simulated by stochastic models. A stochastic simulation may track each individual particle, describing its diffusion by a random walk. If molecules are in close vicinity, they may participate in a chemical reactions and be transformed into product molecules. The numerical effort for such simulations is high, especially if many particles are modeled. Instead of tracking the histories of individual particles, we can also split the cell into subvolumes and simulate the particle numbers within subvolumes by a random process describing reaction and diffusion (see Section 7.1.3 and Chapter 14).

3.4.1.3 Cellular Automata

In *cellular automata* models [53], space is represented by a discrete array of nodes, so-called cells. Each cell can show different discrete states, which are updated in discrete time steps; the new state can be chosen deterministically or stochastically and depends typically on the current states of the cell and its neighbors. A prominent example of a cellular automaton is Conway's *game of life* [54]. In this model, cells form a square lattice and can assume two different states, "dead" (or 0) and "live" (or 1). The states are updated synchronously according to the following rules: (i) a live cell with fewer than 2 or more than 3 neighbors dies; a live cell with 2 or 3 neighbors remains alive. (ii) If a dead cell has exactly three neighbors, it comes to life, otherwise it remains dead. These simple rules give rise to a surprisingly rich dynamic behavior (see exercise 4). More complicated models can be used to simulate the proliferation of cells and organisms in space.

3.4.2
Compartment Models

In compartment models, we assume that concentrations are homogeneous within each compartment. Transport between compartments –, e.g., diffusion across membranes –, is modeled by transport reactions. Passive exchange through membranes or pores, for instance, may be described as diffusion with a rate

$$v^*(s_1, s_2) = AP(s_1 - s_2), \tag{3.33}$$

where the permeability P (in $m \cdot s^{-1}$) depends on the physicochemical properties of membrane, channels, and molecules, and A denotes the membrane area; the indices 1 and 2 refer to the compartments. Active transport by transporter proteins may be modeled by a saturable rate law, for instance, irreversible Michaelis–Menten kinetics. Importantly, transport rates are measured as *amounts* per time (in $mol \cdot s^{-1}$), but for

physical reasons, their values depend on compound *concentrations* in mM (e.g., the difference $s_1 - s_2$ in Eq. (3.33)).

So, although compartment models are not very different from usual kinetic models, we need to pay some attention to the correct conversion between substance amounts, concentrations, and compartment volumes. It is practical to start with the amounts a_i (where the subscript i indicates a substance located in a compartment). With the reaction velocities v^* (in $mol \cdot s^{-1}$), we obtain the rate equation

$$\frac{da_i}{dt} = \sum_l n_{il} v_l^*(\boldsymbol{s}), \tag{3.34}$$

where the n_{il} are the stoichiometric coefficients. Each amount a_i is defined in a compartment with index $k(i)$ and a volume $V_{k(i)}$ (in m^3). After introducing the concentrations $s_i = a_i / V_{k(i)}$, we can rewrite the time derivative in Eq. (3.34) as

$$\frac{da_i}{dt} = \frac{d}{dt}\left(V_{k(i)} s_i\right) = V_{k(i)} \frac{ds_i}{dt} + \frac{dV_{k(i)}}{dt} s_i. \tag{3.35}$$

By combining Eqs. (3.34) and (3.35), we obtain the rate equation for concentrations

$$\frac{ds_i}{dt} = \sum_l \frac{n_{il}}{V_{k(i)}} v_l^*(\boldsymbol{s}) - \frac{dV_{k(i)}/dt}{V_{k(i)}} s_i. \tag{3.36}$$

It shows that concentration changes can be caused by chemical reactions (first term) and volume changes (second term). If all compartments in Eq. (3.36) have the same time-independent volume, we can replace $v_l^* / V_{k(i)}$ by the usual reaction velocity v_l in $mM \cdot s^{-1}$; the second term vanishes, so we obtain the usual form of kinetic models. But we can also consider the transport of a substance between two compartments (1 and 2) of different volume. If the volume sizes are constant in time, the second term vanishes and we obtain, for this reaction alone,

$$V_1 \frac{ds_1}{dt} = -V_2 \frac{ds_2}{dt}. \tag{3.37}$$

The minus sign stems from the stoichiometric coefficients. The volumes play an important role in transport between cells and the external medium: intra- and extracellular concentration changes are converted to each other by the volume ratio V_{cell}/V_{ext}, where V_{cell} is the volume of a single cell and V_{ext} denotes the extracellular volume divided by the number of cells.

The second term in Eq. (3.36) describes the effect of temporal volume changes: substances in growing cells are diluted, so their concentration will decrease even if they are not consumed by chemical reactions. If a cell population grows at a rate $\mu(t)$, the total cell volume V increases according to

$$\frac{dV}{dt} = \mu(t) V(t), \tag{3.38}$$

so the prefactor in the second term in Eq. (3.36) is just the growth rate $\mu(t)$. Dilution of molecules in a growing cell population formally resembles linear degradation, with the cell growth rate μ appearing as an effective degradation constant.

3.4.3
Reaction–Diffusion Systems

3.4.3.1   The Diffusion Equation

The diffusion equation describes the space- and time-dependent concentration $s(r, t)$ of a diffusing substance, where r is a position in space, and t is a moment in time. In spatial models, positions are generally represented by three-dimensional vectors $r = (x, y, z)^T$, but in the following, we will sometimes consider a single space dimension only. This simplification is justified if we model a long, thin compartment or if we assume homogeneity along two space directions. The flow of a substance can be described by a vectorial flow field $j(r, t)$; we can interpret the flow as a product $j(r, t) = s(r, t)\, w(r, t)$, where $w(r, t)$ is the locally averaged particle velocity. If a substance is conserved (no production or degradation by chemical reactions), its concentration obeys the continuity equation

$$\frac{\partial s(r, t)}{\partial t} = -\nabla \cdot j(r, t). \tag{3.39}$$

Fick's law states that a small concentration gradient in a homogeneous, isotropic medium will evoke a flow

$$j(r, t) = -D\, \nabla s(r, t), \tag{3.40}$$

with a *diffusion constant D*. By inserting Eq. (3.40) into the continuity equation (3.39), we obtain the diffusion equation

$$\frac{\partial s(r, t)}{\partial t} = D\, \nabla^2 s(r, t), \tag{3.41}$$

with the *Laplace operator*

$$\nabla^2 s = \frac{\partial^2 s}{\partial x^2} + \frac{\partial^2 s}{\partial y^2} + \frac{\partial^2 s}{\partial z^2}. \tag{3.42}$$

In one space dimension, the Laplace operator simply reads $\nabla^2 s(r, t) = \partial^2 s/\partial r^2$. The diffusion equation (3.41) for concentrations corresponds to the Fokker–Planck equation for Brownian random motion of individual particles (see Chapter 14).

To solve it in a region in space, we need to specify initial conditions (a concentration field $s(r, 0)$ at time $t = 0$) and boundary conditions for all points r_0 on the boundary. It is common to fix concentrations $s(r_0, t)$ on the boundary (a *Dirichlet boundary condition*) or to assume that the boundary is impermeable, i.e., the flow orthogonal to the boundary vanishes. As the flow points along the concentration gradient, this is an example of a *von Neumann boundary condition*, which in general sets the values of $\nabla s(r_0) \cdot n(r_0)$, where n is a unit vector orthogonal to the surface. In one space dimension, an impermeable boundary implies that $\partial s(r, t)/\partial r|_{r=r_0} = 0$, so the slope of the concentration is always zero at the boundary. The diffusion equation, together with proper initial and boundary conditions, determines the time-dependent concentration field $s(r, t)$ at times $t \geq 0$.

(a)

(b)
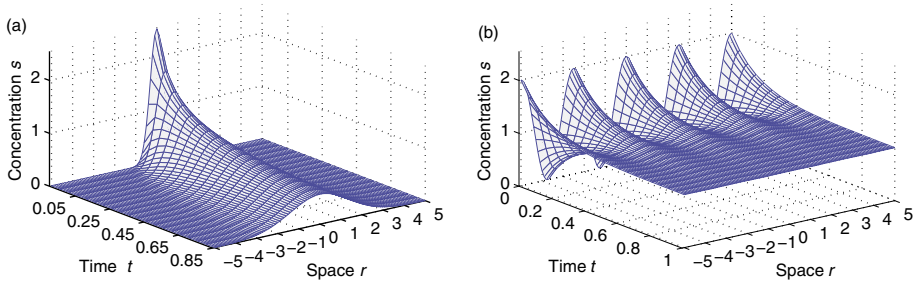
Figure 3.29 Diffusion tends to blur spatial concentration patterns. (a) A localized substance amount leads to a Gaussian-like cloud of increasing width. Parameters $a = 2$, $D = 1$. Time, space, and concentration in arbitrary units. (b) An initial cosine wave pattern keeps its shape, but its amplitude decreases exponentially in time. Parameters $s_0 = 1$, $D = 1$, $k = 2\pi/(5/2)$, base line concentration 1.

3.4.3.2 Solutions of the Diffusion Equation

Diffusion tends to remove spatial heterogeneity: local concentration maxima (with negative curvature $\nabla^2 s$) will shrink and local minima are filled. This is illustrated by some special solutions of the diffusion equation in one space dimension.

1. Stationary concentration profiles in one space dimension have vanishing curvature. If concentrations at the boundaries $r = 0$ and $r = L$ are fixed, one obtains a linear stationary profile $s^{st}(r)$ in which substance flows down the concentration gradient. For impermeable boundaries, the stationary solution is a homogeneous, constant profile $s^{st}(r) = \text{const}$ corresponding to a thermodynamic equilibrium.

2. If a substance amount a is initially concentrated in the point $r = 0$ and if we impose the boundary condition $s(r, t) \to 0$ for $r \to \pm\infty$, diffusion will lead to a Gaussian-shaped concentration profile (see Figure 3.29(a))

$$s(r, t) = \frac{a}{\sqrt{2\pi(2Dt)}} e^{-\frac{r^2}{2(2Dt)}}.$$ (3.43)

The width $\sqrt{2Dt}$ increases with the square root of diffusion constant D and time t.

3. Now we consider a finite region $0 \leq r \leq L$ with impermeable boundaries, i.e., $\partial s/\partial r = 0$ at both $r = 0$ and $r = L$ and choose, as initial condition, a cosine pattern, i.e. an eigenmode of the diffusion operator. Under diffusion, the pattern will keep its shape, but the amplitude decreases exponentially (Figure 3.29(b)):

$$s(r, t) = s_0 e^{-\lambda(k)t}\cos(k r).$$ (3.44)

To ensure positive concentration values, a base line concentration can be added. Due to the boundary conditions, the possible wave numbers k are restricted

to values $k = n\pi/L$ with integer n. The time constant λ is given by the dispersion relation $\lambda(k) = -D k^2$, so narrow-spaced cosine patterns (with large wave numbers k) are smoothed out faster than broad patterns.

As the diffusion equation is linear, general solutions can be obtained by convolution integrals or linear combinations of the profiles (3.43) or (3.44).

3.4.3.3 Reaction–Diffusion Equation

A reaction–diffusion system consists of several substances that diffuse and participate in chemical reactions. By combining a kinetic model for the chemical reactions with the diffusion equation (3.41), we obtain a reaction–diffusion equation

$$\frac{\partial s_i(\boldsymbol{r}, t)}{\partial t} = \sum_l n_{il}\, v_l(\boldsymbol{s}(\boldsymbol{r}, t)) + D_i \nabla^2 s_i(\boldsymbol{r}, t) \tag{3.45}$$

for the concentrations s_i. The first term represents local chemical reactions, while the second term describes diffusion with substance-specific diffusion constants D_i. As the rate laws $v_l(\boldsymbol{s})$ are usually nonlinear, most reaction–diffusion models can only be solved numerically, e.g., by finite-element methods. Reaction–diffusion equations can show various kinds of dynamic behavior including pattern formation, traveling and spiraling waves, or chaos, some of which is also observed in biological systems (Figure 3.30). For instance, traveling waves arising from
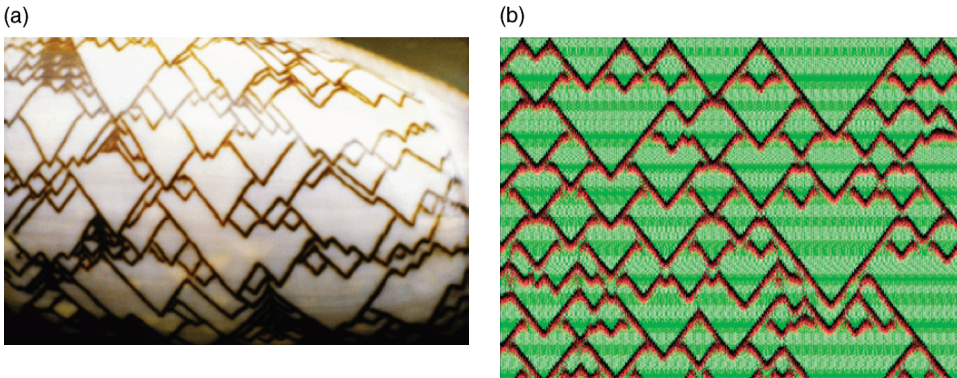
Figure 3.30 Patterns on sea shells arising from a reaction–diffusion system. (a) Color patterns on the shell of *Oliva porphyria* are formed as more material is added to the growing edge of the shell, so the vertical direction in the picture can be interpreted as a time axis. The patterns are preformed by a chemical reaction–diffusion system: in this case traveling waves lead to diagonal lines. (b) The patterns can be simulated by an activator-inhibitor system (black and red) with an additional global signaling substance (green) that counteracts the pairwise annihilation of waves [55, 56]. The vertical axis represents time from top to bottom (Courtesy of H. Meinhardt).

simple reaction–diffusion systems have been used to model the patterns on sea shells [55, 56].

Pattern Formation in Tissue Development

The body plan of multicellular organisms is established in embryonic development by coordinated growth and differentiation of cells. Organisms can develop very specific shapes in a robust manner, which we can see from the similarity between twins and the symmetry of our bodies.

The development process is organized by spatial patterns of *morphogens,* which act as a coordinate system in the developing tissue. If a morphogen level shows a gradient along the anterior–posterior axis of the embryo, cells can sense their positions on this axis and differentiate accordingly [57]. Morphogen fields follow a spatiotemporal dynamics, which arises from its interactions with the growing tissue and is implicitly determined by the way cells sense and produce the morphogens.

Comparable forms of cell communication and collective dynamics also appear in bacteria (in quorum sensing) or in colonies of the social amoeba *Dictyostelium discoideum,* which can turn temporarily into a multicellular organism. Another example is the hydra, a multicellular animal that can regrow its main organs, foot and head, after it is cut into halves, and which can even re-associate from individual cells. The spontaneous development of a new body axis in the hydra by biochemical pattern formation has been described qualitatively by mathematical models [58, 59].

The fly *Drosophila melanogaster* is a prominent model organism for embryonic development: its anterior–posterior body axis is established in early oocyte stage by a gradient of a morphogen protein called Bicoid. Bicoid is produced from mRNA that is attached to microtubules at the anterior end of the unfertilized egg; it then forms a gradient that marks the anterior part of the embryo and serves as a reference for further patterning processes (see Figure 3.31(a)). To compute a stationary Bicoid profile in a simple model, we assume a steady-state balance of production, diffusion, and linear degradation. The concentration $s(r,t)$ in one dimension (pointing along the anterior–posterior axis) can be described by the reaction–diffusion equation

$$\frac{\partial s(r,t)}{\partial t} = D\nabla^2 s(r,t) - \kappa s(r,t), \tag{3.46}$$

with diffusion constant D and degradation constant κ. The stationary profile $s^{st}(r)$ has to satisfy the steady-state condition

$$0 = D\nabla^2 s^{st}(r) - \kappa s^{st}(r), \tag{3.47}$$

which can be solved by a sum of exponential profiles

$$s^{st}(r) = a_1 e^{-r/L_0} + a_2 e^{r/L_0}, \tag{3.48}$$

(a)

(b)
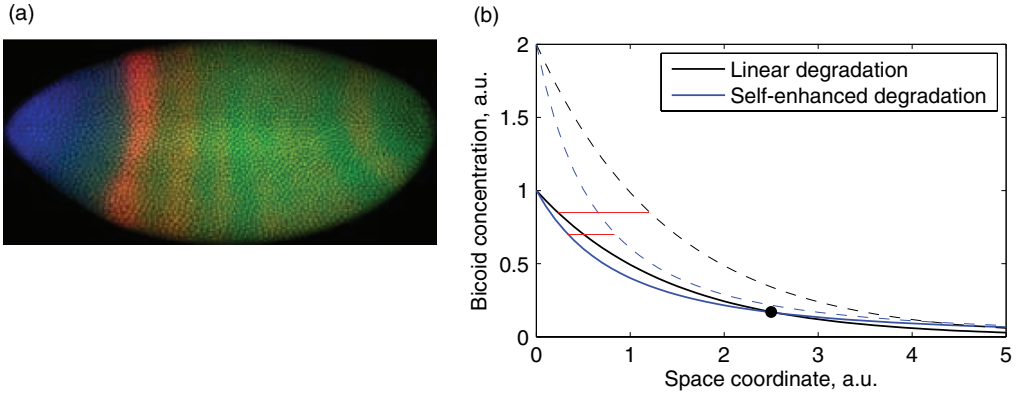
Figure 3.31 Spatial pattern of the morphogen Bicoid. (a) Microscope image [60] showing expression patterns of the genes *even-skipped* (red), *caudal* (green), and *bicoid* (blue). From the FlyEx database [61]. (b) Model results. Solid curves show simulated profiles obtained from models with linear degradation (black) or self-enhanced degradation (blue) and parameters $D = 0.01$, $\kappa = 0.02$, $s_0 = 1$. The Bicoid concentrations in both models coincide at $r = 0$ and $r \approx 2.5$ (dot). The broken curves show profiles that would result from an increased concentration $s_0 = 2$ at the anterior end. The change of this boundary condition shifts profiles to the right by a constant amount (shift sizes marked by red lines).

with the characteristic degradation length $L_0 = \sqrt{D/\kappa}$. The coefficients a_1 and a_2 need to be chosen according to the boundary conditions. We describe Bicoid production by fixing a constant concentration $s(r = 0) = s_0$ at the anterior boundary of the cell; s_0 is proportional to the protein production rate and therefore to the amount of mRNA. On the posterior end, Bicoid cannot leave the cell, so we set $ds^{st}/dr|_{r=L} = 0$. With these boundary conditions, the coefficients in Eq. (3.48) read

$$a_1 = \frac{\beta^2 s_0}{1 + \beta^2} \quad a_2 = \frac{s_0}{1 + \beta^2}, \tag{3.49}$$

with the abbreviation $\beta = \exp(L/L_0)$. If the characteristic length L_0 is much shorter than the length L of the embryo, we can also use the boundary condition $\lim_{r \to \infty} s^{st}(r) = 0$ as an approximation. In this case, the second term in Eq. (3.48) vanishes, and we obtain the exponential profile

$$s^{st}(r) = s_0\, e^{-r/L_0}. \tag{3.50}$$

In an alternative model [62], Bicoid is assumed to catalyze its own degradation, which leads to a steeper profile near the source; with a degradation rate $\kappa s^2(r, t)$ instead of $\kappa s(r, t)$ and boundary conditions as above, the steady-state profile reads (see exercise 6)

$$s^{st}(r) = \frac{6D/\kappa}{\left(r + \sqrt{6D/(\kappa s_0)}\right)^2}. \tag{3.51}$$

This pattern combines two properties that are favorable for reliable patterning [62]. The amounts of mRNA, and therefore morphogen production, may vary from embryo to embryo: an increased production, for example, will shift the emerging pattern to the right (see Figure 3.31(b)). This effect can only be suppressed by a steep initial decrease around $r = 0$. However, in the exponential profile (3.50), a steep decrease would automatically lead to small Bicoid levels along the embryo, which could easily be distorted by noise. The profile implemented by Eq. (3.51), on the other hand, combines a steep decrease near the source with relatively high levels along the embryo. In Figure 3.31(b), for instance, both profiles show the same Bicoid level at the center of the embryo, but model (3.51) shows a much smaller shift after overexpression of Bicoid.

3.4.5
Spontaneous Pattern Formation

Some color patterns, e.g,. on the furs of zebras and leopards, are thought to arise from a self-organized pattern formation. Even if the identity of the biological morphogens and the biochemical interactions in these cases remain elusive, the geometries of these patterns can be well reproduced by simple reaction–diffusion models [63]. Figure 3.32 shows, as an example, the formation of spots in the Gierer–Meinhardt model

$$
\begin{aligned}
\frac{\partial a}{\partial t} &= \frac{\rho a^2}{b(1 + \kappa a^2)} - \mu_{\mathrm{a}} a + D_{\mathrm{a}} \nabla^2 a \\
\frac{\partial b}{\partial t} &= \rho a^2 - \mu_{\mathrm{b}} b + D_{\mathrm{b}} \nabla^2 b.
\end{aligned}
\tag{3.52}
$$

with parameters ρ and κ (for production), μ_{a} and μ_{b} (for degradation), and D_{a} and D_{b} (for diffusion). The concentrations a and b correspond, respectively, to an activator (which has a positive influence on both production terms) and an inhibitor (which

(a) (b) (c) (d)
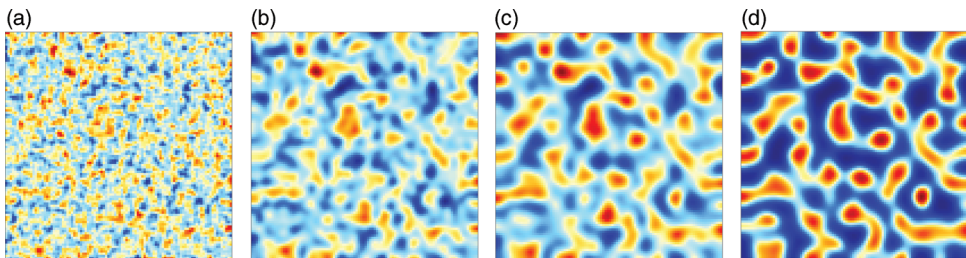
Figure 3.32 Stripe formation in the Gierer–Meinhardt model. The pictures show snapshots (activator concentration) from a simulation at time points $t = 50$ (a), $t = 200$ (b), $t = 50$ (c), $t = 200$ (d). A stripe pattern emerges spontaneously from a noisy initial concentration profile (uniform random values from the interval [0.1, 1]). Parameters $D_{\mathrm{a}} = 0.002$, $D_{b} = 0.2$, $r = 1$, $\mu_a = 0.01$, $\mu_b = 0.015$, $\kappa = 0.1$, discretization $\Delta x = 0.2$, $\Delta t = 1$ (arbitrary units).

inhibits production of the activator). Variants of this model with different parameter sets can lead to spots, stripes, and gradients. The pattern in Figure 3.32 has a typical length scale (distance between spots), which depends on the reaction and diffusion parameters, but not on the size of the tissue. The exact shape is random and depends on the initial random fluctuations.

In reaction–diffusion systems, spatial patterns can emerge spontaneously from an almost homogeneous distribution – a paramount example of spontaneous symmetry breaking. Similar patterns arise in clouds or sand ripples. Although the underlying physical systems are completely different, their ability to form patterns relies on the same general mechanism called *Turing instability* [64]. For spontaneous pattern formation, the system must have a homogeneous steady state. This steady state must be stable against homogeneous concentration changes, but unstable against spatial variation. Fluctuations of a certain finite wavelength must be amplified more strongly than fluctuations of smaller or larger wavelength.

These conditions can be fulfilled in simple reaction–diffusion systems [58] with two substances called "activator" and "inhibitor" as shown in Figure 3.33(a). If the homogeneous steady state of the system is unstable against local fluctuations, even smallest fluctuations will be amplified and lead to a stable pattern with separated regions (typically spots or stripes) of high or low activator levels. Even if the full nonlinear behavior of reaction–diffusion systems may be complicated, the necessary conditions for pattern formation can be obtained from a linear stability analysis (see web supplement). Pattern formation in activator–inhibitor systems requires that the inhibitor diffuses faster than the activator, so whereas pure diffusion removes patterns, diffusion is necessary for pattern formation in this case. Propagating waves (as shown in Figure 3.30), in contrast, require that the inhibitor has a longer life-time and that it diffuses more slowly than the activator.
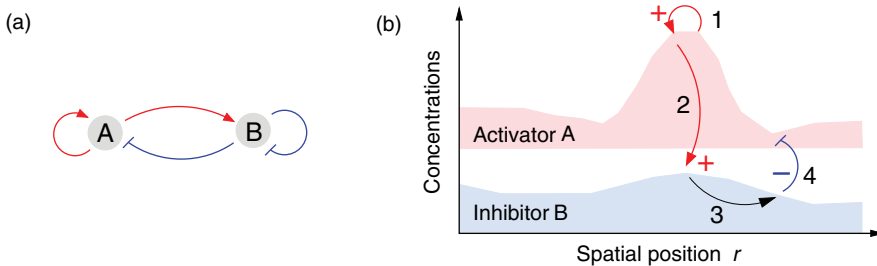
Figure 3.33 Activator–inhibitor system. (a) High levels of A (the activator) locally increase both concentrations, while B (the inhibitor) decreases them. In a nonspatial model, this system is assumed to have a stable steady state. (b) A reaction-diffusion mechanism can amplify existing local inhomogeneities: a local elevation of A catalyzes its own further increase (1). In addition, it increases the level of B (2), which diffuses faster than A (3) and represses the level of A in a distance (4). By the same mechanism, the resulting valley will further increase the original elevation and create another concentration peak nearby.

3.5
Apoptosis

Summary

Similarly as cells always divide, damaged or excess cells can be removed by a kind of cell suicide called *programmed cell death*. Apoptosis, a well-studied form of programmed cell death, can be elicited by extracellular or intracellular signals. Both extracellular signals of death receptors or intracellular signals, e.g., due to DNA damage or oxidative stress activate a signaling cascade. Extracellular or intracellular signals activate initiator caspases, which vice versa activate executioner caspases that finally lead to the death of the cell. The activation of the apoptotic program is an irreversible process – once the "point of no return" has been passed, the process cannot be reverted. The mathematical modeling of the apoptotic signaling cascade can be used for the identification of potential therapeutic targets. Furthermore, the model can be used for the analysis of certain characteristics of the apoptotic signaling cascade, such as bistability and irreversibility.

Multicellular organisms begin their life as a single cell that develops into a fully formed individual. This developmental process is controlled by a precise execution of the organism's genetic program. Although it is obvious that developmental processes require cell division and differentiation, it turned out that a specific and coordinated cell death is essential, too. The crucial role of cell death usually continues into adulthood. As well as our cells permanently proliferate, billions of cells die each day by a suicide program that is precisely coordinated and known as programmed cell death. Cells dying by apoptosis, the most common and best-understood form of programmed cell death, undergo characteristic morphological changes. The cells shrink, their cytoskeleton collapses, the nuclear envelope disassembles, the chromatin breaks up into fragments, and finally, they form so-called apoptotic bodies, which have a chemically altered surface and are usually rapidly engulfed by neighboring cells or macrophages. In contrast to cells dying accidentally by necrosis, apoptosis does not elicit an inflammatory response. Apoptosis plays an important role during development; e.g., the removal of specific cells during embryogenesis helps to sculpt the fingers of the hand, or during frog's metamorphosis it is causative for the degeneration of the tadpole's tail. Moreover, apoptosis functions as a quality control, eliminating abnormal or nonfunctional cells.

3.5.1
Molecular Biology of Apoptosis

Apoptosis depends on an intracellular proteolytic cascade mediated by caspases, a family of proteases with a cystein at their active site, which cleave their target proteins at specific aspartic acids. Caspases are synthesized in the cell as inactive precursors, or procaspases, which then become activated by proteolytic cleavage. Caspases

involved in apoptosis are classified as initiator caspases (caspases 2, 8, 9, 10) and executioner caspases (caspases 3, 6, 7). Initiator caspases act at the start of the proteolytic cascade and activate downstream executioner procaspases. Executioner caspases conduct the cell death by, e.g., activating other executioner procaspases, cleavage of nuclear lamins that results in the breakdown of the nuclear lamina, cleavage of DNA-endonuclease inhibitors that results in the fragmentation of the genomic DNA, and the cleavage of components of the cytoskeleton and cell–cell adhesion. Initiator caspases can be activated either by intracellular or extracellular signals. Figure 3.34 gives an overview of the apoptotic signaling cascade. The extracellular or extrinsic apoptotic pathway is mediated by so-called death receptors and can be induced, e.g., by immune cells that display an appropriate ligand able to
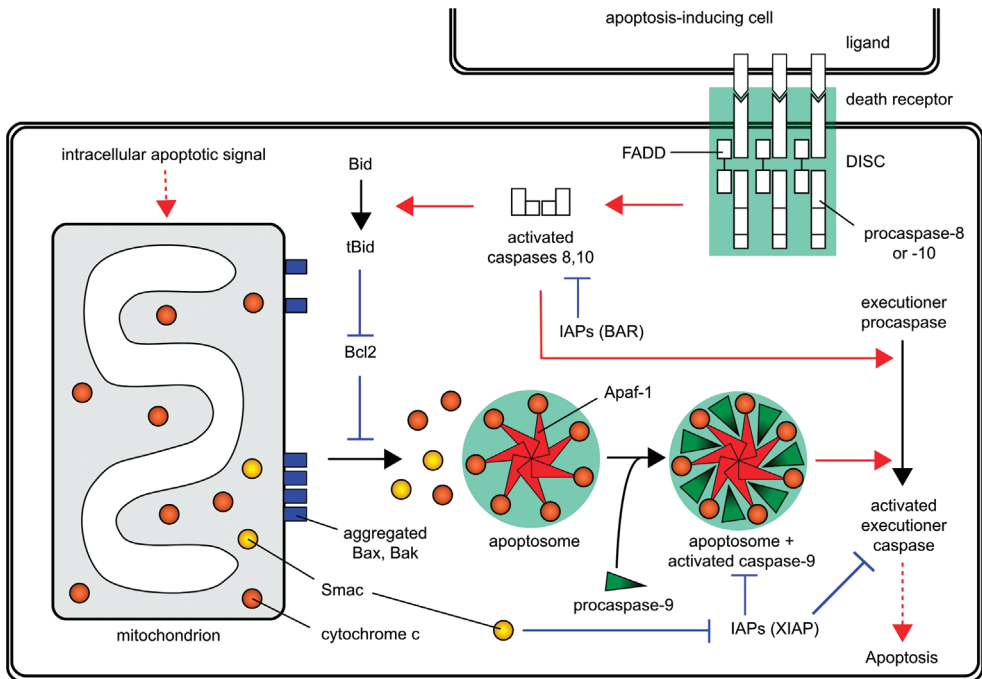
Figure 3.34 Molecular processes of the apoptotic signaling cascade. Apoptosis can be activated via extrinsic or intrinsic signals. The extrinsic apoptotic pathway is initiated by ligands binding to the death receptor, the formation of the DISC complex and the subsequent activation of the initiator caspase-8 or caspase-10. Intracellular signals, such as stress or DNA damage, can lead to an aggregation of Bax or Bak proteins on the surface of the mitochondrial membrane and initiate the release of cytochrome c from the mitochondrial intermembrane space into the cytosol. Together with Apaf-1, cytochrome c can form the apoptosome, which can bind and activate caspase-9. Both, caspases 8 and 10 of the extrinsic pathway and caspase-9 of the intrinsic pathway can cleave and activate executioner procaspases (caspases 3, 6, 7) that subsequently mediate cell death. Intrinsic apoptosis can also be activated by the extrinsic pathway by the truncation of Bid and formation of active tBid. tBid is an inhibitor of Bcl-2, which, under normal condition, binds Bax or Bak and inhibits their aggregation.

bind to its respective death receptor. Death receptor ligands are members of the tumor necrosis factor (TNF) protein family such as TNF-α, TRAIL, or the Fas ligand (FasL). Death receptors belong to the TNF receptor family, which includes a receptor for TNF itself and the Fas receptor (FasR). Binding of a ligand to a respective death receptor induces in the target cell the formation of a complex termed DISC (death-inducing signaling complex). DISC consists of the activated death receptor, the protein FADD (Fas-associated death domain protein), and one of the initiator procaspases (caspase-8 or caspase-10). This complex triggers the self-cleavage of the procaspase and thereby the formation of the respective activated initiator caspase, which in turn activates executioner caspases that finally lead to the progression of apoptosis.

On the other hand, the intracellular or intrinsic apoptotic pathway can be initiated by intracellular signals such as DNA damage or the lack of oxygen, nutrients, or extracellular survival signals. Intracellular apoptotic signals can lead to the aggregation of the pro-apoptotic proteins Bax and Bak, which mediate the release of cytochrome c and Smac from the mitochondrial intermembrane space into the cytosol. Cytochrome c is a water-soluble protein that is usually involved in the mitochondrial electron-transport chain. In the cytosol, cytochrome c binds a procaspase-activating adaptor protein called Apaf1 (apoptotic protease activating factor-1) and leads to the formation of a wheel-like heptamer called apoptosome. The apoptosome recruits the initiator procaspase-9, which then gets activated and subsequently leads to the downstream activation of the executioner procaspases.

Via a crosstalk between the extrinsic and the intrinsic pathway, an extracellular apoptotic signal can be amplified. Activated initiator caspases of the extrinsic pathway cleave the protein Bid. The truncated Bid protein, tBid, acts as a pro-apoptotic protein that is able to inhibit antiapoptotic proteins, such as Bcl2 or Bcl-X_L. Under non-apoptotic conditions, these antiapoptotic proteins oppose the aggregation of Bax or Bak and thereby suppress the onset of apoptosis.

Apoptosis cannot only be inhibited by antiapoptotic proteins belonging to the Bcl2-like protein family, but also by proteins that specifically inhibit active caspases. These proteins are called inhibitors of apoptosis (IAPs). One of the most potent IAP is the X-linked inhibitor of apoptosis protein (XIAP), which is known to inhibit the initiator caspase caspase-9 and the executioner caspases 3 and 7. The function of XIAP in turn can be inhibited by interaction with Smac.

Another protein that has a major effect on the regulation of apoptosis is the protein p53 (sometimes also termed Trp53 in mice or TP53 in humans). Often, p53 is also called a tumor suppressor gene, since it is able to cause cell cycle arrest or apoptosis. It has been shown that several DNA-damaging agents, such as X-rays, ultraviolet radiation, or certain drugs, increases the p53 protein level. p53 can hold the cell cycle and provide the cell with time to repair the DNA damage before the cell cycle proceeds. If the DNA damage cannot be repaired, an increasing amount of p53 acting as a transcription factor can lead to the expression of pro-apoptotic regulators of the Bcl2-family, such as Bax, and initiate by this intrinsic apoptosis.

Once apoptosis is initialized, essential structures of the cell become destructed. This implies that apoptosis should show an irreversible all-or-none behavior, since,

e.g., already a partial destruction of the genomic DNA would introduce irreparable damage to the cell. The existence of an all-or-none behavior, i.e., of a bistability, implies a nonlinear behavior of the system.

Dysregulation of apoptosis is associated with various pathological conditions, such as cancer and neurodegenerative disorders. Dysregulation of apoptosis might be due to an overexpression or dysfunction of its regulatory proteins. For example, an overexpression of XIAP that is inhibiting caspase-9 leads to a decrease of the amount of pro-apoptotic proteins and thus shifts the balance between antiapoptotic and pro-apototic proteins in favor of the former and would lead to a survival of cells that are devoted to die. This can be a reason for the onset of cancer. On the other hand, an overexpression of pro-apoptotic proteins or the dysfunction of antiapoptotic proteins due to mutations could result in an unintended apoptosis leading to, e.g., neurode-generative disorders such as Alzheimer's disease or Parkinson's disease.

3.5.2
Modeling of Apoptosis

Several mathematical models describing different parts and aspects of apoptosis have been developed. A large-scale model of intrinsic and extrinsic apoptosis has been proposed by Fussenegger *et al.* [65]. The model was used to investigate the impact of the overexpression or mutation of several key components of the apoptosis signaling cascade. Using the mathematical model, they analyzed the impact of different combined therapies on simultaneous extrinsic- and intrinsic-induced apoptosis. Table 3.5. shows predicted effects of such combined therapies. This table indicates therapies that are expected to decrease the executioner caspase activation during simultaneous extrinsic- and intrinsic-induced apoptosis. It turned out that no single therapy (results in the diagonal of Table 3.5.), with the exception of IAPs over-expression, is able to block executioner caspase activation. Some combinations of overexpression/disruption or mutation also show an effect, but several combinations

Table 3.5 Predicted effects of combined therapies based on simultaneous extrinsic- and intrinsic-induced apoptosis[a].

	Overexpression				Disruption or mutation	
	Bcl-2/Bcl-X_L	Bax/Bad/Bik	FLIPs	IAPs	FADD	P53
Bcl-2/Bcl-X_L	−	−	+	+	+	−
Bax/Bad/Bik	−	−	−	+	−	−
FLIPs	+	−	−	+	−	+
IAPs	+	+	+	+	+	+
FADD	+	−	−	+	−	+
P53	−	−	−	+	+	−

[a]Entries in the diagonal denote therapies with a single target; others are combinations of potential therapies. A plus sign (+) denotes therapies with decreased activation of executioner caspase, and the minus sign (−) denotes the opposite [65].
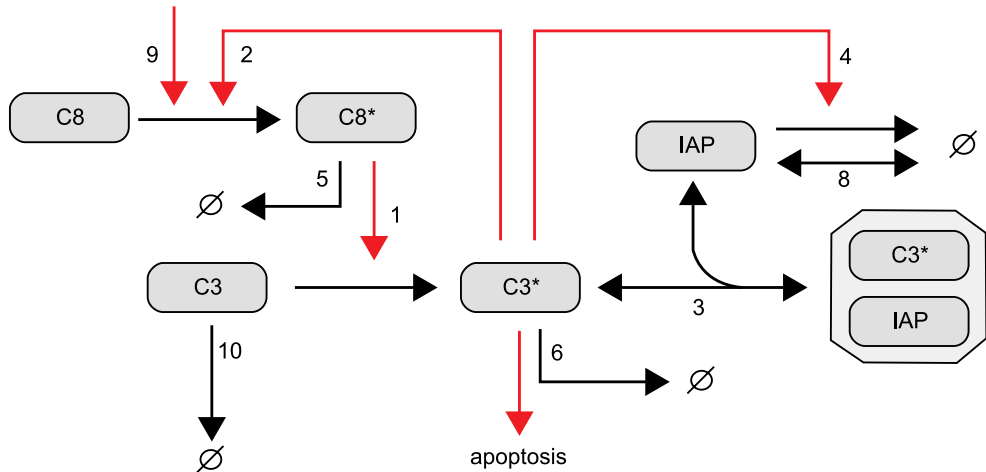
Figure 3.35 Outline of the apoptotic model developed by Eissing *et al.* [66]. It comprises the components of the extrinsic pathway of apoptosis. The asterisk (*) denotes the activated form of a caspase.

do not, because they target only a single activation route. For example, the over-expression of several antiapoptotic members of the Bcl-2 protein family does not block receptor-mediated activation and thus apoptosis can proceed. Similarly, a disruption or mutation of FADD does not block the stress-induced activation of apoptosis via the intrinsic pathway.

Another model describing the extrinsic pathway of apoptosis was developed by Eissing *et al.* [66]. The reaction schema of the model is depicted in Figure 3.35. The model is described by a system of eight ordinary differential equations.

$$
\begin{aligned}
\frac{\mathrm{d}[C8]}{\mathrm{d}t} &= -v_2 - v_9 \\
\frac{\mathrm{d}[C8^*]}{\mathrm{d}t} &= v_2 - v_5(-v_{11}) \\
\frac{\mathrm{d}[C3]}{\mathrm{d}t} &= -v_1 - v_{10} \\
\frac{\mathrm{d}[C3^*]}{\mathrm{d}t} &= v_1 - v_3 - v_6 \\
\frac{\mathrm{d}[IAP]}{\mathrm{d}t} &= -v_3 - v_4 - v_8 \\
\frac{\mathrm{d}[C3^* \sim IAP]}{\mathrm{d}t} &= -v_2 - v_9 \\
\frac{\mathrm{d}[BAR]}{\mathrm{d}t} &= -v_{11} - v_{12} \\
\frac{\mathrm{d}[C8^* \sim BAR]}{\mathrm{d}t} &= -v_{11} - v_{13}.
\end{aligned}
\tag{3.53}
$$

The rate equations read as follows:

$$v_1 = k_1 \cdot [C8^*] \cdot [C3]$$
$$v_2 = k_2 \cdot [C3^*] \cdot [C8]$$
$$v_3 = k_3 \cdot [C3^*] \cdot [IAP] - k_{-3} \cdot [C3^* \sim IAP]$$
$$v_4 = k_4 \cdot [C3^*] \cdot [IAP]$$
$$v_5 = k_5 \cdot [C8^*]$$
$$v_6 = k_6 \cdot [C3^*]$$
$$v_7 = k_7 \cdot [C3^* \sim IAP] \qquad\qquad (3.54)$$
$$v_8 = k_8 \cdot [IAP] - k_{-8}$$
$$v_9 = k_9 \cdot [C8] - k_{-9}$$
$$v_{10} = k_{10} \cdot [C3] - k_{-10}$$
$$v_{11} = k_{11} \cdot [C8^*] \cdot [BAR] - k_{-11} \cdot [C8^* \sim BAR]$$
$$v_{12} = k_{12} \cdot [BAR] - k_{-12}$$
$$v_{13} = k_{13} \cdot [C8^* \sim BAR].$$

In this model, procaspase-8 ($C8$, denoting initiator procaspases 8 and 10) is activated by an extracellular signal mediated by death receptors. Activated caspase-8 ($C8^*$) subsequently cleaves and activates procaspase-3 ($C3$, representing the executioner caspases in general, e.g., caspases 3, 6, 7) by forming active caspase-3 ($C3^*$). Caspase-3 leads to apoptosis and acts in terms of a positive feedback loop onto procaspase-8. The caspase inhibitor IAP can bind caspase-3 reversibly by forming the complex $C3^* \sim IAP$. Activated caspases as well as $C3^* \sim IAP$ are continuously degraded. Furthermore, IAP degradation is mediated by caspase 3. In addition to this, an inhibitor of $C8^*$ called BAR [67] was introduced by Eissing *et al.* [66].

The model was used for the study of the bistable switch from the status "alive" into the apoptotic state. Therefore, simulations were performed by Eissing *et al.* [66] using the following initial concentrations and parameter values. Concentrations of the model components are given as molecules per cell. With an estimated cell volume of 1 pl, one can easily transform these values into more common units. Initial concentrations for caspase-8 and -3 are 130,000 and 21,000 molecules/cell, respectively. The initial concentrations of active caspase-3 and the complexes $C3^* \sim IAP$ and $C8^* \sim BAR$ are assumed to be 0 molecules/cell. Concentrations of the inhibitors IAP and BAR are assumed to be 40,000 molecules/cell at the beginning. The initial amount of activated caspase-8 ($C8^*$) represents the input signal of the signaling cascade. In the example displayed here, it varies between 0 and 3000 molecules/cell. The kinetic parameters of the model as elaborated by Eissing *et al.* [66] mostly from literature are displayed in Table 3.6.

As outlined above, apoptosis should display a bistable behavior, but the status "alive" must be stable and resistant toward minor accidental trigger signals, i.e., noise. However, once the apoptotic signal is beyond a certain threshold, the cell must irreversibly enter apoptosis.

Simulations of the model, using the parameters shown in Table 3.6, show a bistable behavior (Figure 3.36). The simulation results, with varying input signals between 0 and 3000 molecules/cell of activated caspase-8, show a low amount of active caspase-3

Table 3.6 Parameter values of the model described by Eissing *et al.* [66].

Parameter	Value	Reverse parameter	Value
k_1	5.8×10^{-5} cell min^{-1} mo^{-1}	K_{-1}	0
k_2	10^{-5} cell min^{-1} mo^{-1}	k_{-2}	0
k_3	5×10^{-4} cell min^{-1} mo^{-1}	k_{-3}	0.21 min^{-1}
k_4	3×10^{-4} cell min^{-1} mo^{-1}	k_{-4}	0
k_5	5.8×10^{-3} min^{-1}	k_{-5}	0
k_6	5.8×10^{-3} min^{-1}	k_{-6}	0
k_7	1.73×10^{-2} min^{-1}	K_{-7}	0
k_8	1.16×10^{-2} min^{-1}	k_{-8}	464 mo cell^{-1} min^{-1}
k_9	3.9×10^{-3} min^{-1}	k_{-9}	507 mo cell^{-1} min^{-1}
k_{10}	3.9×10^{-3} min^{-1}	k_{-10}	81.9 mo cell^{-1} min^{-1}
k_{11}	5×10^{-4} min^{-1}	k_{-11}	0.21 min^{-1}
k_{12}	10^{-3} min^{-1}	k_{-12}	40 mo cell^{-1} min^{-1}
k_{13}	1.16×10^{-2} min^{-1}	k_{-13}	0

until the concentration of active caspase-8 exceeds a threshold. Then the model switches from the status "alive" into the apoptotic state indicated by a steep rise in the amount of active caspase-3. The apoptotic state is reached with a time delay that is inversely proportional to the initial input signal. Both the states ("alive" and apoptotic)
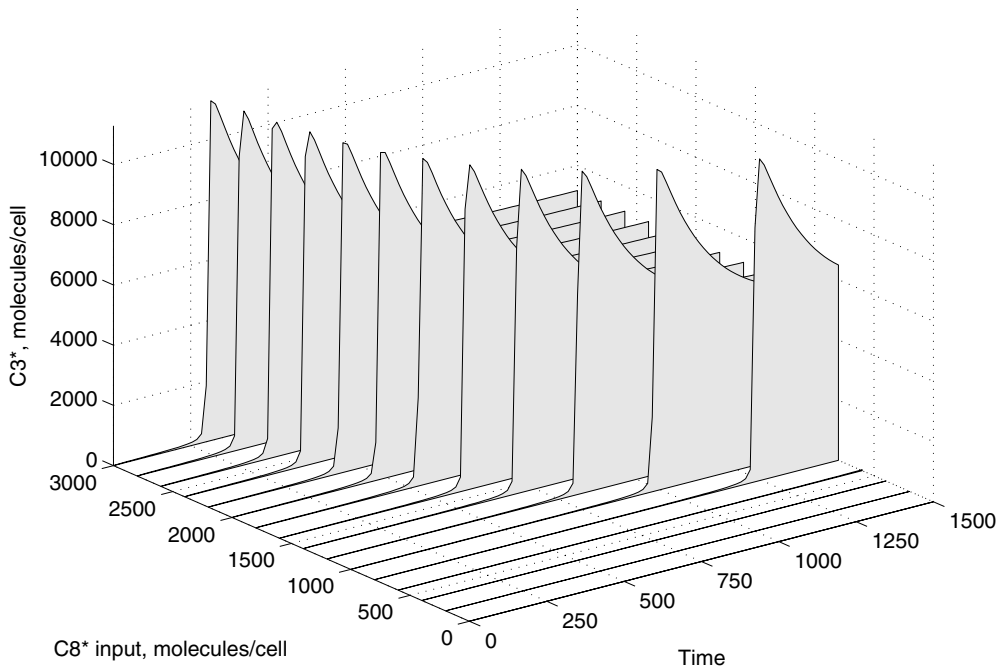
Figure 3.36 Bistable behavior of the extrinsic apoptosis model versus varying input signals. The input signal is modeled by the initial concentration of the activated caspase-8 [66].
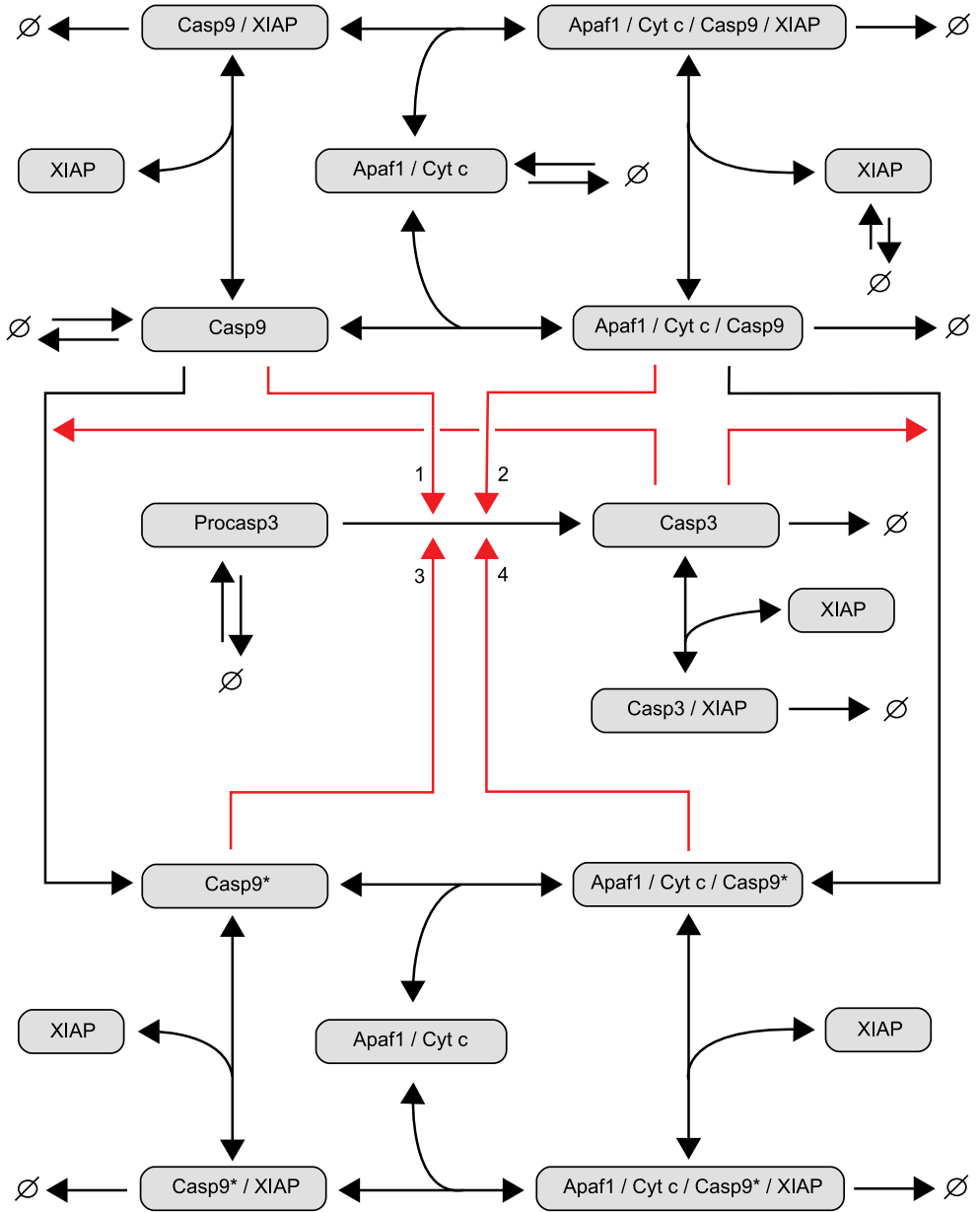
Figure 3.37 Schematic representation of central components of the intrinsic apoptotic signaling pathway developed by Legewie *et al.* [68]. Casp9 denotes the autoproteolytically processed form of caspase-9 that is cleaved at Asp^{315}, and Casp9* is the form processed by caspase-3 at Asp^{330}.

are stable states with the used parameter values for this model. Eissing *et al.* [66] showed that the same model without the inhibition of activated caspase-8 by BAR ("single inhibition model") also shows a bistable behavior, but with an unstable life steady state within the used kinetic parameter space.

Legewie *et al.* [68] developed a model of a central part of the intrinsic apoptotic pathway that describes the activation of caspase-3 by active caspase-9 (Figure 3.37). Caspase-9 can be activated in two different ways (Figure 3.38). First of all recruited by the apoptosome, it can be autoproteolytically processed at amino acid Asp^{315} that results into the formation of the two subunits p35/p12. Furthermore, caspase-9 can also be activated by active caspase-3 through proteolysis at Asp^{330} that results in the formation of the two subunits p37 and p10. The activation of caspase-9 by caspase-3 results in a positive feedback activation and signal amplification. The stimulation of intrinsic apoptosis is given in this model by the amount of the apoptosomes (Apaf1/Cyt c). It is assumed that caspase-9, which is associated with the apoptosome, cleaves procaspase-3 much more efficiently (70 times) than free caspase-9. Furthermore, caspase-9 that was processed by caspase-3 at Asp^{330} is 10 times more efficient than caspase-9 that was processed autocatalytically at Asp^{315}. Both caspase-3 and caspase-9 can be inhibited by XIAP (and other IAPs that are not explicitly modeled). Legewie *et al.* [68] have demonstrated that the inhibition of caspase-3 and caspase-9 by XIAP results in an implicit positive feedback. Cleaved caspase-3 augments its own activation by sequestering the inhibitor XIAP away from caspase-9. This implicit positive feedback brings about bistability, which is an essential claim on apoptosis. Furthermore, the authors show that this positive feedback cooperates with caspase-3-mediated feedback cleavage of caspase-9 to generate irreversibility in the caspase activation.
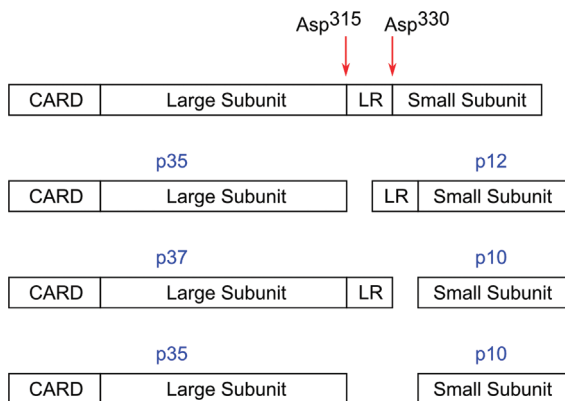
Figure 3.38 Diagram of procaspase-9 and its proteolytic products by caspase-9-mediated cleavage at Asp^{315}, caspase-3-mediated cleavage at Asp^{330}, or both [69].

Exercises and Problems

1. Calculate the flux control coefficients for the model of the threonine synthesis pathway. If required, use a computational tool providing the necessary functions.

2. Consider the Ras activation cycle shown in Figure 3.14 with the parameters given there. The concentration of GAP be 0.1. GEF gets activated according to $GEF = \begin{cases} 0, t < 0 \\ e^{-0.2t}, t \geq 0 \end{cases}$. Calculate the signaling time $\tau_{Ras_{GTP}}$ and the signal duration $\vartheta_{Ras_{GTP}}$ (Eqs. (3.26) and (3.27)).

3. MAP kinase cascades comprise kinases and phosphatases. How would such a cascade behave if there were no phosphatases?

4. Game of Life. (a) Invent two initial configurations that remain unchanged under the updating rules of the game of life. (b) Simulate the following patterns (called "glider" and "lightweight spaceship") with paper and pencil. The surrounding cells are supposed to be empty ("dead"). (c) Implement the game of life as a computer program and play with random initial configurations.
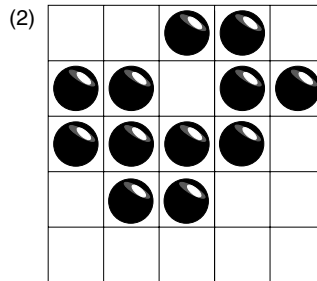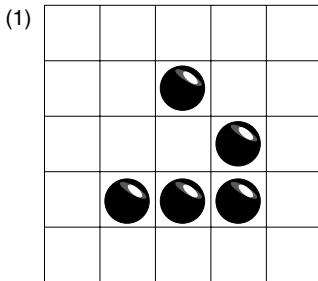
5. Show that the diffusion equation is solved by spatial cosine profiles with temporally decreasing amplitude

$$s(x, t) = s_o \, e^{-\lambda(k)t} \cos(kx)$$

and compute the dispersion relation $\lambda(k)$.

6. Show that the stationary profile

$$s^{st}(x) = \frac{6D/\kappa}{\left(x + \sqrt{6D/(\kappa s_o)}\right)^2} = \frac{6D/\kappa}{\left(x + (2Da/j(0))^{1/3}\right)^2}$$

where $a = 6D/\kappa$ is a solution of the Bicoid reaction–diffusion system with autocatalytic degradation term $-\kappa \cdot s(x, t)^2$ (see Section 3.4.4). Hint: use the ansatz $s^{st}(x) = a/(x + b)^2$.

7. The pair-rule gene *eve* is expressed in seven stripes in the blastoderm of the fruit fly *Drosophila melanogaster*. The stripes do not arise from spontaneous pattern formation, but from a response to existing patterns of the regulatory proteins *Krüppel*, *Bicoid*, *Giant*, and *Hunchback*. The response is hard-coded in the regulatory region of the *eve* gene. Speculate in broad terms about advantages and disadvantages of spontaneous and "hardwired" pattern formation.

8. Describe the different phases of the eukaryotic cell cycle. What are the three most important regulatory cell-cycle checkpoints?

9. Describe the crosslink between the intrinsic and the extrinsic apoptotic pathway.

10. How can a mathematical model of, e.g., apoptosis be used for the identification of potential drug targets?

References

1 Snoep, J.L. and Olivier, B.G. (2002) Java Web Simulation (JWS); a web-based database of kinetic models. *Molecular Biology Reports*, **29**, 259–263.

2 Hynne, F. *et al.* (2001) Full-scale model of glycolysis in *Saccharomyces cerevisiae*. *Biophysical Chemistry*, **94**, 121–163.

3 Rizzi, M. *et al.* (1997) *In vivo* analysis of metabolic dynamics in *Saccharomyces cerevisiae*: II. Mathematical model. *Biotechnology and Bioengineering*, **55**, 592–608.

4 Theobald, U. *et al.* (1997) *In vivo* analysis of metabolic dynamics in *Saccharomyces cerevisiae*: I. Experimental observations. *Biotechnology and Bioengineering*, **55**, 305–316.

5 Yi, T.M. *et al.* (2003) A quantitative characterization of the yeast heterotrimeric G protein cycle. *Proceedings of the National Academy of Sciences of the United States of America*, **100**, 10764–10769.

6 Neer, E.J. (1995) Heterotrimeric G proteins: organizers of transmembrane signals. *Cell*, **80**, 249–257.

7 Dohlman, H.G. (2002) G proteins and pheromone signaling. *Annual Review of Physiology*, **64**, 129–152.

8 Blumer, K.J. and Thorner, J. (1991) Receptor-G protein signaling in yeast. *Annual Review of Physiology*, **53**, 37–57.

9 Dohlman, H.G. *et al.* (1991) Model systems for the study of seven-transmembrane-segment receptors. *Annual Review of Biochemistry*, **60**, 653–688.

10 Buck, L.B. (2000) The molecular architecture of odor and pheromone sensing in mammals. *Cell*, **100**, 611–618.

11 Banuett, F. (1998) Signalling in the yeasts: an informational cascade with links to the filamentous fungi. *Microbiology and Molecular Biology Reviews*, **62**, 249–274.

12 Dohlman, H.G. *et al.* (1998) Regulation of G protein signalling in yeast. *Seminars in Cell & Developmental Biology*, **9**, 135–141.

13 Wang, P. and Heitman, J. (1999) Signal transduction cascades regulating mating, filamentation, and virulence in *Cryptococcus neoformans*. *Current Opinion in Microbiology*, **2**, 358–362.

14 Offermanns, S. (2000) Mammalian G-protein function *in vivo*: new insights through altered gene expression. *Reviews of Physiology, Biochemistry and Pharmacology*, **140**, 63–133.

15 Dohlman, H.G. and Thorner, J.W. (2001) Regulation of G protein-initiated signal

transduction in yeast: paradigms and principles. *Annual Review of Biochemistry,* **70**, 703–754.

16 Meigs, T.E. *et al.* (2001) Interaction of Galpha 12 and Galpha 13 with the cytoplasmic domain of cadherin provides a mechanism for beta-catenin release. *Proceedings of the National Academy of Sciences of the United States of America*, **98**, 519–524.

17 Dohlman, H.G. and Thorner, J. (1997) RGS proteins and signaling by heterotrimeric G proteins. *The Journal of Biological Chemistry*, **272**, 3871–3874.

18 Siderovski, D.P. *et al.* (1999) Whither goest the RGS proteins? *Critical Reviews in Biochemistry and Molecular Biology*, **34**, 215–251.

19 Burchett, S.A. (2000) Regulators of G protein signaling: a bestiary of modular protein binding domains. *Journal of Neurochemistry*, **75**, 1335–1351.

20 Ross, E.M. and Wilkie, T.M. (2000) GTPase-activating proteins for heterotrimeric G proteins: regulators of G protein signaling (RGS) and RGS-like proteins. *Annual Review of Biochemistry*, **69**, 795–827.

21 Takai, Y. *et al.* (2001) Small GTP-binding proteins. *Physiological Reviews*, **81**, 153–208.

22 Postma, P.W. *et al.* (1989) The role of the PEP: carbohydrate phosphotransferase system in the regulation of bacterial metabolism. *FEMS Microbiology Reviews*, **5**, 69–80.

23 Postma, P.W. *et al.* (1993) Phosphoenolpyruvate: carbohydrate phosphotransferase systems of bacteria. *Microbiological Reviews*, **57**, 543–594.

24 Rohwer, J.M. *et al.* (2000) Understanding glucose transport by the bacterial phosphoenolpyruvate: glycose phosphotransferase system on the basis of kinetic measurements *in vitro*. *The Journal of Biological Chemistry*, **275**, 34909–34921.

25 Francke, C. *et al.* (2003) Why the phosphotransferase system of *Escherichia coli* escapes diffusion limitation. *Biophysical Journal*, **85**, 612–622.

26 Klipp, E. *et al.* (2005) Integrative model of the response of yeast to osmotic shock. *Nature Biotechnology*, **23**, 975–982.

27 Hohmann, S. (2002) Osmotic stress signaling and osmoadaptation in yeasts. *Microbiology and Molecular Biology Reviews*, **66**, 300–372.

28 Wilkinson, M.G. and Millar, J.B. (2000) Control of the eukaryotic cell cycle by MAP kinase signaling pathways. *The FASEB Journal*, **14**, 2147–2157.

29 Huang, C.Y. and Ferrell, J.E. Jr (1996) Ultrasensitivity in the mitogen-activated protein kinase cascade. *Proceedings of the National Academy of Sciences of the United States of America*, **93**, 10078–10083.

30 Kholodenko, B.N. (2000) Negative feedback and ultrasensitivity can bring about oscillations in the mitogen-activated protein kinase cascades. *European Journal of Biochemistry*, **267**, 1583–1588.

31 Force, T. *et al.* (1994) Enzymatic characteristics of the c-Raf-1 protein kinase. *Proceedings of the National Academy of Sciences of the United States of America*, **91**, 1270–1274.

32 Kisseleva, T. *et al.* (2002) Signaling through the JAK/STAT pathway, recent advances and future challenges. *Gene*, **285**, 1–24.

33 Schindler, C.W. (2002) Series introduction. JAK–STAT signaling in human disease. *The Journal of Clinical Investigation*, **109**, 1133–1137.

34 Goldbeter, A. (1991b) A minimal cascade model for the mitotic oscillator involving cyclin and cdc2 kinase. *Proceedings of the National Academy of Sciences of the United States of America*, **88**, 9107–9111.

35 Heinrich, R. *et al.* (2002) Mathematical models of protein kinase signal transduction. *Molecular Cell*, **9**, 957–970.

36 Komarova, N.L. *et al.* (2005) A theoretical framework for specificity in cell signalling. *Molecular Systems Biology* 1:2005.0023.

37 Schaber, J. *et al.* (2006) A modelling approach to quantify dynamic crosstalk between the pheromone and the starvation pathway in baker's yeast. *FEBS Journal*, **273**, 3520–3533.

38 Hartwell, L.H. (1974) *Saccharomyces cerevisiae* cell cycle. *Bacteriological Reviews*, **38**, 164–198.

39 Hartwell, L.H. *et al.* (1974) Genetic control of the cell division cycle in yeast. *Science*, **183**, 46–51.

40 Pardee, A.B. (1974) A restriction point for control of normal animal cell proliferation. *Proceedings of the National Academy of Sciences of the United States of America*, **71**, 1286–1290.

41 Nurse, P. (1975) Genetic control of cell size at cell division in yeast. *Nature*, **256**, 547–551.

42 Nurse, P. and Bissett, Y. (1981) Gene required in G1 for commitment to cell cycle and in G2 for control of mitosis in fission yeast. *Nature*, **292**, 558–560.

43 Goldbeter, A. (1991a) A minimal cascade model for the mitotic oscillator involving cyclin and cdc2 kinase. *Proceedings of the National Academy of Sciences of the United States of America*, **88**, 9107–9111.

44 Fall, C.P. *et al.* (2002) *Computational Cell Biology*, Springer, New York.

45 Tyson, J.J. *et al.* (1996) Chemical kinetic theory: understanding cell-cycle regulation. *Trends in Biochemical Sciences*, **21**, 89–96.

46 Novák, B. *et al.* (1999) Finishing the cell cycle. *Journal of Theoretical Biology*, **199**, 223–233.

47 Chen, K.C. *et al.* (2000) Kinetic analysis of a molecular model of the budding yeast cell cycle. *Molecular Biology of the Cell*, **11**, 369–391.

48 Chen, K.C. *et al.* (2004) Integrative analysis of cell cycle control in budding yeast. *Molecular Biology of the Cell*, **15**, 3841–3862.

49 Barberis, M. *et al.* (2007) Cell size at S phase initiation: an emergent property of the G1/S network. *PLoS Computational Biology*, **3**, e64.

50 Murray, J.D. (2003) *Mathematical Biology. II: Spatial Models and Biomedical Applications*, Springer, Berlin.

51 Poulin, P. and Theil, F. (2002) Prediction of pharmacokinetics prior to *in vivo* studies.

II. Generic physiologically based pharmacokinetic models of drug disposition. *Journal of Pharmaceutical Sciences*, **91** (5), 1358–1370.

52 Theil, F., Guentert, T.W., Haddad, S. and Poulin, P. (2003) Utility of physiologically based pharmacokinetic models to drug development and rational drug discovery candidate selection. *Toxicology Letters*, **138**, 29–49.

53 Deutsch, A. and Dormann, S. (2004) *Cellular Automaton Modeling and Biological Pattern Formation*, Birkhäuser Verlag AG, Basel.

54 Gardner, M. (1970) Mathematical games: The fantastic combinations of John Conway's new solitaire game "Life". *Scientific American*, **223**, 120–123.

55 Meinhardt, H. and Klingler, M. (1987) A model for pattern formation on the shells of molluscs. *Journal of Theoretical Biology*, **126**, 63–69.

56 Meinhardt, H. (2003) *The Algorithmic Beauty of Sea Shells*, Springer, Heidelberg, New York.

57 Gurdon, J.B. and Bourillot, P.-Y. (2001) Morphogen gradient interpretation. *Nature*, **413**, 797–803.

58 Meinhardt, H. and Gierer, A. (1974) Applications of a theory of biological pattern formation based on lateral inhibition. *Journal of Cell Science*, **15**, 321–346.

59 Meinhardt, H. (1993) A model for pattern formation of hypostome, tentacles, and foot in hydra: how to form structures close to each other, how to form them at a distance. *Developmental Biology*, **157**, 321–333.

60 Kosman, D., Small, S. and Reinitz, J. (1998) Rapid preparation of a panel of polyclonal antibodies to Drosophila segmentation proteins. *Development Genes and Evolution*, **208**, 290–294.

61 Poustelnikova, E., Pisarev, A., Blagov, M., Samsonova, M. and Reinitz, J. (2004) A database for management of gene expression data *in situ*. *Bioinformatics*, **20**, 2212–2221.

62 Eldar, A., Rosin, D., Shilo, B.Z. and Barkai, N. (2003) Self-enhanced ligand degradation underlies robustness of morphogen gradients. *Developmental Cell*, **5**, 635–646.

63 Gierer, A. and Meinhardt, H. (1972) A theory of biological pattern formation. *Kybernetik*, **12**, 30–39.

64 Turing, A.M. (1952) The chemical basis of morphogenesis. *Philosophical Transactions of the Royal Society of London*, **237** (641), 37–72.

65 Fussenegger, M. *et al.* (2000) A mathematical model of caspase function in apoptosis. *Nature Biotechnology*, **18**, 768–774.

66 Eissing, T. *et al.* (2004) Bistability analyses of a caspase activation model for receptor-induced apoptosis. *The Journal of Biological Chemistry*, **279**, 36892–36897.

67 Stegh, A.H. *et al.* (2002) Inactivation of caspase-8 on mitochondria of Bcl-xL-expressing MCF7-Fas cells: role for the bifunctional apoptosis regulator protein. *The Journal of Biological Chemistry*, **277**, 4351–4360.

68 Legewie, S. *et al.* (2006) Mathematical modeling identifies inhibitors of apoptosis as mediators of positive feedback and bistability. *PLoS Computational Biology*, **2**, e120.

69 Zou, H. *et al.* (2003) Regulation of the Apaf-1/caspase-9 apoptosome by caspase-3 and XIAP. *The Journal of Biological Chemistry*, **278**, 8091–8098.

4
Model Fitting

4.1
Data for Small Metabolic and Signaling Systems

Summary

The mathematical equations that are used to develop kinetic models of biochemical systems are so complex that, except for the most simple cases, it is impossible to solve them analytically. Therefore, numerical simulations are required to predict how concentrations develop over time and when and if the system will reach a steady state. But numerical simulations need numerical data to assign specific values to a large number of molecule properties. Among these properties are Michaelis–Menten constants, K_m, and maximal velocities, $V_{max,}$ (for enzymes), but also biological half-lives, binding constants, molecule concentrations, and diffusion rates. In the early days of mathematical modeling, it was very difficult to obtain enough data of sufficient quality to make reliable model predictions. In such a situation, only qualitative models can be constructed that investigate the question if a certain behavior is at all possible or not. Although such a model provides valuable information about a system of biochemical reactions, most models today aim to be quantitative. This means that the model should agree well with measured concentrations and also predictions regarding changes of molecule concentrations are given as specific numbers instead of a qualitative up or down statement. To develop quantitative models, it is therefore essential to obtain a large number of reliable data for the model parameters. One source are specialized databases, which will be discussed in this section. But the process of filling these databases is currently very time-consuming, since most kinetic data have to be extracted by hand from the existing literature. Recently developed experimental techniques aim to improve the situation by enabling researchers to measure large numbers of kinetic data with high accuracy. Some of these techniques will be described at the end of chapter 4.1.

4.1.1
Databases for Kinetic Modeling

BRENDA is a database that aims to be a comprehensive enzyme information system (http://www.brenda-enzymes.info). BRENDA is a curated database that contains a large number of functional data for individual enzymes (Figure 4.1). These data are gathered from the literature and made available via a web interface. Table 4.1 gives an overview of the types of information that is collected and the number of entries for the different information fields (as of November 2007). For instance, enzymes representing 4762 different EC numbers and almost 80,000 different K_m values exist in the database.

One of BRENDA's strengths is the multitude of ways the database can be searched. It is easy to find all enzymes that are above a specific molecular weight, belong to *C. elegans*, or have a temperature optimum above 30 °C. If desired, the list of results can then be downloaded as a tab separated text file for later inspection. Using the Advanced Search feature, it is possible to construct arbitrarily complex search queries involving the information fields shown in Table 4.1.

Sometimes it is desirable to search for all enzymes that are glycosylases without knowing the corresponding EC number, or to find all enzymes that are found in horses without knowing the exact scientific name. In this situation the ECTree

Figure 4.1 The curated database BRENDA (http://www.brenda-en2ymes. info) provides detailed information for more than 4000 different enzymes, including kinetic data such as K_m values.

Table 4.1 BRENDA collects many types of information regarding enzymes. Each information field can be used for search queries, which makes it possible to perform very complex and specific searches.

Information field	Entries	Information field	Entries
Enzyme nomenclature		*Functional parameters*	
EC number	4762	K_m value	79,435
Recommended name	4757	Turnover number	240,77
Systematic name	3650	Specific activity	30,420
Synonymes	53,396	pH range and optimum	6609/25,681
CAS Registry Number	4383	Temperature range and optimum	2186/12,319
Reaction	10,731	*Molecular properties*	
Reaction type	7783	pH stability	4650
Enzyme structure		Temperature stability	13,149
Molecular weight	24,424	General stability	6653
Subunits	22,750	Organic solvent stability	787
Sequence links	283,733	Oxidation stability	599
Posttranslational modifications	4687	Storage stability	9084
Crystallization	5105	Purification	25,927
3D-structure, PDB links	35,400	Cloned	16,303
Enzyme–ligand interactions		Engineering	23,235
Substrates/products	222,285	Renatured	625
Natural substrates	51,126	Application	4760
Cofactor	16,302	*Organism-related information*	
Activating compound	18,466	Organism	364,770
Metals/ions	27,668	Source tissue, organ	65,938
Inhibitors	11,2470	Localization	29,906
Bibliographic data			
References	30,0190		

browser and the TaxTree search are helpful by providing a browser like interface to search down the hierarchy of EC number descriptions or taxonomic names.

BRENDA is also well connected to other databases that can provide further information about a specific enzyme. Associated GO terms are directly linked to the AmiGO browser, substrates and products of the catalyzed reactions can be displayed as chemical structures, links to the taxonomic database NEWT (http://www.ebi.ac.uk/newt) exist for information on the organism, sequence data can be obtained form Swiss-Prot and if crystallographic data exist, a link to PDB (see Chapter 16) is provided. Finally, literature references (including PubMed IDs) are provided and the implemented web service allows programmatic access to the data via a SOAP (Simple Object Access Protocol) interface (http://www.brenda-enzymes.org/soap).

SABIO-RK (http://sabio.villa-bosch.de/SABIORK) is another web-based database for information about biochemical reactions, kinetic rate equations, and numerical values for kinetic parameters. The information contained in SABIO-RK is partly extracted from KEGG (see Chapter 16) and partly from the literature. Currently the

database (version 20090312) is much smaller than BRENDA, containing for instance K_m values for 367 reactions of *E. coli*, 817 reactions of *H. sapiens*, or 128 reactions of *S. cerevisiae*. The main access to the data is via a search for reactions. Several constraints for the reaction like participating enzyme and reactants, biochemical pathway, organism and cellular location can be used to narrow down the search. The results page provides further information about the reaction (with links to EC information, UniProt, and PubMed) and available kinetic data. A potentially very useful feature of SABIO-RK is that the kinetic information for selected reactions can be exported as SBML format (see Section 6), which could considerably speed up the development in models for simulations. However, there are several points that need special consideration. It is advisable to search only reactions for which K_m, V_{max} and a rate law exists, otherwise the SBML file will contain no reaction and unknown parameters will be set to zero. For SBML export it is also important to select "export parameters normalized to SI base units" to ensure that always standard units are used. In addition the produced SBML file should be inspected manually to check the result. Finally, like BRENDA, the contents of SABIO-RK can be accessed via web services.

4.1.2
Measuring Promoter Activities Using GFP Reporter Genes

The kinetic data in BRENDA or SABIO-RK are extracted from the literature of the last decades. This is not only very time-consuming, but it also means that the data were obtained from a multitude of different organisms under different experimental conditions from different experimenters. Recently green fluorescent protein (GFP)-based high throughput techniques have been developed that have the potential to improve the situation considerably. GFP is a 27 kDa protein found in jellyfish [1], and is frequently used as reporter gene (see also Section 11.14). Work by [2] shows that kinetic parameters of *E. coli* promoters can be determined in parallel by using GFP reporter constructs to measure promoter activity with high accuracy and temporal resolution. For this purpose the promoter region of interest is cloned in front of a GFP gene and the whole construct is placed on a plasmid together with a selection marker and a low copy origin of replication (see also Section 11.2). The authors used this approach to study eight operons of the bacterial SOS repair system by measuring fluorescence and optical density (OD) every 3 min. From the resulting 99 data points per operon kinetic parameters of the promoters can be derived using a simple mathematical approach.

The activity of promoter i, X_i, is proportional to the number of GFP molecules synthesized per time interval per cell. Since degradation of GFP can be neglected, promoter activity is given by the derivative of the amount G_i of GFP, normalized by the optical density.

$$X_i(t) = \frac{dG_i(t)/dt}{OD_i(t)}.$$

A single transcription factor suppresses all operons of the SOS system without influence from other transcription factors. It is therefore reasonable to model the

promoter activity by a Michaelis–Menten type kinetics, where $A(t)$ is the repressor concentration, β_i is the activity of the unrepressed promoter i, and K_i is the repressor concentration at half maximal repression.

$$X_i(t) = \frac{\beta_i}{1 + A(t)/K_i}.$$

All kinetic parameters as well as the time-dependent activities $A(t)$ of the repressor LexA were estimated by a least-squares fit. For the fitting, all time series $X_i(t)$ were normalized to the same maximal activity. The values of $A(t)$ and the K_i can only be determined up to a scaling factor because a rescaling $A \rightarrow \lambda A$, $K_i \rightarrow \lambda K_i$ does not affect the model predictions. As further constraints, it was required that $A(t) > 0$ (no negative concentrations) and $A(0) = 1$ (normalization). The following table shows the obtained values for the eight studied promoters. For six of the eight cases the mean error for the predicted promoter activity is below 22%, which is a very good quantitative prediction. The genes *uvrY* and *polB*, however, showed errors of 30–45%, indicating that these genes are possibly influenced by additional factors. This study shows that kinetic data can be obtained using an approach that can, in principle, be scaled up to the whole genome.

Gene	K	β	Error	Function
uvrA	0.09 ± 0.04	2800 ± 300	0.14	Nucleotide excision repair
lexA	0.15 ± 0.08	2200 ± 100	0.10	Transcriptional repressor
recA	0.16 ± 0.07	3300 ± 200	0.12	LexA autocleavage, replication fork blocking
umuD	0.19 ± 0.1	330 ± 30	0.21	Mutagenesis repair
polB	0.35 ± 0.15	70 ± 10	0.31	Translesion DNA synthesis, replication fork recovery
ruvA	0.37 ± 0.1	30 ± 2	0.22	Double strand break repair
uvrD	0.65 ± 0.3	170 ± 20	0.20	Nucleotide excision repair, recombination repair
uvrY	0.51 ± 0.25	300 ± 200	0.45	Unknown function

The use of GFP and its variants for measuring kinetic and other data has several advantages over traditional experimental techniques.

- It opens the possibility to obtain kinetic data in a high throughput approach.
- The measurements have a high time resolution (one data point every few minutes).
- The kinetic parameters are measured under *in vivo* conditions.
- Using high throughput flow cytometry and microscopy it is possible to perform single cell measurements (see also Section 11.14).
- The reproducibility of the measurements is very good (around 10% error).

These attractive features have led to a number of very interesting studies in recent years. One limitation of the algorithm used by [2] is that it cannot be applied to systems where more than one transcription factor controls the promoter activity.

For this it is necessary to have a quantitative understanding how the input signals of different transcription factors are combined into the output signal (promoter activity). Section 6.1. describes, in detail, how this has been achieved for the promoter of the *lac* operon of *E. coli*.

In another study, 52 promoters of *E. coli* amino acid biosynthesis pathways were investigated by placing the regulatory regions in front of a GFP gene [3]. Cells were shifted from a medium without any amino acids to a medium that contained a single amino acid and GFP expression was measured every 8 min for 8 h. The results showed that the promoters of enzymes early in unbranched pathways have the shortest response time and strongest activity. This design principle agree nicely with the results of a mathematical model that was optimized to achieve a flux goal with minimal enzyme production. The same group extended this GFP-based approach to a genomic scale by generating reporter strains for all intergenic regions in *E. coli* that are larger than 40 bp [4]. The resulting library of 2000 constructs was used in a diauxic shift experiment, where cells first feed on glucose and then switch to lactose once the glucose levels are depleted. This led to the discovery of 80 previously unknown promoters.

In another high throughput experiment, GFP constructs were used to provide genome wide information about protein localization in *S. cerevisiae* [5]. For each annotated ORF, a pair of oligonucleotides was synthesized with homologies to the desired chromosomal insertion site. After placing the GFP sequence between these short sequences, the whole construct was inserted at the C terminus of each ORF using homologous recombination. This resulted in 4156 fusion proteins (75% of the yeast proteome) with a C terminal GFP tag. The information regarding the cellular localization of these proteins is publicly available at http://yeastGFP.ucsf.edu. Together with the spatial information, the website also provides information about individual protein numbers per cell.

4.2
Parameter Estimation

Summary

Parameters in a model can be determined by fitting the model to experimental data. In the method of least squares, a common approach in parameter estimation, the sum of squared residuals between model predictions and data is minimized. For data with additive standard Gaussian errors, this method is equivalent to maximum likelihood estimation. The variability of parameter estimates due to noisy and insufficient data can be assessed by repeating the estimation with resampled data ("bootstrapping") and the quality of model predictions can be tested by cross-validation. In Bayesian parameter estimation, parameter sets are scored by how well they agree with both available data and with certain prior assumptions, which are expressed by probability distributions of the parameters. The parameter estimation often leads to minimization problems, which can be solved with a variety of local or

global optimization algorithms. Local optimizers are relatively fast, but they may get stuck in suboptimal local optima. Global optimizers like simulated annealing or genetic algorithms can evade local minima, but they may be numerically demanding.

In modeling of biochemical systems, the mathematical structure of a model (e.g., the stoichiometric matrix and the kinetic laws) is often known, while the parameter values (e.g., kinetic constants or external concentrations) still need to be determined. Parameter values can be obtained by fitting the model outputs (e.g., concentration time series) to a set of experimental data. If a model is correct and the data are free of experimental errors, the parameters can be adjusted such that model outputs and data coincide. Moreover, if the model is structurally identifiable (a property that will be explained below) and if enough data are available, this procedure will allow us to determine exactly the true parameter set because for all other parameter sets, data and model output would differ.

In reality, however, experimental data are noisy. A common assumption is that the measured values (possibly on logarithmic scale) represent true values – which correspond to the model outputs – plus Gaussian-distributed random errors. Despite these errors, we can use such data to obtain *parameter estimates* that approximate the true parameter values. Statistical methods can help us to find good estimation procedures and to assess the uncertainty of the estimates [6]. Common modeling tools contain routines for parameter estimation [7]. For an example of parameter estimation and model selection, see [8].

4.2.1
Regression

Regression is a good example of parameter estimation. Here, we shall discuss regression problems to introduce concepts like estimators and likelihood. Later, in Section 4.4 on model selection, we shall apply the same concepts to dynamical models. In the linear regression problem shown in Figure 4.2, a number of data points (t_m, y_m) have to be approximated by a straight line $x = f(t, \theta) = \theta_1 t + \theta_2$. If the data points were already located on a straight line, we could choose a parameter vector $\theta = (\theta_1, \theta_2)^T$ such that $\forall i : y_m = f(t_m, \theta)$. In practice, experimental data points will rather be scattered around a line, so we require that the regression line should be as close as possible to the data points. The deviation between line and data can be quantified by the sum of squared residuals (SSR), $R(\theta) = \sum_m (y_m - f(t_m, \theta))^2$. With this choice, the regression problem leads to an optimization problem, namely, finding the minimum of the function $R(\theta)$.

4.2.2
Estimators

The use of the SSR as a distance measure can be justified by statistical arguments, assuming that the data have been generated by a known model with unknown

(a)

(b)

(c)
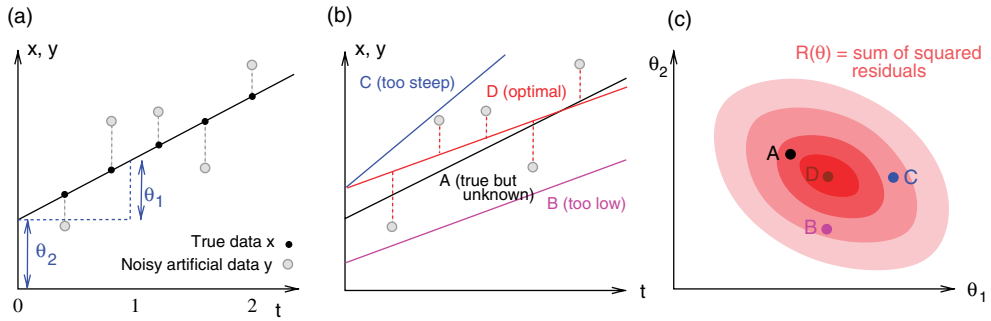
Figure 4.2 Linear regression leads to an optimization problem. (a) Artificial data points (t_m, y_m) (grey) are created by adding Gaussian noise to data points (black) from a model $x(t) = \theta_1(t) + \theta_2$ (straight line). Each possible line is characterized by two parameters, the slope θ_1 and the offset θ_2. The aim in linear regression is to reconstruct the unknown true parameters from noisy data (in this case, the artificial data set y). (b) The distance between a possible line (four lines A, B, C, and D are shown) and the data points can be measured by the sum of squared residuals (SSR). The residuals are shown for line D (red dashed lines). (c) Each of the lines A, B, C, and D corresponds to a point (θ_1, θ_2) in parameter space. The SSR as a function $R(\theta)$ forms a landscape in parameter space (schematically shown by shades of pink, dark pink indicates small SSR). Line D minimizes the SSR value.

parameters. As an example, we consider a curve $f(t, \theta)$ with the independent variable t (e.g., time) and curve parameters $\theta_1, \ldots, \theta_N$. For a given number of values t_m, the model yields the output values $x_m = f(t_m, \theta)$, which form a vector $x = x(\theta)$. By adding random errors ξ_m, we obtain the noisy data

$$y_m = f(t_m, \theta) + \xi_m. \tag{4.1}$$

If the random errors are independent Gaussian with mean 0 and variance σ_m^2, then each of the data points y_m is a Gaussian-distributed random number with mean $f(t_m, \theta)$ and variance σ_m^2.

In parameter estimation, the process of data generation is inverted: we start with a model (given as a function $x(\theta)$ and noise variances σ_m^2) and a set of noisy data y (a specific realization of the above random numbers) and try to infer approximately the unknown parameter set θ. This is done by an *estimator* $\hat{\theta}(y)$; a function of the data that is supposed to approximate the true parameter vector θ.

A practical and fairly simple estimator can be derived from the *principle of maximum likelihood*: given a generative model $y = x(\theta) + \xi$, the probability density for observing a data set y given the true parameter set θ is called $p(y|\theta)$. If a certain data set y is given, this probability density, as a function of the parameter set θ, is called the *likelihood* function $L(\theta|y) = p(y|\theta)$. The maximum likelihood estimate $\hat{\theta}_{ML}(y)$ is defined as the parameter set that maximizes the likelihood:

$$\hat{\theta}_{ML}(y) = \text{argmax}_\theta \, L(\theta|y). \tag{4.2}$$

We assume here that there is a unique maximum point. If this is not the case, the model is not identifiable (see Section 4.2.3).

4.2.2.1 Method of Least Squares and Maximum-Likelihood Estimation

Let us now compute the likelihood function for the model (Eq. (4.1)) with additive Gaussian noise. If the model yields the true value x_m, a noisy value y_m will be observed with a probability density $p_\xi(y_m - x_m)$, where $p_\xi(\xi)$ is probability density of the error term. We assume that each ξ_m is independently Gaussian distributed with mean 0 and variance σ_m^2, so its density reads

$$p_{\xi_m}(\xi) = \frac{1}{\sqrt{2\pi}\sigma_m} e^{-\frac{\xi^2}{2\sigma_m^2}}. \tag{4.3}$$

From a single data point y_m, we would obtain the likelihood function

$$L(\theta|y_m) = p(y_m|\theta) = p_{\xi_m}(y_m - x_m(\theta)). \tag{4.4}$$

As the noise for different data points is supposed to be independent, the probability to observe an entire data set y is the product of the probabilities for the individual data points. Hence, the likelihood is given by

$$L(\theta|y) = p(y|\theta) = \prod_m p_{\xi_m}(y_m - x_m(\theta)). \tag{4.5}$$

By inserting the probability density (4.3) into Eq. (4.5) and taking the logarithm, we obtain

$$\ln L(\theta|y) = \sum_m -\frac{(y_m - x_m(\theta))^2}{2\sigma_m^2} + \text{const.} \tag{4.6}$$

If we assume that the noise for all data points has the same variance σ^2, the logarithmic likelihood reads

$$\begin{aligned}\ln L(\theta|y) &= -\frac{1}{2\sigma^2} \sum_m (y_m - x_m(\theta))^2 + \text{const.} \\ &= -R(\theta)/(2\sigma^2) + \text{const.},\end{aligned} \tag{4.7}$$

where $R(\theta) = ||y - x(\theta)||^2$ is the sum of squared residuals. Thus, with the error model (4.3), maximizing the likelihood is equivalent to the principle of least squares.

The above argument also holds for data values on a logarithmic scale. The additive Gaussian errors for logarithmic data are equivalent to multiplicative log-normally distributed errors for the original, non-logarithmic data. By assuming the same variance σ^2 for all the logarithmic data, we imply that the non-logarithmic data have the same range of *relative errors*.

4.2.3
Identifiability

The likelihood function forms a landscape in parameter space (just like the SSR shown in Figure 4.2) and the maximum likelihood estimate $\hat{\theta}$ is the maximum point of this landscape – provided that it is indeed a single isolated point. In this case, the logarithmic likelihood function $\ln L(\theta|y)$ can be expanded to second order based on the local curvature matrix $\partial^2 \ln L(\theta|y)/\partial\theta_i\partial\theta_k$ and in a unique maximum point, the

(a)

θ_2 R(θ) = sum of squared residuals

θ_1

(b)

θ_2

θ_1
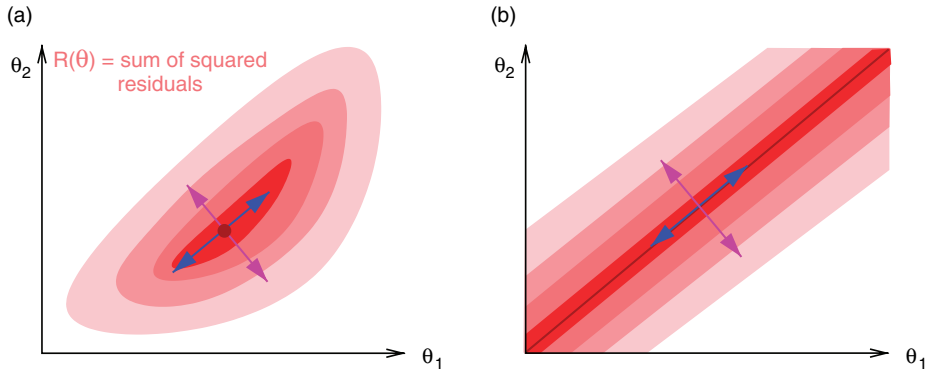
Figure 4.3 Identifiability. (a) In an identifiable model, the sum of squared residuals (SSR, schematically shown as shades of pink) is minimized in a single point (dot). The second derivatives (i.e., the curvatures) of the SSR form a matrix. In the two-dimensional case shown, its two eigenvectors point toward directions of maximal (blue) and minimal curvature (magenta), respectively. (b) In a nonidentifiable model, the SSR is minimal on a line (or in general, a manifold) in parameter space. Some linear combinations of parameters (magenta arrow) can be inferred from the data, while others (blue arrow) are nonidentifiable – accordingly, the curvature of the SSR vanishes in these directions.

curvatures are strictly negative. Directions with a small curvature correspond to parameter deviations that would only have little effect on the likelihood.

In parameter estimation, different parameter sets may happen to agree equally well with the data. In this case, the maximum likelihood criterion cannot be applied and the estimation problem is underdetermined (Figure 4.3). Often, the likelihood function becomes maximal on an entire curve or surface in parameter space rather than in a single point. Such cases of *non-identifiability* can have two reasons:

1. *Structural non-identifiability.* If two parameters θ_a and θ_b appear in a model only in the form of the product $c = \theta_a\theta_b$, then any choice $\theta'_a = \lambda\theta_a$ and $\theta'_b = \theta_b/\lambda$ would yield the same result $\theta'_a\theta'_b = \theta_a\theta_b$, leading to the same model predictions and to the same likelihood value. Thus, a maximum likelihood estimation (which compares model predictions to data) may suffice to determine the product $c = \theta_a\theta_b$, but not the individual parameter values θ_a and θ_b. In such cases, the model is called *structurally non-identifiable.* To resolve the problem in this example, we could replace the product $\theta_a\theta_b$ by a new, possibly identifiable parameter θ_c. Structural non-identifiability can arise from various kinds of formulas and may be difficult to detect and to resolve.

2. *Practical non-identifiability.* Even if a model is structurally identifiable, parameters may still be *practically non-identifiable* if the data are insufficient, i.e., either too few or the wrong kind of data are used for the estimation. In particular, if the number of parameters exceeds the number of data points, the parameters cannot be determined. Let us assume that each possible parameter set θ corresponds to a data set $x(\theta)$ (no experimental noise) and that the function $x(\theta)$ is continuous. If the dimensionality of θ is larger than the dimensionality of x, it is certainly impossible to invert the function $x(\theta)$ and to reconstruct the parameters from a

given data set. A rule for the minimum number of experimental data needed to reconstruct differential equation models is given in [9].

If a model is not identifiable, numerical parameter optimization with different starting points will lead to different estimates $\hat{\theta}$, which may all lie on the same manifold in parameter space. In the above example, for instance, the parameter estimates for θ_a and θ_b would be different every time, but they would always satisfy the relation $\ln \theta_a + \ln \theta_b = \ln c$ with the same value for c, so on a logarithmic scale, all estimates would lie on a straight line (provided that all other model parameters are identifiable).

The task of parameter identification from given data is often called an *inverse problem*. If the solution of an inverse problem is not unique, the problem is *ill-posed* and additional assumptions are required to pinpoint a unique solution. For instance, we may postulate that the sum of squares of all parameter values is supposed to be minimal. This additional requirement can help to determine a particular solution, a trick called "regularization".

4.2.4
Bootstrapping

A noisy data set $\gamma = x(\theta) + \xi$ will not allow us to determine the true model parameters θ, but only an estimate $\hat{\theta}(\gamma)$. Each time we repeat the estimation with different data sets, we deal with a different realization of the random error ξ and obtain a different estimate $\hat{\theta}$. Ideally, the mean value $\langle \hat{\theta} \rangle$ of these estimates should be identical to the true parameter value (in this case, the estimator is called "unbiased"), and their variance should be small. In practice, however, only a single data set is available, so we obtain a single point estimate $\hat{\theta}$ without knowing its distribution. *Bootstrapping* [10] provides a way to determine, at least approximately, the statistical properties of the estimator $\hat{\theta}$. First, hypothetical data sets (of the same size as the original data set) are generated from the original data by resampling with replacement (see Figure 4.4) and the estimate $\hat{\theta}$ is calculated for each of them. The empirical distribution of these estimates is then taken as an approximation of the true distribution of $\hat{\theta}$. The bootstrapping method is asymptotically consistent, that is, the approximation becomes exact as the size of the original data set goes to infinity. However, for finite data sets, it does not provide any guarantees.

Example 4.1: Bootstrapping applied to the estimation of mean values

Ten numbers $(x_1, \ldots, x_{10})$ are drawn from a random distribution. We use the empirical mean $\bar{x} = 1/10 \sum_{m=1}^{10} x_m$ of this sample to estimate the true expected value $\langle x \rangle$ of the underlying random variable X. Our aim is to assess the mean and the variance of the estimator $\bar{x}$. In the bootstrapping method, we randomly draw numbers z from the given sample $(x_1, \ldots, x_{10})$. Using these random numbers, we form new tuples (bootstrap samples) $z^{(k)} = (z_1^{(k)}, \ldots, z_{10}^{(k)})$ and compute the empirical mean $\bar{z}^{(k)} = 1/10 \sum_{i=1}^{10} z_i^{(k)}$ for each of them. A statistics of the values $\bar{z}^{(k)}$ is used as an approximation of the true distribution of $\bar{x}$.

(a)   Bootstrap   (b)   Distribution of estimates
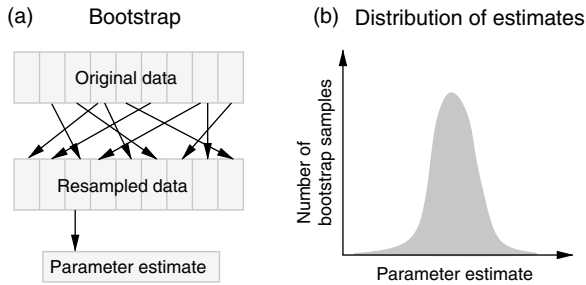
Figure 4.4 The bootstrapping method. (a) Hypothetical data sets are created by resampling data values from the original data set. Each resampled data set yields a parameter estimate $\hat{\theta}$. (b) The distribution of the parameter estimates, obtained from the bootstrap samples, approximates the true distribution of the estimator $\hat{\theta}$. A good approximation requires a large original data set.

4.2.5
Crossvalidation

There exists a fundamental difference between model fitting and prediction. If a model has been fitted to a given data set, it will probably show a better agreement with these *training data* than with new *test data* that have not been used for model fitting. The reason is that in model fitting, we enforce an agreement with the data. Therefore, a fitted model will often fit the data better than the true model itself, a phenomenon called *overfitting*. Despite its good fit, however, an overfitted model will not predict new data as reliably as the true model does. Moreover, the parameters of an overfitted model may differ strongly from the true parameter values. Therefore, strong over-fitting should be avoided.

We have seen an example in Figure 4.2: the least-squares regression line yields a lower SSR than the true model itself – because it has been optimized for it. This apparent improvement is achieved by fitting the noise, i.e., by adjusting the line to this very specific realization of the random errors in the data. However, this adjustment does not help when it comes to predicting points from a new data set; here, the true model is likely to perform better.

How can we check how a model performs in prediction? In *crossvalidation* (see Figure 4.5), a given data set (size N) is split into two parts: a training set of size n and a test set consisting of all remaining data. The model is fitted to the training data and the prediction error is evaluated for the test data. Then, a different part of the data is chosen as the test set. By repeating this procedure for many choices of test sets, we can judge how well the model, after being fitted to n data points, will predict new data. The mean prediction error is an important quality measure of a model. It allows to reject models that are prone to overfitting (e.g., because they contain too many parameters, see Section 4.4.). However, crossvalidation – just like bootstrapping – is numerically demanding because of the repeated estimation runs.
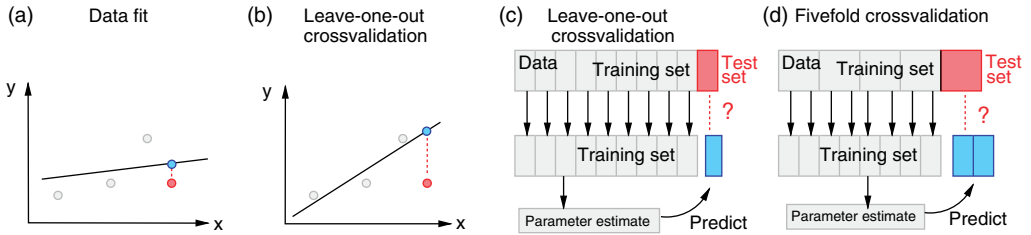
Figure 4.5 Crossvalidation can be used to detect overfitting. (a) In a linear regression, a straight line is fitted to four data points (grey and pink). The fitting error (dotted red line) is the distance between a data point (pink) and the corresponding value of the regression line (blue). The regression line is optimized for small fitting errors. (b) In leave-one-out crossvalidation, we pretend that a point (pink) is unknown and has to be predicted from the model. As the regression line is fitted to the remaining (grey) points, the deviation for the pink point (prediction error) will be larger than the fitting error shown in (a). (c) Scheme of leave-one-out crossvalidation. The model is fitted to all data points except for one ("training set") and the remaining data point ("test set") is predicted. This procedure is repeated for every data point to be predicted and yields an estimate of the average prediction error. (d) In *k*-fold crossvalidation, the data are split into *k* subsets. In every run, $k - 1$ subsets serve as training data, while the remaining subset is used as test data.

4.2.6
Bayesian Parameter Estimation

In parameter estimation as explained above, we suppose that there exists a single true parameter set, which is fixed, but unknown. Bayesian parameter estimation, an alternative approach, is based on a completely different premise: The parameter set θ is not fixed, but described as a random variable. By choosing its probability distribution, called the *prior*, we can state which parameter sets we regard as most plausible in advance. For each possible parameter set θ, we assume that a specific data set y will be observed with a probability density (likelihood) $p(\tilde{y}|\theta)$. Hence, parameters and data follow a joint probability distribution with density $p(y, \theta) = p(y|\theta)p(\theta)$ (see Figure 4.6).

From this joint distribution, we can also compute the conditional probabilities of parameters given the data. If a data vector y has been observed, the conditional probability of a parameter set given these data is called the *posterior probability*. With the Bayesian formula, the posterior probability density can be written as

$$p(\theta|y) = \frac{p(y|\theta)p(\theta)}{p(y)}. \tag{4.8}$$

It is proportional to the product of likelihood and prior density and represents a compromise between them. For a given data set y, the denominator $p(y)$ is a fixed number, which appears only as a normalization term.

Bayesian parameter estimation and maximum likelihood estimation differ both in their interpretation and in their practical use. In maximum likelihood estimation, we ask "which hypothesis about the parameters would make the data look probable?", while in Bayesian estimation, we directly ask "which parameters appear most

(a)

(b)

(c)
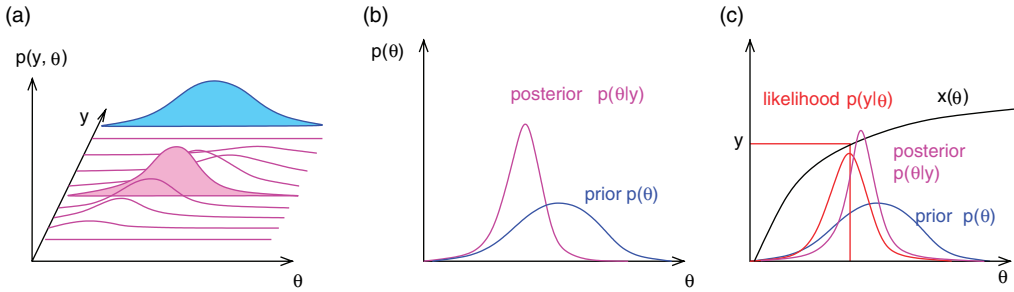
Figure 4.6 Bayesian parameter estimation. (a) In Bayesian estimation, the parameters θ and the data *y* follow a joint probability distribution with density $p(y, θ)$. The marginal probability density $p(θ)$ of the parameters is called the prior (blue), while the conditional density $p(θ|y)$ given a certain data set is called the posterior (magenta). (b) The posterior (magenta) is more narrow than the prior (blue), which reflects the information gained by considering the data. (c) Prior, likelihood and posterior. In a model, the data *y* are given by a mean prediction $x(θ)$ (black line) plus Gaussian noise. An observed value *y* gives rise to a likelihood function $L(θ|y) = p(y|θ)$ in parameter space. The posterior is proportional to the product of prior and likelihood function.

probable given the data?". Moreover, the aim in Bayesian statistics is usually not to choose a single parameter set, but to characterize the entire probability distribution (e.g., marginal distributions of individual parameters, probabilities for model predictions). For complicated problems, this is usually done by sampling parameter sets θ from the posterior $p(θ|y)$, for instance, using the Metropolis–Hastings algorithm described below.

The prior in Bayesian parameter estimation is usually used to express general beliefs or previous knowledge about the parameter values. Besides this, it can also be used as a regularization term to make models identifiable. By taking the logarithm of Eq. (4.8), we obtain the logarithmic posterior

$$\ln p(θ|y) = \ln L(θ|y) + \ln p(θ) + \text{const.} \tag{4.9}$$

If the logarithmic likelihood (the first term) does not have a unique maximum point in parameter space (for instance, as in Figure 4.3, right), the model will not be identifiable by maximum likelihood estimation. Nevertheless, if the logarithmic prior $\ln p(θ|y)$ is added in Eq. (4.9), a unique maximum point can emerge at least for the posterior density.

4.2.7
Local and Global Optimization

Model fitting often leads to an optimization problem of the form

$$\min \overset{!}{=} f(x), \tag{4.10}$$

where *x* is a vector and the function *f* is real and differentiable twice. In the method of least squares, for instance, *x* denotes the parameter vector θ and *f* is the sum of squared residuals (SSR). In addition to Eq. (4.10), we may restrict the allowed vectors *x* by constraints such as $x_i^{\min} \leq x_i \leq x_i^{\max}$. Global and local minima are

defined as follows. A parameter set x^* is a global minimum point if no allowed parameter set x has a smaller value of the objective function. A parameter set x^* is a local minimum point if no other allowed parameter set x in a neighborhood around x^* has a smaller value of the objective function. To find such optimal points numerically, algorithms usually evaluate the objective function f (and possibly its derivatives) in a series of points x leading to better and better points until a convergence criterion is met.

4.2.7.1 Local Optimization

Local optimizers are used to find a local optimum point in the vicinity of a given starting point. Usually, they evaluate the local gradient and improve the objective function step be step until convergence. Simple *gradient descent* is based on the local gradient $\nabla f(x)$, a vector that indicates the direction of the strongest increase of f. A sufficiently small step in the opposite direction of the gradient will lead to lower function values. Thus for a sufficiently small coefficient c,

$$f(x - c\nabla f(x)) < f(x). \tag{4.11}$$

In gradient descent, we iteratively jump from the current point $x^{(n)}$ to the new point by

$$x^{(n+1)} = x^{(n)} - c\nabla f(x^{(n)}). \tag{4.12}$$

The coefficient c can be adapted in each step, e.g., by a numerical line search

$$c = \operatorname{argmin}_{c'} f(x - c'\nabla f(x)). \tag{4.13}$$

Newton's method is based on a local second-order approximation of the objective function

$$f(x + \Delta x) \approx f(x) + \nabla f(x)\Delta x + \frac{1}{2}\Delta x^{\mathrm{T}} H(x)\Delta x \tag{4.14}$$

with the Hessian matrix $H_{ij} = \partial^2 f / \partial x_i \partial x_j$. If we disregard the approximation error in Eq. (4.14), a direct jump Δx to an extremum would require that

$$\nabla f(x) + H(x)\Delta x = 0. \tag{4.15}$$

In the iterative Newton method, we therefore jump from the current point $x^{(n)}$ to the new point

$$x^{(n+1)} = x^{(n)} - H(x^{(n)})^{-1}\nabla f(x^{(n)}). \tag{4.16}$$

Again, the second term can be multiplied by a relaxation coefficient $0 < c < 1$ to make the iteration process more stable.

4.2.7.2 Global Optimization

Theoretically, a global optimum point could be found by scanning the entire parameter space using an arbitrarily fine grid. However, for a problem with n

(a)

f(x)

nonglobal
optimum

global optimum

x

(b)

f(x)

up: accept
sometimes

C

A

down: accept
always

B

x
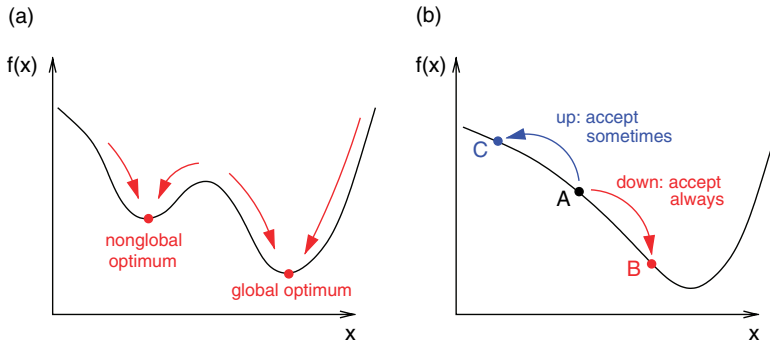
Figure 4.7 Global optimization. (a) In a local minimum point **x**, the function f assumes a minimal value for a neighborhood around **x**. A function may display different local minima with different function values. (b) The Metropolis–Hastings algorithm employs an iterative jump process in which points **x** are sampled with probabilities related to their function values $f(\mathbf{x})$. A jump that leads to lower f values (A → B) is always accepted, while an upward jump (A → C) is only accepted with probability $p = \exp(f(\mathbf{x}_A) - f(\mathbf{x}_C))$.

parameters and m values for each of them, this would require m^n function evaluations, which soon becomes intractable. In practice, most global optimization algorithms scan the parameter space by series of random jumps (Figure 4.7). Their objective is to find high quality solutions (preferably solutions very close to a global optimum or the global optimum itself as it usually happens) in short computation times (or in an affordable number of function evaluations). In order to be able to surmount basins of attraction containing local solutions, the algorithm may have to allow movements toward worse solutions in some stages of the search. There is a variety of global optimization algorithms [11, 12]. Examples of popular stochastic algorithms are *simulated annealing* and *genetic algorithms*.

Besides pure local and global methods, there are also hybrid methods [13, 14], which combine the robustness of global optimization algorithms with the efficiency of local methods. They work by applying a local search from a selection of points created in the global phase, which can accelerate the convergence to optimal solutions up to some orders of magnitude. Hybrid methods usually implement a set of filters to avoid local searches leading to optima that had been found previously.

4.2.7.3 Sampling Methods

Sampling methods like simulated annealing have been inspired by statistical thermodynamics. In a physical analogy, we consider a particle with position x (scalar or vectorial) that moves by stochastic jumps in an energy landscape $E(x)$. In a thermal equilibrium at temperature T, the particle position x follows the *Boltzmann distribution* with density

$$p(x) \sim e^{-E(x)/(k_B T)}, \tag{4.17}$$

where k_B is Boltzmann's constant. The Boltzmann distribution can be realized by the following random jump process ("Monte Carlo Markov chain") called *Metropolis–Hastings algorithm* [15, 16].

1. Given the current position $x^{(n)}$ with energy $E(x^{(n)})$, choose randomly a new potential position x^*.
2. If x^* has an equal or lower energy $E(x^*) \leq E(x^{(n)})$, the jump is accepted, and we set $x^{(n+1)} = x^*$.
3. If the new position has a higher energy $E(x^*) \geq E(x^{(n)})$, the jump is only accepted with a probability

$$p = \exp\left(\frac{E(x^{(n)}) - E(x^*)}{k_{\mathrm{B}}T}\right).$$

To accept or reject a potential jump in the algorithm, we draw a uniform random number z between 0 and 1; if $z < p$, we accept the jump and set $x^{(n+1)} = x^*$. Otherwise, we keep the old position and set $x^{(n+1)} = x^{(n)}$.

Programming the Metropolis–Hastings algorithm is straightforward; an important restriction is that the potential jump in step 1 has to satisfy the following property: the probability for a potential jump from position x' to position x'' must be the same as for the potential jump from x'' to x'. Otherwise, the different probabilities need to be taken into account by a modified acceptance function in step 3. Problems can also arise if the potential jumps are too small. In this case, the particle will tend to stay close to its current position, so the distribution will converge only very slowly to the true Boltzmann distribution.

According to the Boltzmann distribution (4.17), the particle will spend more time – and will yield more samples – in positions with lower energies, and this effect becomes more pronounced if the temperature is low. At temperature $T = 0$, only jumps to lower or same energies will be accepted, so the particle ends up, possibly after a long time, in a global energy minimum. The Metropolis–Hastings algorithm can be used to (i) sample from given probability distributions and (ii) to minimize arbitrary objective functions $f(x)$, which replace the energy function $E(x)$.

1. The Metropolis–Hastings algorithm at fixed temperature can be used to sample the posterior distribution (4.8) in Bayesian statistics: we set $k_{\mathrm{B}}T = 1$ and choose $E(\theta) = p(\gamma|\theta)p(\theta)$, ignoring the constant factor $1/p(\gamma)$. From the resulting samples, we can compute, for instance, the posterior mean values and variances of individual parameters θ_i.

2. For simulated annealing [17], $E(x)$ is replaced by a function to be minimized, the factor k_{B} is set to 1, and the temperature is varied during the optimization process. Simulated annealing starts with a high temperature, which is then continuously lowered during the sampling process. If the temperature decrease is slow enough, the system will end up in almost all cases (i.e., with probability 1) in a global optimum. In practice, the temperature has to be decreased faster, so convergence to a global optimum is not guaranteed.

4.2.7.4 Genetic Algorithms

Genetic algorithms like differential evolution [18] are inspired by the process of mutation and selection occurring in the evolution of species. Instead of improving a single possible solution (as in simulated annealing), genetic algorithms simulate

an entire population of possible solutions (called "individuals") with subsequent generations. In each generation, the fitness of every individual is evaluated. Individuals with good scores (as compared to the other individuals in the population) can have offspring, which then forms the following generation. In addition, mutations (i.e., small random changes) or crossover (random exchange of properties between individuals) allow the population to explore larger regions of the parameter space. For problems with additional constraints, stochastic ranking [19] provides an efficient way to trade the objective function against the need to obey the constraints.

4.3
Reduction and Coupling of Models

Summary

The aim in model reduction is to simplify complex models, i.e., to capture their key dynamical properties with fewer equations and parameters. This facilitates understanding, numerical and analytical calculations, and model fitting. A reduced model has to emulate the behavior of relevant variables under relevant conditions and on the relevant time scale. To reduce a model, elements can be omitted, lumped, or replaced by effective descriptions, and global model behavior can be approximated by global modes or simplified black-box models. Important simplifying concepts like quasi-equilibrium or quasi-steady state can be justified by a distinction between fast and slow processes. Once models for parts of the cell have been established, they may be combined to form move complex models, which may show new emergent behavior.

Biochemical systems are complex, but in order to understand them, we can use simple mental pictures that neglect many details and show processes as if they happened in isolation. Simplicity is just a matter of perspective: if we average over many microscopic events, we will obtain a smooth behavior of macroscopic substance concentrations. If we observe a fast complex system over a long period of time, its effective average behavior may look simple. In computational models, we can choose a level of detail that suits our needs: we may consider smaller or larger pathways and simplify, lump, or disregard substances and reactions. We can do this either from the very beginning by *model assumptions*, or we can simplify an existing model by *model reduction*. If a model turns out to be too simple, we may zoom into the system and acknowledge details that we neglected before, or zoom out and include more parts of the environment into the model.

4.3.1
Model Simplification

Any biochemical model represents a compromise between biological complexity and practical simplicity. Its form will depend on data and biological knowledge available
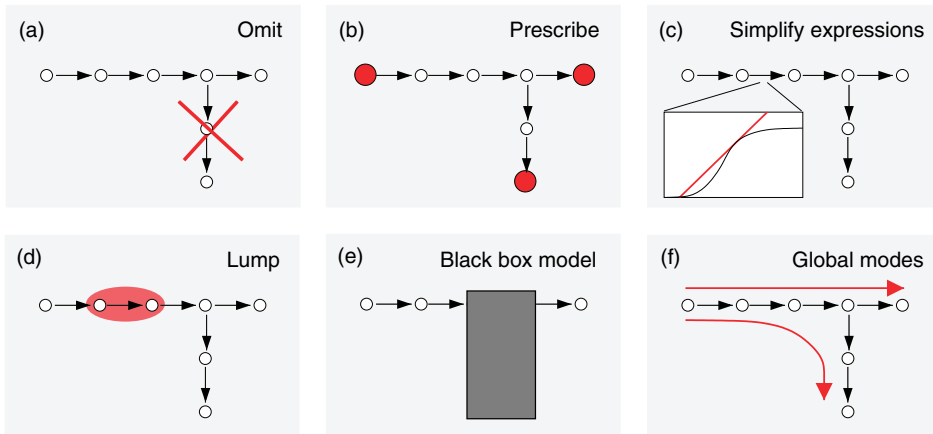
Figure 4.8 Simplifications in biochemical models. The scheme shows a branched pathway of metabolites (circles) and reactions (arrows). (a) Omitting substances or reactions. (b) Predefining the values of concentrations or fluxes or relations between them. (c) Simplifying the mathematical expressions (e.g., omitting terms in a kinetic law, using simplified kinetic laws [21], neglecting insensitive parameters [22]). (d) Lumping the substances, for instance, similar metabolites, protonation states of a metabolite, or metabolite concentrations in different compartments. Likewise, subsequent reactions in a pathway or elementary steps in a reaction can be replaced by a single reaction of the same velocity; for parallel reactions, like the action of isoenzymes, the velocities are summed up; for the two directions of a reaction, the velocities are subtracted. (e) Replacing the model parts by a dynamic black-box model that mimics the input–output behavior [23]. (f) Describing the dynamic behavior by global modes (e.g., elementary flux modes or eigenmodes of the Jacobian).

and on the questions to be answered. Small models provide several advantages: it is easier to understand them, the effort for simulations is lower, and with fewer parameters, model fitting is easier and more reliable.

Different ways to simplify a given model [20] are shown schematically in Figure 4.8. A basic rule for keeping models simple is to omit all elements that have little influence on the model predictions, for instance, reactions with very small rates. Often, elements cannot be omitted, but they can be described in a simplified or effective manner for conditions or time scales of interest. Examples are constant concentrations or flux ratios, effective kinetic laws fitted to measurements, or linearization of nonlinear kinetics that hold within the physiological range.

Such simplifications can speed up model building and simulations because fewer equations, variables, and parameters are needed, differential equations can be replaced by algebraic equations, and stiff differential equations can be avoided. All simplifications, though, have to be justified: a reduced model should yield a good approximation of the original model for certain quantities of interest, a certain time scale, and certain conditions (a range of parameter values, the vicinity of a certain steady state, or a certain qualitative behavior under study).

Even the most detailed biochemical model is still a simplified, reduced picture of a much more complex reality. Therefore, considerations about model reduction

do not only help to simplify existing models, but also to justify common basic model assumptions and our use of mental models in general.

4.3.2
Tacit Model Assumptions

Mathematical models describe biological systems in two complementary ways: in a positive way, by how processes *are* modeled and in a negative way, by omission of processes, simplification of mechanisms, and the decision to treat certain quantities as constant. The positive facts about the system are stated explicitly, while the negative ones – which are just as important – remain hidden in the model assumptions. Arguably, the most important negative statement is that a system as a whole can be seen as a module, that is, its environment – e.g., the cell surrounding a pathway – can be neglected. Experiments test both kinds of statements at the same time, and they should be designed from the very beginning such that the simplifying model assumptions will later be justified.

Example 4.2: Stabilization by negative feedback

Consider a simple kinetic model [24]

$$\frac{ds}{dt} = \frac{a}{1 + s/K_I} - b\,s \tag{4.18}$$

of self-inhibited protein production (with the protein level s, maximal production rate a, inhibition constant K_I, and degradation constant b). The model predicts that the protein level can be stabilized against noise by self-inhibition. Without inhibition ($K_I \rightarrow \infty$), the Jacobian of the system reads $A = -b$; with inhibition, the Jacobian $A = -aK_I/(K_I + s^{st})^2 - b$ has a larger negative value, so s becomes more stable against small random perturbations. Becskei and Serrano [24] have approved this stabilization effect in an experiment with synthetic genetic circuits.

However, the experiment does not only test the model (4.18) itself – the positive statements –, but also all kinds of simplifying assumptions made: (i) in the model, details of transcription and translation, as well as stochastic effects due to small particle numbers, are ignored; (ii) the behavior of the protein level s is entirely determined by s itself and interactions with other processes are neglected; (iii) the model parameters are assumed to be constant while in reality, they may depend on the cell state, be noisy or influenced by s itself, thus forming an additional feedback loop.

The model in Example 4.2 predicts stabilization for an isolated, deterministic system, but only the experiment can prove that an actual biochemical implementation of this loop, embedded in a living cell, shows the predicted behavior. Moreover, the successful prediction shows that the behavior is *robust* against typical perturbations that would occur in living cells. All this supports the working hypothesis that a subsystem can be modeled *at all* without considering the complexity of the surrounding cell.

4.3.3
Reduction of Fast Processes

If processes take place on different time scales (see Chapter 1), this may allow us to reduce the number of differential equations. In gene expression, for instance, binding and unbinding of transcription factors can happen on the order of microseconds, changes in transcription factor activity on the order of minutes, while the culture conditions may change on the order of hours. In a model, we may use a fast equilibrium or time averages for transcription factor binding, a dynamical model for signal transduction and gene expression, and constant values for the culture conditions.

The characteristic time scale of biochemical processes concerns both their internal dynamics (e.g., relaxation to steady state, periodic oscillations) and their susceptibility to external fluctuations. Cellular processes occur on a wide range of time scales from microseconds to hours, and also the time scale of enzymatic reactions can differ strongly due to the very different enzyme concentrations and kinetic constants.

4.3.3.1 Response Time
One way to define time constants is by observing how a system relaxes to steady state, like in the following example. We consider a substance that is produced at a rate v and linearly degraded with rate constant λ; its concentration s satisfies the rate equation

$$\frac{\mathrm{d}s(t)}{\mathrm{d}t} = v(t) - \lambda s(t). \tag{4.19}$$

If the production rate v is constant, then the concentration s will relax from an initial value $s(0) = s_0$ to its steady-state value $s^{\mathrm{st}} = v/\lambda$ according to

$$s(t) = s^{\mathrm{st}} + (s_0 - s^{\mathrm{st}})e^{-\lambda t}. \tag{4.20}$$

We can define the response time $\tau = 1/\lambda$ as the time at which the initial deviation $\Delta s(t) = s^{\mathrm{st}}$ from the steady state has decreased by a factor $1/e$. The response time is closely related to the response half time $\tau_{(1/2)} = \ln 2/\lambda$, at which half of the relaxation has been reached.

4.3.3.2 Time-Scale Separation
In numerical simulations, a single fast process, e.g., a rapid conversion between two substances $A \rightleftarrows B$ (as in Figure 4.9(b)), can force the numerical solver to use very small integration steps. If the same model also contains slow processes, simulations have to cover a long time scale, and the numerical effort can become enormous. However, fast reactions can be approximated rather easily because the concentration ratio s_B/s_A will always be close to the equilibrium constant. If we approximate this by an exact equilibrium in every moment in time, we can replace the reaction by the algebraic relation $s_B/s_A = K_{\mathrm{eq}}$ and get rid of the stiff differential equation that caused the big numerical effort.
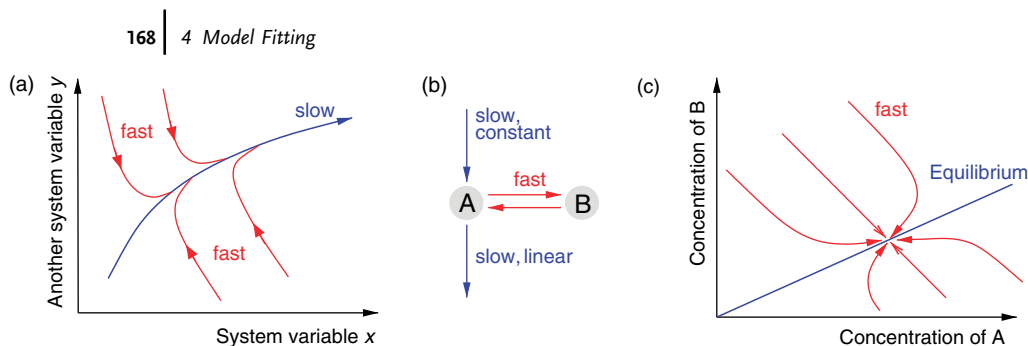
Figure 4.9 Time-scale separation. (a) The dynamics of a system can be illustrated by its trajectories in state space. If the system state is attracted by a submanifold (in the two-dimensional case, a curve), trajectories starting from any point (red) will rapidly approach this manifold (blue). Later, the system will move slowly on the manifold, satisfying an algebraic equation. (b) A small reaction system with different time scales. Fast conversion between metabolites A and B will keep their concentration ratio s_b/s_a close to the equilibrium constant K_{eq}, while slow production and degradation of A only changes the sum $s_a + s_b$. (c) Schematic trajectories for the system shown in (b). For any initial conditions, the concentrations s_A and s_B will rapidly approach the line $s_B/s_A = K_{eq}$ and then move slowly toward the steady state.

The mathematical justification for such an effective algebraic equation is illustrated in Figure 4.9: In state space, fast processes may rapidly move the system state toward a submanifold, on which certain relationships hold (e.g., an equilibrium between different concentrations). After an initial relaxation phase, the system state will change more slowly and remain close to this manifold. In the approximation, the system moves exactly within the manifold. In general, there may be a hierarchy of such manifolds which are related to different time scales [25].

Time-scale arguments can be used to justify various kinds of simplifications: (i) fast movements in molecular dynamics average out behind slow changes of the thermodynamic ensemble (e.g., fast jittering movements versus slow conformation changes in proteins). (ii) Fast diffusion leads to homogeneous concentrations, so spatial structure can be neglected. (iii) In a quasi-equilibrium as considered above, the ratios between substance concentrations are replaced by the equilibrium constant. (iv) In a quasi-steady state, the concentration of a substance may be determined by its production rate. The latter two approximations can be used, for instance, to justify the Michaelis–Menten rate law (see Section 2.1.3).

Example 4.3: Quasi-steady-state and quasi-equilibrium

We shall illustrate two types of approximation, quasi-steady state and quasi-equilibrium, with a simple model of upper glycolysis (see Section 3.1.2).
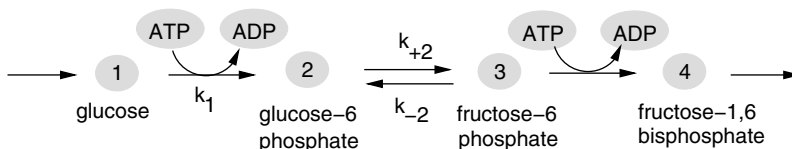
Glucose (GLC) is taken up at a rate v_0 and converted subsequently into glucose-6-phosphate (G6P), fructose-6-phosphate (F6P), and fructose-1,6-bisphosphate (FBP), which is then consumed by the following steps of glycolysis. In this model, the cofactors ATP and ADP have fixed concentrations. With mass-action kinetics and a reversible reaction between G6P and F6P, the rate equations read:

$$\frac{ds_1}{dt} = v_0 - k_1 s_A s_1 \tag{4.21}$$

$$\frac{ds_2}{dt} = k_1 s_A s_1 - k_{+2} s_2 + k_{-2} s_3 \tag{4.22}$$

$$\frac{ds_3}{dt} = k_{+2} s_2 - k_{-2} s_3 - k_3 s_A s_3 \tag{4.23}$$

$$\frac{ds_4}{dt} = k_3 s_A s_3 - k_4 s_4. \tag{4.24}$$

The numbers refer to the metabolites and reactions in the scheme and s_A denotes the constant ATP concentration. We first assume that all reactions take place on a similar time scale, setting $k_{+2} = 2$ and all other rate constants and the ATP concentration to a value of 1 (arbitrary units). Figure 4.10(a) shows simulated concentration curves of GLC, G6P, F6P, and FBP; the initial concentrations are chosen to be zero. For the first 5 time units, the influx has a value of $v_0 = 2$, and the intermediate levels rise one after the other. Then, the influx is reduced to $v_0 = 1$, and the levels decrease again.

How would the system behave if either the first or the second reaction was very fast? The two scenarios can be approximated, respectively, by a quasi-steady-state for glucose or a quasi-equilibrium between G6P and F6P.

If k_1 is increased to a value of 5 (Figure 4.10(b)), glucose is rapidly consumed, so its steady-state level will stay low; due to its high turnover, glucose will also adapt almost instantaneously to changes of the input flux. This behavior can be approximated by a quasi-steady-state approximation for the slow time scale: we replace the glucose concentration in each time point by the steady-state value $s_1^{st}(t) = v_0(t)/(k_1 s_A)$ based on the current value of $v_0(t)$. This algebraic equation replaces the differential equation (4.21) for s_1. Formally, we could obtain the same result by setting the left-hand side of the differential equation to zero.

Next, we assume a rapid and reversible conversion between the hexoses G6P and F6P. We increase both rate constants at the same time by a large factor ($k_{+2} = 10$ and $k_{-2} = 5$ in Figure 4.10(c)) while keeping their ratio $k_{eq} = k_{+2}/k_{-2}$ fixed: in the simulation, the ratio of F6P to G6P levels rapidly approaches the equilibrium constant [F6P]/[G6P] = $s_3/s_2 = K_{eq}$. In the quasi-equilibrium approximation, we assume that this ratio is exactly maintained in every moment. By adding Eqs. (4.22) and (4.23), we obtain the equation

$$\frac{ds_{2+3}}{dt} = \frac{d(s_2 + s_3)}{dt} = k_1 s_A s_1 - k_3 s_A s_3. \tag{4.25}$$

Given s_{2+3} and K_{eq}, we can substitute $s_3 = s_{2+3}K_{eq}/(1 + K_{eq})$ in Eq. (4.24) and obtain a simplified differential equation system in which the fast reaction does not

appear any more. The two differential equations for s_2 or s_3 are replaced by a single differential equation (for the sum of the two variables) and an algebraic equation $s_3/s_2 = K_{eq}$ for the concentration ratio.
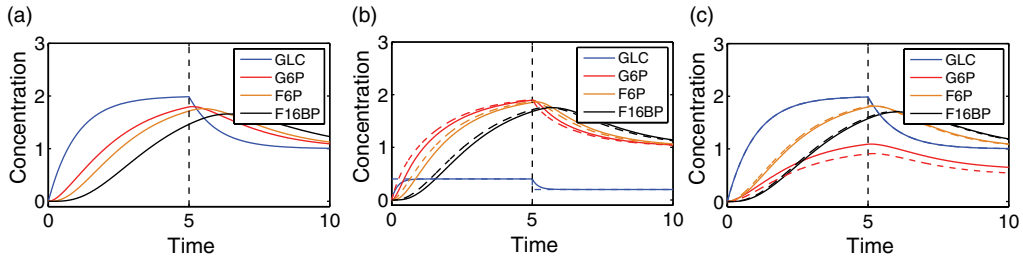
Figure 4.10 Simulation results for the model of upper glycolysis. (a) Results from the original model, showing levels of GLC, G6P, F6P, and FBP (abbreviations see text, time and concentrations measured in arbitrary units). (b) Results from the model with fast glucose turnover $k_1 = 5$ (solid lines) and the quasi-steady-state approximation (broken lines). (c) Results from the model with fast reversible conversion G6P $\leftrightarrow$ F6P (solid lines), parameters $k_{+2} = 10$, $k_{-2} = 5$ and the quasi-equilibrium approximation (broken lines).

4.3.4
Global Model Reduction

If the state of a system is constrained to a submanifold in state space (as shown in Figure 4.9(a)), its movement on the manifold can be described by a smaller number of variables. Such constraints can, for instance, arise from linear conservation relations between metabolite concentrations (see Section 2.2.4): If rows of the stoichiometric matrix N are linearly dependent, the system state can be described by a number of independent metabolite concentrations (effective variables), from which all other concentrations could be computed by algebraic equations. The vector of metabolite concentrations is confined to a linear subspace. Other constraints may arise from fast processes that effectively lead to algebraic relationships, as we saw in the quasi-steady-state and quasi-equilibrium approximation.

The effective variables do not have to describe individual substances: For a general linear manifold, they may consist of linear combinations of all substance concentrations, representing global modes of the system's dynamics. Such global modes appear, for instance, in metabolic systems that are linearized around a steady state: Each mode will represent a pattern of metabolite levels (actually, their deviations from steady state), which follows a certain temporal dynamics (e.g., exponential relaxation). Such modes are comparable to harmonics on a guitar string, which display spatial patterns with a characteristic temporal behavior. Actual movements of the string can be obtained by linear superposition of these modes.

4.3.4.1 Linearized Biochemical Models

Most biochemical models are nonlinear; one way to simplify them is by linearizing them around a steady state. Consider a kinetic model (see Section 2.3.1)

$$\frac{d\boldsymbol{v}}{dt} = \boldsymbol{N}\,\boldsymbol{v}(\boldsymbol{s}, \boldsymbol{p}) \tag{4.26}$$

with stoichiometric matrix $\boldsymbol{N}$, reaction velocity vector $\boldsymbol{v}$, and parameter vector $\boldsymbol{p}$. We assume that for given parameter sets $\boldsymbol{p}$, the system shows a stable steady state $\boldsymbol{s}^{\text{st}}(\boldsymbol{p})$. To linearize Eq. (4.26), we determine the steady state $\boldsymbol{s}_0^{\text{st}} = \boldsymbol{s}^{\text{st}}(\boldsymbol{p}_0)$ at a reference parameter vector $\boldsymbol{p}_0$ and compute the elasticity matrices $\tilde{\varepsilon} = \partial\boldsymbol{v}/\partial\boldsymbol{s}$ and $\tilde{\pi} = \partial\boldsymbol{v}/\partial\boldsymbol{p}$ (see Chapter 2). For small deviations of concentrations $\boldsymbol{x}(t) = \boldsymbol{s}(t) - \boldsymbol{s}_0^{\text{st}}$ and parameters $\boldsymbol{u}(t) = \boldsymbol{p}(t) - \boldsymbol{p}_0$, linearizing Eq. (4.26) leads to

$$\frac{d\boldsymbol{x}(t)}{dt} = \boldsymbol{A}\boldsymbol{x}(t) + \boldsymbol{B}\,u(t) \tag{4.27}$$

with the Jacobian $\boldsymbol{A} = \boldsymbol{N}\,\tilde{\varepsilon}$ and the matrix $\boldsymbol{B} = \boldsymbol{N}\,\tilde{\pi}$. In general, the approximation (4.27) holds only close to the expansion point, so for larger deviations $\boldsymbol{u}$ or $\boldsymbol{x}$, the accuracy decreases. In addition, linearized models may not be able to reproduce certain kinds of dynamic behavior, e.g., a stable limit cycle.

Biochemical systems show characteristic responses to external perturbations, so we can try to mimic complex models by linearized black-box models with the same input–output relation. An important special case are small perturbations of a stable system: if parameter perturbations are slow, the entire system will follow them in a quasi-steady-state. To linear order, the system's input–output relation $\gamma(\boldsymbol{u})$ (for parameter deviations $\boldsymbol{u}$ and steady-state output variables like fluxes or concentrations) can be approximated by the linear response

$$\Delta\gamma \approx \tilde{\boldsymbol{R}}_{\text{p}}^{\gamma}\Delta\boldsymbol{u} \tag{4.28}$$

with the metabolic response matrix $\tilde{\boldsymbol{R}}_{\text{p}}^{\gamma}$. The response to oscillating parameter perturbations [26, 27] and the response of transient behavior to stationary perturbations [28] can be treated accordingly.

4.3.4.2 Linear Relaxation Modes

With Eq. (4.27), we can express the model behavior as a superposition of global modes z_j, each corresponding to one of the eigenvectors of $\boldsymbol{A}$ (see Section 2.3.1). For constant system parameters ($\boldsymbol{u} = 0$), small deviations $\boldsymbol{x} = \boldsymbol{s} - \boldsymbol{s}_0^{\text{st}}$ follow approximately

$$\frac{d\boldsymbol{x}}{dt} = \boldsymbol{A}\boldsymbol{x}. \tag{4.29}$$

In the following, we assume that the Jacobian is diagonalizable, $\boldsymbol{A} = \boldsymbol{Q}\boldsymbol{\Lambda}\boldsymbol{Q}^{-1}$ with a diagonal matrix $\boldsymbol{\Lambda} = \text{Dg}(\lambda_i)$ and a transformation matrix $\boldsymbol{Q} = \{q_{ji}\}$. Furthermore, we assume that all its eigenvalues λ_i have negative (or, possibly, vanishing) real parts. We introduce the transformed vector $\boldsymbol{z} = \boldsymbol{Q}^{-1}\boldsymbol{x}$, which follows the equation

$$\frac{d\boldsymbol{z}}{dt} = \boldsymbol{\Lambda}\boldsymbol{z}, \tag{4.30}$$

so whenever A is diagonalizable, we obtain an individual equation

$$\frac{d}{dt}z_j = \lambda_j\, z_j \tag{4.31}$$

for each global mode z_j. The behavior of the original variables x_i can be written as

$$x_i(t) = \sum_j q_{ij}\, z_j(t) = \sum_j q_{ij}\, z_j(0)e^{-\gamma_j t} \tag{4.32}$$

with the initial value $z(0) = Q^{-1}x(0)$.

The different modes can be characterized by response times as introduced above. If the eigenvalue λ_i is a real number, z_j relaxes exponentially to the value 0 with a response time $\tau_j = 1/\lambda_j$. A pair of complex conjugated eigenvalues, in contrast, leads to a pair of oscillatory modes with time constant $\tau_i = 1/\text{Re}(\lambda_i)$. An eigenvalue $\lambda_i = 0$ (corresponding to an infinitely slow mode) can arise, for instance, from linear conservation relations.

To simplify the system, we can neglect fast global modes (with small τ_j) in the sum (4.32), assuming that they will relax immediately. In metabolic network models, this will reduce the accuracy at fast time scales, but none of the metabolites or reactions will be omitted from the model. The system state is projected to the space of slow modes and the number of variables is effectively reduced.

Even if A cannot be diagonalized, the state space can still be split into subspaces related to fast and slow dynamics: by neglecting the fast subspace, the number of variables can then be reduced adaptively during computer simulations [29]. Powerful methods for linear model reduction like balanced truncation [23, 30] have been developed in control engineering (see the web supplement).

4.3.5
Coupled Systems and Emergent Behavior

All biological systems, from organisms down to cellular pathways, are embedded in larger environments that influence their dynamics. A metabolic pathway, for instance, is part of a larger network and coupled to a transcription network that adjusts its enzyme levels. For the dynamics of such a system, it can make a big difference if the environment's state is kept fixed or if both systems interact dynamically. In our terminology, a system is either studied *in isolation* (with fixed or controlled environment) or *coupled* to a dynamic environment. This fundamental distinction does not only hold for models, but also for experimental systems: in an *in vitro* enzyme assay, for instance, conditions like pH or the levels of cofactors can be experimentally controlled; in living cells, these values may be regulated dynamically, usually in an unknown manner.

When systems are coupled, new dynamic behavior can emerge. Single yeast cells, for instance, can communicate by the exchange of chemicals: Such interactions can lead, for instance, to synchronized glycolytic oscillations, which have been observed both in experiments and in models [31]. The following two examples illustrate the difference between isolated and coupled systems.

(a)

X $\rightarrow$ Y

(b)

X $\rightleftarrows$ Y
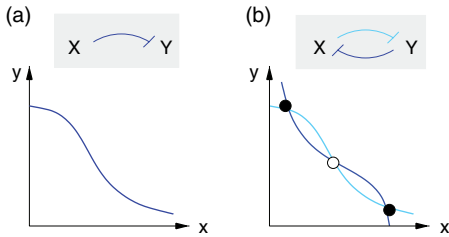
Figure 4.11 Bistability can emerge from mutual inhibition. (a) A gene level y is modeled in isolation with another gene level x acting as a regulatory input. The steady-state level y^{st} (blue) depends on the given value of x. (b) Two mutually interacting genes show bistability as an emergent property, with two stable fixed points (black dots) and one unstable fixed point (white dot) at the intersection of the two nullclines.

Example 4.4: Bistable switch

Let us consider two genes X and Y that mutually inhibit each other (Figure 4.11); we describe their levels x and y by the differential equation model

$$\frac{dx}{dt} = f(x, y)$$

$$\frac{dy}{dt} = g(x, y).$$

(4.33)

By setting the second equation to zero and solving for y, we obtain the steady-state value of y as a function of x. The curve $y^{st}(x)$ in Figure 4.11(a) is called the *nullcline* of y. Likewise, we obtain another nullcline $x^{st}(y)$ from the first equation. These nullclines represent response curves for the individual systems. When both systems are coupled, both steady-state requirements $y^{st} = f(x^{st})$ and $x^{st} = g(y^{st})$ have to be satisfied at the same time. We obtain three fixed points, two of which are stable, as indicated by the slopes of the nullclines. Due to the positive feedback loop, a bistable switch has emerged. The bistability is not a property of the individual genes X and Y – it is an systemic property which is only caused by their coupling.

Example 4.5: Reaction velocity and steady-state flux

Figure 4.12 shows two coupled chemical reactions. To study the first reaction in isolation, we fix the concentrations of substrate X and product Y. The reaction rate is given by the kinetic law $v_1(s_X, s_Y, E_1)$, and the response to a small increase of enzyme activity is described by the elasticity coefficient $\tilde{\pi}^{v_1}_{E_1} = \partial v_1/\partial E_1$. As the enzyme activity increases, the reaction rate can be made arbitrarily large.

Alternatively, we can study the stationary flux in the two coupled reactions, with the levels of X and Z fixed and the level of Y determined by a steady-state requirement. Now the rate of the first reaction equals the steady-state flux $j(x, z, E_1, E_2)$ and the effect of an increased enzyme activity is given by a response coefficient $R^j_{E_1} = \partial j/\partial E_1$.

> In this setting, the first enzyme will have a limited effect on the reaction rate: As its activity increases, the enzyme will lose its control and the reaction flux will be mostly controlled by the second enzyme.

The two approaches – whether isolated and coupled dynamics – are characteristic for two contrary views on complex systems. *Reductionism* studies the parts of a system in isolation and great detail. In this view, which is dominant in molecular biology and biochemistry, the global behavior of a system is explained in terms of interactions between the system's parts, and the dynamics is explained in terms of causal chains. *Holism,* on the contrary, emphasizes the fact that new dynamic behavior can emerge from the coupling of subsystems. Instead of tracing individual causal effects, it emphasizes how the global system dynamics responds to changes of external conditions.

4.3.6
Modeling of Coupled Systems

4.3.6.1 Bottom-Up and Top-Down Modeling
According to the concepts of reductionism and holism, there are two complementary modeling approaches, called bottom-up and top-down modeling; both proceed from simplicity to complexity, but in very different ways. In *bottom-up* modeling [32, 33], one studies elementary processes in isolation and aggregates them to a model. An example is the glycolysis model of Teusink et al. [32] that was built from kinetic rate laws measured *in vitro*. *In vitro* measurements of enzyme kinetics allow for an exact characterization and manipulation of quantitative parameters. A metabolic pathway model was constructed by merging the reactions. Without further tuning, it yielded a fairly plausible steady-state description of glycolysis. In *top-down* modeling, on the contrary, a model is built by refining a coarse-grained model of the entire system. If the model structure is biologically reasonable, such a model can be expected to yield fairly good data fits, but there is no general guarantee that it will remain valid as part of
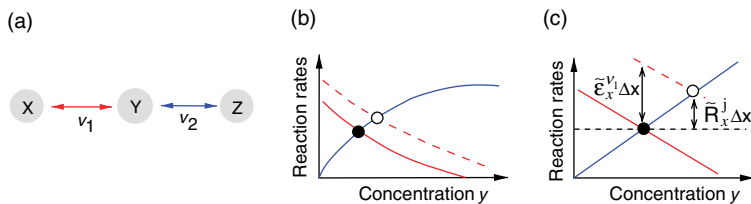
Figure 4.12 Elasticities and response coefficients describe local and global response to external changes. (a) Chain of two reactions with external metabolites X and Z and an intermediate Y. (b) The reaction rates v_1 (red) and v_2 (blue) depend on the intermediate level y. A steady state requires that both rates are identical (black dot). If v_1 is increased – e.g, by an increase of the external substrate X (broken red line), the steady-state flux and concentration are shifted (white dot). (c) The magnified scheme compares the direct increase of the reaction rate $\tilde{\varepsilon}_x^{v_1} \Delta x$ (depending on the reaction elasticity $\tilde{\varepsilon}_x^{v_1}$) to the steady-state flux increase $\tilde{R}_x^j \Delta x$ (depending on the response coefficient $\tilde{R}_x^j$).

a merged model. The two approaches pursue different goals: A bottom-up model is constructed to be locally correct (describing individual reactions by correct rate laws and parameters), while a top-down model, on the other hand, is optimized for a good global fit to *in vivo* behavior. In a model of limited size, it is unlikely that both requirements will be fulfilled at the same time.

4.3.6.2 Modeling the System Boundary

When building a biochemical model, we distinguish between a *system of interest* (which is explicitly modeled) and its *environment*, which is either not modeled or described only very roughly. Although this distinction is artificial, it cannot be avoided. The communicating quantities on the boundary may be external substance levels or fluxes, and their values have to be specified by model assumptions.

If the boundary variables of a system are kept fixed, the system is modeled as if it was in isolation. To ensure that this assumption is at least approximately justified, one should carefully choose the experimental system and the description of communicating variables. The system boundary should be chosen such that the interactions are weak, constant in time, or average out (because they are fast or random) and can thus be buried in the parameters. If the communicating variables are supposed to change in time, time series of the communicating variables can be obtained from experiments or from a separate environment model and be inserted into the model as given, time-dependent functions. Alternatively, the environment can be described as part of the model, either by effective algebraic relationships [34] or by simplified dynamic black-box models [23].

4.3.6.3 Coupling of Submodels

The coupling of several submodels (often called "modules") works quite similarly. The communicating variables *connect* the subsystems, but they also *shield* them from each other: If their temporal behavior was known, then the dynamics of each module could be computed without referring to the other modules. If the influences between modules form an acyclic graph, we can first simulate the dynamics of upstream modules, compute their outputs, and use them later as inputs for the downstream modules. If the coupling involves feedback loops, all modules need to be simulated together. We will come back to this point in Section 8.3.4.

An important consequence is that metabolic pathways can be driven by both supply and demand [35]. In a chain of chemical reactions, the steady-state flux depends on the concentration of the initial substrate. However, if the reactions are reversible or if enzyme activities are controlled by metabolite concentrations, also the end product may exert control on the flux. Supply–demand analysis [35] dissects metabolism into individual blocks, which are coupled by matching their supply and demand variables. The elasticities of supply and demand, which are experimentally measurable properties of the individual blocks, are then used to describe the behavior, control, and regulation of metabolism.

4.3.6.4 Model Merging

As more and more models become available (see Section 3.4.4), it is a tempting idea to build cell models by merging preexisting models of subsystems [36–39]. As the
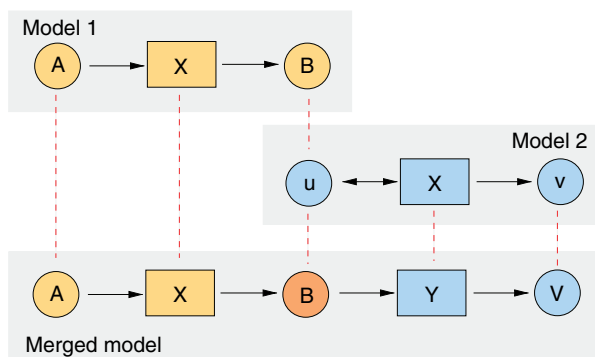
Figure 4.13 Merging of models. Two models (top and center) are merged to a single model (bottom) containing all model elements. Symbols represent model elements, for instance, substances and reactions. For merging, model elements are aligned (red dashed lines) according to their biological meaning as indicated by annotations (not shown). A simple name comparison would be unreliable because models can use different naming conventions.

models can overlap in their elements (e.g., substances or reactions described), elements from different models have to be matched to each other, as shown in Figure 4.13.

Model merging is based on the reductionist assumption that a mechanistic model will remain correct in different environments. However, both manual and computer-assisted merging (e.g., with SemanticSBML, see [38] and Chapter 17) pose various kinds of challenges [39]: (i) Model elements (variables, parameters, chemical reactions) have to be compared according to their biological meaning, which requires a clear description by (possibly computer-readable) annotations (e.g., MIRIAM-compliant RDF annotations [40]). (ii) Units must be compared and unified. (iii) Explicit conflicts between the models – e.g., different kinetics for the same reaction – have to be detected and resolved. (iv) Implicit conflicts may arise if the input models make contradicting assumptions or obey contradicting constraints (e.g., thermodynamic relationships between kinetic parameters). (v) If the model parameters have been determined by global fits, they possibly need to be refitted in the merged model. Some of these difficulties can be avoided if submodels are already designed with a common nomenclature and modeling framework. Model merging is greatly facilitated by standardization efforts for experiments and model building [41].

4.4
Model Selection

Summary

Mathematical models have to meet various requirements: they should fit experimental data, allow for prediction of biological behavior, represent complex biological mechanisms under study, and describe them in a simple, understandable form.

> Systems biology models are often refined in iterative cycles until they agree with all relevant data. Alternative models may include different levels of detail or represent different biological hypotheses, and statistical model selection can help to choose between them. Complex models tend to overfit the data, so for choosing a reliable model, the number of free model parameters needs to be restricted, e.g., by likelihood ratio tests, by selection criteria like the Akaike criterion, or by Bayesian model selection.

One of the main issues in mathematical modeling is to choose between alternative model structures and to justify this choice. It is often arguable which biological elements need to be considered. Models may cover different cellular subsystems, different components or interactions within a subsystem (e.g., feedback interactions), different descriptions of the same process (e.g., different kinetic laws, fixed or variable concentrations), and different levels of detail (subprocesses or time scales). Alternative versions of model parts can lead to a combinatorial explosion of model variants, so we need to rule out models that are incorrect or too complicated [42, 43]. With limited and inaccurate data, we will not be able to pinpoint a single very detailed model, but statistical criteria can at least tell us which of the models are best supported by the data.

4.4.1
What is a Good Model?

A good model need not describe a biological system in all details. Borges writes in a story [44]: "In that empire, the art of cartography attained such perfection that the map of a single province occupied the entirety of a city, and the map of the empire, the entirety of a province. In time, those unconscionable maps no longer satisfied, and the cartographers guilds struck a map of the empire whose size was that of the empire, and which coincided point for point with it."

Systems biology models range from very simple to very complex maps of the cell, but just like usual maps, they never become an exact copy of the biological system. If they did, they would be almost as hard to understand as the biological system itself. Or, as George Box put it [45], "Essentially, all models are wrong, but some are useful." But – useful for what? As models are made for different purposes, they have to meet different requirements (see Figure 4.14):

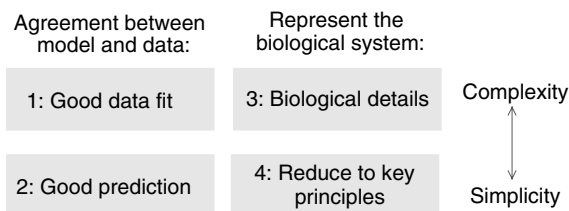| Agreement between model and data:	Represent the biological system:	
1: Good data fit	3: Biological details	Complexity
2: Good prediction	4: Reduce to key principles	Simplicity

Figure 4.14 Possible requirements for a good model.

1. In *data fitting*, we aim to describe individual data points by a general mathematical function. Instead of storing many data pairs (x, y) that lie on a curve, we can store a few curve parameters (e.g., offset and slope for a straight line). If the points are not exactly on a curve, we may attribute the discrepancy between model and data to statistical errors in the measurement. Given a model structure, we can adjust the model parameters such as to optimize the fit, e.g., by minimizing the sum of squared residuals (SSR) (see Section 4.2). Fitting equally applies to dynamical models, which effectively define a mapping between parameters and data curves.

2. When used for *prediction*, a model is supposed to state general relationships between measured quantities that will also hold for future observations: In the language of statistical learning, the model should generalize well to new data.

3. A *detailed mechanistic model* is supposed to describe processes "as they happen in reality." Of course, the description of an entire cell will never be complete down to molecular or lower levels. In practice, mechanistic models will focus on parts of the cell only and use simplifying assumptions and model reduction to simplify them to a tractable level.

4. To emphasize the *key principles* of a biological process, a model needs to be *as simple as possible*. Simplicity is especially important if a model is supposed to serve as a didactic or prototypic example. This also holds for experimental model systems, e.g., the Lac operon as a model for microbial gene regulation.

These properties are partially interrelated. A good data fit supports the hypothesis that a model is biologically correct and covers the key features of a system. But – it does not prove it: a complex model – even with an implausible structure – may achieve better fits than a simpler, biologically plausible model. As a rule of thumb, a model with many free parameters may fit given data more easily ("With four parameters I can fit an elephant, and with five I can make him wiggle his trunk." J. von Neumann, quoted in [46]). But as the fit becomes better and better, the average amount of experimental information per parameter decreases, so the parameter estimates and predictions from the model become poorly determined. Such overfitting is a notorious problem when many free parameters are fitted to few data points or if a large number of possible models is prescreened for good data fits (Freedman's paradox [47]). It can be detected and avoided, though, by making proper use of statistics.

4.4.2
Statistical Tests and Model Selection

Let us suppose that a number of alternative models have been proposed for a biological process. We intend to choose between them based on experimental data, in particular, time series of substance concentrations.

As a running example, we will consider two alternative models for a chemical reaction S $\leftrightarrow$ P. The first model ("A") assumes mass-action kinetics with rate constants k_+ and k_- and a fixed product concentration c. The substrate concentration s follows the rate equation

$$\frac{ds}{dt} = -k_+ s + k_- c. \tag{4.34}$$

The second model ("B") assumes that the reaction is irreversible, i.e., the rate constant k_- vanishes. For the concentration of S, the two models predict a temporal behavior

$$\text{Model A}: \; s(t) = s^{\text{st}} + (s_0 - s^{\text{st}})\, e^{-k_+ t} \tag{4.35}$$

$$\text{Model B}: \; s(t) = s_0\, e^{-k_+ t} \tag{4.36}$$

with the initial concentration s_0 and the steady-state concentration $s^{\text{st}} = c\, k_-/k_+$ in model A. The solution of model A depends on the values of k_+, k_-, s_0, and c. However, the parameters k_- and c only appear in the form of a product $a = k_- c$, which means that they are not identifiable individually (see 4.2.3). For parameter estimation and model selection, we keep three model parameters, k_+, s_0, and a. Model B contains only two parameters, k_+ and s_0.

In model selection, we compare the two models to experimental data, e.g., to a concentration time series for S consisting of triples (t_i, y_i, σ_i) for the ith measurement, each containing a time point t_i, a measured concentration value y_i, and a standard error σ_i. By the approach of model selection, we aim to find out if there is a considerable backward flux from P to S.

We can choose between competing models by statistical tests and model selection criteria. In *statistical tests*, we compare a more complex model to a simpler background model. According to the null hypothesis, both models perform equally well. In the test, we favor the background model unless it statistically contradicts the observed data. In this case, we would conclude that the data support the more complex model. A test at a confidence level α will ensure that if the null hypothesis is correct, there is only an α% chance that we wrongly reject it.

Alternatively, several candidate models can be compared by a *selection criterion* [48–51]. Selection criteria are mathematical scoring functions that balance agreement with experimental data against model complexity. To compensate for the advantage of complex models in fitting large numbers of free parameters in the model are punished. Selection criteria can be used to rank the models, choose between them, and to weight them in averaging. In model selection, we choose between model structures just as we choose between parameter values in parameter fitting: In both cases, we intend to find a model that agrees with biological knowledge and that matches experimental data. The two tasks are interrelated:

In parameter estimation, parameter values are determined for a given model structure, while model selection often involves a parameter estimation run for each of the candidate models.

4.4.3
Maximum-Likelihood Estimation and χ^2-Test

We can judge the quality of a model by comparing its predictions to experimental data. The structure and parameters of a model can be scored by its *likelihood* (see Chapter 13), the probability that the model assigns to actual observations. Consider the model "Tomorrow, the sun will shine with 80% probability": If sunshine is observed, the model has a likelihood of 0.8. Mathematically, the likelihood for a model or parameter set θ is defined as $L(\theta|y) = p(y|\theta)$, that is, the conditional probability to observe the data y given the model.

To compute likelihood values for biochemical models, we need to relate the model predictions to experimental data. In a simple statistical model, we regard the experimental data y_i as a sum

$$y_i = x_i(\theta) + \xi_i \tag{4.37}$$

of the model results and measurement errors ξ_i, described by independent Gaussian random variables with mean 0 and width σ_i. The subscript i can refer to both substances and time points. The assumption of additive Gaussian errors greatly simplifies calculations, but it need not hold in all cases. With Eq. (4.37) and the probability density $p_{\xi i}(\xi)$, the likelihood $L(\theta|y)$ can be written as a function of the model parameters (see Eq. (4.5)). For further calculations, we consider the expression

$$-2 \log L(\theta|y) = -2 \log p(y|\theta) = -2 \sum_{i=1}^{n} \log p_{\xi_i}(y_i(t) - x_i(\theta)). \tag{4.38}$$

By inserting the Gaussian probability density $p_\xi(\xi) \sim \exp(-\xi^2/(2\sigma^2))$, we obtain

$$-2 \log L(\theta|y) = \sum_{i=1}^{n} \frac{(y_i - x_i(\theta))^2}{\sigma_i^2} + \text{const.} \tag{4.39}$$

The quality of the model (4.37) can be judged from the sum in expression (4.39), the weighted sum of squared residuals (wSSR). If our model is correct, the y_i will be independent Gaussian random variables with means x_i and variances σ_i^2, so the weighted SSR will follow a χ^2-distribution with n degrees of freedom. On the contrary, if the result of (4.39) for a given model and given data falls in the upper 5% quantile of the χ_n^2-distribution, the model can be rejected on a 5% confidence level. We would conclude in this case that the model is wrong. If parameters have been fitted before, the number of degrees of freedom in the χ^2-distribution should be reduced to account for possible overfitting. In *maximum-likelihood estimation*, we determine a parameter set $\hat{\theta}(y)$ that maximizes the likelihood

$p(y|\theta)$ for a given data set y (see 4.2.2.1): The resulting likelihood value measures the *goodness of fit*.

The likelihood can also be used to choose between different model structures. For instance, the above statement A, "Tomorrow, the sun will shine with 80% probability" can be compared to the statement B, "Tomorrow, the sun will shine with 50 percent probability". If sunshine has been observed, statement A will have a higher likelihood (Prob(data$|A$) $=0.8$) than statement B, (Prob(data$|B$) $=0.5$), and should be chosen if likelihood is used to select models. Biochemical models can be selected in the same manner, but only if their parameters have been fixed in advance, as we shall explain now.

4.4.4
Overfitting

If models were selected by their maximized likelihood (and not by the likelihood arising from predefined, fixed parameters) overfitting could severely distort the selection of models. Consider a statistical model with true parameters θ and data y: The maximum-likelihood estimator $\hat{\theta}(y)$ will lead to a higher likelihood $L(\hat{\theta}(y)|y) > L(\theta|y)$ than the true parameter set θ just because it was optimized for high likelihood for the observed data. The empirical (maximized) log-likelihood will exceed the log-likelihood of the true parameters, on average, by a certain amount $\Delta \log L$. This bias depends on how easily the model can fit the noise; usually, it increases with the number of free model parameters.

Before using real experimental data, it is often instructive to consider artificial data obtained from model simulations. If we generated the data ourselves, we can judge more easily if a model selection method is able to recover the original, supposedly true, model.

Example 4.7: Likelihood values

For our running example, we assume an original model of form A with parameters $k_{\pm} = 1$, $s_0 = 1$, $c = 0.1$. Figure 4.15 shows a simulation run of this model. Artificial noisy data were generated by adding Gaussian random numbers with a standard deviation of 25% of the true value. These data can now be compared to potential candidate models, using the wSSR, $\sum_{i=1}^{n} (y_i - x_i(\theta))^2 / \sigma_i^2$ to measure the goodness of fit. For models A and B with predefined parameter values (see Figure 4.15(a)), the fit is rather poor. After maximum-likelihood parameter estimation (by minimizing the weighted SSR), we obtain a much closer match (Figure 4.15(b), numerical values in Table 4.2). In fact, both models fit the data even better than the original model does. This is a case of slight overfitting. As expected, model A (with 3 parameters) performs better than model B (with 2 parameters only). The question remains: which of them should we choose?
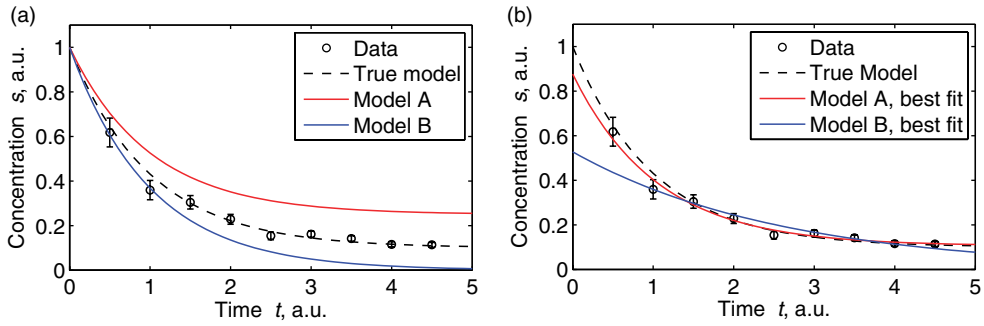
Figure 4.15 Fit of the example models. (a) Artificial data (a concentration time series, black dots) were generated by adding Gaussian noise to results of the true model (dashed line). Solid curves show simulations from model A (red) and B (blue) with fixed parameters. (b) After estimating the parameters of models A and B, a better fit is obtained.

4.4.5
Likelihood Ratio Test

A philosophical principle called *Ockham's razor* (*Entia non sunt multiplicanda praeter necessitatem*, entities should not be multiplied without necessity) states that a theory should not contain unnecessary elements. In statistical model selection, complexity in a model always needs to be supported by data. A good fit by itself will not suffice as a support if the same data have been used twice, for parameter estimation and model selection. To find models with reliable parameter estimates and good potential for predictions, we need to give all models equal chances. To correct for the advantage of complex models, we may apply the likelihood ratio test or selection criteria, which both favor models with few parameters.

The *likelihood ratio test* [52] compares two models A and B (with k_A and k_B free parameters, respectively) by their maximal likelihood values L_A and L_B. The two models have to be nested, that is, model B must be obtainable from model A by fixing a number of parameters in advance. In the test, the null hypothesis states that both models explain the data equally well. But even if model B is correct, model A will show a higher empirical likelihood because its additional parameters make it easier to fit the

Table 4.2 Parameter sets and goodness of fit for versions of the example model (compare Fig. 4.15)

	k_+	a	s_0	Weighted SSR
Original model	1	1	1	7.32
A, fixed parameters	1	0.25	1	102.59
B, fixed parameters	1	–	1	65.92
A, optimized parameters	0.8345	0.0921	0.6815	4.98
B, optimized parameters	0.3123	–	0.4373	6.13

[a]The last column shows the wSSR, $\sum_i (y_i - x_i)^2 / \sigma_i^2$ describing the goodness of fit.

noise. The test accounts for this fact. For large numbers of data points and independent, Gaussian-distributed measurement errors, the expression $r = 2\ln(L_A/L_B)$ asymptotically follows a χ^2-distribution, with $k_A - k_B$ degrees of freedom. This distribution is used for the statistical test: if the empirical value of r is significantly high, we reject the null hypothesis and accept model A. Otherwise, we accept the simpler model B. The likelihood ratio test can also be applied sequentially to more than two models, provided that subsequent models are nested. For a practical example, see [53].

Example 4.8: Likelihood ratio test

In our running example, the test statistics has a value of $2\ln(L_A/L_B) \approx 6.13 - 4.98 = 1.15$. The 95% quantile for χ^2-distribution with $3 - 2 = 1$ degree of freedom is much higher, about 3.84. So according to the likelihood ratio test, we cannot reject model B. However, the likelihood values depend on the noise levels $\sigma_i(t)$ assumed in the likelihood function: With a smaller noise level (same artificial data, noise level corresponding to 10% of the original values), the weighted SSR for the two models read approximately 5.0 (model A) and 19.8 (model B). In this case, the test statistics has a value of $19.8 - 5.0 = 14.8$, which is highly significant, so the data would support model A.

4.4.6
Selection Criteria

We saw that the maximal likelihood contains a certain bias $\Delta\log L$, so for model selection, it would be better to score models by an unbiased estimator of the true likelihood $\Delta\log L(\hat{\theta}(y)|y) - \Delta L$. The value of $\Delta\log L$ is unknown in general, but mathematical expressions for it, so-called *selection criteria*, have been proposed for certain forms of models. By minimizing these objective functions (instead of the likelihood itself), we attempt to find a model that best explains the data, while taking into account the possibility of overfitting. The Akaike information criterion [54]

$$\text{AIC} = -2\log L(\hat{\theta}(y)|y) + 2k, \tag{4.40}$$

for instance, directly penalizes the number k of free parameters. If we assume additive Gaussian measurement noise of width 1, the term $-2\log L(\theta|y)$ in Eq. (4.40) equals the sum of squared residuals $R(\theta)$ and we obtain

$$\text{AIC} = R(\theta) + 2k \tag{4.41}$$

A correction for small sample sizes yields

$$\text{AICc} = \text{AIC} + \frac{2k(k+1)}{n-k-1} \tag{4.42}$$

where n is the number of data. The Schwarz criterion [55]

$$\text{BIC} = -2\log L(\theta|y) + k\log n \tag{4.43}$$

penalizes free parameters more strongly. In contrast to AIC, the BIC is consistent, i. e., as the number of data n goes to infinity, the true model will be selected with probability 1. The selection criteria allow to rank models and to choose between them, but there is no notion of significance for the result of such a model selection.

Example 4.9: Selection criteria

Table 4.3 shows the values of different model selection criteria for the running example 4.6. To produce the artificial data, the standard deviation for the noise in each data point was 25% of the true values. If we assume the same noise levels for the model selection procedure, all selection criteria favor the simpler model B. However, if we refit the models to the same artificial data, but assuming a smaller noise level in the model selection (corresponding to 10% of the original values), model A is favored because in this case, a good fit becomes more important.

In some cases, the selection criteria may suggest that none of the models is considerably better than all others. In this situation, we may decide not to select a single model and instead consider several models. For example, to estimate a model parameter, we may average over the parameter values obtained from different models. To assign higher weight to parameters from the more reliable models, weighting factors can be constructed from the selection criteria [54].

4.4.7
Bayesian Model Selection

Practical reasoning in everyday life is contrary to the logic of maximum likelihood. In real life, we would not ask: "Under which explanation would our observations seem most likely?", but rather: "What is the most plausible explanation for our observations?"

Table 4.3 Calculation of selection criteria for the running example.[a]

	σ large		σ small	
	Model A	**Model B**	**Model A**	**Model B**
n	3	2	–	
k	9	9		
$2k$	6	4	–	
$2k + \frac{2k(k+1)}{n-k-1}$	4.67	2.33		
$k \log n$	6.59	4.39		
Weighted SSR	4.98	6.13	4.99	19.81
AIC	10.98	10.13	10.99	23.81
AICc	9.64	8.46	9.66	22.14
BIC	11.57	10.52	11.58	24.20

[a] For each of the criteria (weighted sum of squared residuals (SSR), Akaike information criteria (AIC and AICc), and Schwarz criterion (BIC)), the more favorable values are shown in red.

Imagine that you toss a coin and obtain heads. Now you have to choose between the statements A: "The coin always shows heads," B: "It shows heads and tails with equal probability." According to the maximum-likelihood criterion, you should choose A – which is counterintuitive, because you know that real coins will not always show heads. But how can such kind of prior knowledge – the probability of different explanations besides our current observations – be included in model selection?

Bayesian statistics is doing just that in a formalized way [56, 57]. Instead of considering distributions of parameter sets (as in Section 4.2.6), we now treat the model structure itself by a probability distribution. Before observing the data, all we know about the model (including its structure $\mathcal{M}$, its parameters θ, or both) is its marginal probability, the *prior* $p(\mathcal{M}, \theta)$. We can compute the posterior from Bayes' theorem about conditional probabilities:

$$p(\mathcal{M}, \theta|y) = \frac{p(y|\mathcal{M}, \theta)p(\mathcal{M}, \theta)}{p(y)}. \tag{4.44}$$

According to this formula, we obtain the posterior by multiplying the likelihood $L(\mathcal{M}, \theta|y) = p(y|\mathcal{M}, \theta)$ (stating how well the model explains the data) with the prior (describing how probable the model is in general). By taking the logarithm, we can rewrite Eq. (4.44) in the form of a sum

$$\ln p(\mathcal{M}, \theta|y) = \ln p(y|\mathcal{M}, \theta) + \ln p(\mathcal{M}, \theta) + \text{const.} \tag{4.45}$$

In practice, the posterior density (4.44) can often not be computed analytically. However, sampling methods like Monte Carlo Markov chains [56] allow to draw representative models and parameter sets from the posterior distribution and to extract all statistical information to arbitrary accuracy. The usual aim in Bayes estimation is not to select a single model, but to assign probabilities to different models. In addition, we can also obtain the marginal distribution of a certain parameter, probabilities for structural features that appear in several models, or probabilities for quantitative model predictions. By considering many possible models and weighting them according to their probabilities, we may obtain more reliable results than from a point estimate by maximum-likelihood estimation.

An application of Bayesian statistics is model selection by the *Bayes factor*. With equal priors $p(\mathcal{M}_1) = p(\mathcal{M}_2)$ for both model structures, the posterior ratio of two models $\mathcal{M}_1$ and $\mathcal{M}_2$, called the *Bayes factor*, reads

$$\frac{p(\mathcal{M}_2|y)}{p(\mathcal{M}_1|y)} = \frac{p(y|\mathcal{M}_2)}{p(y|\mathcal{M}_1)}. \tag{4.46}$$

In contrast to the likelihood ratio, the Bayes factor does not score a model based on a single optimized parameter set; instead, it is computed from weighted averages over all possible parameter vectors θ_1 and θ_2,

$$\frac{p(y|\mathcal{M}_2)}{p(y|\mathcal{M}_1)} = \frac{\int p(y|\theta_2, \mathcal{M}_2)p(\theta_2|\mathcal{M}_2)d\theta_2}{\int p(y|\theta_1, \mathcal{M}_1)p(\theta_1|\mathcal{M}_1)d\theta_1}. \tag{4.47}$$

For complex models, these integrals can be approximated by Monte Carlo sampling.

The prior probability can also be seen as a regularization term: if the data alone are insufficient to identify a parameter set or a model structure, model selection is an underdetermined (or *ill-posed*) problem; with the prior, a single solution can be selected, and model selection becomes well determined.

The posterior distribution depends strongly on how we choose the priors for model structures and parameter values. With a uniform prior (the same prior probability for each model $\mathcal{M}$), the posterior is proportional to the likelihood. The choice of the prior can reflect both our biological expectations and our demands for simplicity. This subjective choice forces modelers to state explicitly their assumptions about the system structure. Furthermore, a prior distribution can be used, like the above-mentioned selection criteria, to punish models with many parameters.

4.4.8
Cycle of Experiments and Modeling

Modeling in systems biology usually starts with literature studies and data collection. The first step toward a quantitative model is to develop hypotheses about the biological system. Which objects and processes (e.g. substances, chemical reactions, cell compartments) are relevant? Which mathematical framework is appropriate (continuous or discrete model, kinetic or stochastic, spatial or nonspatial)?

After the model parameters have been fixed tentatively, models (structure and parameters) can be judged by how well their results agree with experimental data. A correct model should explain or predict the data within their error range; a χ^2-test or a parametric bootstrap can be used to rule out models seem to be wrong. Then, different model variants are formulated and fitted to experimental data, and their dynamic behavior is studied (e.g. by bifurcation analysis or sensitivity analysis). In practice, modeling often involves several cycles of model generation, fitting, testing, and selection [42, 58].

Sometimes, model structures can be selected according to known qualitative properties: for instance, the chemotaxis system in bacteria is known to show precise adaptation to external stimuli and a model of it should account for this fact. In certain chemotaxis models, this robustness property follows from the network structure, and other model structure, which do not ensure precise adaptation, can be ruled out (see Section 7.4). Such requirements can also be stated in the form of model priors.

In the model selection process, a number of models may still perform equally well, and additional data are needed to choose between them. Optimal experimental design [59] is aimed to determine experiments that are most likely to yield the information needed to distinguish between the models; The resulting cycle of experiments and modeling can overcome many of the limitations of one-step model selection.

4.4.9
Models are Growing in Complexity

Systems biology modeling is usually intended to yield fairly plausible mechanistic models that include all relevant key processes for a biochemical system. In practice,

models are selected for various aspects: Does the model reflect the basic biological facts about the system? Is it simple enough to be simulated and fitted? Does it explain the existing data and can it predict anything that was not known before? If data are limited – and they always are – there is a trade-off between these requirements, and statistical model selection can help to avoid overfitting.

As more data or more accurate data become available, models can resolve more and more details of biological reality. This is illustrated by the development of models during the last decades: With increasing amounts of data, models of metabolism, cell cycle, or signaling pathways have become more complex, more accurate, and more predictive. By the time, simple initial models are replaced by detailed biochemical models that account for many experimental observations and come closer and closer to biological reality.

Exercises and Problems

Problems

1. Use BRENDA to search for all hydrolases from *Rattus norvegicus* that have a K_m value below 0.001 mM.

2. What are the advantages of using GFP constructs for measuring the cellular response to perturbations compared to DNA microarrays?

3. Use http://yeastGFP.ucsf.edu to find out how many copies of the mitochondrial DNA polymerase catalytic subunit exist in a yeast cell. The gene name can be found with the help of http://www.yeastgenome.org.

4. *Linear regression*. A data set $\{(t_1, y_1), (t_2, y_2), \ldots\}$ has been obtained from a linear model

$$y(t) = \theta_1 t + \theta_2 + \xi_t$$

with random errors ξ_t. (a) Given the vectors $\boldsymbol{t} = (t_1, t_2, \ldots)^\mathsf{T}$ and $\boldsymbol{y} = (y_1, y_2, \ldots)^\mathsf{T}$, explain how to estimate the model parameters θ_1 and θ_2 by maximizing the likelihood. Assume that the errors ξ_t are independent Gaussian random variables with mean 0 and variance σ^2.

5. *Bootstrapping procedure for the empirical mean*. The expected value of a random number X can be estimated by the empirical mean value $\bar{x} = 1/n \sum_{m=1}^{n} x^{(m)}$ of n realizations $x^{(1)}, \ldots, x^{(n)}$. (a) Compute the mean and the variance of the estimator $\bar{x}$. (b) Choose a distribution of X and approximate the mean and the variance of $\bar{x}$ numerically, by repeatedly drawing samples $(x^{(1)}, \ldots, x^{(n)})$. (c) Implement a bootstrapping procedure and assess the distribution of the estimate $\bar{x}$ based on a single sample $(x^{(1)}, \ldots, x^{(n)})$. (d) Explain why these three results differ.

6. *One-norm and two-norm*. The method of least squares can be derived from the maximal likelihood estimator, assuming independent standard Gaussian errors. (a) Assume that the experimental noise ξ is not Gaussian, but follows an

exponential distribution with density $p(\xi) \sim \exp(-|\xi|/a)$. Find the minimization principle that would replace in this case the method of least squares. (b) Assume that a model is fitted to the same data set (i) by the principle of least squares or (ii) by the minimization principle derived in (a). What will be the qualitative difference between the two fitting results?

7. *Local and global optimization* (a) Why is it important in parameter estimation to find a global optimum rather than a suboptimal local one? Do local optimum points also have a relevance?

8. A substance appears in a kinetic model in two forms, either free or bound to proteins; only the free form participates in chemical reactions, and there is a fast conversion between both forms. Explain how the model could be modified in order to describe the substance by its total concentration.

9. (a) Discuss Aristotle's proposition "The whole is more than the sum of its parts" in the context of biochemical systems and mathematical models describing them. (b) Speculate about the advantages and disadvantages of reductionist and holistic approaches in systems biology.

10. Does the concept of a complete cell model make any sense at all? (a) Speculate about possible definitions. (b) Estimate roughly the number of variables and parameters in models of living cells. Consider the following types of model: (i) Kinetic model of the entire metabolism without spatial structure. (ii) Compartment model including organelles. (iii) Particle-based model describing single molecules and their complexes in different conformation states. (iv) Model with atomic resolution.

11. Discuss the phrase by George Box: "Essentially, all models are wrong, but some are useful." What do you think of it? Does it give any helpful advice for modeling?

12. A kinetic model has been fitted to an experimental concentrations time series. An additional data point can be measured in the time series, and you can choose the time point at which the measurement will take place. How would you choose the best point in time for the measurement, and what circumstances would influence your choice?

13. Three models A, B, C have been fitted to experimental data ($n = 10$ data points) by a maximum-likelihood parameter fit. The respective optimized likelihood values and the numbers k of free parameters are given below. (a) Calculate the selection criteria AIC, AICc, and BIC, and use the results to choose between the models. (b) Assume that the models are nested, that is, A is a submodel of B, and B is a submodel of C. Decide for one of the models by using the likelihood ratio test.

Model	A	B	C
k	2	3	4
$\ln L$	10.0	5.0	2.0

References

1 Tsien, R.Y. (1998) The green fluorescent protein. *Annu Rev Biochem*, **67**, 509–544.

2 Ronen, M. *et al.* (2002) Assigning numbers to the arrows: parameterizing a gene regulation network by using accurate expression kinetics. *Proc Natl Acad Sci USA*, **99**, 10555–10560.

3 Zaslaver, A. *et al.* (2004) Just-in-time transcription program in metabolic pathways. *Nat Genet*, **36**, 486–491.

4 Zaslaver, A. *et al.* (2006) A comprehensive library of fluorescent transcriptional reporters for *Escherichia coli*. *Nat Methods*, **3**, 623–628.

5 Huh, W.K. *et al.* (2003) Global analysis of protein localization in budding yeast. *Nature*, **425**, 686–691.

6 Seber, G.A.F. and Wild, C.J. (2005) *Nonlinear Regression*. Wiley-IEEE.

7 Hoops, S., Sahle, S., Gauges, R., Lee, C., Pahle, J., Simus, N., Singhal, M., Xu, L., Mendes, P. and Kummer, U. (2006) COPASI - a COmplex PAthway SImulator. *Bioinformatics*, **22**, 3067–3074.

8 Timmer, J., Müller, T.G., Swameye, I., Sandra, O. and Klingmüller, U. (2004) Modelling the nonlinear dynamics of cellular signal transduction. *Int. J. of Bifurcation and Chaos*, **14** (6), 2069–2079.

9 Sontag, E.D. (2002) For differential equations with r parameters, $2r + 1$ experiments are enough for identification. *Journal of Nonlinear Science*, **12** (6), 553–583.

10 Efron, B. and Tibshirani, R. (1993) *An Introduction to the Bootstrap*, Chapman & Hall/CRC, London.

11 Mendes, P. and Kell, D.B. (1998) Non-linear optimization of biochemical pathways: application to metabolic engineering and parameter estimation. *Bioinformatics*, **14** (10), 869–883.

12 Moles, C.G., Mendes, P. and Banga, J.R. (2003) Parameter estimation in biochemical pathways: a comparison of global optimization methods. *Genome Research*, **13** (11), 2467–2474.

13 Rodriguez-Fernandeza, M., Mendes, P. and Banga, J.R. (2006) A hybrid approach for efficient and robust parameter estimation in biochemical pathways. *Biosystems*, **83** (2–3), 248–265.

14 Rodriguez-Fernandez, M., Egea, J.A. and Banga, J.R. (2006) Novel metaheuristic for parameter estimation in nonlinear dynamic biological systems. *BMC Bioinformatics*, **7** (483).

15 Rosenbluth, M.N., Teller, A.H., Metropolis, N., Rosenbluth, A.W., and Teller, E. (1953) Equations of state calculations by fast computing machines. *Journal of Chemical Physics*, **21** (6), 1087–1092.

16 Hastings, W.K. (1970) Monte Carlo sampling methods using Markov chains and their applications. *Biometrika*, **57** (1), 97–109.

17 Kirkpatrick, S., Gelatt, C.D. and Vecchi, M.P. (1983) Optimization by simulated annealing. *Science*, **220** (4598), 671–680.

18 Storn, R. and Price, K. (1997) Differential evolution – a simple and efficient heuristic for global optimization over continuous spaces. *Journal of Global Optimization*, **11**, 341–359.

19 Runarsson, T.P. and Yao, X. (2000) Stochastic ranking for constrained evolutionary optimization. *IEEE Transaction on Evolutionary Computation*, **4** (3), 284–294.

20 Okino, M.S. and Mavrovouniotis, M.L. (1998) Simplification of mathematical models of chemical reaction systems. *Chemical reviews*, **98** (2), 391–408.

21 Visser, D., Schmid, J.W., Mauch, K., Reuss, M. and Heijnen, J.J. (2004) Optimal re-design of primary metabolism in Escherichia coli using linlog kinetics. *Metab Eng*, **6** (4), 378–390.

22 Degenring, D., Frömel, C., Dikta, G. and Takors, R. (2004) Sensitivity analysis for the reduction of complex metabolism models. *J. Process Contr.*, **14**, 729–745.

23 Liebermeister, W., Baur, U. and Klipp, E. (2005) Biochemical network models simplified by balanced truncation. *FEBS Journal*, **272** (16), 4034–4043.

24 Becskei, A. and Serrano, L. (2000) Engineering stability in gene networks by autoregulation. *Nature*, **405**, 590–592.

25 Roussel, M.R. and Fraser, S.J. (2001) Invariant manifold methods for metabolic model reduction. *Chaos*, **11** (1), 196–206.

26 Ingalls, B.P. (2004) A frequency domain approach to sensitivity analysis of biochemical systems. *J Phys Chem B*, **108**, 1143–1152.

27 Liebermeister, W. (2005) Metabolic response to temporal parameter fluctuations in biochemical networks. *J Theor Biol*, **234** (3), 423–438.

28 Ingalls, B.P. and Sauro, H.M. (2003) Sensitivity analysis of stoichiometric networks: an extension of metabolic control analysis to non-steady state trajectories. *J Theor Biol*, **222** (1), 23–36.

29 Zobeley, J., Lebiedz, D., Ishmurzin, A. and Kummer, U. (2003) A new time-dependent complexity reduction method for biochemical systems. In *Transactions on Computational Systems Biology*, ed. C. Prami *et al.*, 90–110. Springer, LNCS 3380.

30 Moore, B.C. (1981) Principal component analysis in linear systems: Controllability, observability, and model reduction. *IEEE Trans AC*, AC-26, 17–32.

31 Wolf, J. and Heinrich, R. (2000) Effect of cellular interaction on glycolytic oscillations in yeast: a theoretical investigation. *Biochemical Journal*, **345**, 312–334.

32 Teusink, B., Passarge, J., Reijenga, C.A., Esgalhado, E., van der Weijden, C.C., Schepper, M., Walsh, M.C., Bakker, B.M., van Dam, K., Westerhoff, H.V. and Snoep, J.L. (2000) Can yeast glycolysis be understood in terms of *in vitro* kinetics of the constituent enzymes? Testing biochemistry. *European Journal of Biochemistry*, **267**, 5313–5329.

33 Chassagnole, C., Raïs, B., Quentin, E., Fell, D.A. and Mazat, J. (2001) An integrated study of threonine-pathway enzyme kinetics in *Escherichia coli*. *Biochem J*, **356**, 415–423.

34 Petersen, S., Lieres, E.v., de Graaf, A.A., Sahm, H. and Wiechert, W. (2004) *Metabolic engineering in the post genomic era*, chapter A multi-scale approach for the predictive modeling of metabolic regulation. Horizon Bioscience, UK.

35 Hofmeyr, J.-H.S. and Cornish-Bowden, A. (2000) Regulating the cellular economy of supply and demand. *FEBS Letters*, **476** (1–2), 47–51.

36 Bhalla, U.S. and Iyengar, R. (1999) Emergent properties of networks of biological signaling pathways. *Science*, **283** (5400), 381–387.

37 Snoep, J.L., Bruggeman, Frank, Olivier, B.G. and Westerhoff, H.V. (2006) Towards building the silicon cell: A modular approach. *Biosystems*, **83**, 207–216.

38 www.semanticsbml.org

39 Liebermeister, W. (2008) Validity and combination of biochemical models. *Proceedings of 3rd International ESCEC Workshop on Experimental, Standard Conditions on Enzyme Characterizations*.

40 Le Novère, N., Finney, A., Hucka, M., Bhalla, U.S., Campagne, F., Collado-Vides, J., Crampin, E.J., Halstead, M., Klipp, E., Mendes, P., Nielsen, P., Sauro, H., Shapiro, B., Snoep, J.L., Spence, H.D. and Wanner, B.L. (2005) Minimum information requested in the annotation of biochemical models (MIRIAM). *Nat Biotech.*, **23** (12), 1509–1515.

41 Klipp, E., Liebermeister, W., Helbig, A., Kowald, A. and Schaber, J. (2007) Systems biology standards - the community speaks. *Nature Biotech.*, **25**, 390–391.

42 Wiechert, W. (2004) Metabolic Engineering in the Post Genomic Era, chapter *Validation of Metabolic Models: Concepts, Tools, and Problems*, Chap 11, Horizon Bioscience.

43 Haunschild, M., Freisleben, B., Takors, R. and Wiechert, W. (2005) Investigating the

dynamic behaviour of biochemical
networks using model families.
Bioinformatics, **21**, 1617–1625.

44 Borges, J.L. Suarez Miranda,Viajes de
varones prudentes, Libro IV, Cap. XLV,
Lerida, 1658, Jorge Luis Borges, Collected
Fictions, Penguin.

45 Box, G.E.P. and Draper, N.R. (1987)
*Empirical Model-Building and Response
Surfaces*, Wiley, New York.

46 Dyson, F. (2004) A meeting with Enrico
Fermi. *Nature*, **427**, 297.

47 Freedman, D.A. (1983) A Note on
Screening Regression Equations.
The American Statistician, **37** (2),
152–155.

48 Atkinson, A.C. (1981) Likelihood Ratios,
Posterior Odds and Information Criteria.
Journal. of Econometrics. **16**, 15–20.

49 Ghosh, J.K. and Samanta, T. (2001) Model
selection - an overview. *Current science*,
80 (9), 1135.

50 Hansen, M.H. and Yu, B. (2001) Model
selection and the principle of minimum
description length. *Journal of the
American Statistical Association*, **454**,
746–774.

51 Johnson Jerald B. and Omland Kristian S.
(2004) Model selection in ecology and
evolution. *Trends in Ecology & Evolution*,
19 (2), 101–108.

52 Vuong, Q.H. (1989) Likelihood ratio tests
for model selection and non-nested
hypotheses. *Econometrica*, **57** (2), 307–333.

53 Timmer, J. and Müller, T.G. (2004) Modeling
the nonlinear dynamics of cellular signal
transduction. *International Journal of
Bifurcation and Chaos*, **14** (6), 2069–2079.

54 Akaike, H. (1974) A new look at the statistical
model identification. *IEEE Transactions on
Automatic Control*, **19** (6), 716–723.

55 Schwarz, G. (1978) Estimating the
dimension of a model. *Annals of Statistics*,
6 (2), 461–464.

56 Gelman, A., Carlin, J.B., Stern, H.S. and
Rubin, D.B. (1997) *Bayesian Data Analysis*,
Chapman & Hall, New York.

57 Stewart, Warren E. and Henson, T.L.
(1996) Model discrimination and criticism
with single-response data. *AIChE Journal*,
42 (11), 3055.

58 Vanrolleghem, P.A. and Heijnen, J.J.
(1998) A structured approach for selection
among candidate metabolic network
models and estimation of unknown
stoichiometric coefficients. *Biotechnol
Bioeng*, **58** (2–3), 133–138.

59 Takors, R., Wiechert, W. and Weuster-Botz,
D. (1997) Experimental Design for the
Identification of Macrokinetic Models and
Model Discrimination. *Biotechnology and
Bioengineering*, **56**, 564–567.